PONTIFICIA **UNIVERSIDAD CATÓLICA** DEL PERÚ

PONTIFICIA UNIVERSIDAD CATÓLICA DEL PERÚ

ESCUELA DE POSGRADO

Energy-independent contribution to the flavour ratios of high-energy astrophysical neutrinos

Tesis presentada para optar el Grado de Magíster en Física que presenta:

Mauricio Bustamante Ramírez

Asesor:
Dr. Alberto M. Gago Medina

Jurado:
Dr. Francisco A. de Zela Martínez
Dr. Hernán A. Castillo Egoavil

Lima, Mayo 2010

Energy-independent contribution to the flavour ratios of high-energy astrophysical neutrinos

Mauricio Bustamante Ramírez

Propuesto para el Grado de Magíster en Física
2010

Resumen

En esta tesis exploramos la posible ruptura de la simetría CPT en el sector de neutrinos, a una energía suficientemente alta, usando para esto el flujo de neutrinos de alta energía que se espera que provenga de fuentes astrofísicas lejanas como galaxias activas y explosiones de rayos gamma. La violación de CPT (CPTV) puede afectar las oscilaciones de neutrinos en dos formas: modificando la longitud de oscilación o la amplitud de la misma. Demostramos que cuando sólo la longitud de oscilación es afectada, tal y como sucede cuando la CPTV es introducida a través de una relación de dispersión modificada, los efectos sobre los flujos de neutrinos de distintos sabores no son visibles. Por lo tanto, con la intención de modificar también la amplitud de oscilación, violamos CPT a través de la adición de una contribución, no diagonal e independiente de la energía, al Hamiltoniano de oscilaciones estándar, dentro del contexto de la Extensión del Modelo Estándar, y permitimos que esta contribución se vuelva comparable en magnitud al término estándar, a una escala de 1 PeV. El término de CPTV introduce tres nuevos ángulos de mezcla, dos nuevos autovalores y tres nuevas fases, todos los cuales tienen valores actualmente desconocidos. Hemos variado estos parámetros, junto con los parámetros asociados a las oscilaciones estándar, y explorado las consecuencias para los flujos de sabor. Hemos explorado también la posible detección en IceCube, y en un detector ficcional más grande, asumiendo diferentes modelos para el flujo de neutrinos. Nuestros resultados sugieren que, cuando las razones de sabor en la producción son $\phi_e^0 : \phi_\mu^0 : \phi_\tau^0 = 1 : 2 : 0$ ó $0 : 1 : 0$, las modificaciones a los flujos en Tierra son más pronunciadas y más claramente separables de las predicciones de las oscilaciones estándar. Cuando las razones son $1 : 0 : 0$, la separación es menos clara. Concluimos que, para ciertos valores de los parámetros de CPTV, IceCube podría ser capaz de detectar desviaciones potencialmente grandes respecto de los valores estándar, incluso para modelos de flujo tan bajos como el límite Waxman-Bahcall. Una medición precisa de los parámetros, sin embargo, será difícil a menos que se utilice un detector Čerenkov mucho más voluminoso, o uno de diferente tipo.

Energy-independent contribution to the flavour ratios of high-energy astrophysical neutrinos

Mauricio Bustamante Ramírez

Presented towards a Master's Degree in Physics
2010

Abstract

We explore the possibility that CPT symmetry is broken in the neutrino sector at a high enough energy, using for this the high-energy neutrino flux that is expected to come from distant astrophysical sources such as active galaxies and gamma-ray bursts. CPT violation (CPTV) can affect neutrino oscillations either by modifying the oscillation length or its amplitude. We show that when only the oscillation length is affected, such as when CPTV is introduced through a modified dispersion relation, the effects on the astrophysical neutrino flavour fluxes are not visible. Hence, in order to modify also the oscillation amplitude, CPT is instead violated by adding a non-diagonal energy-independent contribution to the standard, mass-driven, neutrino oscillation Hamiltonian, within the context of the Standard Model Extension, and allowing it to become comparable in magnitude to the latter at a scale of 1 PeV. The CPTV term introduces three new mixing angles, two new eigenvalues and three new phases, all of which have currently unknown values. We have allowed these new parameters to vary, together with the ones associated to pure standard oscillations, and explored the consequences on the flavour fluxes. Detection prospects at the IceCube neutrino telescope, and in a fictional larger detector, have been studied, assuming different models for the neutrino flux. Our results suggest that, when the flavour fluxes at production are in the ratios $\phi_e^0 : \phi_\mu^0 : \phi_\tau^0 = 1 : 2 : 0$ or $0 : 1 : 0$, the modifications to the flavour fluxes at Earth are larger and more clearly separable from the standard-oscillations predictions. When the ratios are $1 : 0 : 0$, the separation is less clear. We conclude that, for certain values of the CPTV parameters, IceCube might be able to detect potentially large deviations from the standard flavour fluxes, even for flux models as low as the Waxman-Bahcall bound. Precision measurements of these parameters, however, are unlikely to be made unless a much larger Čerenkov detector or a one of a different kind are used.

Agradecimientos

El trabajo contenido en esta tesis fue elaborado entre el 2006 y el 2009, en la Pontificia Universidad Católica del Perú (PUCP) y en otras instituciones en las que el tesista tuvo oportunidad de realizar estancias.

Durante el 2006 y 2007, los cálculos relacionados a relaciones de dispersión modificadas y un primer contacto con la violación de simetría CPT fueron realizados bajo la asesoría del Dr. Omar Miranda, del CINVESTAV de México, durante estancias realizadas por el tesista en la segunda mitad del 2006 y del 2007, bajo el auspicio del programa HELEN (High-Energy Latinamerican-European Network). En el 2007, se presentaron resultados preliminares, en forma de poster, en el XI Taller Mexicano de Partículas y Campos, realizado en Tuxtla Gutiérrez, México, del 7 al 12 de Noviembre.

En la segunda mitad del 2008, el tratamiento más general de la violación de CPT fue empezado durante una estancia realizada en el Instituto de Física Corpuscular (IFIC), en Valencia, España, bajo la asesoría del Dr. Carlos Peña-Garay, y auspiciada nuevamente por el programa HELEN. En esa oportunidad, los nuevos resultados obtenidos durante la estancia fueron presentados en la conferencia DISCRETE'08, sobre simetrías discretas, llevada a cabo del 11 al 16 de Diciembre del 2008, en el IFIC.

A Omar y Carlos, mis más sinceros agradecimientos: sin su paciencia, su crítica constructiva y voluntad por compartir su experiencia, este trabajo habría sufrido mucho. A Luciano Maiani y Verónica Riquer, organizadores del programa HELEN, gracias por las oportunidades brindadas.

Especiales agradecimientos van para mi asesor, el Dr. Alberto Gago, por las innumerables y enormemente fructíferas y entretenidas discusiones de trabajo, presenciales, telefónicas y electrónicas, y por enseñarme, de manera empírica, cómo hacer ciencia. Sin tal cantidad de retroalimentación, este trabajo no habría llegado a tener la presente forma. Agradezco también a los profesores e investigadores que componen la Sección Física de la PUCP, especialmente a Francisco de Zela, Hernán Castillo y Eduardo Massoni.

Finalmente, a mis padres. Por mostrarme, mediante el ejemplo, a nunca, bajo ninguna circunstancia, darme por vencido. Por esto y por todos los años de apoyo incondicional, tienen mi gratitud por todo lo que dure mi vida.

El presente trabajo fue financiado por los siguientes proyectos de investigación de la Dirección Académica de Investigación de la PUCP: DAI-3256, DAI-4075 y DAI-L009. El proyecto de tesis asociado fue ganador del Programa de Apoyo a la Investigación para Estudiantes de Posgrado (PAIP) 2009.

Published material in this thesis

Partial and final results contained in Chapters 7 and 8 of the present thesis work have been published in the following journal articles and proceedings:

- M. Bustamante, A. M. Gago, J. L. Bazo, and O. G. Miranda, "On the sensitivity of neutrino telescopes to a modified dispersion relation," *AIP Conf. Proc.* **1026** (2008) 251–253.
- J. L. Bazo, M. Bustamante, A. M. Gago, and O. G. Miranda, "High energy astrophysical neutrino flux and modified dispersion relations," *Int. J. Mod. Phys.* **A24** (2009) 5819–5829, `arXiv:0907.1979 [hep-ph]`.
- M. Bustamante, A. M. Gago, and C. Pena-Garay, "Extreme scenarios of new physics in the UHE astrophysical neutrino flavour ratios," *J. Phys. Conf. Ser.* **171** (2009) 012048, `arXiv:0906.5329 [hep-ph]`.
- M. Bustamante, A. M. Gago, and C. Pena-Garay, "Energy-independent new physics in the flavour ratios of high-energy astrophysical neutrinos," *JHEP* **04** (2010) 066, `arXiv:1001.4878 [hep-ph]`.

Additionally, the review of the Standard Model presented in Section 2.1 was published as part of the following review article from the proceedings of the 2009 Latin-American CERN School of High-Energy Physics, in Medellín, Colombia:

- M. Bustamante, L. Cieri, and J. Ellis, "Beyond the Standard Model for Montaneros," `arXiv:0911.4409 [hep-ph]`.

Contents

List of Figures

List of Tables

Note on units and conventions

Unless otherwise stated, throughout this thesis we use natural units in which

$$\hbar = c = 1 \ ,$$

and the spacetime metric is defined as

$$g^{\mu\nu} = \begin{pmatrix} +1 & & & \\ & -1 & & \\ & & -1 & \\ & & & -1 \end{pmatrix} \ .$$

We have chosen to represent neutrino mass eigenstates using latin indices, and flavour states using greek indices, i.e.,

$$\begin{aligned} &\text{mass eigenstates:} && |\nu_i\rangle \ \ (i = 1, 2, 3, \ldots) \\ &\text{flavour neutrinos:} && |\nu_\alpha\rangle \ \ (\alpha = e, \mu, \tau, \ldots) \ . \end{aligned}$$

Chapter 1

Introduction

Experiments performed over the last thirty years have established that neutrinos can change flavour: careful measurements of solar [1–3], atmospheric [4,5], reactor [6] and accelerator [7, 8] neutrinos have established that there is a nonzero probability that a neutrino created with a certain flavour is detected with a different one after having propagated for some distance, and that this probability is a periodic function of the propagated distance, L, and the neutrino energy, E. The standard mechanism of neutrino flavour change requires neutrinos to be massive and results in a probability of flavour change that is oscillatory, with oscillation lengths that have a distinct $1/E$ dependence (see Section 4.2).

So far, the experiments that have studied neutrino flavour transitions [9] have been designed to detect neutrinos with energies that range from a few MeV (solar neutrinos) to the TeV scale (atmospheric neutrinos). Notably, data from the Super-Kamiokande atmospheric neutrino experiment [10] was used to find an energy dependence of the oscillation probability of E^n, with $n = -0.9 \pm 0.4$ at 90% confidence level, thus confirming the dominance of the mass-driven mechanism in this energy range, and relegating any other potential mechanisms to subdominance. It is possible, however, that one or more of such subdominant mechanisms become important at higher energies.

In the present paper, we have explored a possible scenario where there is an additional oscillation mechanism present which results in an energy-independent contribution to neutrino oscillations. This mechanism, though subdominant in the MeV–TeV range, might become dominant at higher energies, where the $1/E$ dependence of the standard oscillation term might render it comparatively unimportant: the higher the energy, the stronger the suppression of the standard oscillation term. The highest-energy flux of neutrinos available is the expected ultra-high-energy (UHE, with energies at the PeV scale and higher) flux from astrophysical

sources (notably, active galaxies; see Section 5.1.1) which are located at distances in the order of tens to hundreds of Mpc.

We will deferr the detailed treatment of how the energy-independent contribution is introduced to Chapters 6 and 7, and focus now on the possible mechanisms that might motivate it. According to the CPT theorem, any Lorentz-invariant local quantum field theory must be built out of a CPT-conserving Lagrangian. However, the Standard Model (SM) is known to be valid at energies well below the Planck scale, $m_{\rm Pl} \simeq 10^{19}$ GeV and, at higher energies, motivated by theories beyond the SM [11, 12], CPT and Lorentz invariance might be broken. At accessible energies, the breaking of these symmetries can be described by an effective field theory that contains the SM. We have explored the possibility that CPT is not an exact symmetry, but rather that it is broken by the addition of a CPT-odd term to an otherwise CPT-even Lagrangian. The observation of the non-conservation of CPT would imply a fundamental revision of the usefulness of local quantum field theories as accurate descriptions of fundamental interactions. A possible realisation of a CPT-violating (CPTV) effective field theory is the Standard Model Extension [13, 14] (see Chapter 3) which contains the SM, conserves $SU(3) \otimes SU(2) \otimes U(1)$, and also considers potential Lorentz- and CPT-violating couplings in the gauge, lepton, quark and Yukawa sectors. It is worth noting that an alternative mechanism that also results in an energy-independent contribution to the oscillations is the nonuniversal coupling of the different neutrino flavours to an external torsion field [15].

The rest of this thesis is organised as follows. In Chapter 2, we review the Standard Model of particle physics, emphasising the mass-generating Higgs mechanism, the contents of the neutrino sector, and the role of the discrete symmetries C, P, and T. Chapter 3 introduces the Standard Model Extension, which incorporates potential Lorentz and CPT violation. In Chapter 4 we review the theory of neutrino oscillations, and the experimental evidence that supports it. We also introduce different models of high-energy neutrino production at astrophysical sites like active galactic nuclei. In Chapter 6 we introduce CPT violation through Lorentz violation in the form of a modified dispersion relation, and find that, within this formalism, any energy-independent modification that results from the breaking of these symmetries is undetectable in the high-energy astrophysical neutrino flux. In Chapter 7, we adopt a more general formalism and introduce the potential CPT violation as a non-diagonal contribution to the neutrino oscillation Hamiltonian. We explore the effects of the potential violation on the neutrino flavour fluxes and study the detection prospects at the IceCube neutrino telescope, and in a similar, but larger, Čerenkov detector. Finally, in Section 8, we summarise and conclude.

Chapter 2

The Standard Model

2.1 The Salam-Glashow-Weinberg electroweak gauge theory

We start by reviewing the electroweak sector of the Standard Model (SM) (for more detailed accounts, see, e.g., [16–18]), with particular emphasis on the nature of electroweak symmetry breaking[1]. The theory grew out of experimental information on charged-current weak interactions, and of the realisation that the four-point Fermi description ceases to be valid above $\sqrt{s} = 600$ GeV [18]. Electroweak theory was able to predict the existence of neutral-current interactions, as discovered by the Gargamelle Collaboration in 1973 [20]. One of its greatest subsequent successes was the detection in 1983 of the $W^{\pm}$ and Z^0 bosons [21–24], whose existences it had predicted. Over time, thanks to the accumulating experimental evidence, the $SU(2)_L \otimes U(1)_Y$ electroweak theory and $SU(3)_C$ quantum chromodynamics, collectively known as the Standard Model, have come to be regarded as the correct description of electromagnetic, weak and strong interactions up to the energies that have been probed so far.

The particle content of the SM is summarized in Table 2.1. Within the SM, the electromagnetic and weak interactions are described by a Lagrangian that is symmetric under local weak isospin and hypercharge gauge transformations, described using the $SU(2)_L \otimes U(1)_Y$ group (the L subindex refers to the fact that the weak $SU(2)$ group acts only the left-handed projections of fermion states; Y is the

[1] Section 2.1 has been adapted from [19].

Bosons	Scalars
γ, W^+, W^-, Z^0, $g_{1...8}$	ϕ (Higgs)
Fermions	
Quarks (each with 3 colour charges)	Leptons
$2/3:$ $\begin{pmatrix} u \\ d \end{pmatrix}$, $\begin{pmatrix} c \\ s \end{pmatrix}$, $\begin{pmatrix} t \\ b \end{pmatrix}$	neutral: $\begin{pmatrix} \nu_e \\ e^- \end{pmatrix}$, $\begin{pmatrix} \nu_\mu \\ \mu^- \end{pmatrix}$, $\begin{pmatrix} \nu_\tau \\ \tau^- \end{pmatrix}$
$-1/3:$	$-1:$

Table 2.1: Particle content of the Standard Model with a minimal Higgs sector. Note that counting antiparticles, the number of fermions is doubled, and that, taking into account quark colour, the number of quarks plust antiquarks is tripled. Only left-handed neutrinos interact

hypercharge). We can write the $SU(2)_L \otimes U(1)_Y$ part of the SM Lagrangian as

$$\begin{aligned} \mathcal{L} &= -\frac{1}{4}\mathbf{F}^a_{\mu\nu}\mathbf{F}^{a\mu\nu} \\ &+ i\overline{\psi}\not{\partial}\psi + h.c. \\ &+ \psi_i y_{ij}\psi_j\phi + h.c. \\ &+ |D_\mu\phi|^2 - V(\phi) \ . \end{aligned} \tag{2.1}$$

The first line is the kinetic term for the gauge sector of the electroweak theory, with a running over the total number of gauge fields: three associated with $SU(2)_L$, which we shall call B^1_μ, B^2_μ, B^3_μ, and one with $U(1)_Y$, which we shall call $\mathcal{A}_\mu$. Their field-strength tensors are

$$F^a_{\mu\nu} = \partial_\nu B^a_\mu - \partial_\mu B^a_\nu + g\varepsilon_{bca}B^b_\mu B^c_\nu \ \text{ for } a = 1,2,3 \tag{2.2}$$

$$f_{\mu\nu} = \partial_\nu \mathcal{A}_\mu - \partial_\mu \mathcal{A}_\nu \ , \tag{2.3}$$

and, hence, $\mathbf{F}^a_{\mu\nu} \equiv \left(F^1_{\mu\nu}, F^2_{\mu\nu}, F^3_{\mu\nu}, f_{\mu\nu}\right)$. In Eq. (2.2), g is the coupling constant of the weak-isospin group $SU(2)_L$, and the ε_{bca} are its structure constants. The last term in this equation stems from the non-Abelian nature of $SU(2)$. At this point, all of the gauge fields are massless, but we will see later that specific linear combinations of the four electroweak gauge fields acquire masses through the Higgs mechanism.

The second line in Eq. (2.1) describes the interactions between the matter fields ψ, described by Dirac equations, and the gauge fields.

The third line is the Yukawa sector and incorporates the interactions between the matter fields and the Higgs field, ϕ, which are responsible for giving fermions their masses when electroweak symmetry breaking occurs.

The fourth and final line describes the scalar or Higgs sector. The first piece is

the kinetic term with the covariant derivative defined here to be

$$D_\mu = \partial_\mu + \frac{ig'}{2}\mathcal{A}_\mu Y + \frac{ig}{2}\tau \cdot \mathbf{B}_\mu \ , \tag{2.4}$$

where g' is the $U(1)$ coupling constant, and Y and $\tau \equiv (\tau_1, \tau_2, \tau_3)$ (the Pauli matrices) are, respectively, the generators of $U(1)$ and $SU(2)$. The second piece of the final line of (2.1) is the Higgs potential $V(\phi)$.

Whereas the first two lines of Eq. (2.1) have been confirmed in many different experiments, there is **no** *experimental evidence for the last two lines and one of the main objectives of the Large Hadron Collider at CERN [25–27] is to discover whether it is right, needs modification, or is simply wrong.*

2.1.1 The Higgs mechanism in $U(1)$

To explain the Higgs mechanism of mass generation, we first apply it to the gauge group $U(1)$, and then extend it to the full electroweak group $SU(2)_L \otimes U(1)_Y$. Thus, we first consider the following Lagrangian for a single complex scalar field:

$$\mathcal{L} = (\partial_\mu \phi)^* (\partial^\mu \phi) - V(\phi^* \phi) \ , \tag{2.5}$$

with the potential defined as

$$V(\phi^* \phi) = \mu^2 (\phi^* \phi) + \lambda (\phi^* \phi)^2 \ , \tag{2.6}$$

where μ^2 and λ are real constants, with $\lambda > 0$. This Lagrangian is clearly invariant under global $U(1)$ phase transformations

$$\phi \to e^{i\alpha}\phi \ , \tag{2.7}$$

for α some rotation angle. Equivalently, it is invariant under a $SO(2)$ rotational symmetry, which is made evident by writing $\mathcal{L}$ in terms of the decomposition of the complex scalar field into two real fields ϕ_1 and ϕ_2: $\phi \equiv \phi_1 + i\phi_2$.

If we choose $\mu^2 > 0$ in Eq. (2.6), the sole vacuum state has $\langle \phi \rangle = 0$. Perturbing around this vacuum reveals that, in this case, the scalar-sector Lagrangian simply factors into two Klein-Gordon Lagrangians, one for ϕ_1 and the other for ϕ_2, with a common mass. The symmetry of the original Lagrangian is preserved in this case.

However, when $\mu^2 < 0$, the Lagrangian (2.5) exhibits spontaneous breaking of the $U(1)$ global symmetry, which introduces a massless scalar particle known as a Goldstone boson, as we now show. In order to make manifest this breaking of the

$U(1)$ symmetry present in Eq. (2.5), we first minimize the potential (2.6) so as to identify the vacuum expectation value, or v.e.v., of the scalar field. To do this, we first write the Higgs potential as

$$V\left(\phi^*\phi\right) = \mu^2\left(\phi_1^2+\phi_2^2\right) + \lambda\left(\phi_1^2+\phi_2^2\right)^2 \ , \tag{2.8}$$

and note that minimisation with respect to $\phi^*\phi$ yields the value

$$\phi_1^2+\phi_2^2 = -\mu^2/\left(2\lambda\right) \ , \tag{2.9}$$

i.e., there is a set of equivalent minima lying around a circle of radius $\sqrt{-\mu^2/\left(2\lambda\right)}$, when $\mu^2 < 0$ as assumed. The quanta of the Higgs field arise when a particular ground state is chosen and perturbed. Reflecting the appearance of spontaneous symmetry breaking we may, without loss of generality, choose for instance

$$\phi_{1,\mathrm{vac}} = \sqrt{-\mu^2/\left(2\lambda\right)} \equiv v/\sqrt{2} \quad , \quad \phi_{2,\mathrm{vac}} = 0 \ . \tag{2.10}$$

Perturbations around this vacuum may be parametrized by

$$\eta/\sqrt{2} \equiv \phi_1 - v/\sqrt{2} \quad , \quad \xi/\sqrt{2} \equiv \phi_2 \ , \tag{2.11}$$

so that the perturbed complex scalar is $\phi = \left(v+\eta+i\xi\right)/\sqrt{2}$, where η and ξ are real fields. In terms of these, the Lagrangian becomes

$$\begin{aligned}\mathcal{L} \ &= \ \left[\frac{1}{2}\left(\partial^\mu\eta\right)\left(\partial_\mu\eta\right) - \frac{\mu^2}{2}\eta^2\right] + \frac{1}{2}\left(\partial^\mu\xi\right)\left(\partial_\mu\xi\right) \\ &\quad - \frac{\lambda}{2}\left[\left(v+\eta\right)^2+\xi^2\right]^2 - \mu^2 v\eta - \frac{\mu^2}{2}\xi^2 - \frac{1}{2}\mu^2 v^2 \ .\end{aligned} \tag{2.12}$$

The first and second terms describe two scalar particles: the first, η, is massive with $m_\eta^2 = -\mu^2 > 0$ (we recall that $\mu^2 < 0$), and the second, ξ, is massless, the Goldstone boson.

We now discuss how this spontaneous symmetry breaking of symmetry manifests itself in the presence of a $U(1)$ gauge field. For this purpose, we make the Lagrangian (2.5) invariant under local $U(1)$ phase transformations, i.e.,

$$\phi \rightarrow e^{i\alpha(x)}\phi \ . \tag{2.13}$$

This requires the introduction of a gauge field $\mathcal{A}_\mu$ that transforms as follows under $U(1)$:

$$\mathcal{A}'_\mu \rightarrow \mathcal{A}_\mu + \left(1/q\right)\partial_\mu\alpha\left(x\right) \ , \tag{2.14}$$

and replacing the space-time derivatives by covariant derivatives

$$D_\mu = \partial_\mu + iq\mathcal{A}_\mu \ , \tag{2.15}$$

where q is the conserved charge. Replacing the derivatives in Eq. (2.5) and adding a kinetic term for the $\mathcal{A}_\mu$ field, the Lagrangian becomes

$$\mathcal{L} = \left[\left(\partial_\mu - iq\mathcal{A}_\mu\right)\phi^*\right]\left[\left(\partial^\mu + iq\mathcal{A}^\mu\right)\phi\right] - V\left(\phi^*\phi\right) - \frac{1}{4}F^{\mu\nu}F_{\mu\nu} \ . \tag{2.16}$$

The last term in this equation, $(1/4)\,F^{\mu\nu}F_{\mu\nu}$, with $F_{\mu\nu} \equiv \partial_\nu\mathcal{A}_\mu - \partial_\mu\mathcal{A}_\nu$, is the kinetic term, which is separately invariant under the transformation (2.14) of the gauge field.

We now repeat the minimization of the potential $V(\phi)$ and write the Lagrangian in terms of the perturbations around the ground state, Eqs. (2.11):

$$\begin{aligned}\mathcal{L} \ = \ & \left\{\frac{1}{2}\left[\left(\partial^\mu\eta\right)\left(\partial_\mu\eta\right) - \mu^2\eta^2\right] + \frac{1}{2}\left(\partial^\mu\xi\right)\left(\partial_\mu\xi\right) - \frac{1}{4}F^{\mu\nu}F_{\mu\nu} + \frac{1}{2}q^2v^2\mathcal{A}^\mu\mathcal{A}_\mu\right\} \\ & + vq^2A^\mu\mathcal{A}_\mu\eta + \frac{q^2}{2}\mathcal{A}^\mu\mathcal{A}_\mu\eta^2 + q\left(\partial^\mu\xi\right)\mathcal{A}_\mu\left(v+\eta\right) - q\left(\partial^\mu\eta\right)\mathcal{A}_\mu\xi \\ & - \mu^2v\eta - \frac{\mu^2}{2}\xi^2 - \frac{\lambda}{2}\left[\left(v+\eta\right) + \xi^2\right]^2 - \frac{\mu^2v}{2} \ .\end{aligned} \tag{2.17}$$

The first three terms again describe a (real) scalar particle, η, of mass $\sqrt{-\mu^2}$ and a massless Goldstone boson, ξ. The fourth term describes the free gauge field. However, whereas previously the Lagrangian described a massless boson field (see Eq. (2.12)), now it contains a term proportional to $\mathcal{A}_\mu\mathcal{A}^\mu$, which gives the gauge field a mass of

$$m_\mathcal{A} = qv \ , \tag{2.18}$$

from which we see that the boson field has acquired a mass that is proportional to the vacuum expectation value of the Higgs field. Indeed, the last two terms in the first line of Eq. (2.12) are identical with the Proca Lagrangian for a $U(1)$ gauge boson of mass m.

The rest of the terms in Eq. (2.17) define couplings between the fields A^μ, η and ξ, among which is a bilinear interaction coupling A^μ and $\partial_\mu\xi$. In order to give the correct propagating particle interpretation of (2.17), we must diagonalize the bilinear terms and remove this term. This is easily done by exploiting the gauge freedom of the $\mathcal{A}_\mu$ field to replace

$$\mathcal{A}_\mu \to \mathcal{A}'_\mu = \mathcal{A}_\mu + \frac{1}{qv}\partial_\mu\xi \ , \tag{2.19}$$

which is accompanied by the local phase transformation

$$\phi \to \phi' = e^{-i\xi(x)/v}\phi = (v+\eta)/\sqrt{2}\ . \tag{2.20}$$

After making this transformation, the field ξ no longer appears, and the Lagrangian (2.12) takes the simplified form

$$\mathcal{L} = \frac{1}{2}\left[(\partial^\mu)(\partial_\mu) - \mu^2\eta^2\right] - \frac{1}{4}F^{\mu\nu}F_{\mu\nu} + \frac{q^2v^2}{2}\mathcal{A}^\mu\,'\mathcal{A}'_\mu + \dots\ . \tag{2.21}$$

where the ellipsis stand for trilinear and quadrilinear interactions.

The interpretation of Eq. (2.21) is that the Goldstone boson ξ that appeared when the global $U(1)$ symmetry was broken by the choice of an asymmetric ground state when $\mu^2 < 0$ has been absorbed (or "eaten") by the gauge field $\mathcal{A}_\mu$, with the effect of generating a mass. Another way to understand this is to recall that, whereas a massless gauge boson has only two degrees of freedom, or polarization states (which are transverse), a massive gauge boson must have a third (longitudinal) polarization state. In the Higgs mechanism, this is supplied by the Goldstone boson of the spontaneously-broken $U(1)$ global symmetry.

At first sight, the Higgs mechanism may seem somewhat artificial. From one point of view, it is merely a description of the breaking of electroweak symmetry, rather than an explanation how a massless gauge boson may become massive. As Quigg says [28], the electroweak symmetry is broken because $\mu^2 < 0$, and we must choose $\mu^2 < 0$, because otherwise electroweak symmetry is not broken. From another point of view, the *only* consistent formulation of an interacting massive gauge boson is via the Higgs mechanism, and the spontaneous breaking of symmetry is a mathematical ruse for describing this phenomenon.

2.1.2 The Higgs mechanism in $SU(2)_L \otimes U(1)_Y$

Following closely in both spirit and notation the book by Quigg [28], we now consider the weak-isospin doublet

$$\mathrm{L} = \begin{pmatrix} \nu \\ e \end{pmatrix}_L\ , \tag{2.22}$$

with the left-handed neutrino and electron states defined by

$$\nu_L = \frac{1}{2}(1-\gamma_5)\,\nu \quad , \quad e_L = \frac{1}{2}(1-\gamma_5)\,e\ . \tag{2.23}$$

The operator $(1-\gamma_5)/2$ is of course the left-handed helicity projector, and ν, e are solutions of the free-field Dirac equation. Within the SM, we consider the neutrino

to be massless, and it does not have a corresponding right-handed component, i.e.,

$$\nu_R = \frac{1}{2}\left(1+\gamma_5\right)\nu = 0 \ . \tag{2.24}$$

Hence, the only right-handed lepton, e_R, constitutes a weak-isospin singlet, i.e.,

$$\mathrm{R} = e_R = \frac{1}{2}\left(1+\gamma_5\right)e \ . \tag{2.25}$$

We write initially the Lagrangian as

$$\begin{aligned}
\mathcal{L} &= \mathcal{L}_{\text{gauge}} + \mathcal{L}_{\text{leptons}} && (2.26)\\
\mathcal{L}_{\text{gauge}} &= -\frac{1}{4}F^a_{\mu\nu}F^{a\mu\nu} - \frac{1}{4}f_{\mu\nu}f^{\mu\nu} && (2.27)\\
\mathcal{L}_{\text{leptons}} &= \overline{\mathrm{R}}\left(\partial_\mu + i\frac{g'}{2}\mathcal{A}_\mu Y\right)\mathrm{R} + \overline{\mathrm{L}}i\gamma^\mu\left(\partial_\mu + i\frac{g'}{2}\mathcal{A}_\mu Y + i\frac{g}{2}\tau\cdot\mathbf{B}_\mu\right)\mathrm{L}\ , && (2.28)
\end{aligned}$$

where the field-strength tensors, $F_{\mu\nu}$ and $f_{\mu\nu}$, were defined in Eqs. (2.2) and (2.3), respectively. Here, $g'/2$ is the coupling constant associated to the hypercharge group $U(1)_Y$, and $g/2$ is the coupling to the weak-isospin group $SU(2)_L$. So far, we are presented with four massless bosons ($\mathcal{A}_\mu$, B^1_μ, B^2_μ, B^3_μ); the Higgs mechanism will select linear combinations of these to produce three massive bosons ($W^\pm$, Z^0) and a massless one (γ).

The Higgs field is now a complex $SU(2)$ doublet

$$\phi = \begin{pmatrix} \phi^+ \\ \phi^0 \end{pmatrix} \ , \tag{2.29}$$

with ϕ^+ and ϕ^0 scalar fields. We need to add the Lagrangian

$$\mathcal{L}_{\text{Higgs}} = \left(D_\mu\phi\right)^\dagger\left(D^\mu\phi\right) - V\left(\phi^\dagger\phi\right) \ , \tag{2.30}$$

with the Higgs potential given by analogy to Eq. (2.6) as

$$V\left(\phi^\dagger\phi\right) = \mu^2\left(\phi^\dagger\phi\right) + \lambda\left(\phi^\dagger\phi\right)^2 \ , \tag{2.31}$$

with $\lambda > 0$. We should also include the interaction Lagrangian between this scalar field and the fermionic matter fields, which occurs through Yukawa couplings,

$$\mathcal{L}_{\text{Yukawa}} = -G_e\left[\overline{\mathrm{R}}\phi^\dagger\mathrm{L} + \overline{\mathrm{L}}\phi\mathrm{R}\right] \ . \tag{2.32}$$

We will see later that these terms give rise to masses for the matter fermions.

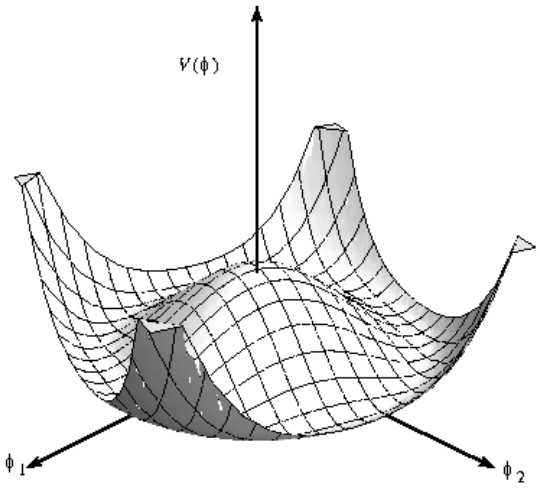

Figure 2.1: Scalar potential $V\left(\phi^{\dagger}\phi\right)$ with $\lambda > 0$ and $\mu^2 < 0$.

A plot of the Higgs potential is presented in Fig. 2.1, where we see that $\langle\phi\rangle = 0$ is an unstable local minimum of the effective potential if $\mu^2 < 0$, and that the minimum is at some $\langle\phi\rangle \neq 0$ with an arbitrary phase, leading to spontaneous symmetry breaking. Minimising the Higgs potential, we obtain

$$\frac{\partial}{\partial\left(\phi^{\dagger}\phi\right)}V\left(\phi^{\dagger}\phi\right) = \mu^2 + 2\lambda\langle\phi\rangle_0 = \mu^2 + 2\lambda\left[\left(\phi^{+}_{\text{vac}}\right)^2 + \left(\phi^{0}_{\text{vac}}\right)^2\right] = 0\ . \tag{2.33}$$

Choosing $\phi^{+}_{\text{vac}} = 0$ and $\phi^{0}_{\text{vac}} = \sqrt{-\mu^2/\left(2\lambda\right)}$, the v.e.v. of the scalar field becomes

$$\langle\phi\rangle_0 = \begin{pmatrix} 0 \\ v/\sqrt{2} \end{pmatrix}\ , \tag{2.34}$$

with $v \equiv \sqrt{-\mu^2/\lambda}$. Selecting a particular v.e.v. breaks, of course, both $SU(2)_L$ and $U(1)_Y$ symmetries. Nevertheless, an invariance under the $U(1)_{\text{EM}}$ symmetry is preserved, with the charge operator as the generator. In the preceding Section, we saw one example of the general theorem that, for every broken generator (i.e., every generator that does not leave the vacuum invariant), there would (in the absence of the Higgs mechanism) be a Goldstone boson.

In general, a generator $\mathcal{G}$ leaves the vacuum invariant if

$$e^{i\alpha\mathcal{G}}\langle\phi\rangle_0 \simeq \left(1 + i\alpha\mathcal{G}\right)\langle\phi\rangle_0 = \langle\phi\rangle_0\ , \tag{2.35}$$

which is satisfied when $\mathcal{G}\langle\phi\rangle_0 = 0$. Let us test whether the generators of $SU(2)_L \otimes$

$U(1)_Y$ satisfy this condition:

$$\tau_1\langle\phi\rangle_0 = \begin{pmatrix} 0 & 1 \\ 1 & 0 \end{pmatrix}\begin{pmatrix} 0 \\ v/\sqrt{2} \end{pmatrix} = \begin{pmatrix} v/\sqrt{2} \\ 0 \end{pmatrix} \tag{2.36}$$

$$\tau_2\langle\phi\rangle_0 = \begin{pmatrix} 0 & -i \\ i & 0 \end{pmatrix}\begin{pmatrix} 0 \\ v/\sqrt{2} \end{pmatrix} = \begin{pmatrix} -iv/\sqrt{2} \\ 0 \end{pmatrix} \tag{2.37}$$

$$\tau_3\langle\phi\rangle_0 = \begin{pmatrix} 1 & 0 \\ 0 & -1 \end{pmatrix}\begin{pmatrix} 0 \\ v/\sqrt{2} \end{pmatrix} = \begin{pmatrix} 0 \\ -v/\sqrt{2} \end{pmatrix} \tag{2.38}$$

$$Y\langle\phi\rangle_0 = \langle\phi\rangle_0 \, . \tag{2.39}$$

Thus, none of the generators leave the vacuum invariant. However, we note that

$$Q\langle\phi\rangle_0 = \frac{1}{2}\left(\tau_3 + Y\right)\langle\phi\rangle_0 = 0 \, , \tag{2.40}$$

which is what we expected: the linear combination of generators corresponding to electric charge remains unbroken. Correspondingly, as we shall now see, whilst the photon remains massless, the other three gauge bosons acquire masses.

To see this, we now consider perturbations around the choice of vacuum. The full perturbed scalar field is

$$\phi = \exp\left(\frac{i\xi\cdot\tau}{2v}\right)\begin{pmatrix} 0 \\ (v+\eta)/\sqrt{2} \end{pmatrix} \, . \tag{2.41}$$

However, in analogy to what we did for the $U(1)$ Higgs in the previous section to rotate the Goldstone boson ξ away, we are also able here to gauge-transform the scalar ϕ and the gauge and matter fields, i.e.,

$$\phi \rightarrow \phi' = \exp\left(\frac{-i\xi\cdot\tau}{2v}\right)\phi = \begin{pmatrix} 0 \\ (v+\eta)/\sqrt{2} \end{pmatrix} \, . \tag{2.42}$$

$$\tau\cdot\mathbf{B}_\mu \rightarrow \tau\cdot\mathbf{B}'_\mu \tag{2.43}$$

$$\mathrm{L} \rightarrow \mathrm{L}' = \exp\left(\frac{-i\xi\cdot\tau}{2v}\right)\mathrm{L} \, , \tag{2.44}$$

while the $\mathcal{A}_\mu$ and R remain invariant. It is possible to show that $\tau\cdot\mathbf{B}'_\mu = \tau\cdot\mathbf{B}_\mu - \xi\times\mathbf{B}_\mu\cdot\tau - (1/g)\,\partial_\mu(\xi\cdot\tau)$.

In the unitary gauge, we can write the perturbed state as

$$\langle\phi\rangle_0 \rightarrow \phi = \begin{pmatrix} 0 \\ (v+\eta)/\sqrt{2} \end{pmatrix} \, , \tag{2.45}$$

and the Lagrangian in the Yukawa sector, Eq. (2.32), becomes

$$\mathcal{L}_{\text{Yukawa}} = -G_e \left[\overline{e}_R \phi^\dagger \begin{pmatrix} \nu_L \\ e_L \end{pmatrix} + (\overline{\nu}_L \ \overline{e}_L)\, \phi e_R \right] = -G_e \frac{v+\eta}{\sqrt{2}} \left(\overline{e}_R e_L + \overline{e}_L e_R \right) \ . \quad (2.46)$$

Defining $\overline{e} \equiv (\overline{e}_R, \overline{e}_L)$ and $e \equiv (e_L, e_R)^T$ yields

$$\mathcal{L}_{\text{Yukawa}} = -\frac{G_e v}{\sqrt{2}} \overline{e} e - \frac{G_e \eta}{\sqrt{2}} \overline{e} e \ , \quad (2.47)$$

so that the electron has acquired a mass

$$m_e = G_e v/\sqrt{2} \ . \quad (2.48)$$

Clearly, this mechanism may be applied to all the SM fermions, with the general feature that their masses are proportional to their Yukawa couplings to the Higgs field [2]. This implies that the preferred decays of a Higgs boson into generic fermions f are into heavier species, as long as the Higgs mass $> 2m_f$.

To see the effect of spontaneous symmetry breaking on the scalar-sector Lagrangian, $\mathcal{L}_{\text{Higgs}}$ in Eq. (2.30), it is useful to calculate first

$$\phi^\dagger \phi = \left(\frac{v+\eta}{\sqrt{2}} \right)^2 \ , \quad (2.49)$$

so that

$$V\left(\phi^\dagger \phi\right) = \mu^2 \left(\frac{v+\eta}{\sqrt{2}} \right)^2 + \lambda \left(\frac{v+\eta}{\sqrt{2}} \right)^4 \ , \quad (2.50)$$

and we also need

$$D_\mu \phi = \partial_\mu \phi + \frac{ig'}{2} \mathcal{A}_\mu Y \phi + \frac{ig}{2} \tau \cdot \mathbf{B}_\mu \phi \ , \quad (2.51)$$

whose first term is simply

$$\partial_\mu \phi = \begin{pmatrix} 0 \\ \partial_\mu \eta/\sqrt{2} \end{pmatrix} \ . \quad (2.52)$$

[2] The Higgs couplings to quarks also induce their Cabibbo-Kobayashi-Maskawa mixing.

Using Eqs. (2.36)–(2.39), we calculate the second and third terms, i.e.,

$$\frac{ig'}{2}\mathcal{A}_\mu Y\phi = \frac{ig'}{2}\mathcal{A}_\mu\phi = \frac{ig'}{2}\mathcal{A}_\mu\begin{pmatrix}0\\(v+\eta)/\sqrt{2}\end{pmatrix}, \tag{2.53}$$

$$\begin{aligned}(\tau\cdot\mathbf{B}_\mu)\,\phi &= B^1_\mu\begin{pmatrix}(v+\eta)/\sqrt{2}\\0\end{pmatrix} + B^2_\mu\begin{pmatrix}-i\,(v+\eta)/\sqrt{2}\\0\end{pmatrix}\\ &\quad + B^3_\mu\begin{pmatrix}0\\-(v+\eta)/\sqrt{2}\end{pmatrix}.\end{aligned} \tag{2.54}$$

Hence,

$$D_\mu\phi = \begin{pmatrix}\frac{ig}{2}\left(\frac{v+\eta}{\sqrt{2}}\right)\left(B^1_\mu - iB^2_\mu\right)\\ \frac{1}{\sqrt{2}}\partial_\mu\eta + \left(\frac{v+\eta}{\sqrt{2}}\right)\frac{i}{2}\left(ig'\mathcal{A}_\mu - igB^3_\mu\right)\end{pmatrix} \tag{2.55}$$

and

$$\begin{aligned}(D^\mu\phi)^\dagger\,(D_\mu\phi) &= \frac{g^2}{8}(v+\eta)^2\,|B^1_\mu - iB^2_\mu|^2 + \frac{1}{2}\,(\partial_\mu\eta)\,(\partial^\mu\eta)\\ &\quad + \frac{1}{8}(v+\eta)^2\left(g'\mathcal{A}_\mu - gB^3_\mu\right)^2.\end{aligned} \tag{2.56}$$

With this, the scalar-sector Lagrangian becomes

$$\begin{aligned}\mathcal{L}_{\text{Higgs}} &= \left\{\frac{1}{2}\,(\partial_\mu\eta)\,(\partial^\mu\eta) - \frac{\mu^2}{2}\eta^2 + \frac{v^2}{8}\left[g^2|B^1_\mu - iB^2_\mu|^2 + \left(g'\mathcal{A}_\mu - gB^3_\mu\right)^2\right]\right\}\\ &\quad + \left\{\frac{1}{8}\left(\eta^2+2v\eta\right)\left[g^2|B^1_\mu - iB^2_\mu|^2 + \left(g'\mathcal{A}_\mu - gB^3_\mu\right)^2\right]\right.\\ &\quad \left. - \frac{1}{4}\eta^4 - \lambda v\eta^3 - \frac{3}{2}\lambda v^2\eta^2 - \left(\lambda v^3 + \mu^2 v\right)\eta - \left(\frac{\lambda v^4}{4} + \frac{\mu^2 v^2}{2}\right)\right\}.\end{aligned} \tag{2.57}$$

From the second term inside the first curly brackets, we see that the η field has acquired a mass; indeed, it is the Higgs boson, with non-zero mass. The terms inside the second curly brackets either describe interactions between the gauge and Higgs fields, or are constants that do not affect the physics.

It is convenient to define the charged gauge fields $W^\pm_\mu$ as linear combinations of the massless fields B^1_μ and B^2_μ, i.e.,

$$W^\pm_\mu \equiv \frac{B^1_\mu \mp iB^2_\mu}{\sqrt{2}}, \tag{2.58}$$

and, analogously,

$$Z_\mu \equiv \frac{-g'\mathcal{A}_\mu + gB^3_\mu}{\sqrt{g^2+g'^{\,2}}} \,, \tag{2.59}$$

$$A_\mu \equiv \frac{g\mathcal{A}_\mu + g'B^3_\mu}{\sqrt{g^2+g'^{\,2}}} \,. \tag{2.60}$$

Writing the original fields $\mathcal{A}_\mu$, B^i_μ in terms of the new fields, we have

$$B^1_\mu = \frac{\sqrt{2}}{2}\left(W^-_\mu + W^+_\mu\right) \,, \tag{2.61}$$

$$B^2_\mu = \frac{\sqrt{2}}{2}\left(W^-_\mu - W^+_\mu\right) \,, \tag{2.62}$$

$$B^3_\mu = \frac{g'}{\sqrt{g^2+g'^{\,2}}}\left(A_\mu + \frac{g}{g'}Z_\mu\right) \,, \tag{2.63}$$

$$\mathcal{A}_\mu = \frac{g}{\sqrt{g^2+g'^{\,2}}}\left(A_\mu - \frac{g'}{g}Z_\mu\right) \,. \tag{2.64}$$

Making these replacements in the broken scalar-sector Lagrangian, Eq. (2.57), leads to

$$\begin{aligned}\mathcal{L}_{\text{Higgs}} = & \left[\frac{1}{2}\left(\partial^\mu\eta\right)\left(\partial_\mu\eta\right) - \frac{\mu^2}{2}\eta^2\right] \\ & + \frac{v^2g^2}{8}W^{+\,\mu}W^+_\mu + \frac{v^2g^2}{8}W^{-\,\mu}W^-_\mu + \frac{\left(g^2+g'^{\,2}\right)v^2}{8}Z^\mu Z_\mu \\ & + \ldots \,,\end{aligned} \tag{2.65}$$

and it is evident now that while the photon field, $\mathcal{A}_\mu$, is massless due to the unbroken $U(1)_{\text{EM}}$ symmetry (i.e., the symmetry under $e^{iQ\alpha(x)}$ rotations), the vector bosons $W^\pm$ and Z^0 have masses

$$m_W = gv/2 \quad , \quad m_Z = (v/2)\sqrt{g^2+g'^{\,2}} \,. \tag{2.66}$$

We see again that the Higgs couplings to other particles, in this case the $W^\pm$ and Z^0, are related to their masses.

We also see that the masses of the neutral and charged weak-interaction bosons are related through

$$m_Z = m_W\sqrt{1+g'^{\,2}/g^2} \,. \tag{2.67}$$

Experimentally, the weak gauge boson masses are known to high accuracy to be [29]

$$m_W = 80.399 \pm 0.023 \text{ GeV} \quad , \quad m_Z = 91.1875 \pm 0.0021 \text{ GeV} \,, \tag{2.68}$$

which can be compared in detail with Eq. (2.67) only after the inclusions of radiative corrections. Meanwhile, the current experimental upper limit on the photon mass, based on plasma physics, is very stringent: $m_\gamma < 10^{-18}$ eV [30]. For the Higgs mass, we see from (2.57) that

$$m_H = -2\mu^2 \ . \tag{2.69}$$

A priori, however, there is no theoretical prediction within the Standard Model, since μ is not determined by any of the known parameters of the Standard Model. Later we will see various ways in which experiments constrain the Higgs mass.

We can introduce a weak mixing angle θ_W to parametrise the mixing of the neutral gauge bosons, defined by

$$\tan(\theta_W) = g'/g \ , \tag{2.70}$$

so that

$$\cos(\theta_W) = \frac{g}{\sqrt{g^2 + g'^{\,2}}} \quad , \quad \sin(\theta_W) = \frac{g'}{\sqrt{g^2 + g'^{\,2}}} \ . \tag{2.71}$$

With this, we can write, from Eqs. (2.59) and (2.60),

$$Z_\mu = -\sin(\theta_W)\,\mathcal{A}_\mu + \cos(\theta_W)\,B^3_\mu \ , \tag{2.72}$$

$$A_\mu = \cos(\theta_W)\,\mathcal{A}_\mu + \sin(\theta_W)\,B^3_\mu \ . \tag{2.73}$$

The relation (2.67) between the masses of $W^\pm$ and Z^0 becomes

$$m_W = m_Z \cos(\theta_W) \ , \tag{2.74}$$

and it is common practice to define the ratio

$$\rho = \frac{m_W^2}{m_Z^2 \cos^2(\theta_W)} \ . \tag{2.75}$$

According to the Standard Model, this is equal to unity at the tree level, a prediction that has been well tested by experiment, including radiative corrections. The value of $\sin^2(\theta_W)$ is obtained from measurements of the Z pole and neutral-current processes, and depends on the renormalisation prescription. The 2008 Particle Data Group review [29] states values of $\sin^2(\theta_W) = 0.2319(14)$ and $\rho = 1.0004^{+0.0008}_{-0.0004}$.

Therefore, after the spontaneous breaking of the electroweak $SU(2)_L \otimes U(1)_Y$ symmetry, we have ended up with what we desired: three massive gauge bosons ($W^\pm$, Z^0) that mediate weak interactions, one massless gauge boson (A) corresponding to the photon, and an extra, massive, Higgs boson (H).

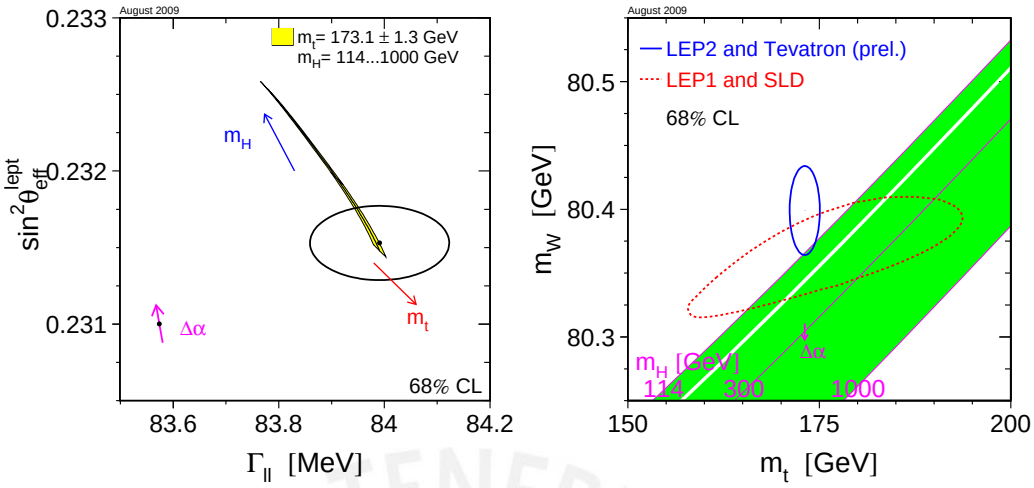

Figure 2.2: *Left:* LEP and SLD measurements of $\sin^2\theta_W$ and the leptonic decay width of the Z^0, Γ_{ll}, compared with the SM prediction for different values of m_t and m_H. *Right:* The predictions for m_t and m_W made in the SM using LEP1 and SLD data (dotted mango-shaped contour) for different values of m_H, compared with the LEP2 and Tevatron measurements (ellipse). The arrows show the additional effects of the uncertainty in the value of α_{em} at the Z^0 peak [31].

2.1.3 Parameters of the Standard Model

The transformation from being one of the possible explanations of electromagnetic, weak and strong phenomena into a description in outstanding agreement with experiments is reflected in the dozens of electroweak precision measurements available today [29, 31, 32]. These are sensitive to quantum corrections at and beyond the one-loop level, which are essential for obtaining agreement with the data. The calculations of these corrections rely upon the renormalizability (i.e, the calculability at all orders of perturbation) of the SM[3], and depend on the masses of heavy virtual particles, such as the top quark and the Higgs boson and possibly other particles beyond the SM. The consistency with the data may be used to constrain the masses of these particles.

Many of these observables have quadratic sensitivity to the mass of the top quark, e.g.,

$$s_W^2 \equiv 1 - m_W^2/m_Z^2 \ni -\frac{2\alpha}{16\pi \sin^2(\theta_W)} \frac{m_t^2}{m_Z^2} . \tag{2.76}$$

This effect was used before the discovery of the top quark to predict successfully its mass [33], and the consistency of the prediction with experiment can be used to

[3] A crucial aspect of this is cancellation of anomalous triangle diagrams between quarks and leptons, which may be a hint of an underlying Grand Unified Theory.

Parameter	Input value	Fit value
M_Z [GeV]	91.1875 ± 0.0021	91.1876 ± 0.0021
Γ_Z [GeV]	2.4952 ± 0.0023	2.4956 ± 0.0015
$\sigma^0_{\rm had}$	41.540 ± 0.037	41.478 ± 0.014
R^0_l	20.767 ± 0.025	20.741 ± 0.018
$A^{0,l}_{\rm FB}$	0.0171 ± 0.0010	0.01624 ± 0.0002
A_l (LEP)	0.1465 ± 0.0033	0.1473 ± 0.0009
A_l (SLD)	0.1513 ± 0.0021	$0.1465^{+0.0007}_{-0.0010}$
$\sin^2\phi^l_{\rm eff}\,(Q_{\rm FB})$	0.2324 ± 0.0012	$0.23151^{+0.00010}_{-0.00012}$
$A^{0,c}_{\rm FB}$	0.0707 ± 0.0035	0.0737 ± 0.0005
$A^{0,b}_{\rm FB}$	0.0992 ± 0.0016	$0.1032^{+0.0007}_{-0.0006}$
A_c	0.670 ± 0.027	$0.6679^{+0.00042}_{-0.00036}$
A_b	0.923 ± 0.020	$0.93463^{+0.00007}_{-0.00008}$
R^0_c	0.1721 ± 0.0030	0.17225 ± 0.00006
R^0_b	0.21629 ± 0.00066	0.21577 ± 0.00005
$\Delta\alpha^{(5)}_{\rm had}\,(M_Z^2)$	2768 ± 22	2764^{+22}_{-21}
M_W [GeV]	80.399 ± 0.023	$80.371^{+0.008}_{-0.011}$
Γ_W [GeV]	2.098 ± 0.048	2.092 ± 0.001
$\overline{m}_c$ [GeV]	1.25 ± 0.09	1.25 ± 0.09
$\overline{m}_b$ [GeV]	4.20 ± 0.07	4.20 ± 0.07
m_t [GeV]	173.1 ± 1.3	173.6 ± 1.2

Table 2.2: Fit and experimental values of some SM quantities, as obtained using the `Gfitter` package [32]. For all the observables listed, except A_l (LEP) and A_l (SLD), the fit values shown are the results of "complete fits", i.e., the results of using all the inputs, including the input value of the parameter that is being fit, to calculate the result. For the two exceptions, the fit values shown were calculated using all inputs except their own. Consult [32] for a description of each observable.

constrain possible new physics beyond the SM, particularly mass-squared differences between isospin partner particles, that would contribute analogously to (2.76). Many electroweak observables are also logarithmically sensitive to the mass of the Higgs boson, e.g.,

$$s^2_W \;\ni\; \frac{5\alpha}{24\pi}\ln\left(\frac{m^2_H}{m^2_W}\right) \tag{2.77}$$

when $m_H \gg m_W$. If there were no Higgs boson, or nothing to do its job, radiative corrections such as (2.77) would diverge, and the SM calculations would become meaningless. Two examples of precision electroweak observables, namely the coupling of the Z^0 boson to leptons and the mass of the W boson, are shown in Fig. 2.2.

Table 2.2 and Fig. 2.3 [32] compare the predicted (fitted) and experimentally measured values for several parameters of the Standard Model; the agreement is usually better than 1σ. This is a remarkable success for a theory that, as we have

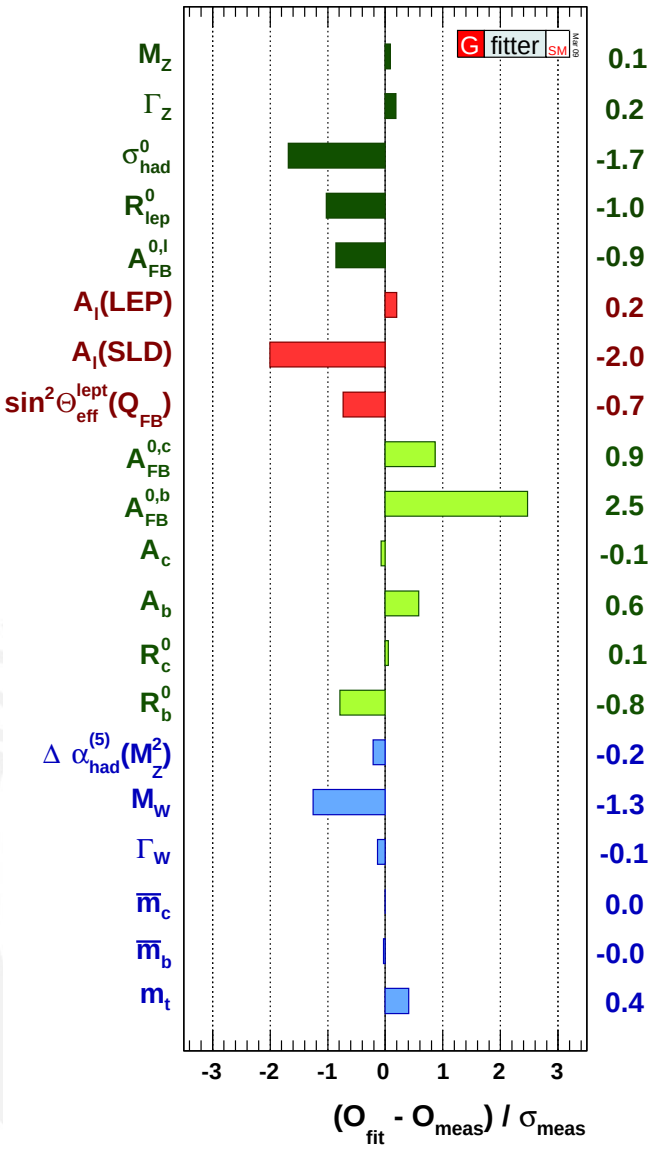

Figure 2.3: Comparison between direct measurements and the results of a fit using the `Gfitter` package [32].

seen, can be written down in only a few lines.

The agreement of the precision electroweak observables with the SM can be used to predict m_H, just as it was used previously to predict m_t. Since the early 1990s [34], this method has been used to tighten the vise on the Higgs, providing ever-stronger indications that it is probably relatively light, as hinted in Fig. 2.4. The latest estimate of the Higgs mass is [31]

$$m_H = 89^{+35}_{-26} \text{ GeV}. \tag{2.78}$$

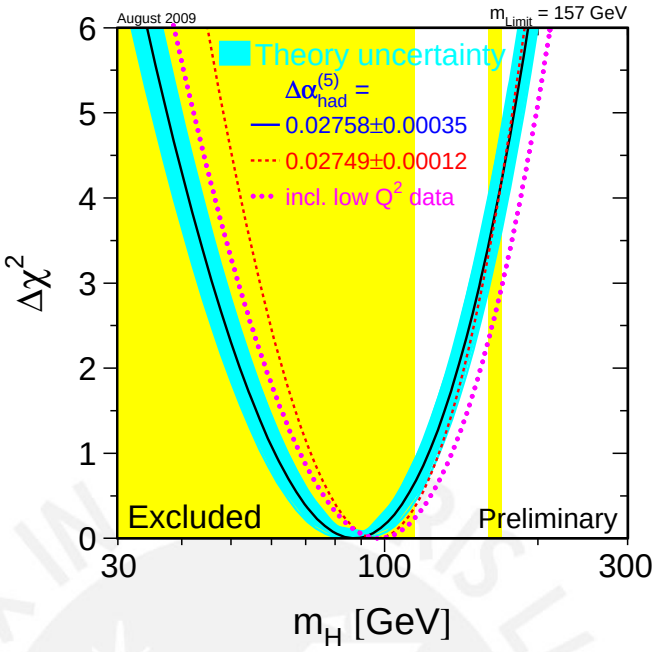

Figure 2.4: The χ^2 likelihood function for m_H in a global electroweak fit. The blue band around the (almost) parabolic solid curve represents the theoretical uncertainty: the other curves indicate the effects of different calculations of the renormalization of α_{em} and of including low-energy data. The shaded regions are those excluded by LEP and by the Tevatron [31].

Although the central value is somewhat below the lower limit of 114.4 GeV set by direct searches at LEP [35], there is consistency at the 1-σ level, and no significant discrepancy. *A priori*, the relatively light mass range (2.78) suggests that the Higgs boson interacts relatively weakly, with a small quartic coupling λ, though there is no theoretical consensus on this.

This success is very impressive. However, our rejoicing is muted by the fact that to specify the SM we need at least 19 input parameters in order to calculate physical processes, namely:

- three coupling parameters, which we can choose to be the strong coupling constant, α_s, the fine structure constant, α_{em}, and the weak mixing angle, $\sin^2(\theta_W)$;
- two parameters that specify the shape of the Higgs potential, μ^2 and λ (or, equivalently, m_H and m_W or m_Z);
- six quark masses (or the six Yukawa couplings for the quarks);
- four parameters (three mixing angles and one weak CP-violating angle) for

the Cabibbo-Kobayashi-Maskawa matrix [see Eq. (4.47) below];

- three charged-lepton masses (or the corresponding Yukawa couplings);
- one parameter to allow for non-perturbative CP violation in QCD, θ_{QCD}.

Moreover, because we now know that neutrinos have mass and that they mix (see, e.g., [36,37]), the Standard Model must be extended to incorporate this fact. Therefore, we also need to specify three neutrino masses and three mixing angles plus a CP-violating phase for the neutrino mixing matrix, bringing the grand total to 26 parameters. Additionally, if neutrinos turn out to be Majorana particles, so that they are their own antiparticles, two more CP-violating phases need to be specified. Notice that at least 20 of the parameters relate to flavour physics.

Many of the ideas for physics beyond the SM, like supersymmetry and extra dimensions, have been motivated by attempts to reduce the number of its parameters, or understand their origins, or at least to make them seem less unnatural.

2.2 Symmetries of the Standard Model

A symmetry is any transformation that leaves the object being transformed unchanged. Along with the $SU(3) \otimes SU(2) \otimes U(1)$ gauge symmetry, the SM has other symmetries, both continuous and discrete.

2.2.1 Continuous Lorentz symmetries

A continuous Lorentz transformation is one that can be built up of infinitesimal Lorentz transformations. Since every relativistic field theory must be invariant under Lorentz transformations, and since the SM is a relativistic (quantum) field theory, then Lorentz transformations must be a symmetry of the theory. Given a four-component Dirac field ψ, i.e., an object that satisfies the Dirac equation, $(i\hbar\partial\!\!\!/ - m)\,\psi(x) = 0$, the coordinate Lorentz transformation

$$x \to x' = \Lambda x \tag{2.79}$$

induces the following transformation [38] of ψ:

$$\psi(x) \to \psi'(x') = U(\Lambda)\,\psi(x)\,U^{-1}(\Lambda) = \Lambda_{1/2}^{-1}\psi(\Lambda x)\ , \tag{2.80}$$

with U a unitary operator. The Lorentz transformation operator for a Dirac field, $\Lambda_{1/2}$, is given by

$$\Lambda_{1/2} = \exp\left(-\frac{i}{2}\omega\mu\nu S^{\mu\nu}\right) , \tag{2.81}$$

where

$$S^{\mu\nu} = \frac{i}{4}[\gamma^{\mu}, \gamma^{\nu}] \tag{2.82}$$

are the generators of field Lorentz transformations. The generators of boosts are

$$S^{0i} = -\frac{1}{2}\begin{pmatrix} \sigma^i & 0 \\ 0 & -\sigma^i \end{pmatrix} , \quad i = 1, 2, 3 , \tag{2.83}$$

with σ_i the Pauli matrices, and the generators of rotations are

$$S^{ij} = \frac{1}{2}\epsilon^{ijk}\begin{pmatrix} \sigma^k & 0 \\ 0 & \sigma_k \end{pmatrix} . \tag{2.84}$$

A four-component field ψ that transforms under boosts and rotations according to Eqs. (2.83) and (2.84), respectively, is a Dirac spinor. Since the S^{0i} are not Hermitian, the field Lorentz transformation $\Lambda_{1/2}$ is not a unitary transformation.

With the knowledge of how a Dirac field transforms, we can see how some of the bilinears made up of combinations of two Dirac fields and gamma matrices, transform. Let us first explore the transformation of the object $\psi^{\dagger}\psi$:

$$\psi^{\dagger}\psi \to \psi^{\dagger}\Lambda_{1/2}^{\dagger}\Lambda_{1/2}\psi \neq \psi^{\dagger}\psi , \tag{2.85}$$

since $\Lambda_{1/2}^{\dagger} \neq \Lambda_{1/2}^{-1}$. However, if we define the adjoint field as

$$\overline{\psi} \equiv \psi^{\dagger}\gamma^0 , \tag{2.86}$$

it can be proved [38] that it transforms as

$$\overline{\psi} \to \overline{\psi}\Lambda_{1/2}^{-1} . \tag{2.87}$$

We can see then that the bilinear $\overline{\psi}\psi$ transforms as

$$\overline{\psi}\psi \to \overline{\psi}\Lambda_{1/2}^{-1}\Lambda_{1/2}\psi = \overline{\psi}\psi . \tag{2.88}$$

Therefore, $\overline{\psi}\psi$ is a Lorentz scalar.

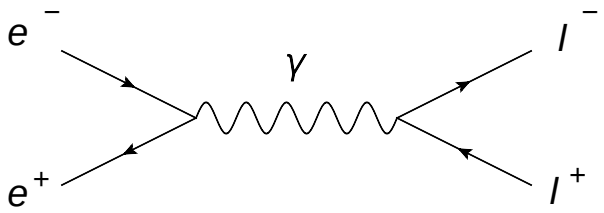

Figure 2.5: Feynmann diagram for photon-mediated e^-e^+ annihilation and l^-l^+ creation.

	name	**number of bilinears of this type**
$\overline{u}u$	scalar	1
$\overline{u}\gamma^\mu u$	vector	4
$\overline{u}\sigma^{\mu\nu}u = \frac{1}{2}\overline{u}\left[\gamma^\mu, \gamma^\nu\right]u$	tensor	6
$\overline{u}\gamma^\mu\gamma^5 u$	pseudo-vector	4
$\overline{u}\gamma^5 u$	pseudo-scalar	1
		16

Table 2.3: Bilinears in the gamma-matrix algebra. Any amplitude written using these bilinears, in any quantum field theory, must be Lorentz-invariant.

On the other hand, the bilinear $\overline{\psi}\gamma^\mu\psi$ is a Lorentz vector. Since [38]

$$\Lambda_{1/2}^{-1}\gamma^\mu\Lambda_{1/2} = \Lambda^\mu_\nu\gamma^\nu \ , \tag{2.89}$$

we find that

$$\overline{\psi}\gamma^\mu\psi \to \overline{\psi}\Lambda_{1/2}^{-1}\gamma^\mu\Lambda_{1/2}\psi = \overline{\psi}\Lambda^\mu_\nu\gamma^\nu\psi \ . \tag{2.90}$$

In a simple example, we will see how a typical SM amplitude is Lorentz-invariant. By writing ψ as

$$\psi\left(x\right) = u\left(\mathbf{p}\right)e^{-ip\cdot x/\hbar} \ , \tag{2.91}$$

we can express the amplitude for the pure-QED process in Figure 2.5 as

$$\mu = ie^2\left[\overline{u}_l\gamma^\alpha v_l\right]\frac{1}{k^2 + i\varepsilon}\left[\overline{v}_e\gamma_\alpha u_e\right] \ . \tag{2.92}$$

The terms in brackets transform as

$$\overline{u}_l\gamma^\alpha v_l \ \to \ \overline{u}_l\gamma^\beta\Lambda^\alpha_\beta v_l \tag{2.93}$$

$$\overline{v}_e\gamma_\alpha u_e \ \to \ \overline{v}_e\gamma_\beta\Lambda^\beta_\alpha u_e \ . \tag{2.94}$$

Hence,

$$\left[\overline{u}_l\gamma^\alpha v_l\right]\left[\overline{v}_e\gamma_\alpha u_e\right] \to \left[\overline{u}_l\gamma^\beta v_l\right]\left[\overline{v}_e\gamma_\beta u_e\right]\Lambda^\alpha_\beta\Lambda^\beta_\alpha \ , \tag{2.95}$$

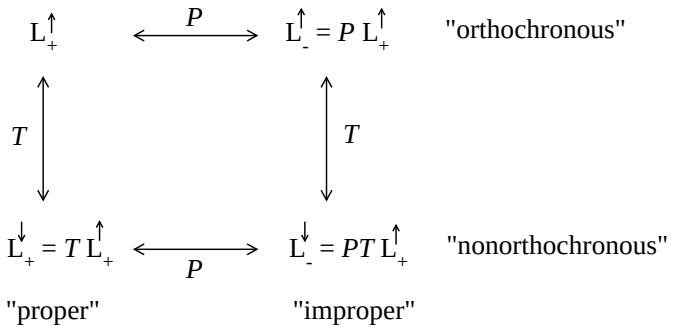

Figure 2.6: The Lorentz group. Adapted from [38].

and, since $\Lambda^{\alpha}_{\beta}\Lambda^{\beta}_{\alpha} = 1$, we find that the amplitude μ is Lorentz-invariant.

Bilinears of the gamma-matrix algebra can be classified according to their Lorentz-transformation properties. Table 2.3 shows a list of the sixteen different bilinears that exist in the SM.

2.2.2 Discrete symmetries

The continuous Lorentz transformations are a symmetry of any relativistic field theory. There are, however, in addition to Lorentz symmetry, two spacetime transformations that are potential symmetries of the Lagrangian: parity, P, and time reversal, T whose action on an arbitrary four-vector $(t, \mathbf{x})$ is given by:

$$\text{parity:} \qquad (t, \mathbf{x}) \xrightarrow{P} (t, -\mathbf{x}) \tag{2.96}$$

$$\text{time reversal:} \qquad (t, \mathbf{x}) \xrightarrow{T} (-t, \mathbf{x}) \ . \tag{2.97}$$

Whereas P changes the handedness of space, T interchanges the past and future light-cones. These transformations cannot be achieved by continuous Lorentz transformations starting from the identity, but they both preserve the metric element $x^2 = t^2 - |\mathbf{x}|^2$. Continuous Lorentz transformations, formally known as the proper, orthochronous Lorentz transformations and denoted by $L^{\uparrow}_{+}$, are only a subset of the full Lorentz group, which is broken down into four sub-groups under the action of the P and T transformations, as seen in Figure 2.6. We will also explore a third, non-spacetime, discrete transformation: charge conjugation, denoted by C, which interchanges particles and anti-particles.

Any relativistic field theory must be invariant under $L^{\uparrow}_{+}$, but they must not necessarily be invariant under P, T, or C. We know that the gravitational, electromagnetic, and strong interactions are symmetric with respect to P, T, and C, and that weak interactions violate C and P separately, but preserve CP and T. However,

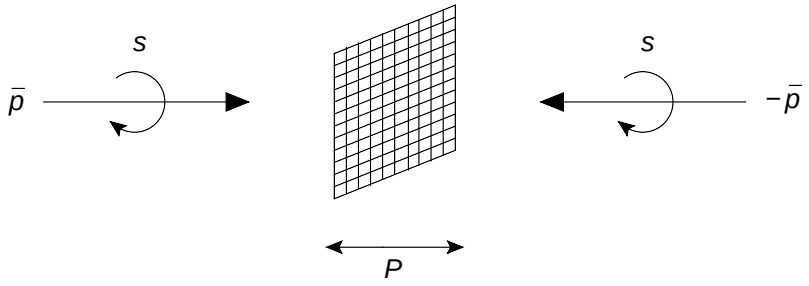

Figure 2.7: Action of the parity operator P on a particle with momentum $\mathbf{p}$ and spin s. While the momentum is flipped, the spin is not affected. Thus, the particle's helicity changes sign.

certain rare processes, so far, observed only in the decay of K and B mesons, violate CP and T. So far, however, observations indicate that CPT is exactly conserved by Nature and therefore the Standard Model has been designed to be invariant under CPT.

Parity

The effect of applying the parity operator is to reverse the direction of the space component, i.e.,

$$\mathbf{x} \to -\mathbf{x} \quad , \quad \mathbf{p} \to -\mathbf{p} \; . \tag{2.98}$$

Since the parity transformation does not affect the particle spins, it effectively changes a particle's helicity, as seen in Figure 2.7.

For concreteness, and following the presentation in [38], let us write general fermion, $\psi(x)$, and anti-fermion operators, $\overline{\psi}(x)$ as the Fourier expansions

$$\psi(x) = \int \frac{d^3p}{(2\pi)^3} \frac{1}{\sqrt{2E_{\mathbf{p}}}} \sum_s \left(a^s_{\mathbf{p}} \; u^s(p) \, e^{-ip\cdot x} + b^{s\dagger}_{\mathbf{p}} \; v^s(p) \, e^{ip\cdot x} \right) \; , \tag{2.99}$$

$$\overline{\psi}(x) = \int \frac{d^3p}{(2\pi)^3} \frac{1}{\sqrt{2E_{\mathbf{p}}}} \sum_s \left(b^s_{\mathbf{p}} \; \overline{v}^s(p) \, e^{-ip\cdot x} + a^{s\dagger}_{\mathbf{p}} \; \overline{u}^s(p) \, e^{ip\cdot x} \right) \; , \tag{2.100}$$

where $a^s_{\mathbf{p}}$, $b^s_{\mathbf{p}}$ are fermion and anti-fermion annihilation operators, respectively, and $a^{s\dagger}_{\mathbf{p}}$, $b^{s\dagger}_{\mathbf{p}}$ are fermion and anti-fermion creation operators, respectively. The sum is over all spin states, s. The creation and operation operators satisfy the canonical anti-conmutation relations

$$\left\{ a^r_{\mathbf{p}}, a^{s\dagger}_{\mathbf{q}} \right\} = \left\{ b^r_{\mathbf{p}}, b^{s\dagger}_{\mathbf{q}} \right\} = (2\pi)^3 \, \delta^{(3)}(\mathbf{p} - \mathbf{q}) \, \delta^{rs} \; , \tag{2.101}$$

and the vacuum $|0\rangle$ is defined by $a^s_{\mathbf{p}}|0\rangle = b^s_{\mathbf{p}}|0\rangle = 0$.

The parity transformation is implemented through the unitary operator P such that

$$Pa^s_{\mathbf{p}}P = \eta_a a^s_{\mathbf{p}} \quad , \qquad Pb^s_{\mathbf{p}}P = \eta_b b^s_{-\mathbf{p}} \ , \tag{2.102}$$

where η_a and η_b are possible phases. We demand that a double application of P leaves the fermion operators unchanged, e.g.,

$$P\left(Pa^s_{\mathbf{p}}P\right)P = a^s_{\mathbf{p}} \ , \tag{2.103}$$

which implies

$$\eta_a^2 = \pm 1 \quad , \qquad \eta_b^2 = \pm 1 \ . \tag{2.104}$$

It is possible (see, e.g., [38]) to prove that

$$P\psi\left(t,\mathbf{x}\right)P = \eta_a\gamma^0\psi\left(t,-\mathbf{x}\right) \quad , \qquad P\overline{\psi}\left(t,\mathbf{x}\right)P = \eta_a^*\overline{\psi}\left(t,-\mathbf{x}\right)\gamma^0 \ . \tag{2.105}$$

With this, we can calculate the action of P on a few of the bilinears:

- scalar:

$$P\overline{\psi}\left(t,\mathbf{x}\right)\psi\left(t,\mathbf{x}\right)P = |\eta_a|^2\overline{\psi}\left(t,-\mathbf{x}\right)\gamma^0\gamma^0\psi\left(t,-\mathbf{x}\right) = \overline{\psi}\left(t,-\mathbf{x}\right)\psi\left(t,-\mathbf{x}\right) \tag{2.106}$$

- vector:

$$P\overline{\psi}\left(t,\mathbf{x}\right)\gamma^\mu\psi\left(t,\mathbf{x}\right)P = \begin{cases} +\overline{\psi}\left(t,-\mathbf{x}\right)\gamma^\mu\psi\left(t,-\mathbf{x}\right) \ , & \mu = 0 \\ -\overline{\psi}\left(t,-\mathbf{x}\right)\gamma^\mu\psi\left(t,-\mathbf{x}\right) \ , & \mu = 1,2,3 \end{cases} \tag{2.107}$$

- pseudo-scalar:

$$Pi\overline{\psi}\left(t,\mathbf{x}\right)\gamma^5\psi\left(t,\mathbf{x}\right)P = -i\overline{\psi}\left(t,-\mathbf{x}\right)\gamma^5\psi\left(t,-\mathbf{x}\right) \tag{2.108}$$

- pseudo-vector:

$$P\overline{\psi}\left(t,\mathbf{x}\right)\gamma^\mu\gamma^5\psi\left(t,\mathbf{x}\right)P = \begin{cases} -\overline{\psi}\left(t,-\mathbf{x}\right)\gamma^\mu\gamma^5\psi\left(t,-\mathbf{x}\right) \ , & \mu = 0 \\ +\overline{\psi}\left(t,-\mathbf{x}\right)\gamma^\mu\gamma^5\psi\left(t,-\mathbf{x}\right) \ , & \mu = 1,2,3 \end{cases} \tag{2.109}$$

We will examine the effects of parity on a pure electromagnetic interaction and on a weak interaction. The basic QED vertex is given by the left Feynmann diagram in Figure 2.8. The initial and final electrons have momenta p and p', respetively, and are represented by the the Dirac spinors $u\left(p\right)$ and $u\left(p'\right)$. The transferred momentum

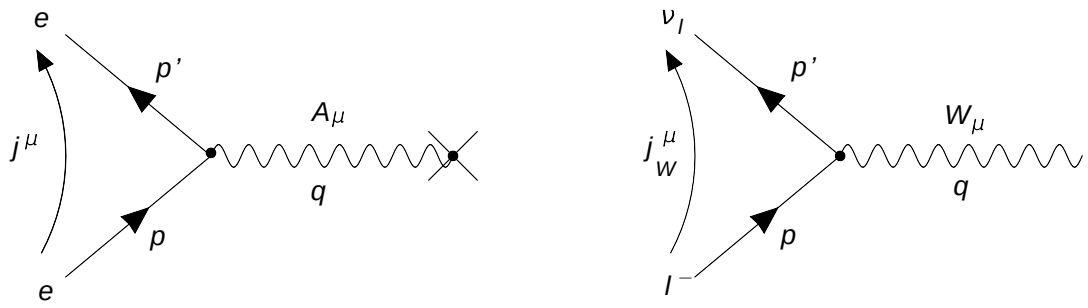

Figure 2.8: *Left:* Basic QED vertex representing electron scattering off an external electromagnetic field. *Right:* One of the vertices in charged-current $\nu_l - l$ scattering, mediated by a W^- weak boson.

$q \equiv p - p'$ and the conserved electromagnetic current is given by (see, e.g., [28,38,39])

$$j^\mu \equiv -ie\overline{u}\left(\mathbf{p}\right)\gamma^\mu u\left(\mathbf{p}'\right) \ , \tag{2.110}$$

and the external field in momentum space, $A_\mu\left(\mathbf{q}\right)$ can be expressed as the Fourier transform of the corresponding field in position space, $A_\mu\left(\mathbf{x}\right)$, i.e.,

$$A_\mu\left(\mathbf{q}\right) = \int d^3x \ e^{-i\mathbf{q}\cdot\mathbf{x}} A_\mu\left(\mathbf{x}\right) \ . \tag{2.111}$$

The amplitude for the process is therefore

$$j^\mu A_\mu = -ie\overline{u}\left(\mathbf{p}\right)\gamma^\mu u\left(\mathbf{p}'\right) A_\mu\left(\mathbf{q}\right) \ . \tag{2.112}$$

Applying the parity operator to this amplitude results in

$$\begin{aligned} Pj^\mu\left(\mathbf{p},\mathbf{p}'\right) A_\mu\left(\mathbf{q}\right) P &= -ie\left[P\overline{u}\left(\mathbf{p}\right)\gamma^0 u\left(\mathbf{p}'\right) A_0\left(\mathbf{q}\right) P - P\overline{u}\left(\mathbf{p}\right)\gamma^i u\left(\mathbf{p}'\right) A_i\left(\mathbf{q}\right) P\right] \\ &= -ie\left[+\overline{u}\left(-\mathbf{p}\right)\gamma^0 u\left(-\mathbf{p}'\right)\right]\left[+A_0\left(-\mathbf{q}\right)\right] \\ &\quad +ie\left[-\overline{u}\left(-\mathbf{p}\right)\gamma^i u\left(-\mathbf{p}'\right)\right]\left[-A_i\left(-\mathbf{q}\right)\right] \\ &= j^\mu\left(-\mathbf{p},-\mathbf{p}'\right) A_\mu\left(-\mathbf{q}\right) \ . \end{aligned} \tag{2.113}$$

Since $j^\mu A_\mu$ and $Pj^\mu A_\mu P$ have the same functional form, but with $\mathbf{p} \to -\mathbf{p}$, $\mathbf{p}' \to -\mathbf{p}'$, and $\mathbf{q} \to -\mathbf{q}$, this amplitude is said to be P-symmetric.

The right Feynmann diagram in Fig. (2.8) represents one vertex of a $\nu_l - l$ charged-current interaction. As in the QED case, the initial particle, the charged lepton, has momentum $\mathbf{p}$ and the final one, the neutrino, has momentum $\mathbf{p}'$. The weab W^- boson is represented by the W_μ field and the conserved charged weak

current is given by [28, 38, 39]

$$j_W^\mu = -ig_W \overline{u}_l(\mathbf{p})\gamma^\mu\left(1-\gamma^5\right)u_\nu(\mathbf{p}') \ , \tag{2.114}$$

where g_W is the coupling constant in the intermediate boson theory of weak interactions [39], and the spinors u_l, u_ν represent the charged lepton and the neutrino, respectively. The amplitude associated to this vertex is therefore given by

$$\begin{aligned} j_W^\mu W_\mu &= -ig_W \overline{u}_l(\mathbf{p})\gamma^\mu\left(1-\gamma^5\right)u_\nu(\mathbf{p}')W_\mu & (2.115)\\ &= -ig_W \overline{u}_l(\mathbf{p})\gamma^\mu u_\nu(\mathbf{p}')W_\mu + ig_W \overline{u}_l(\mathbf{p})\gamma^\mu\gamma_5 u_\nu(\mathbf{p}')W_\mu \ . & (2.116)\end{aligned}$$

Note that the amplitude for this process has a vector-coupling part, reminiscent of the QED coupling, and a pseudo-vector coupling part, characteristic of the weak interaction. The application of the parity transformation results in

$$\begin{aligned} Pj_W^\mu(\mathbf{p},\mathbf{p}')W_\mu(\mathbf{q})P &= -ig_W \overline{u}_l(-\mathbf{p})\gamma^\mu u_\nu(-\mathbf{p}')W_\mu(-\mathbf{q}) \\ &\quad +ig_W\left[-\overline{u}_l(-\mathbf{p})\gamma^0\gamma_5 u_\nu(-\mathbf{p}')\right][W_0(-\mathbf{q})] \\ &\quad -ig_W\left[+\overline{u}_l(-\mathbf{p})\gamma^i\gamma_5 u_\nu(-\mathbf{p}')\right][-W_i(-\mathbf{q})] \\ &= -ig_W \overline{u}_l(\mathbf{p})\gamma^\mu(1+\gamma_5)u_\nu(\mathbf{p}')W_\mu \ . \end{aligned} \tag{2.117}$$

Notice, in the last step, that the sign of γ_5 has been flipped with respect to the original amplitude, Eq. (2.115). To interpret this change, recall the form of the helicity operators in the limit of zero mass, or equivalently in the limit where the particle energy is much larger than its mass:

$$\Pi^\pm \equiv \frac{1}{2}(1\pm\gamma_5) \ . \tag{2.118}$$

The result of applying the positive (negative) helicity operator on a general particle state is a state with positive (negative) helicity, that is, one in which the spin direction is (anti-)parallel to the momentum direction. Using these operators, we can write Eqs. (2.115) and (2.117) as

$$\begin{aligned} j_W^\mu(\mathbf{p},\mathbf{p}')W_\mu(\mathbf{q}) &= -2ig_w \overline{u}_l(\mathbf{p})\gamma^\mu\Pi^- u_\nu(\mathbf{p}')W_\mu(\mathbf{q}) \ , & (2.119)\\ Pj_W^\mu(\mathbf{p},\mathbf{p}')W_\mu(\mathbf{q})W_\mu P &= -2ig_w \overline{u}_l(-\mathbf{p})\gamma^\mu\Pi^+ u_\nu(-\mathbf{p}')W_\mu(-\mathbf{q}) \ . & (2.120)\end{aligned}$$

In other words, the amplitude $j_W^\mu W_\mu$ couples left-handed (negative helicity) particles with the weak boson field, a fact that has been throughly confirmed experiment and that is incorporated in the structure of the SM. On the other hand, after the

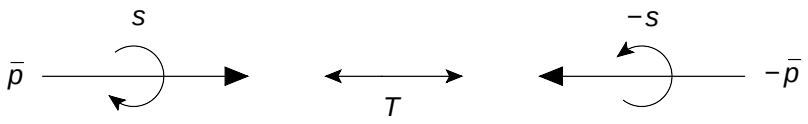

Figure 2.9: Action of the time-reversal operator T on a particle with momentum $\mathbf{p}$ and spin s. Both the momentum and the spin directions are flipped. Therefore, the helicity is preserved.

application of the parity operator, we end up with a situation in which right-handed (positive helicity) particles couple with the weak boson field, a situation which is not observed in Nature. Therefore, weak interactions violate the P symmetry.

Time reversal

The effect of applying the time-reversal operator is to reverse the direction of the tie component, i.e.,

$$t \to -t \quad , \quad x_0 \to -x_0 \quad , \quad p_0 \to -p_0 \ . \tag{2.121}$$

The time-reversal operator, T, is required to reverse the direction of the momentum of the particle and to flip its spin. In terms of the fermion annihilation operators, this means

$$T a^s_{\mathbf{p}} T = a^{-s}_{-\mathbf{p}} \quad , \quad T b^s_{\mathbf{p}} T = b^{-s}_{-\mathbf{p}} \ , \tag{2.122}$$

and similar expressions for the creation operators. Therefore, whereas the parity transformation preserves the spin direction, but flips the helicity, the time-reversal transformation flips the spin direction, but preserves the helicity, as shown in Figure 2.9.

Since, in quantum mechanics, the evolution of a system is performed by an evolution operator of the form e^{-iHt}, with H the Hamiltonian of the system, then the T operator should conjugate all complex quantities, namely

$$T z = z^* T \ , \tag{2.123}$$

where z is any c-number. Hence the evolution operator becomes, under the action of T,

$$T e^{-iHt} = e^{iHt} T \ , \tag{2.124}$$

effectively changing the sign of t. Note that there is no unitary operator able to perform such an operation; therefore, T is not unitary. On the other hand, it can be proved (see, e.g., [38]) that the action of T on the fermion fields can be accomplished

by

$$T\psi\left(t,\mathbf{x}\right)T=\left(\gamma^{1}\gamma^{3}\right)\psi\left(-t,\mathbf{x}\right)\quad,\quad T\overline{\psi}\left(t,\mathbf{x}\right)T=\overline{\psi}\left(-t,\mathbf{x}\right)\left(-\gamma^{1}\gamma^{3}\right)\ . \tag{2.125}$$

The action of T on some of the bilinears of the theory is as follows:

- scalar:

$$T\overline{\psi}\left(t,\mathbf{x}\right)\psi\left(t,\mathbf{x}\right)T=+\overline{\psi}\left(-t,\mathbf{x}\right)\psi\left(-t,+\mathbf{x}\right) \tag{2.126}$$

- vector:

$$T\overline{\psi}\left(t,\mathbf{x}\right)\gamma^{\mu}\psi\left(t,\mathbf{x}\right)T=\begin{cases}+\overline{\psi}\left(-t,\mathbf{x}\right)\gamma^{\mu}\psi\left(-t,\mathbf{x}\right)\ , & \mu=0\\ -\overline{\psi}\left(-t,\mathbf{x}\right)\gamma^{\mu}\psi\left(-t,\mathbf{x}\right)\ , & \mu=1,2,3\end{cases} \tag{2.127}$$

- pseudo-scalar:

$$Ti\overline{\psi}\left(t,\mathbf{x}\right)\gamma^{5}\psi\left(t,\mathbf{x}\right)T=-i\overline{\psi}\left(-t,\mathbf{x}\right)\gamma^{5}\psi\left(-t,\mathbf{x}\right) \tag{2.128}$$

- pseudo-vector:

$$T\overline{\psi}\left(t,\mathbf{x}\right)\gamma^{\mu}\gamma^{5}\psi\left(t,\mathbf{x}\right)T=\begin{cases}+\overline{\psi}\left(-t,\mathbf{x}\right)\gamma^{\mu}\gamma^{5}\psi\left(-t,\mathbf{x}\right)\ , & \mu=0\\ -\overline{\psi}\left(-t,\mathbf{x}\right)\gamma^{\mu}\gamma^{5}\psi\left(-t,\mathbf{x}\right)\ , & \mu=1,2,3\end{cases} \tag{2.129}$$

The application of the T operator on the QED amplitude, Eq. (2.112), written in the position space, results in

$$\begin{aligned}Tj^{\mu}\left(x,x'\right)A_{\mu}\left(\mathbf{y}\right)T &= T\left[-ie\overline{t,\mathbf{x}}\gamma^{\mu}\psi\left(t',\mathbf{x}'\right)A_{\mu}\left(\mathbf{y}\right)\right]T\\ &= -ie\overline{\psi}\left(-t,\mathbf{x}\right)\gamma^{0}\psi\left(-t',\mathbf{x}'\right)A_{0}\left(\mathbf{y}\right)\\ &\quad +ie\left[-\overline{\psi}\left(-t,\mathbf{x}\right)\gamma^{i}\psi\left(-t',\mathbf{x}'\right)\right]\left[-A_{0}\left(\mathbf{y}\right)\right]\\ &= -ie\overline{\psi}\left(-t,\mathbf{x}\right)\gamma^{\mu}\psi\left(-t',\mathbf{x}'\right)A_{\mu}\left(\mathbf{y}\right)\ ,\end{aligned} \tag{2.130}$$

where, for the external electromagnetic field in position space, we have used

$$A_{\mu}\left(\mathbf{y}\right)=\int d^{3}q\ e^{i\mathbf{q}\cdot\mathbf{y}}A_{\mu}\left(\mathbf{q}\right)\ . \tag{2.131}$$

Clearly, since the functional for of the QED amplitude is maintained under T (there is only a change $t\rightarrow-t$), it is T-invariant.

Repeating the calculation for the weak interaction amplitude, Eq. (2.115), one

obtains

$$\begin{aligned} T j_W^{\mu}(x,x') W_{\mu}(\mathbf{y}) T &= T\left[-i g_W \overline{\psi}(t,\mathbf{x}) \gamma^{\mu}(1-\gamma_5) \psi(t',\mathbf{x}') W_{\mu}(\mathbf{y})\right] T \\ &= -i g_W \overline{\psi}(-t,\mathbf{x}) \gamma^{\mu}(1-\gamma_5) \psi(-t',\mathbf{x}') W_{\mu}(\mathbf{y}) \end{aligned} \quad (2.132)$$

Therefore, weak interactions are also T-invariant.

Charge conjugation

Charge conjugation takes a fermion with a given spin orientation into an anti-fermion with the same spin orientation, i.e.,

$$C a_{\mathbf{p}}^s C = b_{\mathbf{p}}^s \quad , \quad C b_{\mathbf{p}}^s C = a_{\mathbf{p}}^s \ . \quad (2.133)$$

This operation can be implemented (see, e.g., [38]) by the unitary operator

$$C\psi(x) C = -i\gamma^2 \left(\psi^{\dagger}\right)^T = -i\left(\overline{\psi}\gamma^0\gamma^2\right)^T \quad , \quad C\overline{\psi}(x) C = -i\left(\gamma^0\gamma^2\psi\right)^T \ . \quad (2.134)$$

Denoting by ψ_1 and ψ_2 two different fermions, the effect of charge conjugation on some of the bilinears that can be built from them is:

- scalar:
$$C\overline{\psi}_1\psi_2 C = +\overline{\psi}_2\psi_1 \quad (2.135)$$
- vector:
$$C\overline{\psi}_1\gamma^{\mu}\psi_2 C = -\overline{\psi}_2\gamma^{\mu}\psi_1 \quad (2.136)$$
- pseudo-scalar:
$$Ci\overline{\psi}_1\gamma^5\psi_2 C = +i\overline{\psi}_2\gamma^5\psi_1 \quad (2.137)$$
- pseudo-vector:
$$C\overline{\psi}_1\gamma^{\mu}\gamma^5\psi_2 C = +\overline{\psi}_2\gamma^{\mu}\gamma^5\psi_1 \quad (2.138)$$

The application of charge conjugation on the QED amplitude, Eq. (2.112), yields

$$C j^{\mu} A_{\mu} C = C\left[-ie\overline{u}_1\gamma^{\mu}u_2 A_{\mu}\right] C = -ie\left[-\overline{u}_2\gamma^{\mu}u_1\right] C A_{\mu} C \ . \quad (2.139)$$

We require that $C A_{\mu} C = -A_{\mu}$ in order for the amplitude to be C-symmetric. With this,

$$C j^{\mu} A_{\mu} C = j_{1\leftrightarrow 2}^{\mu} A_{\mu} \ , \quad (2.140)$$

and the amplitude is invariant under C.

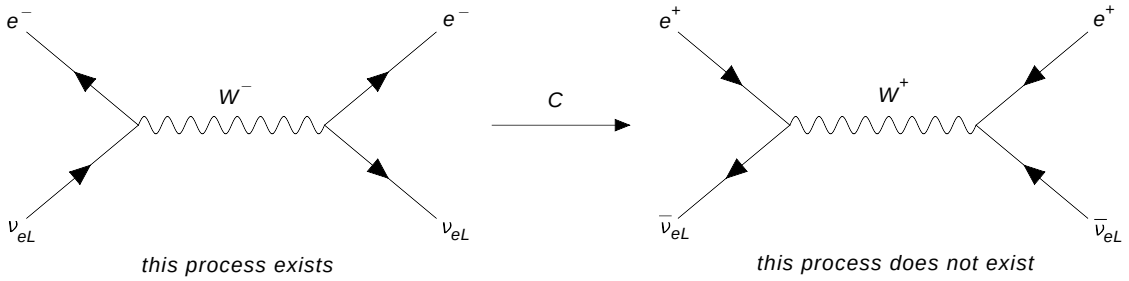

Figure 2.10: Applying charge conjugation on the ampltude for $\nu_e - e$ scattering (*left plot*), where the neutrino is left-handed (ν_{eL}), yields the amplitude for $\overline{\nu}_e$- $- e$ scattering (*right plot*), with a left-handed anti-neutrino ($\overline{nu}_{eL}$). Since all anti-neutrinos in the Standard Model are right-handed, the C-symmetric process of $\nu_e - e$ scattering does not exist and weak interactions are not C-invariant.

In addition, charge conjugation applied on the weak amplitude, Eq. (2.115), results in

$$\begin{aligned} C j^{\mu}_{W} A_{\mu} C &= C\left[-ig_W \overline{u}_1 \gamma^{\mu}\left(1-\gamma_5\right) u_2 W_{\mu}\right] C \\ &= -ig_W \overline{u}_2 \gamma^{\mu} u_1 W_{\mu} + ig_W \left[\overline{u}_2 \gamma^{\mu} \gamma_5 u_1\right]\left[-W_{\mu}\right] \\ &= -ig_W \overline{u}_2 \gamma^{\mu}\left(1+\gamma_5\right) u_1 W_{\mu} \ . \end{aligned} \tag{2.141}$$

Because of the sign change of γ_5, the weak amplitude is not C-invariant.

Let us consider, as an example, neutrino-electron scattering. As we mentioned earlier, only left-handed (negative helicity) neutrinos couple with other particles in the SM. The left Feynmann diagram in Figure 2.10 features said scattering process; we have denoted the neutrinos by ν_{eL}. Applying the charge conjugation operator to this process yields the diagram on the right, representing the scattering of left-handed anti-neutrinos, $\overline{\nu}_{eL}$, and positrons. Within the SM, however, anti-neutrinos are always right-handed; therefore, the process represented by the diagram on the right does not occur in the SM. In other words, weak interactions are not C-invariant.

CP and CPT

Since QED is invariant under both C and P transformations, it follows that it is also CP-invariant. On the other hand, weak processes are neither C- nor P-invariant, but they are CP-invariant as well. We know, from Eq. (2.141), the result of charge conjugation on $j^{\mu}_{W} W_{\mu}$; applying a parity transformation to this, we obtain

$$P\left(C j^{\mu}_{W} W_{\mu} C\right) P = -ig_W \overline{u}_2 \gamma^{\mu}\left(1-\gamma_5\right) u_1 W_{\mu} \ , \tag{2.142}$$

	$\overline{\psi}\psi$	$i\overline{\psi}\gamma^5\psi$	$\overline{\psi}\gamma^\mu\psi$	$\overline{\psi}\gamma^\mu\gamma^5\psi$	$\overline{\psi}\sigma^{\mu\nu}\psi$	∂_μ
P	$+1$	-1	$(-1)^\mu$	$-(-1)^\mu$	$(-1)^\mu(-1)^\nu$	$(-1)^\mu$
T	$+1$	-1	$(-1)^\mu$	$(-1)^\mu$	$-(-1)^\mu(-1)^\nu$	$-(-1)^\mu$
C	$+1$	$+1$	-1	$+1$	-1	$+1$
CPT	$+1$	$+1$	-1	-1	$+1$	-1

Table 2.4: Effect of the P, T, C, and CPT operators on the bilinears of the Standard Model.

which, unlike $Cj^\mu_W W_\mu C$, has the correct sign for γ_5. Therefore, weak processes are mostly CP-conserving.

The exception exists in the decays of certain neutral mesons, namely the K and B mesons, in which CP is seen to be violated. A complete treatment of CP violation lies outside the focus of the current work, but the interested reader is referred to the introductory material in [40–42]. It should be mentioned, however, that T violation is assumed to be violated as well in such processes, in such a way that CPT is so far assumed to be an exact symmetry of Nature.

To conclude the section on discrete symmetries of the SM, we present in Table 2.4 a summary of the effect of the operators P, T, C, and CPT on the different bilinears. Each term in the SM Lagrangian consists of one of the bilinears, coupled to a field, or accompanied by a numerical coefficient (say, a mass). In constructing each term, care must be taken that the CPT properties of the bilinear and of the field are such that the resulting term is invariant under CPT transformations and, therefore, that the whole Lagrangian is as well.

2.3 Massive neutrinos

2.3.1 Dirac masses

In the minimal SM, neutrinos are massless, i.e., their Yukawa coupling constants are zero. However, by introducing a right-handed neutrinos in the lepton-Higgs Yukawa sector, Eq. (2.32), we can make neutrinos massless. Denoting the left- and right-handed lepton multiplets, respectively by

$$L_l = \begin{pmatrix} \nu_l \\ l_l \end{pmatrix}_L \quad , \quad R_l = (l)_R \quad , \quad R_{\nu_l} = (\nu_l)_R \ , \tag{2.143}$$

with $l = e, \mu, \tau$ and $\nu_l = \nu_e, \nu_\mu, \nu_\tau$, we can write the new, modified, Yukawa Lagrangian as

$$\mathcal{L}'_{\text{Yukawa}} = -G_l \left[\overline{L}_l R_l \Phi + \Phi^\dagger \overline{R}_l L_l\right] - G_{\nu_l} \left[\overline{L}_l R_{\nu_l} \tilde{\Phi} + \tilde{\Phi}^\dagger \overline{R}_{\nu_l} L_l\right] \ , \tag{2.144}$$

with the Higgs field, in an arbitrary gauge, represented as

$$\Phi(x) = \begin{pmatrix} \phi_a(x) \\ \phi_b(x) \end{pmatrix} \ , \quad \tilde{\Phi}(x) = \begin{pmatrix} \phi_b^*(x) \\ -\phi_a^*(x) \end{pmatrix} \ . \tag{2.145}$$

In the unitary gauge, Eq. (2.45), the Higgs field is

$$\Phi(x) = \frac{1}{\sqrt{2}} \begin{pmatrix} 0 \\ v + \sigma(x) \end{pmatrix} \ , \quad \tilde{\Phi} = \frac{1}{\sqrt{2}} \begin{pmatrix} v + \sigma(x) \\ 0 \end{pmatrix} \ . \tag{2.146}$$

Recalling that

$$\psi_L \equiv P_L \psi \equiv \frac{1}{2}(1 - \gamma_5)\psi \ , \quad \psi_R \equiv P_R \psi \equiv \frac{1}{2}(1 + \gamma_5)\psi \ , \tag{2.147}$$

the Yukawa Lagrangian becomes, in the unitary gauge,

$$\begin{aligned} \mathcal{L}'_{\text{Yukawa}} \ = \ & -m_l \overline{l} l - m_{\nu_l} \overline{\nu}_l \nu_l \\ & -\frac{1}{v} m_l \overline{l} l \sigma - \frac{1}{v} m_{\nu_l} \overline{\nu}_l \nu_l \sigma \ , \end{aligned} \tag{2.148}$$

where

$$m_l = v G_l / \sqrt{2} \ , \quad m_{\nu_l} = v G_{\nu_l} / \sqrt{2} \ . \tag{2.149}$$

The first line of Eq. (2.148) contains the mass terms for the charged lepton and the neutrino, with respective masses m_l and m_{ν_l} given by Eq. (2.149). The second line contains interaction terms between the two fermions and the Higgs boson, σ.

The Lagrangian describing neutrino interactions can therefore written as

$$\mathcal{L}^\nu = \overline{\nu}_l \left(i\partial\!\!\!/ - m_{\nu_l}\right) \nu_l + \mathcal{L}^\nu_{\text{I}} \ , \tag{2.150}$$

where $\mathcal{L}^\nu_{\text{I}}$ contains interactions terms between the neutrino and other particles of the SM, e.g.,

$$\mathcal{L}^\nu_{\text{I}} \supset = -\frac{g}{2\sqrt{2}} \overline{\nu}_l \gamma^\mu (1 - \gamma_5) l W_\mu - \frac{g}{4\cos(\theta_W)} \overline{\nu}_l \gamma^\mu (1 - \gamma_5) \nu_l Z_\mu - \frac{1}{v} m_{\nu_l} \overline{\nu}_l \nu_l \sigma \ . \tag{2.151}$$

An interesting generalisation (see, e.g., [39]) is to replace the second bracketed

term in Eq. (2.144) by

$$\mathcal{L}''_{\text{Yukawa},\nu} = -G_{\nu_l\nu_{l'}}\overline{L}_{l'}R_{\nu_{l'}}\tilde{\Phi} - G^*_{\nu_l\nu_{l'}}\tilde{\Phi}^\dagger\overline{R}_{\nu_l}L_{l'}\tilde{\Phi}\ , \tag{2.152}$$

where G is now a Hermitian coupling matrix known as a "Yukawa matrix". Let U be the unitary matrix that diagonalises the Yukawa matrix, i.e.,

$$\left(UGU^\dagger\right)_{ij} = \lambda_i\delta_{ij}\ , \tag{2.153}$$

and define a second basis of neutrino states through

$$\nu_i = \sum_l U_{jl}\nu_l\ . \tag{2.154}$$

On account of the unitarity of U, we can invert this relation to yield

$$\nu_l = \sum_j U^*_{jl}\nu_j\ . \tag{2.155}$$

Replacing Eq. (2.155) in Eq. (2.152), we obtain, in the unitary gauge,

$$\begin{aligned}
\mathcal{L}''_{\text{Yukawa},\nu} &= -\frac{(\nu+\sigma)}{2\sqrt{2}}\left[G_{\nu_{l'}\nu_l}\left(\sum_j U_{jl'}\overline{\nu}_j\right)(1+\gamma_5)\left(\sum_k U^*_{kl}\nu_k\right)\right.\\
&\qquad\left. + G^*_{\nu_{l'}\nu_l}\left(\sum_k U_{kl}\overline{\nu}_k\right)(1-\gamma_5)\left(\sum_j U^*_{jl'}\nu_j\right)\right]\\
&= -\frac{(\nu+\sigma)}{2\sqrt{2}}\left[\sum_{j,k}\left(U_{jl'}G_{\nu_{l'}\nu_l}U^*_{kl}\right)\overline{\nu}_j\,(1+\gamma_5)\,\nu_k\right.\\
&\qquad\left. + \sum_{j,k}\left(U_{jl'}G_{\nu_{l'}\nu_l}U^*_{kl}\right)^*\overline{\nu}_k\,(1-\gamma_5)\,\nu_j\right]\\
&= -\frac{(\nu+\sigma)}{2\sqrt{2}}\left[\sum_{j,k}\lambda_j\delta_{jk}\overline{\nu}_j\,(1+\gamma_5)\,\nu_k + \sum_{j,k}\lambda_k\delta_{jk}\overline{\nu}_k\,(1-\gamma_5)\,\nu_j\right]\\
&= -\sum_j\frac{-1}{\sqrt{2}}\lambda_j\overline{\nu}_j\nu_j\,(\nu+\sigma)\ ,
\end{aligned} \tag{2.156}$$

where we have used the fact that the eigenvalues of any Hermitian matrix, like G, are real. Defining the masses of the eigenstates ν_j as

$$m_j = \lambda_j v/\sqrt{2}\ , \tag{2.157}$$

we can finally write

$$\mathcal{L}''_{\text{Yukawa},\nu} = \sum_j -m_j \overline{\nu}_j \nu_j - \frac{1}{v} m_j \overline{\nu}_j \nu_j \sigma \ . \tag{2.158}$$

This generalisation of the neutrino sector naturally incorporates the idea that a neutrino of a certain flavour is a linear combination of the different neutrino mass eigenstates, and that they are connected by means of a unitary transformation U. The Yukawa Lagrangian in its final form, Eq. (2.158), is written in the mass basis, opposite to Eq. (2.150), where it is written in the flavour basis. In Chapter 4, we will introduce neutrino oscillations, which is based precisely on a generalisation of the type presented here.

2.3.2 Majorana neutrinos

The Dirac equation for an arbitrary fermion field ψ of mass m is

$$(i\gamma^\mu \partial_\mu - m)\,\psi = 0 \ . \tag{2.159}$$

Expressing ψ as a combination of two chiral fields, one with negative helicity, or "left-handed", ψ_L, and the other with positive helicity, or "right-handed", ψ_R, the Dirac equation, Eq. (2.159), can be separated into the system of equations

$$i\partial\!\!\!/ \psi_L = m\psi_R \ , \tag{2.160}$$

$$i\partial\!\!\!/ \psi_R = m\psi_L \ , \tag{2.161}$$

which are coupled through the parameter m. For a massless fermion, this reduces to

$$i\partial\!\!\!/ \psi_L = 0 \ , \tag{2.162}$$

$$i\partial\!\!\!/ \psi_R = 0 \ . \tag{2.163}$$

Eqs. (2.162) and (2.163) are called the *Weyl equations*, and the chiral fields ψ_L and ψ_R are *Weyl spinors*, each of which has only two independent components.

In the SM, massless neutrinos are described the left-handed Weyl spinors. This is an example of the fact that a two-component spinor is sufficient to describe a massless fermion. In 1937, however, E. Majorana found that a four-component spinor is not necessary to describe a massive particle, but rather that a Weyl spinor can be used also in this case (provided, as we will see later, that the particle is

electrically neutral). At the core of this lies the realisation that ψ_L and ψ_R need not be independent. They still have, however, to conform to Eqs. (2.160) and (2.161). Hence, these two equations must be two different ways of describing the same field, say, ψ_L.

To show this, we will obtain Eq. (2.160) from Eq. (2.161). In order to do this, we take the Hermitian conjugate of Eq. (2.161) and multiply by γ^0 on the right, i.e.,

$$-i\partial_\mu \psi_R^\dagger \gamma^{\mu\dagger}\gamma^0 = m\overline{\psi}_L \ , \tag{2.164}$$

where, as usual, $\overline{\psi} \equiv \psi^\dagger\gamma^0$. Using the identity $\gamma^{\mu\tau} = \gamma^0\gamma^\mu\gamma^0$ (see, e.g., [39]), we find

$$i\partial_\mu \overline{\psi}_R \gamma^\mu = m\overline{\psi}_L \ . \tag{2.165}$$

Before continuing, note that, under charge conjugation [43], the fermion field transforms as

$$\psi \xrightarrow{C} \psi^C \equiv \xi C\overline{\psi}^T = -\xi_C\gamma^0 C\psi^* \ , \tag{2.166}$$

$$\overline{\psi} \xrightarrow{C} \overline{\psi^C} \equiv -\xi^*\psi^T C^\dagger \ , \tag{2.167}$$

where ξ is an arbitrary phase factor such that $|\xi|^2 = 1$. Three properties of the C operator which we will use are:

$$C\gamma_\mu^T C^{-1} = -\gamma_\mu \ , \tag{2.168}$$

$$C^\dagger = C^{-1} \ , \tag{2.169}$$

$$C^T = -C \ . \tag{2.170}$$

In order to make the structure of Eq. (2.165) similar to that of Eq. (2.160), we now need to take the transpose of Eq. (2.165) and multiply the result on the left by the charge conjugation operator C. Doing this and applying the property in Eq. (2.168) yields

$$i\gamma^\mu\partial_\mu C\overline{\psi}_R^T = mC\overline{\psi}_L^T \ , \tag{2.171}$$

which is identical to the Weyl equation Eq. (2.160) if we set

$$\psi_R = \xi C\overline{\psi}_L^T \ . \tag{2.172}$$

Eq. (2.172) is the Majorana relation between the left-handed field ψ_L and the right-handed[4] field ψ_R.

[4]The proof of the right-handedness of ψ_R can be found in [43].

From Eqs. (2.160) and (2.172), we obtain the Majorana equation for the chiral field ψ_L:

$$i\partial\!\!\!/\psi_L = m\xi C\overline{\psi}_L^T \ . \tag{2.173}$$

By a suitable rephasing of the field, i.e.,

$$\psi_L \to \xi^{1/2}\psi_L \ , \tag{2.174}$$

we can hide the arbitrary phase ξ, so that Eq. (2.173) becomes simply

$$i\partial\!\!\!/\psi_L = mC\overline{\psi}_L^T \ . \tag{2.175}$$

For the full fermion field $\psi = \psi_L + \psi_R$, this translates into

$$\psi = \psi_L + \psi_R = \psi_L + C\overline{\psi}_L^T \ , \tag{2.176}$$

and, therefore,

$$\psi = C\overline{\psi}^T \ . \tag{2.177}$$

Choosing the charge parity of the chiral field ψ_L to be equal to unity, i.e., making $\xi = 1$, we can write

$$\psi_L^C = C\overline{\psi}_L^T \ . \tag{2.178}$$

This implies that

$$\psi = \psi_L + \psi_L^C \ , \tag{2.179}$$

and, so,

$$\psi = \psi^C \ . \tag{2.180}$$

Eq. (2.180) implies the equality of particles and antiparticles. Therefore, only neutral fermions can be described by a Majorana field. This is also evidenced in the fact that the electromagnetic current, $j^\mu \equiv q\overline{\psi}\gamma^\mu\psi$, with q the electric charge, is identically zero:

$$\overline{\psi}\gamma^\mu\psi = \overline{\psi^C}\gamma^\mu\psi^C = -\psi^T C^\dagger\gamma^\mu C\overline{\psi}^T = \overline{\psi}C\gamma^{\mu T}C^\dagger\psi = -\overline{\psi}\gamma^\mu\psi = 0 \ . \tag{2.181}$$

In the SM, the only elementary fermion that is neutral is the neutrino.

The Majorana theory is simpler and more economical than the Dirac theory; in fact, neutrinos are Majorana particles in most theories beyond the SM. The Dirac and Majorana descriptions differ in their phenomenological consequences only if the neutrino is massive, a fact that we now know to be true from neutrino oscillation experiments (see Chapter 4). In massless Dirac theory, the chiral fields $\nu_L \equiv \psi_L$

and $\nu_R \equiv \psi_R$ obey the coupled Weyl equations. The same is true in massless Majorana theory, buy here ν_L and ν_R are not independent. In the massless limit, since ν_L follows Eq. (2.162) in both the Dirac and Majorana descriptions, the right-handed chiral field ν_R is irrelevant for neutrino interactions, i.e., the descriptions are effectively equivalent.

Therefore, in order to distinguish between the two of them, we need to measure effects related to the neutrino mass. The mass effect must not be of a kinematic nature, since kinematic effects are the same for Dirac and Majorana neutrinos. Indeed, neutrino oscillations are not affected by the Dirac or Majorana nature of neutrinos. Currently, the most promising measurement where the nature of the neutrino might be revealed is neutrinoless double beta decay [44, 45].

2.3.3 Majorana mass terms

A Majorana mass term is generated by a Lagrangian mass term with a chiral fermion alone. Since neutrinos are left-handed, we will use ν_L. For simplicity, we will consider only one neutrino flavour.

For a Dirac neutrino field $\nu = \nu_L + \nu_R$, we can build the mass term

$$\mathcal{L}^{\mathrm{D}}_{\mathrm{mass}} = -m\overline{\nu}\nu = -m\left(\overline{\nu}_R\nu_L + \overline{\nu}_L\nu_R\right) = -m\overline{\nu}_R\nu_L + \mathrm{H.c.} \tag{2.182}$$

The terms proportional to $\overline{\nu}_L\nu_L$ and $\overline{\nu}_R\nu_R$ do not appear, since $P_R\nu_L = 0$ and

$$\overline{\nu}_L\nu_L = \nu_L^\dagger\gamma^0\nu_L = \nu_L^\dagger\gamma^0 P_L\nu_L = \nu_L^\dagger P_R\gamma^0\nu_L = \left(P_R\nu_L\right)^\dagger\gamma^0\nu_L = 0\ , \tag{2.183}$$

and similarly for $\overline{\nu}_R\nu_R$ (for which $P_L\nu_R = 0$ is used).

The terms $\overline{\nu}_R\nu_L$ and $\overline{\nu}_L\nu_R$ are Lorentz scalars. If we wish to write a Majorana mass term using only ν_L, we need to find a right-handed function of ν_L that transforms as ν_L under Lorentz transformations and that can be substituted in place of ν_R. Such a function is precisely the charge-conjugated field

$$\nu_L^C = C\overline{\nu}_L^T\ , \tag{2.184}$$

where, again, we have taken the arbitrary phase $\xi = 1$. The Majorana mass term is therefore given by

$$\mathcal{L}^{\mathrm{M}}_{\mathrm{mass}} = -\frac{1}{2}m\overline{\nu_L^C}\nu_L + \mathrm{H.c.} \tag{2.185}$$

The full Majorana Lagrangian, containing the kinetic terms for ν_L and ν_L^C, and the

mass terms in Eq. (2.185), is

$$\mathcal{L}^{\mathrm{M}} = \frac{1}{2}\left[\overline{\nu}_L i \overleftrightarrow{\partial} \nu_L + \overline{\nu_L^C} i \overleftrightarrow{\partial} \nu_L^C - m\left(\overline{\nu_L^C}\nu_L + \overline{\nu}_L \nu_L^C\right)\right] . \tag{2.186}$$

The factor 1/2 is introduced to avoid double counting on account of the fact that ν_L and ν_L^C are not independent.

Since

$$\overline{\nu_L^C} = \left(C\overline{\nu}_L^T\right)^\dagger \gamma^0 = \nu_L^T \left(\gamma^0\right)^T C^\dagger \gamma^0 = -\nu_L^T C \ , \tag{2.187}$$

we can write the Majorana Lagrangian also as

$$\mathcal{L}^{\mathrm{M}} = \frac{1}{2}\left[\overline{\nu}_L i \overleftrightarrow{\partial} \nu_L + \nu_L^T i \overleftrightarrow{\partial}^T \overline{\nu}_L^T - m\left(-\nu_L^T C^\dagger \nu_L + \overline{\nu}_L C \overline{\nu}_L^T\right)\right] . \tag{2.188}$$

With the Lagrangian in this form, we can find the Euler-Lagrange equation,

$$\partial_\mu \frac{\partial \mathcal{L}^{\mathrm{M}}}{\partial\left(\partial_\mu \overline{\nu}_L\right)} - \frac{\partial \mathcal{L}^{\mathrm{M}}}{\partial \overline{\nu}_L} = 0 \ . \tag{2.189}$$

Seeing that

$$\frac{\partial \mathcal{L}^{\mathrm{M}}}{\partial\left(\partial_\mu \overline{\nu}_L\right)} = -\frac{1}{2} i\gamma^\mu \nu_L \ , \tag{2.190}$$

$$\frac{\partial \mathcal{L}^{\mathrm{M}}}{\partial \overline{\nu}_L} = \frac{1}{2} i\gamma^\mu \nu_L - mC\overline{\nu}_L^T \ , \tag{2.191}$$

Eq. (2.189) becomes

$$i\partial\!\!\!/ \nu_L = mC\overline{\nu}_L^T \ , \tag{2.192}$$

which is just the Weyl equation, Eq. (2.175), that had to be satisfied.

By writing

$$\nu = \nu_L + \nu_L^C \ , \tag{2.193}$$

implying $\nu^C = \nu$, the Majorana Lagrangian in Eq. (2.188) can be simplified to

$$\mathcal{L}^{\mathrm{M}} = \frac{1}{2}\overline{\nu}\left(i \overleftrightarrow{\partial} - m\right)\nu \ . \tag{2.194}$$

The factor 1/2 distinguishes the Majorana from the Dirac Lagrangian. A more convenient form of the Majorana Lagrangian, however, is given by [43]

$$\mathcal{L}^{\mathrm{M}} = \overline{\nu}_L i \overleftrightarrow{\partial} \nu_L - \frac{m}{2}\left(-\nu_L^T C^\dagger \nu_L + \overline{\nu}_L C \overline{\nu}_L^T\right) \ , \tag{2.195}$$

in which the kinetic term has the same form as that of a massless neutrino in the

SM. The remaining Majorana mass terms represent effects beyond the SM.

2.3.4 Dirac-Majorana mass terms

The chiral fields ν_L and ν_R are the building blocks of the neutrino Lagrangian. We know that ν_L exists: it is present in the SM and enters in the charged-current weak interaction Lagrangian. We dow not know if ν_R exists, but it is allowed by the symmetries of the SM.

If only ν_L exists, the only mass term allowed is the Majorana mass term

$$\mathcal{L}^{L}_{\text{mass}} = \frac{1}{2} m_L \nu_L^T C^\dagger \nu_L + \text{H.c.} \,, \tag{2.196}$$

and the neutrino is a Majorana particle. If ν_R also exists, the Dirac mass term

$$\mathcal{L}^{\text{D}}_{\text{mass}} = -m_D \overline{\nu}_R \nu_L + \text{H.c.} \tag{2.197}$$

is allowed, and implies that the neutrino is a Dirac particle. However, in addition to the Dirac mass term, Eq. (2.197), the neutrino Lagrangian can also contain the Majorana mass term for ν_L, Eq. (2.196), and the Majorana mass term

$$\mathcal{L}^{R}_{\text{mass}} = \frac{1}{2} m_R \nu_R^T C^\dagger \nu_R + \text{H.c.} \,, \tag{2.198}$$

for ν_R.

Hence, in general, it is possible to have Dirac-Majorana mass terms, i.e.,

$$\mathcal{L}^{\text{D+M}}_{\text{mass}} = \mathcal{L}^{\text{D}}_{\text{mass}} + \mathcal{L}^{L}_{\text{mass}} + \mathcal{L}^{R}_{\text{mass}} \,. \tag{2.199}$$

Among all particles in the SM, only neutrinos can have the Majorana mass terms $\mathcal{L}^{L}_{\text{mass}}$ and $\mathcal{L}^{R}_{\text{mass}}$, which introduce physics beyond the SM. The Majorana mass term in Eq. (2.196) for ν_L is not allowed by the SM, since it is not invariant under $SU(2)_L \otimes U(1)_Y$ transformations. The corresponding Majorana mass term for ν_R, Eq. (2.198), is, however, allowed by the symmetries of the SM, since ν_R is a singlet of $SU(3)_C \otimes SU(2)_L \otimes U(1)_Y$. Thus, the Dirac-Majorana mass term in Eq. (2.199) with $m_L = 0$ is allowed within the SM, with the only addition of the right-handed chiral field ν_R.

Let us define the column matrix of left-handed chiral fields

$$N_L = \begin{pmatrix} \nu_L \\ \nu_R^C \end{pmatrix} = \begin{pmatrix} \nu_L \\ C\overline{\nu}_R^T \end{pmatrix} \,. \tag{2.200}$$

Making use of Eq. (2.187), we can write the Dirac-Majorana mass terms in Eq. (2.199) as

$$\mathcal{L}_{\text{mass}}^{\text{D+M}} = \frac{1}{2} N_L^T C^\dagger M N_L + \text{H.c.} \ , \tag{2.201}$$

where the antisymmetric mass matrix is defined as

$$M = \begin{pmatrix} m_L & m_D \\ m_D & m_R \end{pmatrix} \ . \tag{2.202}$$

From the fact that M has non-zero off-diagonal terms, it is clear that the chiral fields ν_L and ν_R do not have a definite mass. Hence, in order to find the massive neutrino fields, it is necessary to diagonalise the mass matrix. This can be done via a unitary transformation of the chiral fields analogous to the one we introduced in Subsection 2.3.1,

$$N_L = U n_L \ , \tag{2.203}$$

where

$$n_L = \begin{pmatrix} \nu_{1L} \\ \nu_{2L} \end{pmatrix} \tag{2.204}$$

is the column matrix of left-handed massive neutrino fields and the unitary matrix U must be such that

$$U^T M U = \begin{pmatrix} m_1 & 0 \\ 0 & m_2 \end{pmatrix} \ , \tag{2.205}$$

with real $m_k \geq 0$ the masses of the massive neutrinos.

Applying the transformation in Eq. (2.203), the Dirac-Majorana mass terms in Eq. (2.201) become

$$\mathcal{L}_{\text{mass}}^{\text{D+M}} = \frac{1}{2} \sum_{k=1,2} m_k \nu_{kL}^T C^\dagger \nu_{kL} + \text{H.c.} = -\frac{1}{2} \sum_{k=1,2} m_k \overline{\nu}_k \nu_k \ , \tag{2.206}$$

where the Majorana massive neutrino field has been defined as

$$\nu_k = \nu_{kL} + \nu_{kL}^C = \nu_{kL} + C \overline{\nu}_{kL}^T \ . \tag{2.207}$$

Thus, we have shown that the existence of a Dirac-Majorana mass term implies that massive neutrinos are Majorana particles, i.e., $\nu_k = \nu_k^C$.

We have seen that in the case of one generation with both left- and right-handed chiral neutrino fields, ν_L and ν_R, the diagonalisation of the most general Dirac-Majorana mass term implies the existence of two massive Majorana neutrino fields, ν_1 and ν_2. Conventionally, ν_L and ν_R^C are referred to as the left-handed fields in the

flavour basis, while ν_1 and ν_2 are known as the fields in the mass basis. The field ν_L is *active*, because ν_L takes part in weak interactions, whereas ν_R is *sterile*, since it is a singlet of the SM gauge symmetries.

The transformation in Eq. (2.203) implies the mixing relations

$$\nu_L = U_{11}\nu_{1L} + U_{12}\nu_{2L} \tag{2.208}$$

$$\nu_R^C = U_{21}\nu_{1L} + U_{22}\nu_{2L} \ , \tag{2.209}$$

so that the active and sterile neutrino fields, ν_L and ν_R, respectively, are linear combinations of the same massive neutrino fields, ν_{1L} and ν_{2L}. Therefore, oscillations between active and sterile states are, in principle, possible, though they have not been observed. Since sterile neutrinos cannot be detected by their charged- or neutral-current weak interactions, their existence could be inferred by measuring the disappearance of active neutrinos, a fact that could be explained by their oscillation into sterile ones.

Chapter 3

The Standard Model Extension

3.1 A simple effective Lagrangian with spontaneous CPT breaking

In this section, we will present a simple model, introduced in [46], of an effective field theory that extends the minimal Standard Model to include spontaneous CPT violation. In doing so, the aim has been to introduce CPT-violating terms without perturbing the usual gauge structure and important properties like renormalisability. In the spirit of the Standard Model Extension which will be introduced in the next section, we assume that the effective four-dimensional action is obtained from a fundamental quantum field theory which satisfies CPT and Poincaré invariance at a higher energy scale M. Motivated by string theory, where spontaneous CPT breaking due to interactions in the Lagrangian may occur, a natural choice for M would the Planck scale, $m_{Pl} \approx 10^{19}$ GeV. We further assume that this fundamental theory undergoes spontaneous CPT and Lorentz-symmetry breaking at a lower energy scale, which yields the effective CPT-violating theory that we will introduce presently.

In this first extension of the Standard Model, we will not include CPT-even terms in the Lagrangian, that is, terms that, while preserving CPT, violate Lorentz symmetry. These, however, are included in the full Standard Model Extension [13]. The present section will contain only CPT-odd terms, i.e., terms that violate both Lorentz and CPT symmetry.

The simplified model considers a single massive Dirac field $\psi(x)$ with Lagrangian density

$$\mathcal{L} = \mathcal{L}_o - \mathcal{L}' \,, \tag{3.1}$$

where

$$\mathcal{L}_o = \frac{1}{2} i\overline{\psi}\gamma^\mu \overleftrightarrow{\partial}_\mu \psi - m\overline{\psi}\psi \tag{3.2}$$

is the free-particle Lagrangian for a fermion ψ of mass m, and $\mathcal{L}'$ contains the CPT-violating terms. Here and in the full Standard Model Extension, we ascribe the C, P, T, and Lorentz properties to ψ as determined by the free-field theory Lagrangian $\mathcal{L}_o$, and these are used to establish the corresponding properties of $\mathcal{L}'$. Seeing as the CPT-violating effects must be small (no CPT violation has been observed so far), in general $\mathcal{L}'$ should be treated perturbatively. In [46], the possibility of re-defining C, P, T, and Lorentz properties that encompass the full Lagrangian $\mathcal{L}$ is considered.

We will not conform to any particular fundamental theory that exhibits spontaneous CPT invariance, like, for instance, string theory. Rather, we will introduce the effects in a general manner: it is only assumed that the spontaneous violation of CPT originates from nonzero expectation values, $\langle T \rangle$, of one or more Lorentz tensors T. Hence, $\mathcal{L}'$ is an effective four-dimensional Lagrangian arising from a fudamental theory that allows for Poincaré-conserving interactions of ψ with T.

Every CPT-breaking contribution to $\mathcal{L}$ must have mass dimension four. Therefore, in the effecive Lagrangian, each combination of fields and derivatives of dimension greater than four must be accompanied by a weighting factor of a negative power $-k$ of at least one mass scale $M \gg m$, with m the natural scale of the effective theory. We can add to $\mathcal{L}'$ possible terms with different suppressions $k = 0, 1, 2, \ldots$. The leading terms with $k \leq 2$ have the form

$$\mathcal{L}' \supset \frac{\lambda}{M^k} \langle T \rangle \cdot \overline{\psi} \Gamma \left(i\partial\right)^k \psi + \text{H.c.} \,, \tag{3.3}$$

where we have omitted Lorentz indices for simplicity. The parameter λ is a dimensionless coupling constant, $(i\partial)^k$ is a four-derivative acting on some combination of the fermion fields, and Γ is some combination of gamma matrices. Evidently, terms with $k \geq 3$ and with more quadratic fermion factors are allowed, but these are further suppressed.

The contributions to $\mathcal{L}'$ are fermion bilinears involving 4×4 spinor matrices that are combinations of the Dirac γ matrices. Out of the 16 basis elements of the gamma-matrix algebra, only those producing CPT-violating bilinears are considered in $\mathcal{L}'$.

For the case $k = 0$, there are two CPT-violating terms, i.e.,

$$\mathcal{L}'_a \equiv a_\mu \overline{\psi}\gamma^\mu\psi \,, \tag{3.4}$$

$$\mathcal{L}'_b \equiv b_\mu \overline{\psi}\gamma_5\gamma^\nu\psi \,, \tag{3.5}$$

whereas for the case $k = 1$, there are three possibilities:

$$\mathcal{L}'_c \equiv \frac{1}{2} i c^\alpha \overline{\psi} \overleftrightarrow{\partial}_\alpha \psi \ , \tag{3.6}$$

$$\mathcal{L}'_d \equiv \frac{1}{2} d^\alpha \overline{\psi} \gamma_5 \overleftrightarrow{\partial}_\alpha \psi \ , \tag{3.7}$$

$$\mathcal{L}'_e \equiv \frac{1}{2} i e^\alpha_{\mu\nu} \overline{\psi} \sigma^{\mu\nu} \overleftrightarrow{\partial}_\alpha \psi \ , \tag{3.8}$$

where $A \overleftrightarrow{\partial}_\mu B \equiv A\partial_\mu B - (\partial_\mu A) B$. The coefficients a_μ, b_μ, c^α, d^α, and $e^\alpha_{\mu\nu}$ must be real on account of their origins in the spontaneous CPT symmetry breaking and of the presumed hermiticity of the fundamental theory [46]. These quantities, which act as effective coupling constants, are combinations of fundamental coupling constants, mass parameters, and coefficients that originate in the decomposition of Γ. Due to their interpretation as effective coupling constants, a_μ, b_μ, c^α, d^α, and $e^\alpha_{\mu\nu}$ are CPT-invariant so that, together with the standard CPT transformation properties of ψ (see Chapter 2), the terms in Eqs. (3.4)–(3.8) break CPT.

Allowing $k = 0$ terms from Eqs. (3.4) and (3.5) into $\mathcal{L}'$ results in

$$\mathcal{L} = \frac{1}{2} i \overline{\psi} \gamma^\mu \overleftrightarrow{\partial}_\mu \psi - a_\mu \overline{\psi} \gamma^\mu \psi - b_\mu \overline{\psi} \gamma_5 \gamma^\mu \psi - m \overline{\psi} \psi \ . \tag{3.9}$$

The associated Euler-Lagrange equation of motion is a generalised Dirac equation:

$$\left(i\gamma^\mu \partial_\mu - a_\mu \gamma^\mu - b_\mu \gamma_5 \gamma^\mu - m \right) \psi = 0 \ , \tag{3.10}$$

and, multiplying this equation by itself with the opposite sign mass, we obtain the generalised Klein-Gordon equation that each spinor component follows, i.e.,

$$\left[(i\partial - a)^2 - b^2 - m^2 + 2i\gamma_5 \sigma^{\mu\nu} b_\mu \left(i\partial_\nu - a_\nu \right) \right] \psi = 0 \ . \tag{3.11}$$

The CPT-violating terms in Eq. (3.9) do not affect the global $U(1)_{\text{em}}$ gauge, so the current $j^\mu = \overline{\psi} \gamma^\mu \psi$ and associated electric charge $Q \equiv \int d^3x j^0$ are still conserved. It is stated in [46] that $\mathcal{L}$ is invariant under translations, as long as the tensor expectation values are taken as constants. Hence, the conserved energy-momentum tensor $\Theta^{\mu\nu}$ has the standard form (see, e.g., [38])

$$\Theta^{\mu\nu} = \frac{1}{2} \overline{\psi} \gamma^\mu \overleftrightarrow{\partial}^\nu \psi \ , \tag{3.12}$$

with

$$\partial_\mu \Theta^{\mu\nu} = 0 \ , \tag{3.13}$$

and a corresponding conserved four-momentum $P^\mu \equiv \int d^3x \Theta^{0\mu}$. The conservation of energy and momentum, however, does not necessarily imply conventional behaviour under boosts or rotations; in particular, the behaviour under Lorentz transformations, i.e., rotations and boosts, will be different due to the CPT-violating contributions.

In special relativity, conventional Lorentz transformations relate observations made in two inertial frames with different orientations and velocities. These are known as "observer Lorentz transformations". Another type of transformation relates the properties of two particles with different spin direction or momentum within a specific inertial frame with a certain orientation. We call these "particle Lorentz transformations". While observer Lorentz transformations amount to coordinate changes, particle Lorentz transformations involve boosts on localised fields and particles (but not on background fields). For free particles under usual circumstances, these two types of transformations are inversely related. Yet a third type of Lorentz transformations boosts all particles and fields, including background ones, simultaneously. They are called (inverse) active Lorentz transformations. For free particles, they coincide with particle Lorentz transformations.

It is relevant to distinguish between observer and particle transformations in the context of the present model, since the CPT-violating terms in Eq. (3.9) can be thought of as arising from constant background fields a_μ and b_μ. Under observer Lorentz transformations, these eight parameters transform as two four-vectors, whereas, under particle Lorentz transformations, they transform as eight scalars. Since they are coupled to currents that transform as four-vectors under both types of transformations, this means that $\mathcal{L}$ still preserves observer Lorentz symmetry, but the particle Lorentz group is partly broken (the terms from $\mathcal{L}_o$ are still invariant under particle Lorentz transformations).

3.2 The Standard Model Extension

Unlike the model in the previous section, where only CPT-odd terms were considered in the context of a single massive fermion field, the Standard Model Extension (SME), introduced in the seminal paper by D. Colladay and V.A. Kostelecký [13], considers Lorentz violating terms, both CPT-odd and CPT-even, in all of the sectors of the minimal $SU(3) \otimes SU(2) \otimes U(1)$ Standard Model: fermion (both leptons and quarks, and three generations for each), gauge, and Higgs sectors. The goal of the SME is to provide a single encompassing theoretical framework with which to describe the numerous and diverse tests of Lorentz and CPT invariance that exist

and that can be performed. Again, the SME, with its Lorentz-violating terms, is assumed to be the low-energy effective limit of a fundamental Lorentz-conserving theory with a higher energy scale, and Lorentz and CPT symmetries are assumed to be spontaneously broken. As stated in [13], in addition to in addition to the desirable features of energy-momentum conservation, observer Lorentz invariance, conventional quantisation of the fields, hermiticity, and the exptected microcausality and positivity of the energy, the SME maintains gauge invariance and power-counting renormalisability.

The SME is built by adding to the SM all possible Lorentz-violating terms that could arise from spontaneous symmetry-breaking, but that preserve the $SU(3) \otimes SU(2) \otimes U(1)$ gauge invariance and power-counting renormalisability. We will denote the left- and right-handed lepton and quark multiplets by

$$L_A = \begin{pmatrix} \nu_A \\ l_A \end{pmatrix}_L , \quad R_A = (l_A)_R , \tag{3.14}$$

$$Q_A = \begin{pmatrix} u_A \\ d_A \end{pmatrix}_L , \quad U_A = (u_A)_R , \quad D_A = (d_A)_R , \tag{3.15}$$

where

$$\psi_L \equiv \frac{1}{2}(1-\gamma_5)\psi , \quad \psi_R \equiv \frac{1}{2}(1+\gamma_5)\psi , \tag{3.16}$$

as usually defined. The index $A = 1, 2, 3$ labels the flavour, such that $l_A \equiv (e, \mu, \tau)$, $\nu_A \equiv (\nu_e, \nu_\mu, \nu_\tau)$, $u_A \equiv (u, c, t)$, and $d_A \equiv (d, s, b)$. The Higgs doublet, ϕ, will be represented in the unitary gauge as

$$\phi = \frac{1}{\sqrt{2}} \begin{pmatrix} 0 \\ r_\phi \end{pmatrix} , \tag{3.17}$$

with ϕ^c the conjugate doublet. The gauge fields associated to the $SU(3)$, $SU(2)$, and $U(1)$ symmetries are denoted by G_μ, W_μ, and B_μ, respectively, with corresponding field strengths $G_{\mu\nu}$, $W_{\mu\nu}$, and $B_{\mu\nu}$ (see, e.g., [28]), the first two of which are Hermitian adjoint matrices, and the latter, a Hermitian singlet. The corresponding coupling constants are g_3, g, and g'. The electromagnetic $U(1)$ charge q and the Weinberg angle θ_W are still defined through $q = g\sin(\theta_W) = g'\cos(\theta_W)$. The covariant derivative is denoted by D_μ and, as before, $A \overset{\leftrightarrow}{\partial_\mu} B \equiv A\partial_\mu B - (\partial_\mu A) B$. Yukawa couplings for leptons, up-type quakrs and down-type quarks are denoted, respectively, by G_L, G_U, and G_D.

Following the presentation in [13], we will first provide the SM terms for the

different particles sectors:

$$\mathcal{L}_{\text{lepton}} = \frac{1}{2} i \overline{L}_A \gamma^\mu \overleftrightarrow{D}_\mu L_A + \frac{1}{2} i \overline{R}_A \gamma^\mu \overleftrightarrow{D}_\mu R_A \ , \tag{3.18}$$

$$\mathcal{L}_{\text{quark}} = \frac{1}{2} i \overline{Q}_A \gamma^\mu \overleftrightarrow{D}_\mu Q_A + \frac{1}{2} i \overline{U}_A \gamma^\mu \overleftrightarrow{D}_\mu U_A + \frac{1}{2} i \overline{D}_A \gamma^\mu \overleftrightarrow{D}_\mu D_A \ , \tag{3.19}$$

$$\mathcal{L}_{\text{Yukawa}} = -\left[(G_L)_{AB} \overline{L}_A \phi R_B + (G_U)_{AB} \overline{Q}_A \phi^c U_B + (G_D)_{AB} \overline{Q}_A \phi D_B \right] + \text{H.c.} \ , \tag{3.20}$$

$$\mathcal{L}_{\text{Higgs}} = (D_\mu \phi)^\dagger D^\mu \phi + \mu^2 \phi^\dagger \phi - \frac{\lambda}{3!} \left(\phi^\dagger \phi \right)^2 \ , \tag{3.21}$$

$$\mathcal{L}_{\text{gauge}} = -\frac{1}{2} \text{Tr} \left(G_{\mu\nu} G^{\mu\nu} \right) - \frac{1}{2} \text{Tr} \left(W_{\mu\nu} W^{\mu\nu} \right) - \frac{1}{4} B_{\mu\nu} B^{\mu\nu} \ . \tag{3.22}$$

The fermion sector of the SME can be divided into CPT-even and CPT-odd Lagrangians:

$$\mathcal{L}^{\text{CPT-even}}_{\text{lepton}} = \frac{1}{2} i \left(c_L \right)_{\mu\nu AB} \overline{L}_A \gamma^\mu \overleftrightarrow{D}^\nu L_B + \frac{1}{2} i \left(c_R \right)_{\mu\nu AB} \overline{R}_A \gamma^\mu \overleftrightarrow{D}^\nu R_B \ , \tag{3.23}$$

$$\mathcal{L}^{\text{CPT-odd}}_{\text{lepton}} = -\left(a_L \right)_{\mu AB} \overline{L}_A \gamma^\mu L_B - \left(a_R \right)_{\mu AB} \overline{R}_A \gamma^\mu R_B \ , \tag{3.24}$$

$$\begin{aligned} \mathcal{L}^{\text{CPT-even}}_{\text{quark}} \ = \ & \frac{1}{2} i \left(c_Q \right)_{\mu\nu AB} \overline{Q}_A \gamma^\mu \overleftrightarrow{D}^\nu Q_B + \frac{1}{2} i \left(c_U \right)_{\mu\nu AB} \overline{U}_A \gamma^\mu \overleftrightarrow{D}^\nu U_B \\ & + \frac{1}{2} i \left(c_D \right)_{\mu\nu AB} \overline{D}_A \gamma^\mu \overleftrightarrow{D}^\nu D_B \ , \end{aligned} \tag{3.25}$$

$$\mathcal{L}^{\text{CPT-odd}}_{\text{quark}} = -\left(a_Q \right)_{\mu AB} \overline{Q}_A \gamma^\mu Q_B - \left(a_U \right)_{\mu AB} \overline{U}_A \gamma^\mu U_B - \left(a_D \right)_{\mu AB} \overline{D}_A \gamma^\mu D_B \ . \tag{3.26}$$

The coupling coefficients $c_{\mu\nu}$ and a_μ are assumed to be Hermitian in generation space, with $c_{\mu\nu}$ dimensionless and a_μ having dimensions of mass. The coefficients $c_{\mu\nu}$ can have both symmetric and antisymmetric parts, but can be assumed to be traceless.

The SME also considers Lorentz-violating terms in the Yukawa sector; the usual gauge structure is maintained, but gamma matrices are introduced. All of the contributions are CPT-even:

$$\begin{aligned} \mathcal{L}^{\text{CPT-even}}_{\text{Yukawa}} \ = \ & -\frac{1}{2} \Big[\left(H_L \right)_{\mu\nu AB} \overline{L}_A \phi \sigma^{\mu\nu} R_B + + \left(H_U \right)_{\mu\nu AB} \overline{Q}_A \phi^c \sigma^{\mu\nu} U_B \\ & + \left(H_D \right)_{\mu\nu AB} \overline{Q}_A \phi \sigma^{\mu\nu} D_B \Big] + \text{H.c.} \end{aligned} \tag{3.27}$$

The coefficients $H_{\mu\nu}$ are dimensionless and antisymmetric, and, like the Yukawa couplings, they are not necessarily Hermitian in generation space.

The Higgs sector receives both a CPT-even and a CPT-odd contribution:

$$\begin{aligned}\mathcal{L}_{\text{Higgs}}^{\text{CPT-even}} &= \frac{1}{2}\left(k_{\phi\phi}\right)^{\mu\nu}\left(D_\mu\phi\right)^\dagger D_\nu\phi + \text{H.c.} \\ &\quad -\frac{1}{2}\left(k_{\phi B}\right)^{\mu\nu}\phi^\dagger\phi B_{\mu\nu} - \frac{1}{2}\left(k_{\phi W}\right)^{\mu\nu}\phi^\dagger W_{\mu\nu}\phi\ , \end{aligned} \tag{3.28}$$

$$\mathcal{L}_{\text{Higgs}}^{\text{CPT-odd}} = i\left(k_\phi\right)^\mu\phi^\dagger D_\mu\phi + \text{H.c.} \tag{3.29}$$

The dimensionless coefficient $k_{\phi\phi}$ in Eq. (3.28) can have symmetric real and antisymmetric imaginary parts. The rest of the coefficients have dimensions of mass and must be real antisymmetric. The coefficient k_ϕ in Eq. (3.29) also has dimensions of mass and can be an arbitrary complex number.

The gauge sector of the SME also has CPT-even and CPT-odd contributions:

$$\begin{aligned}\mathcal{L}_{\text{gauge}}^{\text{CPT-even}} &= -\frac{1}{2}\left(k_G\right)_{\kappa\lambda\mu\nu}\text{Tr}\left(G^{\kappa\lambda}G^{\mu\nu}\right) - \frac{1}{2}\left(k_W\right)_{\kappa\lambda\mu\nu}\text{Tr}\left(W^{\kappa\lambda}W^{\mu\nu}\right) \\ &\quad -\frac{1}{4}\left(k_B\right)_{\kappa\lambda\mu\nu}B^{\kappa\lambda}B^{\mu\nu}\ , \end{aligned} \tag{3.30}$$

$$\begin{aligned}\mathcal{L}_{\text{gauge}}^{\text{CPT-odd}} &= \left(k_3\right)_\kappa\epsilon^{\kappa\lambda\mu\nu}\,\text{Tr}\left(G_\lambda G_{\mu\nu} + \frac{2}{3}ig_3G_\lambda G_\mu G_\nu\right) \\ &\quad + \left(k_2\right)_\kappa\epsilon^{\kappa\lambda\mu\nu}\,\text{Tr}\left(W_\lambda W_{\mu\nu} + \frac{2}{3}igW_\lambda W_\mu W_\nu\right) \\ &\quad + \left(k_1\right)_\kappa\epsilon^{\kappa\lambda\mu\nu}B_\lambda B_{\mu\nu} + \left(k_0\right)_\kappa B^\kappa\ . \end{aligned} \tag{3.31}$$

In Eq. (3.30), the dimensionless coefficients $k_{G,W,B}$ are real. In Eq. (3.31), the coefficients $k_{1,2,3}$ are real and have dimensions of mass, while k_0 is real and has dimensions of mass cubed. According to [13], if any of these CPT-odd terms do indeed appear, they would generate instabilities in the minimal SM. They are associated with negative contributions to the energy and, in addition, the k_0 term would generate a linear instability in the potential. Hence, it would seem desirable that $k_{0,1,2,3}$ are all identically zero. However, radiative corrections (e.g., from the fermion sector) might generate nonzero values. However, it turns out that the structure of the SME is such that no corrections arise, at least to one loop.

Note that field redefinitions are able to eliminate Lorentz-breaking terms [13,46]. Alternatively, some Lorentz-violating terms may be absorbed into others, provided the terms that are being grouped have the same discrete-symmetry properties. The issue of electroweak $SU\left(3\right)\otimes SU\left(2\right)\otimes U\left(1\right)$ symmetry breaking within the SME is briefly examined in [13], but this analysis lies beyond the scope of the current work.

No Lorentz violation has been observed so far, but there are indications of

nonzero values of the SME parameters with weak confidence levels. Ref. [47] contains the latest experimental bounds on the SME Lorentz-violating parameters.

3.2.1 Extended QED

A generalised quantum electrodynamics (QED) including Lorentz-violating terms can be extracted from the SME. Since QED has been tested to high precision in various kinds of experiments, it might be possible to tightly constraing the Lorentz-violating coefficients. A direct way to obtain QED from the full SME is the following [13]. After $SU(2) \otimes U(1)$ symmetry breaking, set to zero the fields G_μ for gluons, $W_\mu^\pm$ and Z_μ^0 for weak bosons, and the Higgs field (but not the Higgs expectation value, since this generates the fermion masses). With this, the only remaining boson is the photon and the only remaining interaction is the electromagnetic one. Since neutrinos are neutral, they decouple and can be discarded. The resulting theory describes the electromagnetic interaction of quarks and charged leptons, including CPT-violating terms inherited from the full SME. Features from the SME are also inherited by the extended QED: $U(1)$ gauge invariance, energy-momentum conservation, observer Lorentz invariance, hermiticity, microcausality, positivity of the energy, and power-counting renormalisability.

Denoting the conventional four-component lepton fields by l_A and their masses by m_A, with $A = 1, 2, 3$ corresponding, respectively, to the electron, muon, and tau, then the standard QED Lagrangian can be written as

$$\mathcal{L}^{\text{QED}}_{\text{lepton-photon}} = \frac{1}{2} i \bar{l}_A \gamma^\mu \overleftrightarrow{D}_\mu l_A - m_A \bar{l}_A l_A - \frac{1}{4} F_{\mu\nu} F^{\mu\nu} \ , \tag{3.32}$$

where $D_\mu \equiv \partial_\mu + iqA_\mu$ and the field strength is defined as usual by $F_{\mu\nu} \equiv \partial_\mu A_\nu - \partial_\nu A_\mu$.

Extended QED inherits both CPT-even and CPT-odd terms from the full SME:

$$\begin{aligned} \mathcal{L}^{\text{CPT-even}}_{\text{lepton}} \quad = \quad & -\frac{1}{2} (H_l)_{\mu\nu AB} \bar{l}_A \sigma^{\mu\nu} l_B + \frac{1}{2} i (c_l)_{\mu\nu AB} \bar{l}_A \gamma^\mu \overleftrightarrow{D}^\nu l_B \\ & + \frac{1}{2} i (d_l)_{\mu\nu AB} \bar{l}_A \gamma_5 \gamma^\mu \overleftrightarrow{D}^\nu l_B \ , \end{aligned} \tag{3.33}$$

$$\mathcal{L}^{\text{CPT-odd}}_{\text{lepton}} = -(a_l)_{\mu AB} \bar{l}_A \gamma^\mu l_B - (b_l)_{\mu AB} \bar{l}_A \gamma_5 \gamma^\mu l_B \ . \tag{3.34}$$

In Eq. (3.33), the coupling coefficients $(H_l)_{\mu\nu AB}$ are antisymmetric in the spacetime indices, Hermitian in generation space, and have dimensions of mass. Their origin is in the coefficients of Eq. (3.27) after electroweak symmetry breaking. The Hermitian dimensionless couplings $(c_l)_{\mu\nu AB}$ and $(d_l)_{\mu\nu AB}$ can be taken traceless; they originate

from Eq. (3.23). The coefficients $(a_l)_{\mu AB}$ and $(b_l)_{\mu AB}$ are Hermitian have dimensions of mass; they originate from Eq. (3.24). As stated in [13], imposing individual lepto-number conservation in $\mathcal{L}^{\text{CPT-even}}_{\text{lepton}}$ and $\mathcal{L}^{\text{CPT-odd}}_{\text{lepton}}$ would render all the coupling coefficients diagonal in flavour space.

The pure-photon sector comprises one CPT-even term and one CPT-odd term:

$$\mathcal{L}^{\text{CPT-even}}_{\text{photon}} = -\frac{1}{4}\left(k_F\right)_{\kappa\lambda\mu\nu} F^{\kappa\lambda}F^{\mu\nu} \ , \tag{3.35}$$

$$\mathcal{L}^{\text{CPT-odd}}_{\text{photon}} = +\frac{1}{2}\left(k_{AF}\right)^{\kappa} \epsilon_{\kappa\lambda\mu\nu}A^{\lambda}F^{\mu\nu} \ . \tag{3.36}$$

The dimensionless couplings $(k_F)_{\kappa\lambda\mu\nu}$ and $(k_{AF})_{\kappa\lambda\mu\nu}$ are real and arise, respectively, from Eqs. (3.30) and (3.31).

Certainly, the extended QED also has a quark sector, which has the same form as Eqs. (3.32), (3.33), and (3.34), but with six quarks replacing the three leptons. Hence, twice the number of Lorentz-violating parameters appear in the quark sector. The extended QED of leptons and photons, however, suffices for certain applications where the initial and final asymptotic states are only leptons and photons, and where weak and atrong interactions are negligible. Examples include the precise measurement of $g-2$ and the decay $\mu \to e\gamma$.

3.2.2 Extended QED with only electrons, positrons, and photons

Another limiting case of SME is extended QED with only electrons, positrones, and photons, which can be directly obtained from the extended QED of leptons and photons by setting the muon and tau fields to zero. Denoting the electron field by ψ and its mass by m_e, the usual QED Lagrangian for electrons and photons is

$$\mathcal{L}^{\text{QED}}_{\text{electron}} = \frac{1}{2}i\overline{\psi}\gamma^{\mu} \overleftrightarrow{D}_{\mu} \psi - m_e\overline{\psi}\psi - \frac{1}{4}F_{\mu\nu}F^{\mu\nu} \ . \tag{3.37}$$

The pure-photon, Lorentz-violating, terms are still given by Eqs. (3.35) and (3.36), but the corresponding electron terms become

$$\begin{aligned}\mathcal{L}^{\text{CPT-even}}_{\text{electron}} \quad = \quad & -\frac{1}{2}H_{\mu\nu}\overline{\psi}\sigma^{\mu\nu}\psi + \frac{1}{2}ic_{\mu\nu}\overline{\psi}\gamma^{\mu} \overleftrightarrow{D}^{\nu} \psi \\ & + \frac{1}{2}id_{\mu\nu}\overline{\psi}\gamma_5\gamma^{\mu} \overleftrightarrow{D}^{\nu} \psi \ ,\end{aligned} \tag{3.38}$$

$$\mathcal{L}^{\text{CPT-odd}}_{\text{electron}} = -a_{\mu}\overline{\psi}\gamma^{\mu}\psi - b_{\mu}\overline{\psi}\gamma_5\gamma^{\mu}\psi \ . \tag{3.39}$$

The real coupling coefficients a, b, c, d, and H are the $(1,1)$-flavour components of the corresponding coefficients in the extended QED of leptons and photons, and so inherit their dimensions and Lorentz-transformation properties. The extended QED model for electrons and photons could also be used to study free composite fermions, such as nucleons, atoms, or ions, after making the necessary replacement of the mass value.

There are other Lorentz-violating terms, not contained in Eqs. (3.35)–(3.39), but that also preserve $U(1)$ symmetry, renormalisability, and that have an origin in spontaneous Lorentz breaking. These terms, all of which are CPT-odd, cannot be obtained by a reduction of the SME:

$$\mathcal{L}_{\text{electron}}^{\text{extra}} = \frac{1}{2} i e_\mu \overline{\psi} \overleftrightarrow{D}^{\mu} \psi - \frac{1}{2} f_\mu \overline{\psi} \gamma_5 \overleftrightarrow{D}^{\mu} \psi + \frac{1}{4} i g_{\lambda\mu\nu} \overline{\psi} \sigma^{\lambda\mu} \overleftrightarrow{D}^{\nu} \psi \,, \tag{3.40}$$

with the couplings e_μ, f_μ, and $g_{\lambda\mu\nu}$ real and dimensionless. These terms are absent from the previous expressions because they are incompatible with the electroweak structure. However, it is possible that nonrenormalisable higher-dimensional operators that are invariant under the $SU(2) \otimes U(1)$ symmetry and involving the Higgs field generate the terms in Eq. (3.40) after the Higgs acquires a v.e.v.

Chapter 4

Neutrino oscillations

The standard mechanism that explains neutrino flavour transitions makes use of two different bases: the basis of neutrino mass eigenstates, which have well-defined masses, and the basis of neutrino interaction states –the flavour basis– which are the ones that take part in weak processes such as W decay. The two bases are connected through a unitary transformation, so that we can write each one of the flavour states $|\nu_\alpha\rangle$ as a linear combination of the mass eigenstates $|\nu_i\rangle$, i.e.,

$$|\nu_\alpha\rangle = \sum_i [U_0]^*_{\alpha i} |\nu_i\rangle \ , \tag{4.1}$$

where the coefficients $[U_0]_{\alpha i}$ are components of the unitary mixing matrix that represents the transformation. The mass eigenstates $|\nu_i\rangle$ are eigenstates of the oscillation Hamiltonian H, i.e.,

$$H|\nu_i\rangle = E_i|\nu_i\rangle \ , \tag{4.2}$$

and satisfy Schrödinger's equation,

$$i\frac{\partial}{\partial t}|\nu_i\rangle = H|\nu_i\rangle \ . \tag{4.3}$$

Taking H as time-independent, then, the mass eigenstates propagate as

$$|\nu_i\,(L)\rangle = e^{-iHL}|\nu_i\rangle = e^{-iE_iL}|\nu_i\rangle \ , \tag{4.4}$$

where we have replaced $L \approx t$ given that neutrinos travel at virtually c.

If the neutrinos propagate in the vacuum, we can write the energy of the i-th mass eigenstates that makes up $|\nu_\alpha\rangle$ as

$$E_i = \sqrt{|\mathbf{p}|^2 + m_i^2} \simeq |\mathbf{p}| + \frac{m_i^2}{2|\mathbf{p}|} \ , \tag{4.5}$$

where we have assumed that all of the mass eigenstates share the same momentum, $|\mathbf{p}|$, and, on account of the relativistic nature of neutrinos, we have obtained the last expression in the limit $m_i \ll |\mathbf{p}|$. Furthermore, because neutrino masses are small, we can approximate $E \approx |\mathbf{p}|$. We can write the Hamiltonian, in the mass basis, as

$$\begin{aligned} H^m &= \operatorname{diag}(E_1, E_2, \ldots) \\ &\simeq \begin{pmatrix} |\mathbf{p}| & & \\ & |\mathbf{p}| & \\ & & \ldots \end{pmatrix} + \begin{pmatrix} \frac{m_1^2}{2E} & & \\ & \frac{m_2^2}{2E} & \\ & & \ldots \end{pmatrix} \to \begin{pmatrix} \frac{m_1^2}{2E} & & \\ & \frac{m_2^2}{2E} & \\ & & \ldots \end{pmatrix} , \end{aligned} \tag{4.6}$$

where we have discarded the part proportional to the identity because it results in a global phase.

The evolved neutrino eigenstate, Eq. (4.4), can thus be written as

$$|\nu_i(L)\rangle = e^{-i|\mathbf{p}|L} e^{-i\frac{m_i^2}{2E}L} |\nu_i\rangle , \tag{4.7}$$

and we can discard the global phase $e^{-i|\mathbf{p}|L}$ because it is common to all the mass eigenstates that make up $|\nu_\alpha\rangle$.

From Eq. (4.1), the evolved state of a neutrino that is created with flavour α is

$$|\nu_\alpha(L)\rangle = \sum_i [U_0]^*_{\alpha i} |\nu_i(L)\rangle = \sum_i [U_0]^*_{\alpha i} e^{-i\frac{m_i^2}{2E}L} |\nu_i\rangle . \tag{4.8}$$

Now we invert Eq. (4.1) to yield

$$|\nu_i\rangle = \sum_\beta [U_0]_{\beta i} |\nu_\beta\rangle , \tag{4.9}$$

where the sum is over all neutrino flavours. Replacing this in Eq. (4.8) results in

$$|\nu_\alpha(L)\rangle = \sum_i \sum_\beta [U_0]^*_{\alpha i} e^{-i\frac{m_i^2}{2E}L} [U_0]_{\beta i} |\nu_\beta\rangle . \tag{4.10}$$

The probability amplitude for the $\nu_\alpha \to \nu_\beta$ transition is therefore

$$\langle \nu_\beta | \nu_\alpha(L)\rangle = \sum_i [U_0]^*_{\alpha i} [U_0]_{\beta i} e^{-i\frac{m_i^2}{2E}L} , \tag{4.11}$$

and hence the probability is

$$P_{\alpha\beta} \equiv P_{\nu_\alpha \to \nu_\beta} = |\langle \nu_\beta | \nu_\alpha(L)\rangle|^2 = \left| \sum_i [U_0]^*_{\alpha i} [U_0]_{\beta i} e^{-i\frac{m_i^2}{2E}L} \right|^2 . \tag{4.12}$$

We have seen that, because of the mixing between mass and flavour eigenstates, Eq. (4.1), a neutrino created with a definite flavour α will, in general, become a superposition of states of different flavour as it propagates, so that a detector placed in its way can, with a certain probability, register it as having a different flavour from the one that it was created with. Since the probability turns out to be oscillatory, the phenomenon of neutrino flavour transitions is also known as "neutrino oscillations".

4.1 Two–neutrino oscillations

Let us consider first two-generation mixing, such as occurs in oscillations of neutrinos from the Sun, where the two intervening flavours are solely electron- and muon-neutrinos.

4.1.1 Standard derivation of vacuum oscillations

In a two–neutrino system, the transformation matrix between mass and flavour eigenstates is a real 2×2 rotation matrix, parametrised by the rotation, or mixing, angle, θ:

$$U = \begin{pmatrix} \cos(\theta) & \sin(\theta) \\ -\sin(\theta) & \cos(\theta) \end{pmatrix} . \tag{4.13}$$

Considering the system of, say, the flavour neutrinos ($|\nu_e\rangle, |\nu_\mu\rangle$), we need the two mass eigenstates ($|\nu_1\rangle, |\nu_2\rangle$), to define them as the linear combinations

$$\begin{pmatrix} |\nu_e\rangle \\ |\nu_\mu\rangle \end{pmatrix} = U \begin{pmatrix} |\nu_1\rangle \\ |\nu_2\rangle \end{pmatrix} \Rightarrow \begin{cases} |\nu_e\rangle = \cos(\theta)\,|\nu_1\rangle + \sin(\theta)\,|\nu_2\rangle \\ |\nu_\mu\rangle = -\sin(\theta)\,|\nu_1\rangle + \cos(\theta)\,|\nu_2\rangle \end{cases} . \tag{4.14}$$

In this case, the Hamiltonian, in the mass basis, is

$$H_2^m = \begin{pmatrix} \frac{m_1^2}{2E} & 0 \\ 0 & \frac{m_2^2}{2E} \end{pmatrix} . \tag{4.15}$$

The probability amplitude, Eq. (4.11), associated to the transition $\nu_e \to \nu_\mu$ is hence

$$\begin{aligned} \langle \nu_\mu | \nu_e(L) \rangle &= U_{e1} U_{\mu 1} e^{-i\frac{m_1^2}{2E}L} + U_{e2} U_{\mu 2} e^{-i\frac{m_2^2}{2E}L} \\ &= \cos(\theta)\sin(\theta)\left(e^{-i\frac{m_2^2}{2E}L} - e^{-i\frac{m_1^2}{2E}L}\right) . \end{aligned} \tag{4.16}$$

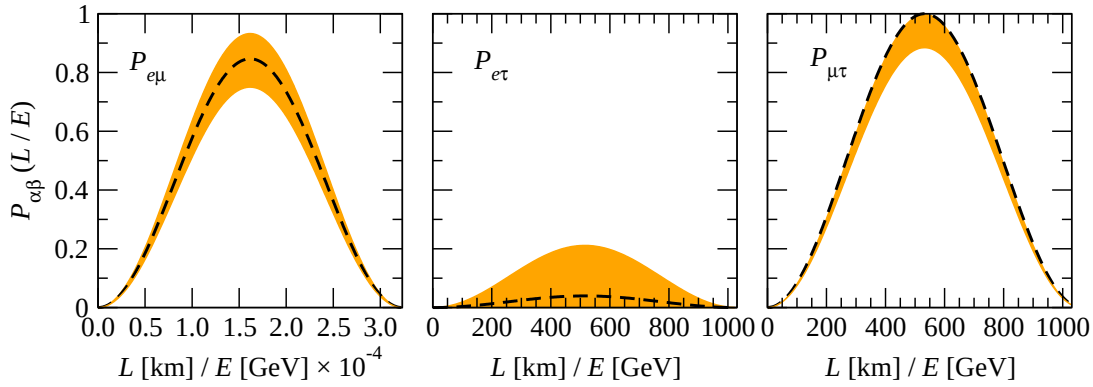

Figure 4.1: Oscillation probabilities in the vacuum within the two-neutrino formalism, Eq. (4.20), as functions of the quotient L/E, with the propagated distance, L, in km, and the neutrino energy, E, in GeV. The dashed black lines are calculated using the central values (Eq. (4.52)) of the mixing angle and squared-mass difference that corresponds to each case: $(\theta_{12}, \Delta m^2_{21})$, $(\theta_{13}, \Delta m^2_{31})$, and $(\theta_{23}, \Delta m^2_{32})$ for the left, central, and right plots, respectively. We have assumed a normal mass hierarchy, so that $\Delta m^2_{32} \equiv \Delta m^2_{31} - \Delta m^2_{21}$. The orange regions are generated by allowing the mixing angle correspondng to each plot to vary within its current 3σ experimental bounds, as given by Eq. (4.52).

Therefore, the associated probability, Eq. (4.12) is

$$\begin{aligned} P_{e\mu}(E,L) &= \frac{1}{4}\sin^2(2\theta)\left(2 + e^{-i\frac{\Delta m^2}{2E}L} - e^{i\frac{\Delta m^2}{2E}L}\right) \\ &= \frac{1}{2}\sin^2(2\theta)\left[1 - \cos\left(\frac{\Delta m^2}{2E}L\right)\right] \\ &= \sin^2(2\theta)\sin^2\left(\frac{\Delta m^2}{4E}L\right) \ , \end{aligned} \tag{4.17}$$

with $\Delta m^2 \equiv m_2^2 - m_1^2$, which is the final expression we were seeking.

In general, for any system of two neutrino flavours, $(|\nu_\alpha\rangle, |\nu_\beta\rangle)$, we can write the transition $(\nu_\alpha \to \nu_\beta)$ and survival $(\nu_\alpha \to \nu_\beta)$ probabilities as

$$P_{\alpha\beta}(E,L) = \sin^2(2\theta)\sin^2\left(\frac{\Delta m^2}{4E}L\right) \ , \quad \alpha \neq \beta \ , \tag{4.18}$$

$$P_{\alpha\alpha}(E,L) = 1 - P_{\alpha\beta}(E,L) \ , \tag{4.19}$$

which is the standard expression for standard two-neutrino mixing. Inserting the necessary factors of $\hbar$ and c, we can write

$$P_{\alpha\beta}(E,L) = \sin^2(2\theta)\sin^2\left(1.27\frac{\Delta m^2\,[\mathrm{eV}^2]}{E\,[\mathrm{GeV}]}L\,[\mathrm{km}]\right) \ , \quad \alpha \neq \beta \ . \tag{4.20}$$

Figure 4.1 shows plots of the vacuum oscillation probabilities $P_{e\mu}$, $P_{e\tau}$, and $P_{\mu\tau}$ as functions of L/E, calculated within the two–neutrino formalism, as given by Eq. (4.20). The dashed black lines are calculated using the central values (Eq. (4.52)) of the mixing angle and squared-mass difference that corresponds to each case: $(\theta_{12}, \Delta m^2_{21})$, $(\theta_{13}, \Delta m^2_{31})$, and $(\theta_{23}, \Delta m^2_{32})$ for the left, central, and right plots, respectively. We have assumed a normal mass hierarchy, so that $\Delta m^2_{32} \equiv \Delta m^2_{31} - \Delta m^2_{21}$. The orange regions are generated by allowing the mixing angle correspondng to each plot to vary within its current 3σ experimental bounds, as given by Eq. (4.52).

4.1.2 Derivation in the flavour basis

An alternative, but completely equivalent, derivation of the oscillation probabilty starts out by writing the evolved state of a neutrino created with flavour α directly as

$$|\nu_\alpha\,(L)\rangle = e^{-iH_2^f L}|\nu_\alpha\rangle\ , \tag{4.21}$$

with H_2^f the oscillation Hamiltonian in the flavour basis. This can be obtained from the Hamiltonian in the mass basis, H_2^m, by a similarity transformation with the mixing matrix U. If the Hamiltonian in the flavour basis is non-diagonal, there will be flavour transitions.

First, however, it will be useful to write H_2^m in a more familiar form, by subtracting and adding multiples of the identity. We have the freedom to do this without affecting the final result because multiples of the identity will only contribute as global phases in the evolved neutrino state, which disappear when the absolute value of the probability amplitude is calculated. By subtracting first $-m_1^2/2E$ and then $\Delta m^2/4E$, and multiplying the result by -1 (this last step just for conventional purposes), we end up with

$$H_2^m = \begin{pmatrix} \frac{\Delta m^2}{4E} & 0 \\ 0 & -\frac{\Delta m^2}{4E} \end{pmatrix}\ . \tag{4.22}$$

Hence, the Hamiltonian in the flavour basis is

$$\begin{aligned} H_2^f &= U H_2^m U^\dagger \\ &= \begin{pmatrix} \cos(\theta) & \sin(\theta) \\ -\sin(\theta) & \cos(\theta) \end{pmatrix} \frac{\Delta m^2}{4E} \begin{pmatrix} 1 & 0 \\ 0 & -1 \end{pmatrix} \begin{pmatrix} \cos(\theta) & -\sin(\theta) \\ \sin(\theta) & \cos(\theta) \end{pmatrix} \\ &= \frac{\Delta m^2}{4E} \begin{pmatrix} -\cos(2\theta) & \sin(2\theta) \\ \sin(2\theta) & \cos(2\theta) \end{pmatrix}\ , \end{aligned} \tag{4.23}$$

where, in the last step, we have multiplied the result by -1, to follow convention.

Considering a $\nu_e - \nu_\mu$ system, the neutrino state is described by the column vector

$$|\nu(L)\rangle = \begin{pmatrix} f_e(L) \\ f_\mu(L) \end{pmatrix} , \tag{4.24}$$

and it satisfies the Schrödinger equation

$$i\frac{\partial}{\partial t}|\nu(t)\rangle = H_2^f|\nu(t)\rangle , \tag{4.25}$$

with $(f_e(0), f_\mu(0)) = (1, 0)$ if the neutrino was created as a ν_e and $(f_e(0), f_\mu(0)) = (0, 1)$ if it was created as a ν_μ.

Now, in order to calculate the oscillation probability given the Hamiltonian in the flavour basis, H_2^m, it is necessary to change it into the mass basis by using an inverse similarity transformation,

$$H_2^m = U^\dagger H_2^f U . \tag{4.26}$$

With this, we just need to repeat the derivation in Section 4.1.1 to recover the probability, Eq. (4.17).

So far, it may seem pointless to write the Hamiltonian in the flavour basis only to change it back into the mass basis in order to obtain the probability. However, notice that in weak processes, the neutrino states that interact are flavour states, not mass eigenstates. Therefore, when in the flavour basis, additional neutrino interactions can be introduced by directly adding extra terms to the vacuum Hamiltonian. When this augmented Hamiltonian is diagonalised, the energy eigenvalues E_i will be modified with respect to the vacuum eigenvalues, and so will the oscillation probability. In the next section, we will illustrate this for neutrino interactions with matter.

An alternative, more general derivation of the two-neutrino oscillation probability, for an arbitrary time-independent Hamiltonian (in the flavour basis) is presented in Appendix A.

4.1.3 Oscillations in matter

When a neutrino beam traverses matter, the oscillation probability will be affected by the forward scattering of neutrinos off the particles they encounter on their way. Within the Standard Model, the scattering can be mediated either by W exchange with an electron, if and only if the neutrinos are ν_e, or by Z exchange with an electron, proton or neutron, which occurs for all flavours. Both interactions

contribute an extra energy which, in lowest perturbation order, will be proportional to G_F.

In $\nu_e - e$ scattering, the extra interaction potential V_W will be proportional to N_e, the number of electrons per unit volume. It is straightforward to find that (see, e.g., [43]),

$$V_W = +\sqrt{2} G_F N_e \tag{4.27}$$

for a neutrino beam. For an anti-neutrino beam, the expression for V_W has the opposite sign.

Assuming that the medium is electrically neutral, i.e., that the electron and proton densities are equal, then the contributions to coherent forward scattering off electrons and protons will cancel out. Thus, the flavour-independent Z-exchange contribution V_Z depends only on N_n, the number of neutrons per unit volume, and is given by

$$V_Z = -\frac{\sqrt{2}}{2} G_F N_n \ . \tag{4.28}$$

Again, the sign of V_Z is flipped for anti-neutrino interactions.

As in the vacuum case, neutrino oscillations in matter can be described by a Schrödinger equation in the flavour basis, Eq. (4.25). Considering a $\nu_e - \nu_\mu$ system, the neutrino state is described by the column vector

$$|\nu(t)\rangle = \begin{pmatrix} f_e(t) \\ f_\mu(t) \end{pmatrix} \ , \tag{4.29}$$

and the Schrödinger equation is

$$i\frac{\partial}{\partial t}|\nu(t)\rangle = H_2^M(t)\,|\nu(t)\rangle \ . \tag{4.30}$$

The total Hamiltonian is given by

$$H_2^M = H_2^{\text{vac}} + V_W \begin{pmatrix} 1 & 0 \\ 0 & 0 \end{pmatrix} + V_Z \begin{pmatrix} 1 & 0 \\ 0 & 1 \end{pmatrix} \ , \tag{4.31}$$

with H_2^{vac} the vacuum Hamiltonian given by Eq. (4.23). Note that V_W has its only non-zero component in the upper left corner, signifying that only in $\nu_e - e$ interactions are W exchanged, whereas the contribution from V_Z affects both ν_e and ν_μ interactions. The time dependence of the matter Hamiltonian comes from the time dependence of the potentials V_W and V_Z, in view of the possibility that the electron and neutron densities are not homogeneous within the medium traversed by the neutrino.

Since the third term on the right in Eq. (4.31) is proportional to the identity, it will result in a global phase in the oscillation amplitude and hence we can discard it already at this point. Therefore,

$$H_2^M = H_2^{\text{vac}} + \frac{V_W}{2}\begin{pmatrix} 1 & 0 \\ 0 & 1 \end{pmatrix} + \frac{V_W}{2}\begin{pmatrix} 1 & 0 \\ 0 & -1 \end{pmatrix} , \tag{4.32}$$

where we have split the V_W contribution into a part that is proportional to the identity and a part that is not. Again, we can drop the part former and obtain, finally,

$$H_2^M = H_2^{\text{vac}} + \frac{V_W}{2}\begin{pmatrix} 1 & 0 \\ 0 & -1 \end{pmatrix} \tag{4.33}$$

$$= \frac{\Delta m^2}{4E}\begin{pmatrix} -(\cos(2\theta) - x) & \sin(2\theta) \\ \sin(2\theta) & (\cos(2\theta) - x) \end{pmatrix} , \tag{4.34}$$

with

$$x \equiv \frac{V_W/2}{\Delta m^2/4E} = \frac{2\sqrt{2}G_F N_e E}{\Delta m^2} \tag{4.35}$$

measuring the relative importance of the matter effects with respect to the vacuum contribution.

If we define

$$\Delta m_M^2 \equiv \Delta m^2 \sqrt{\sin^2(2\theta) + (\cos(2\theta) - x)^2} \tag{4.36}$$

and

$$\sin^2(2\theta_M) \equiv \frac{\sin^2(2\theta)}{\sin^2(2\theta) + (\cos(2\theta) - x)^2} , \tag{4.37}$$

then we can write the matter Hamiltonian as

$$H_2^M = \frac{\Delta m_M^2}{4E}\begin{pmatrix} -\cos(2\theta_M) & \sin(2\theta_M) \\ \sin(2\theta_M) & \cos(2\theta_M) \end{pmatrix} . \tag{4.38}$$

Thus, H_2^M has the same form as H_2^{vac}, with the replacementes $\Delta m^2 \to \Delta m_M^2$ and $\theta \to \theta_M$. Hence, we can interpret Δm_M^2 and θ_M as the effective mass-splitting and mixing angle in matter, respectively.

In a homogeneous medium, where N_e is constant, the $\nu_e \to \nu_\mu$ oscillation probability has the same functional form as the vacuum case, with the replacements $\Delta m^2 \to \Delta m_M^2$ and $\theta \to \theta_M$, i.e.,

$$P_{M,e\mu}(E, L) = \sin^2(2\theta_M)\sin^2\left(\frac{\Delta m_M^2}{4E}L\right) . \tag{4.39}$$

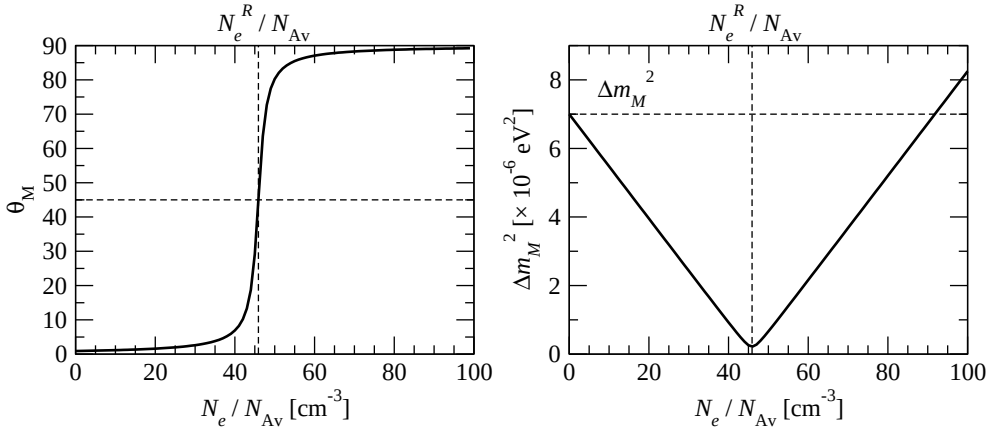

Figure 4.2: Effective mixing angle (*left*) and mass splitting (*right*) in the presence of matter effects, as functions the electron number density, N_e. For illustration purposes, we have set $\Delta m^2 = 7 \times 10^{-6}$ eV^2, $\sin(\theta) = 10^{-3}$ and $E = 1$ MeV. $N_{\rm Av}$ is Avogadro's number.

This may be the case, for instance, in a long-baseline neutrino experiment, where a neutrino beam originated at an accelerator traverses the crust of the Earth for 1000 km before reaching the detector.

It is interesting to note that, for certain values of N_e, there is a resonance that enforces maximal mixing between the neutrinos, i.e., $\theta_M = \pi/4$, regardless of the value of the vaccum value of the angle, θ. We can see this by writing

$$\tan(2\theta_M) = \frac{\tan(2\theta)}{1 - x/\cos(2\theta)} \,, \tag{4.40}$$

and noting that the resonance occurs when

$$1 - x/\cos(2\theta) = 0 \,, \tag{4.41}$$

or, equivalently, when, for a fixed energy E, the electron number density is

$$N_e^R = \frac{\Delta m^2 \cos(2\theta)}{2\sqrt{2} G_F E} \,. \tag{4.42}$$

When this resonance condition is fulfilled, the effective mass splitting and mixing angle are, from Eqs. (4.36) and (4.37), respectively,

$$\Delta m^2_{M,R} = \Delta m^2 \sin(2\theta) \;\;, \quad \theta_{M,R} = \pi/4 \,. \tag{4.43}$$

This effect is known as the MSW effect, after Mikheev, Smirnov, and Wolfenstein. In ordinary matter, x is positive, so a resonance can only occur if $\theta < \pi/4$, in order

for $\cos(2\theta) > 0$. Hence, oscillations in matter are different for neutrinos and anti-neutrinos, for which the sign of the potential is flipped: for the former, there can only be a resonance if $\theta < \pi/4$ while, for the latter, there can only be one if $\theta > \pi/4$.

Figure 4.2 shows the variation of θ_M (left plot) and Δm^2_M (right plot) with $N_e/N_{\rm Av}$, with $N_{\rm Av}$ Avogadro's number. To produce these plots, we have set the vacuum mixing parameters at $\Delta m^2 = 10^{-6}$ eV^2 and $\sin(\theta) = 10^{-3}$, and the neutrino energy at 1 MeV. The vertical, dashed, lines indicate where the MSW resonance occurs, at $N_e = N_e^R$. At this value, $\theta_M = \pi/4$ and Δm^2_M reaches its minimum value.

Scenarios with an inhomogeneous medium can be treated in the adiabatic approximation, if the density gradient is low enough, and, more generally, by considering the V_W contribution perturbatively. We will not explore these cases in details, but the interested reader can consult, e.g., [43]. Hereafter, we will not consider matter effects in the oscillations; however, the introduction of the V_W contribution due to matter effects will serve to illustrate how new physics effects can be considered, by adding extra terms to the Hamiltonian in the flavour basis (see Chapter 7).

4.2 Three–neutrino oscillations

While the two-generation case can be successfully used to analyse solar, accelerator, atmospheric and reactor neutrino data, a three-generation analysis is needed when performing combined fits to data from all of the aforementioned diverse source. Also, the formalism of three-generation mixing is typically required when studying neutrinos originated at distant astrophysical sources, such as active galactic nuclei, supernovae and gamma-ray bursts. Due to travelled distances of the order of hundreds of Mpc or more, the transitions between all three flavour states must be considered when calculating the expected flavour ratios at neutrino detectors on Earth.

Assuming the existence of three active neutrino families ($\alpha = e, \mu, \tau$), as indicated by LEP [48], three mass eigenstates are required ($i = 1, 2, 3$ in the sum) and so U_0 is a 3×3 matrix. The mass eigenstates $|\nu_i\rangle$ satisfy Schrödinger's equation and so propagate, sans a flavour-independent common phase e^{-iEL}, as

$$|\nu_i(L)\rangle = e^{-iHL}|\nu_i\rangle = e^{-i\frac{m_i^2}{2E}L}|\nu_i\rangle \ , \tag{4.44}$$

where we have assumed that $m_i \ll E$, so that $p = \sqrt{E^2 - m_i^2} \simeq E - m_i^2/(2E)$, and that, because neutrinos are highly relativistic particles, $t \simeq L$ (in natural units).

That a neutrino created with a definite flavour α becomes, in general, a superposition of states of different flavour as it propagates is made evident by writing the

Hamiltonian in the basis of flavour eigenstates, a choice which will also allow us to introduce contributions from new physics later in a more straightforward manner. In this basis, if a neutrino is produced with flavour α, then, after having propagated for a distance L, its evolved state will be

$$|\nu_\alpha\left(L\right)\rangle = e^{-iH_m L}|\nu_\alpha\rangle \ , \tag{4.45}$$

where the oscillation Hamiltonian H_m is the one corresponding to the standard, mass-driven, mechanism, and is written in the flavour basis. H_m is related to the Hamiltonian in the mass basis -the "mass matrix"- through a similarity transformation that makes use of the unitary mixing matrix U_0:

$$H_m = U_0 H U_0^\dagger = U_0 \frac{\mathrm{diag}\left(0, \Delta m^2_{21}, \Delta m^2_{31}\right)}{2E} U_0^\dagger \ . \tag{4.46}$$

U_0 is the Pontecorvo-Maki-Nakagawa-Sakata (PMNS) mixing matrix, which in the PDG parametrisation [29] can be written in terms of three mixing angles, θ_{12}, θ_{13} and θ_{23}, and one CP-violation phase, δ_{CP}, as

$$U_0\left(\{\theta_{ij}\}, \delta_{\mathrm{CP}}\right) = \begin{pmatrix} c_{12}c_{13} & s_{12}c_{13} & s_{13}e^{-i\delta_{\mathrm{CP}}} \\ -s_{12}c_{23} - c_{12}s_{23}s_{13}e^{i\delta_{\mathrm{CP}}} & c_{12}c_{23} - s_{12}s_{23}s_{13}e^{i\delta_{\mathrm{CP}}} & s_{23}c_{13} \\ s_{12}s_{23} - c_{12}c_{23}s_{13}e^{i\delta_{\mathrm{CP}}} & -c_{12}s_{23} - s_{12}c_{23}s_{13}e^{i\delta_{\mathrm{CP}}} & c_{23}c_{13} \end{pmatrix} \tag{4.47}$$

with $c_{ij} \equiv \cos\left(\theta_{ij}\right)$, $s_{ij} \equiv \sin\left(\theta_{ij}\right)$.

The standard flavour-oscillation probability $P_{\alpha\beta} = \left|\langle\nu_\beta|\nu_\alpha\left(L\right)\rangle\right|^2$ can hence be calculated, using Eq. (4.45) for the evolved neutrino state and Eq. (4.46) for the standard Hamiltonian, to be

$$P_{\alpha\beta} = \delta_{\alpha\beta} - 4\sum_{i>j} \mathrm{Re}\left(J^{ij}_{\alpha\beta}\right) \sin^2\left(\frac{\Delta m^2_{ij}}{4E}L\right) + 2\sum_{i>j} \mathrm{Im}\left(J^{ij}_{\alpha\beta}\right) \sin\left(\frac{\Delta m^2_{ij}}{2E}L\right) \ , \tag{4.48}$$

where $\Delta m^2_{ij} \equiv m^2_i - m^2_j$, with m_i the mass of the i-th eigenstate, and

$$J^{ij}_{\alpha\beta} \equiv \left[U_0\right]^*_{\alpha i}\left[U_0\right]_{\beta i}\left[U_0\right]_{\alpha j}\left[U_0\right]^*_{\beta j} \ . \tag{4.49}$$

(For a detailed deduction, see Appendix B and, e.g., [49].) The unitarity of the PMNS matrix, i.e., $U_0 U_0^\dagger = U_0^\dagger U_0 = 1$, implies the conservation of probability, in the form

$$\sum_{\beta=e,\mu,\tau} P_{\alpha\beta} = 1 \quad , \qquad \alpha = e, \mu, \tau \ , \tag{4.50}$$

which should be compared to Eq. (4.19) from the two–neutrino formalism.

It is straightforward to conclude from Eq. (4.48) that flavour transitions occur because neutrinos are massive, particularly, because different mass eigenstates have different masses (clearly, if $\Delta m^2_{ij} = 0$, no transitions occur), and because flavour states are not mass eigenstates. Note the $1/E$ dependence on the energy associated with this standard, mass-driven, oscillation mechanism. Note also that the full form of the PMNS matrix includes two extra Majorana CP-violation phases, α_1 and α_2, which are identically zero if neutrinos are Dirac, so that the complete matrix is given by

$$U_0 \times \text{diag}\left(e^{i\alpha_1/2}, e^{i\alpha_2/2}, 1\right) \ . \tag{4.51}$$

However, these phases do not affect the oscillations, so we have not included them in the definition of the standard mixing matrix U_0.

Using the latest data from solar, atmospheric, reactor (KamLAND and CHOOZ) and accelerator (K2K and MINOS) experiments, the authors of [50] performed a global three-generations fit and found the best-fit values of the standard oscillation parameters and their 3σ intervals to be

$$\Delta m^2_{21} = 7.65^{+0.69}_{-0.60} \times 10^{-5} \text{ eV}^2 \ , \ |\Delta m^2_{31}| = 2.40^{+0.35}_{-0.33} \times 10^{-3} \text{ eV}^2 \tag{4.52}$$

$$\sin^2(\theta_{12}) = 0.304^{+0.066}_{-0.054} \ , \ \sin^2(\theta_{13}) = 0.01^{+0.046}_{-0.01} \ ,$$
$$\sin^2(\theta_{23}) = 0.50^{+0.17}_{-0.14} \ . \tag{4.53}$$

Throughout this work, we have assumed a normal mass hierarchy, so that $\Delta m^2_{32} = \Delta m^2_{31} - \Delta m^2_{21}$.

A value of the CP-violation phase δ_{CP} different from zero implies a violation of the CP symmetry which, so far, has only been observed in the quark sector. Currently, there are no experimental values of or bounds on the value of δ_{CP}. The main difficulty in measuring it lies in the fact that, in the PMNS matrix, Eq. (4.47), it always appears multiplied by $\sin(\theta_{13})$, which is a very small number, given that θ_{13} is close to zero [51]. Numerous proposals for measuring or restricting the value of δ_{CP}, however, circulate in the literature [51–55]. Also, note that in the two–neutrino treatment of oscillations, no CP-violation phase appears. This is because, in the two–flavour formalism, the CP phase can be rotated away by a redefinition of the neutrino states (see, e.g., [43]).

Figure 4.3 shows plots of $P_{e\mu}$, $P_{e\tau}$, and $P_{\mu\tau}$ as functions of L/E, within the

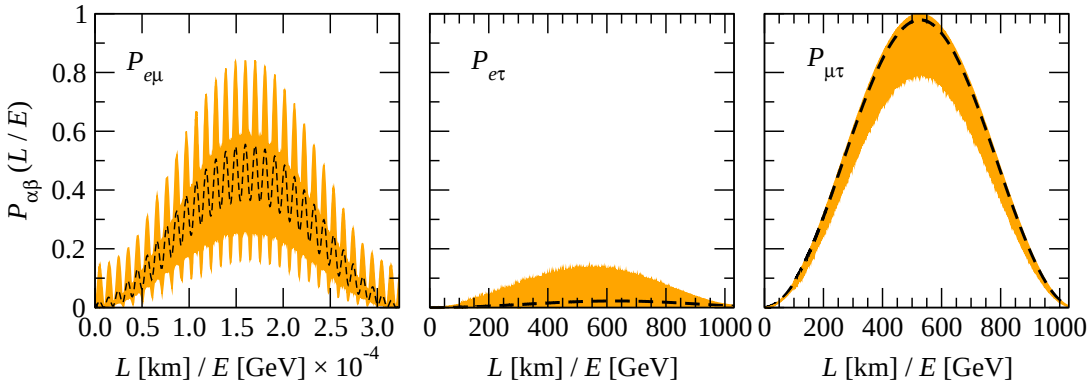

Figure 4.3: Oscillation probabilities within the full three-neutrino formalism, Eq. (4.54), as functions of the quotient L/E, with the propagated distance, L, in km, and the neutrino energy, E, in GeV. The dashed black lines are calculated using the central values (Eq. (4.52)) of the mixing angles and squared-mass differences. We have assumed a normal mass hierarchy, so that $\Delta m^2_{32} \equiv \Delta m^2_{31} - \Delta m^2_{21}$. The orange regions are generated by allowing the mixing angles to vary within their respective 3σ experimental bounds, as given by Eq. (4.52). The CP violating phase was set to $\delta_{\rm CP} = 0$.

three–neutrino formalism, as given by

$$P_{\alpha\beta} = \delta_{\alpha\beta} - 4\sum_{i>j} \mathrm{Re}\left(J^{ij}_{\alpha\beta}\right) \sin^2\left(1.27\frac{\Delta m^2_{ij}\,[\mathrm{eV}^2]}{E\,[\mathrm{GeV}]} L\,[\mathrm{km}]\right) + 2\sum_{i>j} \mathrm{Im}\left(J^{ij}_{\alpha\beta}\right) \sin\left(2.54\frac{\Delta m^2_{ij}\,[\mathrm{eV}^2]}{E\,[\mathrm{GeV}]} L\,[\mathrm{km}]\right) , \quad (4.54)$$

which is just Eq. (4.48) after the necessary factors of $\hbar$ and c have been inserted. These plots should be compared to the ones in Fig. 4.1. The dashed black lines are calculated using the central values (Eq. (4.52)) of the mixing angles and squared-mass differences. We have assumed a normal mass hierarchy, so that $\Delta m^2_{32} \equiv \Delta m^2_{31} - \Delta m^2_{21}$. The orange regions are generated by allowing the mixing angles to vary within their respective 3σ experimental bounds, as given by Eq. (4.52). Note that, in the three–neutrino formalism, three different oscillatory signals are superposed: this is particularly clear for $P_{e\mu}$. Note also that $P_{e\mu}$ is suppressed when using three– instead of two–neutrino oscillations. While, in the two–neutrino case, $P_{\mu\tau}$ was maximised when using the central value of $\theta_{23} = \pi/4$, in the three–neutrino case the curve corresponding to this value of the mixing angle is nearly, but not quite, a maximum, due to the suppression introduced by the extra oscillatory terms. Finally, $P_{e\tau}$ is not greatly affected when replacing two– for three–neutrino oscillations: this is because the dominating mixing angle in this transition, θ_{13} is

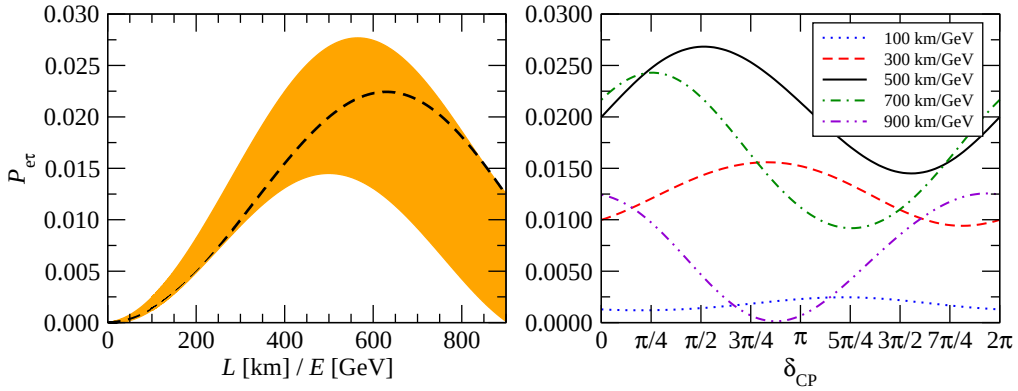

Figure 4.4: *Left:* Three–neutrino oscillation probability $P_{e\tau}$ as a function of L/E, when $\delta_{\rm CP}$ is allowed to vary between 0 and 2π, while keeping the other mixing parameters, θ_{ij} and Δm^2_{ij}, at their best-fit values. This variation generates the orange region, while the dashed black curve corresponds to the particular case of $\delta_{\rm CP} = 0$. *Right:* $P_{e\tau}$ as a function of $\delta_{\rm CP}$, for different choices of L/E. Again, the rest of the mixing parameters have been set to their best-fit values.

close to zero, so that the mixing between ν_e and ν_τ is very small.

As there are no experimental values for $\delta_{\rm CP}$ presently, we have shown, for illustration purposes, in Figure 4.4 the variation of the three–neutrino probability $P_{e\tau}$ with $\delta_{\rm CP}$. The left plot shows $P_{e\tau}$ as a function of L/E when $\delta_{\rm CP}$ is allowed to vary between 0 and 2π, while keeping the other mixing parameters (mixing angles and squared-mass differences) fixed at their best-fit values. The variation of $\delta_{\rm CP}$ generates the orange region, while the black dashed curve corresponds to the particular case when this phase is zero. The right plot shows $P_{e\tau}$ as a function of $\delta_{\rm CP}$, for different choices of L/E.

Because, as was mentioned in Chapter 1, we will be considering UHE neutrinos of extragalactic origin, the flavour-transition probability in Eq. (4.48) oscillates very rapidly, and we use instead the average probability, which is obtained by averaging the oscillatory terms in the expression, thus yielding

$$\langle P_{\alpha\beta} \rangle = \sum_i |[U_0]_{\alpha i}|^2 |[U_0]_{\beta i}|^2 \ . \tag{4.55}$$

When using the average probability, the information in the oscillation phase, including any potential CPTV energy-independent contribution, is lost, as we will see in Chapter 6. The modifications to the mixing angles due to CPTV, however, will still be present in the averaged version of the probability, and this will be the subject of Chapter 7.

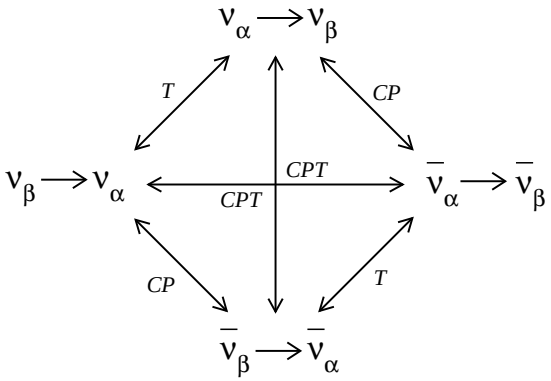

Figure 4.5: Schematic representation of the action of the symmetry operators T, CP, and CPT. Adapted from [43].

4.3 Discrete symmetries in neutrino oscillations

In Section 2.2.2 we explored how the C, P, and T operators (and their combinations) associated to the charge conjugation, parity, and time reversal symmetries, respectively, affect the bilinears that make up the terms of the Standard Model. In the present section, we will see how these operators affect neutrino oscillations.

Neutrinos and anti-neutrino flavour states can be transformed into one another by a CP transformation which changes the quantum numbers from those of a particle to those an anti-particle and reverses helicity, i.e.,

$$\nu_\alpha \overset{CP}{\longleftrightarrow} \overline{\nu}_\alpha \ . \tag{4.56}$$

On the other, applying the T operator interchanges the initial and final states.

Hence, a CP transformation interchanges the $\nu_\alpha \to \nu_\beta$ and $\overline{\nu}_\alpha \to \overline{\nu}_\beta$ channels, i.e.,

$$\nu_\alpha \to \nu_\beta \overset{CP}{\longleftrightarrow} \overline{\nu}_\alpha \to \overline{\nu}_\beta \ , \tag{4.57}$$

while a T transformation interchanges the $\overline{\nu}_\alpha \to \overline{\nu}_\beta$ and $\overline{\nu}_\beta \to \overline{\nu}_\alpha$ channels, namely,

$$\overline{\nu}_\alpha \to \overline{\nu}_\beta \overset{T}{\longleftrightarrow} \overline{\nu}_\beta \to \overline{\nu}_\alpha \ . \tag{4.58}$$

Therefore, a CPT transformation interchanges the $\nu_\alpha \to \nu_\beta$ and $\overline{\nu}_\beta \to \overline{\nu}_\alpha$ channels:

$$\nu_\alpha \to \nu_\beta \overset{CPT}{\longleftrightarrow} \overline{\nu}_\beta \to \overline{\nu}_\alpha \tag{4.59}$$

Figure 4.5 is a schematic representation of the action of the T, CP and CPT operators in the different channels.

4.3.1 CPT

CPT is a symmetry of the Standard Model (see Chapter 2). In fact, it is a symmetry of any local quantum field theory. Since conventional neutrino oscillations are derived within the Standard Model, the oscillation probabilities are expected to be CPT-symmetric. In other words,

$$P_{\nu_\alpha \to \nu_\beta} = P_{\overline{\nu}_\beta \to \overline{\nu}_\alpha} \ , \tag{4.60}$$

where we have used the more explicit notation $P_{\nu_\alpha \to \nu_\beta}$ to avoid confusion. From Eq. (4.48), we find that

$$P_{\nu_\beta \to \nu_\alpha}(U) = P_{\nu_\alpha \to \nu_\beta}(U^*) \ . \tag{4.61}$$

Thus, if CPT invariance holds, then

$$P_{\overline{\nu}_\alpha \to \overline{\nu}_\beta} = \delta_{\alpha\beta} - 4 \sum_{i>j} \mathrm{Re}\left(J^{ij}_{\alpha\beta}\right) \sin^2\left(\frac{\Delta m^2_{ij}}{4E} L\right) \pm 2 \sum_{i>j} \mathrm{Im}\left(J^{ij}_{\alpha\beta}\right) \sin\left(\frac{\Delta m^2_{ij}}{2E} L\right) \ , \tag{4.62}$$

where the plus sign in the third term applies to neutrinos, and the minus sign, to anti-neutrinos. A possible measure of CPT invariance in neutrino oscillations would therefore be

$$A^{CPT}_{\alpha\beta} \equiv P_{\nu_\alpha \to \nu_\beta} - P_{\overline{\nu}_\beta \to \overline{\nu}_\alpha} \ . \tag{4.63}$$

4.3.2 CP

As shown in Fig. (4.5) and the accompanying text, the CP transformation interchanges neutrinos of negative helicity with anti-neutrinos of positive helicity, i.e., it interchanges the $\nu_\alpha \to \nu_\beta$ channel and the $\overline{\nu}_\alpha \to \overline{\nu}_\beta$ one. CP asymmetry is possible in three-neutrino mixing because, in general, the mixing matrix U is complex.

As we did in the case of CPT symmetry, a possible CP asymmetry can be measured in neutrino oscillation experiments through the parameter

$$A^{CP}_{\alpha\beta} \equiv P_{\nu_\alpha \to \nu_\beta} - P_{\overline{\nu}_\alpha \to \overline{\nu}_\beta} \ . \tag{4.64}$$

Since, due to CPT symmetry, $P_{\overline{\nu}_\alpha \to \overline{\nu}_\beta} = P_{\nu_\beta \to \nu_\alpha}$, then, clearly, CP asymmetry can only be measured in transitions between different flavours.

Using Eq. (4.62), we see that the terms that contribute to the CP asymmetry are the imaginary parts of the quartic products of the PMNS matrix components,

i.e.,

$$A^{CP}_{\alpha\beta} = 4\sum_{i>j} \mathrm{Im}\left(J^{ij}_{\alpha\beta}\right) \sin\left(\frac{\Delta m^2_{ij}}{2E}L\right) \ . \tag{4.65}$$

Note that if $\alpha = \beta$, the imaginary parts are identically zero, thus confirming that the CP asymmetry can only be measured in transitions between different flavours. Also, since the imaginary part the PMNS matrix is associated with the phase δ, if this phase is zero, then the asymmetry vanishes.

4.3.3 T

If CPT is a true symmetry, then the violation of CP symmetry implies the violation of T symmetry necessarily. A T asymmetry can be measured in neutrino and anti-neutrino oscillation experiments through the quantities

$$A^{T}_{\alpha\beta} \equiv P_{\nu_\alpha\to\nu_\beta} - P_{\nu_\beta\to\nu_\alpha} \ , \tag{4.66}$$

$$\overline{A}^{T}_{\alpha\beta} \equiv P_{\overline{\nu}_\alpha\to\overline{\nu}_\beta} - P_{\overline{\nu}_\beta\to\overline{\nu}_\alpha} \ . \tag{4.67}$$

From the action of the CPT operator, Eq. (4.60), and from Eq. (4.64) we find that

$$A^{T}_{\alpha\beta} = -\overline{A}^{T}_{\alpha\beta} = A^{CP}_{\alpha\beta} \ . \tag{4.68}$$

Hence, measuring a CP asymmetry is equivalent to measuring a T asymmetry. Therefore, T violation occurs only if $\delta = 0$.

Chapter 5

Astrophysical neutrinos

High-energy gamma ray experiments such as H.E.S.S. [56–58], MAGIC [59–62], VERITAS [63–65] and Milagro [66, 67] have observed during the last decade events with energies ranging from $\sim$ 100 GeV to several TeV coming from identified extragalactic sources, notably Active Galactic Nuclei (AGN) and Gamma Ray Bursts. While the correlation between observed gamma rays and catalogue sources is strong (signals at separation of 5σ or more from the background are not unusual), the generating mechanism of these emissions remains unknown [68]: high-energy gamma rays may be created at the sources as synchrotron radiation, in inverse Compton processes or in the decay of neutral pions resulting from pp and $p\gamma$ collisions. Current data is not sufficient to distinguish between these scenarios. The observation of neutrino emission correlated with the gamma-ray emission from these sources, however, would be enough to establish the decay of pions generated in the interactions of high-energy protons (and nuclei) as the generating mechanism: the same processes that create the neutral pions are also expected to create charged pions which would decay into neutrinos, yielding both a gamma-ray and a neutrino signal from the source, with the neutrino energy about a factor of two or three below the gamma-ray energy. Neutrino telescopes such as AMANDA [69], IceCube [70] and ANTARES [71] have been designed to detect this high-energy neutrino emission and, if possible, to correlate it with the known positions of gamma-ray sources.

5.1 Astrophysical neutrino flavour fluxes

We have seen that, in order for a potential energy-independent contribution to the flavour transitions to be visible, we would need to use the expected UHE astrophysical neutrino flux. The sources of this flux, e.g., active galaxies, are located at distances of tens to hundreds of Mpc, so that the average flavour transition proba-

bility, Eq. (7.47), can be used.

If, at the sources, neutrinos of different flavours are produced in the ratios $\phi_e^0 : \phi_\mu^0 : \phi_\tau^0$, then, because of flavour transitions during propagation, the ratios at detection will be

$$\phi_\alpha = \sum_{\beta=e,\mu,\tau} \langle P_{\beta\alpha} \rangle \phi_\beta^0 \ , \tag{5.1}$$

for $\alpha = e, \mu, \tau$. Note that the ratio in Eq. (5.1) is the proportion of ν_α to the sum of all flavours detected at Earth. We will later denote the actual neutrino fluxes, in units of $\mathrm{GeV}^{-1}\ \mathrm{cm}^{-2}\ \mathrm{s}^{-1}\ \mathrm{sr}^{-1}$, by Φ_α. Evidently, the initial flavour ratios depend on the astrophysics at the source, which is currently not known with high certainty, while the detected ratios depend also on the oscillation mechanism and could be affected by the presence of an energy-independent contribution at high energies. Thus, the reconstruction of the initial neutrino fluxes from the detected ones is a difficult task [72–78].

AGN have long been presumed to be sites of high-energy neutrino production. In the scenario of neutrino production by meson decay [75], it is assumed that within the AGN protons are accelerated by strong magnetic fields and that pions are produced in high-energy proton-proton and proton-photon collisions, i.e.,

$$p + \gamma \to \Delta^+ \to \begin{cases} p + \pi^0 \\ n + \pi^+ \end{cases} \quad , \qquad n + \gamma \to p + \pi^- \ , \tag{5.2}$$

with branching ratios $\mathrm{Br}\,(\Delta^+ \to p\pi^0) = 2/3$ and $\mathrm{Br}\,(\Delta^+ \to n\pi^+) = 1/3$. The neutral pions decay into gamma rays through $\pi^0 \to \gamma\gamma$, while the charged pions decay into electron and muon neutrinos through

$$\pi^+ \to \nu_\mu + \mu^+ \to e^+ + \nu_e + \overline{\nu}_\mu \quad , \qquad \pi^- \to \overline{\nu}_\mu + \mu^- \to e^- + \overline{\nu}_e + \nu_\mu \ . \tag{5.3}$$

The gamma rays thus created may be obscured and dispersed by the medium, and the protons will in addition be deviated by magnetic fields on their journey to Earth. Neutrinos, on the other hand, escape from the production site virtually unaffected by interactions with the medium, so that, if their direction can be reconstructed at detection, they could point back to their sources. Such process yields approximately $\phi_e^0 : \phi_\mu^0 : \phi_\tau^0 = 1 : 2 : 0$ (see [76] for a more detailed treatment), where we have not discriminated between neutrinos and antineutrinos, as is the case with current Čerenkov-based neutrino telescopes. In the standard oscillation scenario, i.e., in the absence of an energy-independent contribution, plugging this initial flux into Eq. (5.1), and using the best-fit values of the mixing angles, Eq. (4.52), results in

Production mechanism	Initial flux $\phi_e^0 : \phi_\mu^0 : \phi_\tau^0$	Std. detected flux $\phi_e^{\rm std} : \phi_\mu^{\rm std} : \phi_\tau^{\rm std}$	$R^{\rm std}$	$S^{\rm std}$
Pion decay	$1 : 2 : 0$	$1 : 1 : 1$	1	1
Muon cooling	$0 : 1 : 0$	$0.22 : 0.39 : 0.39$	1.77	1
Beta decay	$1 : 0 : 0$	$0.57 : 0.215 : 0.215$	0.38	1

Table 5.1: Standard values (without energy-independent new physics contributions) of the detected flavour ratios ϕ_α ($\alpha = e, \mu, \tau$) and of the ratios R, S, for the three different scenarios of initial flavour ratios considered in the text. The detected ratios were calculated using the average flavour-transition probability in Eq. (4.55) with the central values of the mixing angles: $\sin^2(\theta_{12}) = 0.304$, $\sin^2(\theta_{13}) = 0.01$, $\sin^2(\theta_{23}) = 0.50$. We have defined $R^{\rm std} = \phi_\mu^{\rm std}/\phi_e^{\rm std}$ and $S^{\rm std} = \phi_\tau^{\rm std}/\phi_\mu^{\rm std}$.

equal detected fluxes of each flavour, i.e., $\phi_e^{\rm std} : \phi_\mu^{\rm std} : \phi_\tau^{\rm std} \approx 1 : 1 : 1$.

In a related production process [76, 79, 80], the muons produced by pion decay lose most of their energy before decaying, so that a pure-ν_μ flux is generated at the source, i.e., $\phi_e^0 : \phi_\mu^0 : \phi_\tau^0 = 0 : 1 : 0$. In the standard oscillation scenario, these initial ratios result in the detected ratios $\phi_e^{\rm std} : \phi_\mu^{\rm std} : \phi_\tau^{\rm std} \approx 0.22 : 0.39 : 0.39$. Alternatively, a pure-$\nu_e$ initial flux, corresponding to $\phi_e^0 : \phi_\mu^0 : \phi_\tau^0 = 1 : 0 : 0$, produced through beta decay has been considered, e.g., in [76]. In this scenario, high-energy nuclei emmitted by the source have sufficient energy for photodisintegration to occur, but not enough to reach the threshold for pion photoproduction. The neutrons created in the process generate $\overline{\nu}_e$ through beta decay. For these initial ratios, the resulting detected ratios, in the standard oscillation scenario, are $\phi_e^{\rm std} : \phi_\mu^{\rm std} : \phi_\tau^{\rm std} \approx 0.57 : 0.215 : 0.215$. The results are summarised in Table 5.1. In the following sections, we will consider the possibility of observing the hypothetical energy-independent contribution of H_b assuming that the initial ratios correspond to one of these three production scenarios.

Using the detected flavour ratios, we have defined the ratios of ratios

$$R = \frac{\phi_\mu}{\phi_e} \quad , \quad S = \frac{\phi_\tau}{\phi_\mu} \, . \tag{5.4}$$

Their standard values, $R^{\rm std}$ and $S^{\rm std}$, i.e., those calculated in the absence of H_b, are shown in Table 5.1 for the three choices of initial flavour ratios. Note that $S^{\rm std} = 1$ for any choice of initial ratios because the value of θ_{23} used was its best-fit value $\pi/4$, which yields equal detected fluxes of ν_μ and ν_τ due to maximal mixing. Deviations from this value result in $S \neq 1$ [81]. In the following sections, when we allow H_b to contribute, we will calculate the extent to which the values of R and S deviate from their standard values.

5.1.1 Cosmic ray flux normalisation using results from Auger

Recently [82], the Pierre Auger Observatory (PAO) claimed to have detected 27 events with energies above 57 EeV, providing evidence of the anisotropy in the arrival directions of utrahigh-energy cosmic rays (UHECRs). Based on the observation of 20 of these events having an angular separation equal to or less than 3.2° from the positions of AGN from the 12th edition Véron-Cetty & Véron catalogue [83], a possible correlation was found with sources lying relatively close, at distances of 75 Mpc or less. Even though the claim on the correlation has since lost some ground [84, 85], it still constitutes a possible hint towards identifying AGN as the sources of the highest-energy cosmic rays. Under the assumption that cosmic ray emission is accompanied by neutrino emission, Auger's claim can be used to normalise the neutrino flux predicted by astrophysical models of AGN. In the present work, we have focused on two such models of neutrino production that take into account Auger's results: one by H.B.J. Koers & P. Tinyakov [86] and another one by J. Becker & P.L. Biermann [87], which we will call hereafter the KT and BB models, respectively. They differ greatly in their assumptions and, within some regions of their parameters spaces, on their predictions of the neutrino fluxes.

The preferred mechanism for cosmic ray acceleration at AGN is second-order Fermi acceleration [88], which results in a power-law differential cosmic ray proton spectrum,

$$\Phi_p\left(E\right) \equiv \frac{dN_p}{dE} = A_p E^{-\alpha_p} \ , \tag{5.5}$$

with E the cosmic ray energy at detection on Earth. Here, A_p is the energy-independent normalisation constant. The integral of this expression,

$$N\left(E_{\rm th}\right) = \int_{E_{\rm th}} \frac{dN_p}{dE} dE \simeq A_p \left(\alpha_p - 1\right)^{-1} E_{\rm th}^{\alpha_p - 1} \ , \tag{5.6}$$

is the integrated cosmic ray flux above a certain threshold energy $E_{\rm th}$. For the ultrahigh-energy cosmic rays detected at the PAO, $E_{\rm th} = 57$ EeV.

On the other hand, the integrated flux can be calculated from experimental data as

$$N\left(E_{\rm th}\right) = N_{\rm evts}\left(E_{\rm th}\right)/\Xi \ . \tag{5.7}$$

where $N_{\rm evts}\left(E_{\rm th}\right)$ is the number of observed cosmic rays above $E_{\rm th}$ and $\Xi = 9000$ km^2 yr sr is the reported [82] total detector exposure of Auger. The KT and BB models use different values for $N_{\rm evts}\left(E_{\rm th}\right)$, according to their assumptions: KT assumes $N_{\rm evts} = 2$ originated at Cen A and uses this to calculate the diffuse neutrino flux assuming that all AGN behave like Cen A, while BB assumes that the $N_{\rm evts} = 20$

events truly originated at the AGN with which the correlation was found. Comparing this expression to Eq. (5.6) yields for the normalisation constant,

$$A_p = \frac{N_{\rm evts}\,(\alpha_p - 1)}{\Xi} E_{\rm th}^{\alpha_p - 1} \ . \tag{5.8}$$

The spectral index α_p is expected to lie between 2 and 3 and is treated in the present work as a free parameter with values in this range. The relation between the cosmic ray normalisation constant and the neutrino normalisation constant (see the next two Sections) is model-dependent.

When calculating the proton spectrum from a single point source, we will need to weigh the normalisation constant using the detector effective area A that is accessible to the observation, which depends on the declination δ_s of the source, i.e.,

$$A_p^{\rm pt} = \frac{N_{\rm evts}\,(\alpha_p - 1)}{\Xi} E_{\rm th}^{\alpha_p - 1} \frac{\int A\,(\delta_s)\,d\Omega}{A\,(\delta_s)} \ . \tag{5.9}$$

5.1.2 Model by Waxman & Bahcall

In [89], Waxman and Bahcall set a model-independent upper bound of $E_\nu^2 \Phi_\nu < 2 \times 10^{-8}$ GeV cm^{-2} s^{-1} sr^{-1} to the flux of high-energy neutrinos from the decay of pions produced in $p\gamma$ interactions that occur at sources that are optically thin to $p\gamma$ interactions. Their calculation estimates the bound on the neutrino flux from observations of the high-energy (greater than 10^9 GeV) cosmic ray flux. We will reproduce here the outline of the calculation presented in [89].

Above 10^8 GeV, cosmic rays are thought to be created at extra-galactic sources. An homogenenous distribution of cosmic ray sources (e.g., AGN or GRBs) is assumed, with injection spectrum

$$\Phi_p^{\rm WB}\,(E_p) \equiv \frac{dN_p}{dE_p} \propto E_p^{-2} \ , \tag{5.10}$$

as expected from Fermi acceleration. From [90], the energy production rate of protons in the range $10^{10} - 10^{12}$ GeV is $\varepsilon_{\rm CR}^{\left[10^{10}, 10^{12}\right]} \sim 5 \times 10^{44}$ erg Mpc^{-3} yr^{-1}, assuming, again, a homogenenous distribution of cosmic ray sources. The generation rate of cosmic rays is hence

$$E_p^2 \frac{d\dot{N}_p}{dE_p} = \frac{\varepsilon_{\rm CR}^{\left[10^{10}, 10^{12}\right]}}{\ln\left(10^{12}/10^{10}\right)} \approx 10^{44} \text{ erg Mpc}^{-3} \text{ yr}^{-1} \ . \tag{5.11}$$

Let $\epsilon < 1$ be the fraction of the energy that extra-galactic high-energy neutrinos lose through photo-meson production of pions before leaving the source. Thus, the

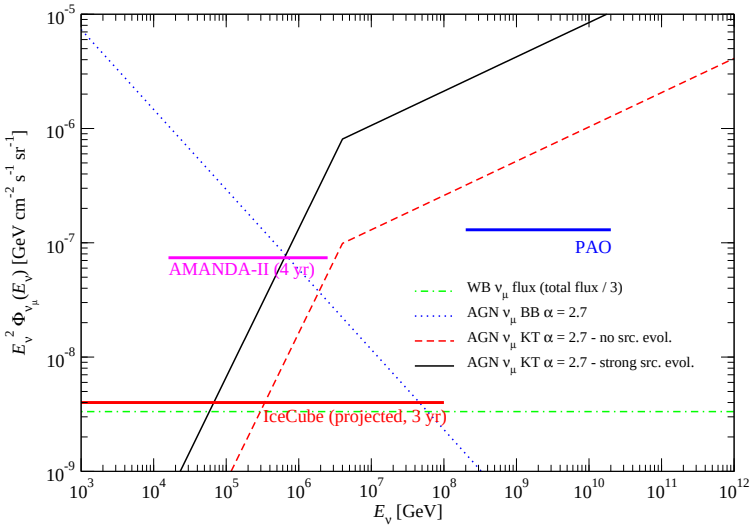

Figure 5.1: AGN ν_μ fluxes according to models WB, KT (with no source evolution and strong evolution) and BB, multiplied by E_ν^2. In this and the other plots, the best-fit values of the model parameters were used: $\alpha = 2.7$, $\Gamma_\nu/\Gamma_{\rm CR} = 3$ and $z_{\rm CR}^{\rm max} = 0.03$. Upper limits for the integrated astrophysical ν_μ flux $E_\nu\Phi_\nu$ from past, present and future neutrino experiments are included for comparison. For the Pierre Auger Observatory (PAO) [91], the limit is 1.3×10^{-7} GeV cm^{-2} s^{-1} sr^{-1}, in the range $2\times10^8 < E_\nu/\text{GeV} < 2\times10^{10}$. (Note that, strictly speaking, the PAO set a limit on the astrophysical ν_τ flux; the limit on the ν_μ flux is obtained by assuming that these two flavours arrive at Earth in equal proportions, due to flavour oscillations.) For IceCube [92], after three years of exposure of the full detector, the limit is 4×10^{-9} GeV cm^{-2} s^{-1} sr^{-1}, for neutrinos with energy $E_\nu < 10^8$ GeV. Finally, for AMANDA-II [93], using data collected in the period 2000-2003, the limit is 7.4×10^{-8} GeV, between 16 TeV and 2.5 PeV. Note that these limits have been calculated assuming a E_ν^{-2} flux, whereas we are showing the KT and BB fluxes for $\alpha = 2.7$ in this plot.

energy density of muon neutrinos at the present epoch ($z = 0$) is

$$E_\nu^2 \frac{d\dot{N}_\nu}{dE_\nu} \simeq \frac{1}{4}\epsilon t_H E_p^2 \frac{d\dot{N}_p}{dE_p} \ , \tag{5.12}$$

where $t_H \approx 10^{10}$ yr is the Hubble time. The factor of 1/4 comes from the fact that neutral pions, which do not decay into neutrinos, are produced with approximately the same probability as charged pions, and because in the decay of charged pions into muon-neutrinos, these carry about half of the pion energy.

Setting $\epsilon = 1$, the muon-neutrino intensity (for ν_μ and $\overline{\nu}_\mu$ combined) obtained is

$$\begin{aligned} I_{\max} &\simeq 0.25 \xi_Z t_H \frac{c}{4\pi} E_p^2 \frac{d\dot{N}_p}{dE_p} \\ &\approx 1.5 \times 10^{-8} \xi_Z \text{ GeV cm}^{-2} \text{ s}^{-1} \text{ sr}^{-1} , \end{aligned} \tag{5.13}$$

with the parameter ξ_Z, of order unity, introduced to describe the possible contribution of so far unobserved high-redshift sources of high-energy cosmic rays, and the effect of the cosmological expansion on the neutrino energy. For a distribution of cosmic ray sources that follows the star formation rate, Eq. (5.18), it was estimated that $\xi_Z \approx 3$, with a weak dependence on the cosmology, while for no source evolution, it is found that $\xi_Z \approx 0.6$.

Therefore, the expected muon-neutrino intensity is

$$E_\nu^2 \Phi_{\nu_\mu} = \frac{c}{4\pi} E_\nu^2 \frac{dN_{\nu_\mu}}{dE_\nu} = \frac{1}{2} \epsilon I_{\max} , \tag{5.14}$$

with the fluxes of all other flavours of neutrinos and anti-neutrinos approximately the same as for ν_μ. Taking $\xi_Z = 3$ and $\epsilon = 0.8$, one finds the Waxman-Bahcall upper bound of $E_\nu^2 \Phi_\nu < 2 \times 10^{-8}$ GeV cm^{-2} s^{-1} sr^{-1}. Note that when this upper bound was first derived, neutrino oscillations of the ν_μ and ν_e produced at the sources were not taken into account and so the upper bound was higher than it should have been.

In this work, we have been more restrictive and set the sum of the fluxes of all neutrino flavours at

$$\Phi_{\nu_{\text{all}}}^{\text{WB}} (E_\nu) = 10^{-8} \left(E_\nu / \text{GeV}\right)^{-2} \text{ GeV cm}^{-2} \text{ s}^{-1} \text{ sr}^{-1} . \tag{5.15}$$

Figure 5.1 features plots of the different flux models, multiplied by E_ν^2. The WB ν_μ flux, defined as one third of the all-flavour WB flux, is ploted as a dash-dotted (green) line.

5.1.3 Model by Koers & Tinyakov

The PAO has reported [82] observing two events correlated with the position of Centaurus A (Cen A), the nearest active galaxy, lying at about 3.5 Mpc. The observed differential flux from a point source lying at proper (luminosity) distance $d_L(z)$ is

$$\Phi(E) = \frac{j^0(E_0)}{4\pi d_L^2 (1+z)} \frac{dE_0}{dE} , \tag{5.16}$$

where E is the observed energy and the energy at the source, $E_0 = E_0(E, z)$, is calculated taking into account energy losses. j^0 is the differential injected spectrum at the source, which for protons and neutrinos behaves like a power-law, i.e., $j^0_\nu \propto E^{-\alpha_\nu}$, $j^0_p \propto E^{-\alpha_p}$. The KT model [86] assumes that Cen A is a typical source of UHECRs and neutrinos, and computes the diffuse flux by assuming that all sources are identical to Cen A by integrating over a cosmological distribution of sources, also taking into account energy losses during the propagation of the particles. Thus, the diffuse neutrino flux is

$$\Phi^{\text{diff}}_\nu(E_\nu) = \frac{cn_0}{4\pi}\int_0^\infty dz \left|\frac{dt}{dz}\right| \frac{dE_0}{dE_\nu}\epsilon(z)\, j^0(E_0) \ , \tag{5.17}$$

where c is the speed of light, n_0 is the local source density and $\epsilon(z)$ parametrises the source distribution. Two limiting cases have been considered: one in which there is no source evolution with redshift ($\epsilon(z) = 1$) and another one, adopted from [94], in which there is a strong source evolution which follows the star formation rate,

$$\epsilon(z) \propto \begin{cases} (1+z)^{3.4} & , \text{ if } z \leq 1.9 \\ (1+1.9)^{3.4} & , \text{ if } 1.9 < z < 3 \\ (z-3)^{-0.33} & , \text{ if } z \geq 3 \end{cases} \ , \tag{5.18}$$

The KT model adopts the ΛCDM cosmology to calculate

$$|dt/dz|^{-1} = H_0(1+z)\sqrt{\Omega_m(1+z)^3 + \Omega_\Lambda} \ , \tag{5.19}$$

with $H_0 = 73$ km s^{-1} Mpc^{-1} the Hubble constant and $\Omega_m = 0.24$, $\Omega_\Lambda = 0.76$ the present matter density and vacuum energy density parameters, respectively.

The diffuse neutrino flux is normalised using the integrated UHECR flux $\varphi^{\text{diff}}_p(E_{\text{th}})$ above the threshold E_{th},

$$\frac{\Phi^{\text{diff}}_\nu(E_\nu)}{j^0_\nu(E_\nu)} = H(E_{\text{th}})\frac{\varphi^{\text{diff}}_p(E_{\text{th}})}{J^0_p(E_{\text{th}})} \ , \tag{5.20}$$

with $J^0_p(E_{\text{th}})$ the integrated UHECR proton spectrum at the source. The proportionality constant, $H(E_{\text{th}})$, is called the "neutrino boost factor" and contains the information on neutrino mean-free path lengths and source evolution. It can be calculated numerically, provided an expression is given for dE_0/dE_ν, from Eqs. (5.17) and (5.20). Proton energy losses are taken into account in the continuous-loss approximation, considering both loss by the adiabatic expansion of the Universe and loss from interactions with the CMB photons resulting in pion photoproduction and

electron-positron pair production; see Appendix A in ref. [86] for details. To obtain the diffuse flux, the source distribution is integrated up to $z = 5$.

The PAO energy threshold is $E_{\rm th} = 57$ EeV. However there is a $\sim 20\%$ systematic uncertainty in the energy determination that affects the neutrino boost factor. Koers & Tinyakov [86] found that this uncertainty is well approximated by

$$H'\left(E_{\rm th}\right) = 10^{(E_{\rm th}/E_0)-1} H\left(E_0\right) \ , \tag{5.21}$$

where $E_{\rm th}$ is the actual threshold and $E_0 = 57$ EeV. This introduces a variation in H of a factor of ~ 1.6 when the energy is mis-reconstructed with 20% accuracy.

The integrated diffuse UHECR neutrino spectrum and the integrated flux from Cen A above 57 EeV can be written, respectively, as

$$\varphi_p^{\rm diff}\left(E_{\rm th}\right) = \frac{N_{\rm tot} - N_{\rm Cen\ A}}{\Xi} = 9 \times 10^{-21}\ {\rm cm^{-2} s^{-1} sr^{-1}} \tag{5.22}$$

$$\varphi_p^{\rm Cen\ A}\left(E_{\rm th}\right) = \frac{N_{\rm Cen\ A}}{\Xi} \frac{\int A\left(\delta_s\right) d\Omega}{A\left(\delta_s\right)} = 5 \times 10^{-21}\ {\rm cm^{-2} s^{-1} sr^{-1}} \ , \tag{5.23}$$

where $\delta_s = -43^\circ$ is the declination of Cen A and $A\left(\delta_s\right)$ is the detector's effective area for this declination. The PAO reported $A\left(\delta_s\right) / \int A\left(\delta_s\right) d\Omega = 0.15\ {\rm sr^{-1}}$ and $N_{\rm tot} = 27$ events above 57 EeV, with $N_{\rm Cen\ A} = 2$ of these coming from the direction of Cen A. From Eq. (5.20), we find

$$\begin{aligned} \frac{\Phi_\nu^{\rm diff}\left(E_\nu\right)}{\Phi_\nu^{\rm Cen\ A}\left(E_\nu\right)} &= H'\left(E_{\rm th}\right) \frac{\varphi_\nu^{\rm diff}\left(E_{\rm th}\right)}{\varphi_\nu^{\rm Cen\ A}\left(E_{\rm th}\right)} \\ &= H'\left(E_{\rm th}\right) \frac{N_{\rm tot} - N_{\rm Cen\ A}}{N_{\rm Cen\ A}} \frac{A\left(\delta_s\right)}{\int A\left(\delta_s\right) d\Omega} \\ &\simeq 1.9 H'\left(E_{\rm th}\right) \ . \end{aligned} \tag{5.24}$$

This relation between the diffuse neutrino flux and the flux from Cen A is the main result of the KT model.

In their paper [86], Koers & Tinyakov used a model by Cuoco & Hannestad [95] to describe the neutrino emission from Cen A, $\Phi_\nu^{\rm Cen\ A}$, itself based on a model by Mannheim, Protheroe & Raschen [96]. In this model, it is assumed that high-energy protons, accelerated by some mechanism (e.g., shock acceleration) are confined within a region close to the source. Because of energy losses in their photopion interactions with the ambient photon field, which is assumed to have an energy spectrum $n\left(\epsilon_\gamma\right) \propto \epsilon_\gamma^{-2}$, their lifetime is much shorter than their diffusive escape time and they decay into neutrons and neutrinos, both of which escape the source. Thereafter, the neutrons decay into UHECR protons; however, because of their interaction with

the photon field before decaying, the neutrons produce a softer proton spectrum than the seed proton spectrum.

Furthermore, the model predicts two spectral breaks in the CR spectrum, at energies at which the optical depths for proton and neutrino photopion production become unity. These two breaks are close in energy, though, so that to simplify the model, only one spectral break is considered, at energy $E_{\rm br}$. Below $E_{\rm br}$, the UHECR proton and neutrino spectra are harder than the seed proton spectra by one power of the energy, while above $E_{\rm br}$, the UHECR proton spectrum is softer than the seed proton by one power of the energy and the neutrino spectrum is harder by one power of the energy. Hence, at high energies, the model predicts a neutrino spectrum that is harder by one power of the energy than the UHECR proton spectrum.

Following [86,95,96], the all-flavour neutrino spectrum from Cen A can be written as

$$\Phi_\nu^{\rm Cen\ A}(E_\nu) = \frac{\xi_\nu}{\xi_n \eta_{\nu n}^2} \min\left(\frac{E_\nu}{\eta_{\nu n} E_{\rm br}}, \frac{E_\nu^2}{\eta_{\nu n}^2 E_{\rm br}^2}\right) \Phi_p^{\rm Cen\ A}\left(\frac{E_\nu}{\eta_{\nu n}}\right) , \tag{5.25}$$

where ξ_i $(i = \nu, n)$ is the fraction of the proton's energy that is transferred to the species i in photopion interactions and $\eta_{\nu n}$ is the ratio of the average neutrino energy to the average neutron energy. The KT model uses for these parameters the values featured in [96], obtained from Monte Carlo simulations: $\xi_\nu \approx 0.1$, $\xi_n \approx 0.5$, $\langle E_\nu \rangle / E_p \approx 0.033$ and $\langle E_n \rangle / E_p \approx 0.83$, with which

$$\xi_\nu / \xi_n = 0.2 \quad , \quad \eta_{\nu n} = 0.04 \ . \tag{5.26}$$

The neutrino break energy, $E_{\rm br}$, is estimated from the gamma-ray break energy as $E_{\rm br} \simeq 3 \times 10^8 E_{\gamma,{\rm br}}$. Ref. [96] uses $E_{\gamma,{\rm br}} = 200$ MeV, so that

$$E_{\rm br} = 10^8 \text{ GeV} \ . \tag{5.27}$$

Under the assumption of equitative flavour ratios at Earth (see Section 5.1), the $\nu_\mu + \overline{\nu}_\mu$ flux is 1/3 the flux in Eq. (5.25). Plugging the power-law proton spectrum, Eq. (5.5), with the normalisation constant for a point source, Eq. (5.9), yields

$$\Phi_{\nu_\mu}^{\rm Cen\ A}(E_\nu) = \frac{\varphi_p^{\rm Cen\ A}(E_{\rm th})}{3} \frac{\xi_\nu \eta_{\nu n}^{\alpha_p - 2}}{\xi_n} \frac{\alpha_p - 1}{E_{\rm th}} \left(\frac{E_\nu}{E_{\rm th}}\right)^{-\alpha_p} \left(\frac{E_\nu}{E_{\nu,{\rm br}}}\right) \min\left(1, \frac{E_\nu}{E_{\nu,{\rm br}}}\right) \tag{5.28}$$

for the muon-neutrino flux from Cen A, with $E_{\nu,{\rm br}} \equiv \eta_{\nu n} E_{\rm br} = 4 \times 10^6$ GeV. Koers & Tinyakov [86] considered mainly a proton spectral index $\alpha_p = 2.7$, which is the value that we have also adopted to calculate the detection prospects in Section 7.3. Giving values to the rest of the parameters, the muon-neutrino flux from Cen A

results in

$$\Phi_{\nu_\mu}^{\text{Cen A}}(E_\nu) \simeq 9.14\times10^{-37}\times\left(2.28\times10^{9}\right)^{\alpha_p}(\alpha_p-1)\,E_\nu^{1-\alpha_p}\min\left(1,\frac{E_\nu}{E_{\nu,\text{br}}}\right)\ . \quad (5.29)$$

Using the scaling relation, Eq. (5.24), the muon-neutrino diffuse flux in the KT model is therefore

$$\Phi_{\nu_\mu}^{\text{diff,KT}}(E_\nu) \simeq 1.9H'(E_{\text{th}})\,\Phi_{\nu_\mu}^{\text{Cen A}}(E_\nu)\ . \quad (5.30)$$

The KT muon-neutrino fluxes, multiplied by E_ν^2, are plotted in Fig. (5.1), for a spectral index $\alpha = 2.7$: the case without source evolution, as a dashed (red) line, and the case with strong source evolution, as a solid (black) line.

We have taken the all-flavour diffuse flux to be three times the ν_μ flux. The factor of three comes from the fact that, in the presence of standard neutrino oscillations, the flux at Earth is evenly divided between the three neutrino flavours. Thus,

$$\Phi_{\nu_{\text{all}}}^{\text{KT}}(E_\nu) \equiv \Phi_{\nu_{\text{all}}}^{\text{diff,KT}}(E_\nu) \simeq 5.7H'(E_{\text{th}})\,\Phi_{\nu_\mu}^{\text{Cen A}}(E_\nu)\ . \quad (5.31)$$

5.1.4 Model by Becker & Biermann

The BB model [87] describes the production of high-energy neutrinos in the relativistic jets of radio galaxies. According to the model, the UHECRs observed by the PAO originated at FR-I galaxies (relatively low-luminosity radio galaxies with extended radio jets, and radio knots distributed along them), which can in principle accelerate protons up to $\sim 10^{20}$ eV. Like in the KT model, here the protons are also shock-accelerated. Unlike the KT model, though, where the neutrino emission occurred in a region close to the AGN core, in the BB model the neutrino emission from $p\gamma$ interactions is expected to peak at the first strong shock along the jet, lying at a distance $z_j \sim 3000$ gravitational radii from the center.

The optical depth corresponding to proton interactions with the disc photon field, $\tau_{p\gamma_{\text{disc}}} \equiv 1/\lambda_{p\gamma_{\text{disc}}} = z_j\theta n_{\gamma_{\text{disc}}}\sigma_{p\gamma}$, for a source with disc luminosity $L_{\text{disc}} \sim 10^{44}$ erg s^{-1} is [87]

$$\tau_{p\gamma_{disc}} = 0.2\epsilon_{\text{Edd}}\left(\frac{\theta}{0.1}\right)\left(\frac{z_j}{3000r_g}\right)^{-1}\left(\frac{L_{\text{disc}}}{10^{44}\ \text{erg s}^{-1}}\right)\ , \quad (5.32)$$

where $\sigma_{p\gamma} \approx 900$ μbarn is the total $p\gamma$ cross-section for the production of the Δ^+ resonance, $\epsilon_{\text{Edd}} \leq 1$ is the accretion rate relative to the maximum, θ is the beam aperture angle, and the gravitational radius $r_g = 1.5\times10^{12}M_{\text{BH}}/\left(10^7M_\odot\right)$ cm, with

$M_{\rm BH}$ and $M_\odot$ the mass of the central supermassive black hole and of the Sun, respectively. The photon density is calculated as

$$n_{\gamma_{\rm disc}} = \frac{L_{\rm disc}}{4\pi z_j^2 ch\nu} \ , \tag{5.33}$$

where h is Planck's constant and the average photon energy in the disc $h\nu = 20$ eV. For $\epsilon_{\rm Edd} = 0.1$, the optical depth is $\tau_{p\gamma_{disc}} \approx 0.02$, and so $p\gamma$ interactions in the disc are not the dominant source of neutrinos. The proton-proton interactions that occur when the jet encounters the AGN's torus, at $z_j \sim 1 - 10$ pc, are also subdominant: given the torus column density $X \sim 4 \times 10^{23}$ cm^{-2} and the pp cross section $\sigma_{pp} \approx 50$ mb, the optical depth results

$$\tau_{pp_{\rm torus}} = X\sigma_{pp} \approx 2 \times 10^{-3} \ . \tag{5.34}$$

Thus, pp interactions are neglected in the BB model.

The dominant mechanism of neutrino production is the interaction between the accelerated protons and the synchrotron photons in the relativistic jet, at one of the jet's knots, which is assumed to contribute a fraction $\epsilon_{\rm knot} \approx 0.1$ of the total synchrotron luminosity, $L_{\rm synch} \sim 10^{40}$ erg s^{-1}. In this case, the optical depth is given by [87]

$$\tau_{p\gamma_{\rm synch}} \approx 0.9 \left(\frac{10}{\Gamma}\right) \left(\frac{\theta}{0.1}\right) \left(\frac{\epsilon_{\rm knot}}{0.1}\right) \left(\frac{L_{\rm synch}}{10^{40}\ {\rm erg\ s^{-1}}}\right) \left(\frac{z_j}{3000 r_g}\right)^{-1} \left(\frac{\nu}{1\ {\rm GHz}}\right)^{-1} \ , \tag{5.35}$$

where $\nu \approx 1$ GHz is the frequency of the synchrotron photons. For boost factors of $\Gamma \sim 10$, the optical depth $\tau_{p\gamma_{\rm synch}} \sim 1$. Hence, it is expected that neutrino emission occurs predomninantly at the foot of the jet, where the beam is still highly collimated. Therefore, the BB model predicts a highly beamed neutrino emission, produced in the first shock ($z_j \sim 3000 r_g$), and consequently observable only from sources whose jets are directed towards Earth. Flat-spectrum radio sources, such as FR-I galaxies whose jets are pointing towards Earth, will have correlated neutrino and proton spectra, while steep-spectrum sources, which are AGN seen from the side, are expected to be weak neutrino sources, but to contribute to the cosmic-ray proton flux.

The BB model assumes that the $N_{\rm evts} = 20$ events that were observed by the PAO to have a positional correlation to sources in the Véron-Cetty & Véron catalogue were indeed originated at AGN lying in the supergalactic plane. The normalisation constant of the proton spectrum, A_p, is given by Eq. (5.8) with this value for $N_{\rm evts}$. We now need a connection between A_p and the corresponding normalisation constant

for neutrinos, A_ν. To this end, consider the total neutrino and total proton energy fluxes radiated in the solid angles Ω_ν and Ω_p, respectively, in the shock rest frame (i.e., denoted by primed variables):

$$\Omega_\nu j'_\nu = \int E'_\nu \frac{dN_\nu}{dE'_\nu} dE'_\nu \quad , \quad \Omega_p j'_p = \int E'_p \frac{dN_p}{dE'_p} dE'_p \ . \tag{5.36}$$

These are connected by

$$\Omega_\nu j'_\nu = \frac{\tau_{p\gamma}}{12} \Omega_p j'_p \ , \tag{5.37}$$

where the factor 1/12 is due to the branching ratio of Δ^+ to charged pions (see Eq. (5.2)) and to the fact that half of the energy of the pion is transferred to the muon neutrinos ($\nu_\mu + \overline{\nu}_\mu$). The energy fluxes at Earth are given by

$$j = \frac{\Gamma}{4\pi} j' n \ , \tag{5.38}$$

where

$$j' \equiv \int_{E'} dE' \ E' \frac{dN}{dE'} \tag{5.39}$$

is the energy flux in the shock rest frame and

$$n \equiv \int_{z_{\min}}^{z_{\max}} \int_{L_{\min}}^{L_{\max}} dz \ dL \frac{1}{4\pi d_L^2 \, (z)} \frac{d^2 n}{dV dL} \frac{dV}{dz} \tag{5.40}$$

is the total number of sources. In this last expression, d_L is the luminosity distance of the source, $d^2n/dVdL$ is the luminosity function of the sources (the distribution of sources as a function of redshift and luminosity) and dV/dL is the differential comoving volume. Because strong neutrino sources are weak CR proton sources, the luminosity function will be different for neutrinos and protons: for the former, the model assumes the FR-I radio luminosity function by Willot [97], while for the latter, the luminosity function by Dunlop & Peacock is employed [98]. The lower redshift integration limit for CR proton sources, $z^{\rm CR}_{\rm min} = 0.0008$, corresponds to the closest FR-I sources, while the one for neutrinos, $z^{\nu}_{\rm min} = 0.018$, corresponds to the closest FRS sources. The absolute upper integration limit, $z^{\rm CR}_{\rm max} = 0.03$, marks the outskirts of the supergalactic plane and is thus common for both neutrinos and protons; we will, however, maintain $z^{\rm CR}_{\rm max}$ as a free parameter in our analysis, with 0.03 as its maximum value. The luminosity integration limits, $L_{\rm min} = 10^{40}$ erg s^{-1} and $L_{\rm max} = 10^{44}$ erg s^{-1}, are obtained from the distribution of FR-I galaxies (FRS galaxies are believed to be a subclass of FR-I, so the limits apply to them as

well [87]). Replacing the expressions for the energy fluxes in Eq. (5.37) yields

$$j_\nu = \frac{\tau_{p\gamma}}{12}\frac{\Gamma_\nu}{\Gamma_p}\frac{\Omega_p}{\Omega_\nu}\frac{n_\nu}{n_p} j_p \ . \tag{5.41}$$

On the other hand, assuming a power-law behaviour for the diffuse differential flux of protons, i.e., $\Phi_p^{\rm diff} \equiv dN_p/dE_p = A_p E_p^{-\alpha_p}$, the integrated energy flux results

$$j_p = A_p \int_{E_{p,\rm min}}^{E_{p,\rm max}} E_p \frac{dN_p}{dE_p}\, dE_p = \begin{cases} A_p \left(\alpha_p - 2\right)^{-1} E_{p,\rm min}^{-\alpha_p+2} & , \text{ if } \alpha_p \neq 2 \\ A_p \ln\left(E_{p,\rm max}/E_{p,\rm min}\right) & , \text{ if } \alpha_p = 2 \end{cases} , \tag{5.42}$$

where the term proportional to $E_{p,\rm max}^{-\alpha_p+2}$ has been neglected, in the case when $\alpha_p \neq 2$. The normalisation constant A_p is given by Eq. (5.8). Assuming that the neutrino spectrum follows the proton spectrum, i.e., $\Phi_{\nu_\mu}^{\rm diff,BB} = A_\nu E_\nu^{-\alpha_\nu}$ with $\alpha_\nu \approx \alpha_p$, the energy flux for neutrinos is

$$j_\nu \simeq \begin{cases} A_\nu \left(\alpha_p - 2\right)^{-1} E_{\nu,\rm min}^{-\alpha_p+2} & , \text{ if } \alpha_p \neq 2 \\ A_\nu \ln\left(E_{\nu,\rm max}/E_{\nu,\rm min}\right) & , \text{ if } \alpha_p = 2 \end{cases} . \tag{5.43}$$

The lower integration limits for protons and neutrinos are, respectively, $E_{p,\rm min} = \Gamma_p m_p \approx \Gamma_p \cdot (1\ \text{GeV})$ and $E_{\nu,\rm min} = \Gamma_\nu \cdot (m_\pi/4) = \Gamma_\nu \cdot (0.035\ \text{GeV})$. Finally, we see that when $\alpha_p \neq 2$, the neutrino normalisation constant is given by

$$A_\nu \simeq \frac{\tau_{p\gamma}}{12}\left(\frac{\Gamma_\nu}{\Gamma_p}\right)^{\alpha_p+1} \frac{n_\nu}{n_p}\left(\frac{m_\pi}{4}\right)^{\alpha_p-2} \frac{N_{\rm evts}\left(\alpha_p - 1\right)}{\Xi} E_{\rm th}^{\alpha_p-1} \ . \tag{5.44}$$

To arrive at this expression[1], it must be noted that because of the relativistic beaming in the jets, the emission solid angles are $\Omega_\nu \sim 1/\Gamma_\nu^2$ and $\Omega_p \sim 1/\Gamma_p^2$. When $\alpha_p = 2$, the logarithms in the two spectra are similar and cancel out, making the previous expression for A_ν valid also for $\alpha_p = 2$. The BB muon-neutrino flux, multiplied by E_ν^2, is plotted in Fig. (5.1), for a spectral index $\alpha_p = 2.7$, $\Gamma_\nu/\Gamma_{\rm CR} = 3$, and $z_{\rm CR}^{\rm max} = 0.03$.

As for the WB and KT fluxes, we have set the all-flavour BB flux of three times the corresponding ν_μ flux, i.e.,

$$\Phi_{\nu_{\rm all}}^{\rm BB}\left(E_\nu\right) = 3\Phi_{\nu_\mu}^{\rm diff,BB}\left(E_\nu\right) \ . \tag{5.45}$$

[1]The reader should be wary that in their paper [87], Becker & Biermann incorrectly reported a dependence of the form $\sim \left(\Gamma_\nu/\Gamma_p\right)^{5-\alpha_p}$.

5.2 Neutrino decay

Since we are considering neutrinos that travel distances of tens or hundreds of Mpc, neutrino decay is a possibility. Flavour mixing and decays in astrophysical neutrinos have been explored before, e.g., in [73, 99, 100] The current strongest direct limit on neutrino lifetime, $\tau/m \gtrsim 10^{-4}$ s eV^{-1}, was obtained using solar neutrino data [101]. More stringent, though indirect, limits can be obtained by considering neutrino radiative decays and using cosmological data [102]: $\tau >$ few $\times 10^{19}$ s or $\tau \gtrsim 5 \times 10^{20}$ s, depending on the mass hierarchy and the absolute mass scale. Assuming that the heaviest mass eigenstates decay into the lightest one plus an undetectable light or massless particle (e.g., a sterile neutrino), then, following [74], the flux of flavour α at Earth will be

$$\phi_\alpha = \sum_{\beta=e,\mu,\tau} \sum_i \phi^0_\beta |[U_0]_{\beta i}|^2 |[U_0]_{\alpha i}|^2 e^{-L/\tau_i} \xrightarrow{L \gg \tau_i} \sum_{\beta=e,\mu,\tau} \sum_{i(\text{stable})} \phi^0_\beta |[U_0]_{\beta i}|^2 |[U_0]_{\alpha i}|^2 \ , \tag{5.46}$$

where τ_i is the lifetime of the i-th mass eigenstate in the laboratory frame. As explained in [74], this expression corresponds to the case where the decay has been completed when the neutrinos arrive at Earth. In a normal hierarchy, ν_1 is the only stable state and so

$$\phi^{\text{dec,norm}}_\alpha = |[U_0]_{\alpha 1}|^2 \sum_{\beta=e,\mu,\tau} \phi^0_\beta |[U_0]_{\beta 1}|^2 \ , \tag{5.47}$$

while in an inverted hierarchy ν_3 is the stable state and

$$\phi^{\text{dec,inv}}_\alpha = |[U_0]_{\alpha 3}|^2 \sum_{\beta=e,\mu,\tau} \phi^0_\beta |[U_0]_{\beta 3}|^2 \ . \tag{5.48}$$

Ref. [74] provides expressions for the flavour fluxes when the decay product accompanying the lightest eigenstate can also be detected, but since the focus of our analysis is the modification of the oscillations through terms of the form Eq. (7.2), we have chosen to include only the simplest case of neutrino decay, described by the two preceding expressions.

Chapter 6

CPT violation through modified dispersion relations

Note: the results in this chapter have been adapted from refs. [103, 104].

Experimental evidence has confirmed that flavour transitions are the solution to the former so-called solar and atmospheric neutrino deficit problems [2, 6, 105]. Further evidence was provided by experiments performed with neutrinos generated in particle accelerators and nuclear reactors, such as KamLAND [106] and K2K [7]. The mechanism responsible for these transitions requires neutrinos to be massive: the probability of a flavour transition is oscillatory, with oscillation length $\lambda^{\text{std}} \equiv 4\pi E/\Delta m^2$, where E is the neutrino energy and Δm^2 is the difference of the squared masses of the different neutrino mass eigenstates. However, even though this mass-driven mechanism is the dominant one in the energy regimes that have been explored experimentally (MeV–TeV), there is still the possibility that alternative mechanisms contribute to the flavour transitions in a subdominant manner, which perhaps can manifest at higher energies.

Although these alternative mechanisms involving new physics (NP) are able to produce flavour transitions, it is known that none of them can explain the combined data from atmospheric, solar, accelerator, and reactor neutrino experiments performed in the MeV–TeV range, unlike the pure Δm^2 oscillation mechanism [10, 107–109]. Some of these alternatives [110] are the violation of the equivalence principle (VEP), of Lorentz invariance [111, 112] (VLI), of CPT invariance (CPTV), the non-universal coupling of neutrinos to a space-time torsion field (NUCQ), decoherence during the neutrino's trip, and non-standard interactions (NSI).

Typically, these mechanisms result in oscillation lengths λ^{NP} that have a different

dependence on E, usually expressed as a power-law, $\lambda^{\rm NP} \sim E^n$, with the value of n depending on which mechanism is being considered: for instance, $n = 0$ for CPTV and NUCQ and $n = 1$ for VEP and VLI, while with $n = -1$ the standard Δm^2 oscillations are recovered. Atmospheric events from Super-Kamiokande (SK) [10] were used to find the value $n = -0.9 \pm 0.4$ at 90% C.L., thus confirming the dominance of the Δm^2 oscillation mechanism and forcing any other mechanisms to be subdominant, at least within the energy range and pathlength considered in said analysis.

So far, searches for NP effects in neutrino oscillations have been limited to energies ranging from a few MeV to a few GeV [10, 107–109] and have turned out negative. However, proposals for analyses of atmospheric neutrinos with energies of up to 10^4 TeV in second-generation neutrino detectors such as IceCube [113] and ANTARES [114] are being considered. Due to the energy dependence of the oscillation lengths, the oscillation phases scale as $\left(2\pi L/\lambda^{\rm NP}\right) / \left(2\pi/\lambda^{\rm std}\right) \sim E^{1-n}$, that is, the relative dominance of the NP contribution grows with the neutrino energy provided that $n \leq 0$, so that the observation of very energetic neutrinos -such as the ones expected from presumed cosmic accelerators like active galaxies and gamma ray bursts- would offer a means to establish whether the Δm^2 oscillation mechanism is still the dominant one at high energies or to otherwise set stronger bounds on the NP parameters.

In this chapter, we have introduced the aforementioned new physics through the use of a modified dispersion relation, and focused our analysis on the case of $n = 0$, corresponding, as we will see, to an energy-independent NP contribution to the neutrino flavour oscillation phase. We have calculated the proportion of each flavour arriving at Earth from distant cosmic accelerators and explored how it is affected by the parameters that control the new physics, and whether these effects are observable at all.

6.1 Flavour-transition probability in the presence of a modified dispersion relation

The NP effects can modify flavour transitions in two ways [114]: by transforming both the oscillation length and the neutrino mixing angles or by altering only the first. The former case occurs, for instance, when considering the low energy phenomenological model of string theory, known as the Standard Model Extension [110] (see Chapter 3) and has been examined using SK and K2K data [107, 113]. The second case can be achieved by considering a modified dispersion relation which departs

from the well-known formula $E^2 = p^2 + m^2$. Because we wish to explore whether solely effects on the phase are observable at high energies, we follow this second alternative and consider the following modified dispersion relation [115], which allows us to study the contributions of NP effects in a model-independent way:

$$E^2 = p^2 + m^2 + \eta' p^2 \left(\frac{E}{m_P}\right)^{\alpha} = p^2 + m^2 + \eta p^2 E^{\alpha} \ , \tag{6.1}$$

where $m_{Pl} \simeq 10^{19}$ GeV is the Planck mass, $\eta' = \eta m_{Pl}^{\alpha}$ is an adimensional parameter that controls the strength of the NP effects and, following the literature, α has been chosen to be of integer value. Such a dispersion relation assumes that the scale of NP effects is the Planck scale where, according to theories of quantum gravity, space-time might become "foamy". Eq. (6.1) was recently [114] used to predict the sensitivity of the ANTARES neutrino telescope to NP effects in the high-energy atmospheric neutrino flux.

We now derive the flavour-transition probability in the presence of NP effects, for neutrinos that propagate over a cosmological distance. As we saw in Chapter 4, flavour transitions arise as a consequence of the fact that flavour eigenstates $|\nu_\alpha\rangle$ $(\alpha = e, \mu, \tau)$ are not also mass eigenstates $|\nu_i\rangle$ $(i = 1, 2, 3)$, but rather a linear combination of them, i.e., $|\nu_\alpha\rangle = \sum_{i=1}^{3} [U_0]^*_{\alpha i} |\nu_i\rangle$, with $[U_0]^*_{\alpha i}$ elements of the neutrino mixing matrix.

Using the standard dispersion relation, it is a common procedure to derive an approximate expression for the momentum of the i-th neutrino mass eigenstate,

$$p_i = \sqrt{E^2 - m_i^2} \simeq E - \frac{m_i^2}{2E} \ , \tag{6.2}$$

where m_i is the mass of the neutrino and E is its energy, and are such that, at the energies that we have considered, $m_i \ll E$. From this equation we obtain the usual expression for the momenta difference:

$$\Delta p_{ij} \equiv p_j - p_i = \frac{\Delta m_{ij}^2}{2E} \ . \tag{6.3}$$

In accordance with the latest bounds obtained from global fits [50], we have set the three mixing angles that parametrise U to $\sin^2(\theta_{12}) = \sqrt{0.304}$, $\theta_{13} = 0$ and $\theta_{23} = \pi/4$. The mass-squared differences have been set to $\Delta m_{21}^2 = 8.0 \times 10^{-5}$ eV^2 and $\Delta m_{32}^2 = 2.5 \times 10^{-3}$ eV^2, and we have assumed a normal mass hierarchy (i.e., $m_3 > m_1$), so that $\Delta m_{31} = \Delta m_{32} + \Delta m_{21}$. The probability that a neutrino created with flavour α is detected as having flavour β after having propagated a distance L

in vacuum is given by (compare this with Eq. (4.48))

$$P_{\alpha\beta}\left(E,L\right)=\delta_{\alpha\beta}-4\sum_{i>j}\mathrm{Re}\left(J_{ij}^{\alpha\beta}\right)\sin^{2}\left(\frac{\Delta p_{ij}}{2}L\right)\ , \tag{6.4}$$

with the $J_{ij}^{\alpha\beta}$ defined in Eq. (4.49). Since we have in this chapter set $\theta_{13}=0$, U_0 is a real matrix, independent of the CP-violation phase, δ_{CP}.

In the case of the modified dispersion relation of Eq. (6.1) we can also find an expression for the momenta difference. To first order in η_i, and discarding terms higher than second power in m_i or involving $\eta_i m_i^2$, we obtain

$$p_i\simeq E-\frac{m_i^2}{2E}-\frac{\eta_i E^n}{2}\ , \tag{6.5}$$

with $n\equiv\alpha+1$, and hence

$$\Delta\tilde{p}_{ij}=\frac{\Delta m_{ij}^2}{2E}+\frac{\Delta\eta_{ij}^{(n)}E^n}{2}\ , \tag{6.6}$$

where $\Delta\eta_{ij}^{(n)}\equiv\eta_i^{(n)}-\eta_j^{(n)}$, for the NP mechanism with an E^n energy dependence. Note that it is necessary that the η_i have different values for different mass eigenstates in order to have a nonzero NP contribution to the momenta difference. The corresponding oscillation probability is Eq. (6.4) with $\Delta p_{ij}\to\Delta\tilde{p}_{ij}$; hence, the NP affects solely the oscillation phase, but not its amplitude.

Since $L\gg 1$ for high-energy astrophysical neutrinos, $\sin^2\left(\Delta p_{ij}L/2\right)$ is a rapidly oscillating function and so, due to the limited energy resolution of neutrino telescopes, the average flavour-transition probability, Eq. (4.55), is sometimes used instead, i.e.,

$$\langle P_{\alpha\beta}\rangle=\sum_i|U_{\alpha i}|^2|U_{\beta i}|^2\ . \tag{6.7}$$

Let $\langle P_{\alpha\beta}\rangle^{\mathrm{std}}$ be the standard average probability, that is, when there are no NP effects present. If the extra term in $\Delta\tilde{p}_{ij}$ has $n>0$, its effect will be that, at high energies, $P_{\alpha\beta}$ will oscillate even more rapidly with energy, but still around the same mean value $\langle P_{\alpha\beta}\rangle^{\mathrm{std}}$. If $n<0$, the oscillations will continue up to high energies, also around the same mean, and at a high enough value, when $\Delta p_{ij}=\Delta m_{ij}^2/2E\to 0$, the probability will tend to zero. However, if $n=0$, then the extra term in $\Delta\tilde{p}_{ij}$ is energy-independent and so when $\Delta p_{ij}\to 0$, $P_{\alpha\beta}$ becomes constant, but different from zero due to the existence of the extra term. Furthermore, when this happens, and depending on the values of the $\Delta\eta_{ij}^{(0)}$, it is in principle possible for the constant probability to be different from $\langle P_{\alpha\beta}\rangle^{\mathrm{std}}$. Such a nonzero, constant probability at

high energies could therefore be interpreted as being due to the contribution from energy-independent new physics. We will focus on this possibility.

Although our analysis of NP effects using Eq. (6.1) is model-independent, $\Delta\eta^{(0)}$ takes a different form depending on the particular mechanism being considered [107, 113]. In the energy-independent oscillation mechanism that we are focusing on, the extra contribution could be due to CPTV through Lorentz invariance violation, in which case

$$\Delta\eta_{ij}^{(0)} = b_i - b_j \equiv b_{ij} \ , \tag{6.8}$$

with b_i the eigenvalues of the Lorentz-violating CPT-odd operator [107] $\overline{\nu}_L b_\mu^{\alpha\beta}\gamma_\mu\nu_L^\beta$. Alternatively, the contribution could be due to NUCQ, and in this case [15] we would consider different couplings, $k_i \neq k_j$ (for mass eigenstates i and j), to a torsion field Q, so that

$$\Delta\eta_{ij}^{(0)} = Q\left(k_i - k_j\right) \equiv Qk_{ij} \ . \tag{6.9}$$

Strict bounds [107] have been set on the parameters that control the energy-independent NP mechanism using data from atmospheric and solar neutrinos, as well as SK and K2K, with energies up to about 1 TeV:

$$b_{21} \leq 1.6 \times 10^{-21} \text{ GeV} \quad , \quad b_{32} \leq 5.0 \times 10^{-23} \text{ GeV} \ . \tag{6.10}$$

Because the relative dominance of the NP energy-independent phase over the standard oscillation phase increases with neutrino energy, i.e., $\left(\Delta\tilde{p}_{ij} - \Delta p_{ij}\right)/\Delta p_{ij} \sim E$, we would like to look at the most energetic neutrinos available. Hence, we will consider neutrinos originating at cosmic accelerators, such as active galactic nuclei (see Chapter 4), where it is presumed that they are created with energies of up to 10^{12} GeV. Because the typical distance to these accelerators is in the order of hundreds of Mpc, we will include in the flavour-transition probability the effect of cosmological expansion. Hence, instead of the argument that appears in the sine of Eq. (6.4), we define an accumulated phase [116] ϕ_{ij} as follows:

$$\phi_{ij}\left(t_f, t_i\right) = \int_{t_i}^{t_f} \Delta p_{ij}\left(\tau\right) d\tau = \int_{t_i}^{t_f} \frac{\Delta m_{ij}^2}{2E_o}\left(\frac{\tau}{t_o}\right)^{2/3} d\tau \tag{6.11}$$

$$= \frac{3}{10}\frac{\Delta m_{ij}^2 t_o}{E_o}\left[\left(\frac{t_f}{t_o}\right)^{5/3} - \left(\frac{t_i}{t_o}\right)^{5/3}\right] \ , \tag{6.12}$$

where t_i and t_f are the times at which the neutrino was produced and detected, respectively; $t_o = 13.7$ Gyr is the age of the Universe [29]; and we have used the relation between the energy at detection (E_o) and production epochs (E), in an

adiabatically expanding universe:

$$E(\tau) = E_o (t_o/\tau)^{2/3} = E_o (1+z) \ . \tag{6.13}$$

Considering the detection time t_f in the present epoch, $t_f = t_o$, we obtain the accumulated phase

$$\phi_{ij}(E_o, z) = 1.97 \times 10^{23} \frac{\Delta m^2_{ij}\,[\mathrm{eV}^2]}{E_o\,[\mathrm{GeV}]} \left[1 - (1+z)^{-5/2}\right] \ , \tag{6.14}$$

where we have made use of the relation $t_i/t_o = (1+z)^{-3/2}$.

By replacing the momenta difference Δp_{ij} with $\Delta \tilde{p}_{ij}$, we obtain, correspondingly,

$$\tilde{\phi}_{ij}(E_o, z) = \phi_{ij}(E_o, z) + \frac{\Delta \eta^{(n)}_{ij} E_o^n t_o}{2} \left[1 - (1+z)^{n-3/2}\right] \tag{6.15}$$

$$\equiv \phi_{ij}(E_o, z) + \xi^{(n)}_{ij}(E_o, z) \ , \tag{6.16}$$

with $\xi^{(n)}_{ij}$ the contribution to the phase due to the NP effects. For $n = 0$,

$$\xi^{(0)}_{ij}(E_o, z) = 3.28 \times 10^{41} b_{ij}\,[\mathrm{GeV}] \left[1 - (1+z)^{-3/2}\right] \ . \tag{6.17}$$

Hence, instead of the traditional expression in Eq. (6.4) for $P_{\alpha\beta}$, we will employ

$$P^{\mathrm{cosm}}_{\alpha\beta}(E_o, z) = \delta_{\alpha\beta} - 4 \sum_i \mathrm{Re}\left(J^{\alpha\beta}_{ij}\right) \sin^2\left(\frac{\phi_{ij}}{2}\right) \ , \tag{6.18}$$

where the explicit expression for $\phi_{ij} \equiv \phi_{ij}(E_o, z)$ is either of Eqs. (6.14) or (6.15), depending on which dispersion relation is being considered[1].

6.2 Observability of the NP effects in the high-energy neutrino flavour ratios

Using the flavour-transition probability obtained in the previous section, Eq. (6.18), we can calculate the ratio of neutrinos of each flavour to the total number of neutrinos that arrive at the detector from a source with redshift z. For α-flavoured neutrinos

[1] In the limit of very small z, Eq. (6.18) reduces to Eq. (6.4), the expression for the transition probability for neutrinos that travel much less than cosmological distances, i.e., solar, atmospheric and reactor neutrinos. This can be seen by making $t_i = t_o - \Delta t$ in Eq. (6.11), with $\Delta t \ll 1$, and discarding terms of order $(\Delta t)^2$ and higher.

$(\alpha = e, \mu, \tau)$ with energy E_o, this is

$$\Upsilon^D_{\nu_\alpha}(E_o, z) = \sum_{\beta=e,\mu,\tau} P^{\text{cosm}}_{\beta\alpha}(E_o, z)\, \Upsilon^S_{\nu_\beta} \,, \tag{6.19}$$

where $\Upsilon^D_{\nu_\alpha}$ is the ratio at the detector and $\Upsilon^S_{\nu_\beta}$ is the ratio at the source. The latter is estimated assuming that neutrinos are secondaries of high-energy proton-proton or proton-photon collisions (see Chapter 4), which produce pions that decay into neutrinos and muons which decay into neutrinos too [75, 117, 118]: $\pi^+ \longrightarrow \mu^+\ \nu_\mu \longrightarrow e^+\ \nu_e\ \overline{\nu}_\mu\ \nu_\mu$, $\pi^- \longrightarrow \mu^-\ \overline{\nu}_\mu \longrightarrow e^-\ \overline{\nu}_e\ \nu_\mu\ \overline{\nu}_\mu$. It is easy to see that $\Upsilon^S_{\nu_e} : \Upsilon^S_{\nu_\mu} : \Upsilon^S_{\nu_\tau} = 1/3 : 2/3 : 0$. (Actually, ν_τ *are* expected to be produced through the decay of $D_s^\pm$ charmed mesons generated also in pp and $p\gamma$ collisions. However, $D_s^\pm$ production is strongly suppressed [75] and $\Upsilon^S_{\nu_\tau} < 10^{-5}$.)

The $\Upsilon^D_{\nu_\alpha}$ are very rapidly oscillating functions of energy. Taking into account the limited energy sensitivity of current and envisioned neutrino telescopes (AMANDA-II, for instance, had an energy resolution of 0.4 in the logarithm of the energy of the ν_μ-spawned muon [119]), we see that they are sensitive not to the instantaneous value of the ratios, $\Upsilon^D_{\nu_\alpha}(E_o, z)$, but rather to the energy-averaged flavour ratios

$$\langle \Upsilon^D_{\nu_\alpha}(E_o, z) \rangle = \frac{1}{\Delta E_o} \int_{E_o^{\min}}^{E_o^{\max}} \Upsilon^D_{\nu_\alpha}(E'_o, z)\ dE'_o \,, \tag{6.20}$$

where $E_o^{\min} = E_o - \delta E_o$, $E_o^{\max} = E_o + \delta E_o$ and $\Delta E_o \equiv E_o^{\max} - E_o^{\min} = 2\delta E_o$, with δE_o a small energy displacement. Without the NP effects, the high-energy neutrino flux from a distant astrophysical source is equally distributed among the three flavours, i.e., $\langle \Upsilon^D_{\nu_e} \rangle : \langle \Upsilon^D_{\nu_\mu} \rangle : \langle \Upsilon^D_{\nu_\tau} \rangle = 1/3 : 1/3 : 1/3$.

In the presence of NP effects, however, the detected flavour ratios might be modified. Given that the relative dominance of the energy-independent NP phase $\xi^{(0)}_{ij}$ over the standard phase ϕ_{ij} grows with energy, i.e., $\xi^{(0)}_{ij}/\phi_{ij} \sim E_o$, we would expect that any modifications became more pronounced in the UHE range, PeV–EeV, or higher. As explained in Section 6.1, while the NP phase remains constant in energy, the standard phase decreases and, as a consequence, beyond a certain threshold (determined by the values of the b_{ij}), the detected ratios $\Upsilon^D_{\nu_\alpha}$ would acquire a constant nonzero value, which might differ from the standard ratios $1/3 : 1/3 : 1/3$, thus providing a distinct phenomenological signature of a possible energy-independent contribution to the oscillation phase.

As a means of estimating the values of the b_{ij} for which the NP phase starts to be of importance, we can demand that $\xi^{(0)}_{ij} \sim \phi_{ij}$. From this requirement, we can calculate, for given values of the b_{ij}, the energy E^{NP} above which the NP effects are

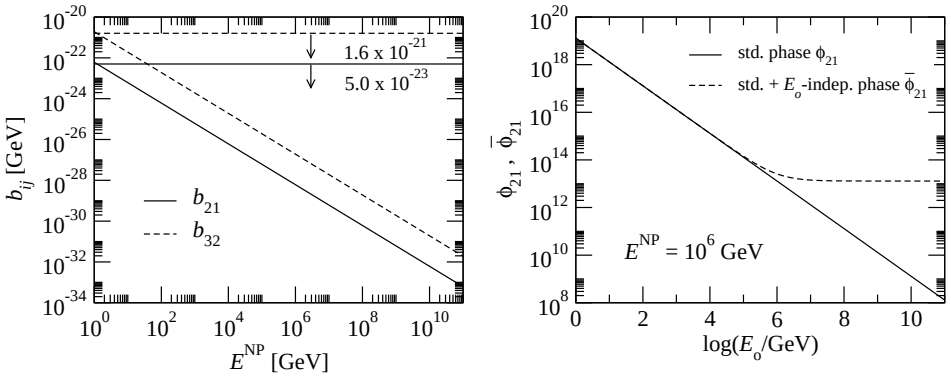

Figure 6.1: *Left:* Eigenvalues b_{21} and b_{32} as functions of $E^{\rm NP}$, the energy at which the standard and NP energy-independent oscillation phases become comparable, i.e., $\phi_{ij} \sim \xi^{(0)}_{ij}$, according to Eq. (6.21). The redshift $z = 1$. The current upper bounds are plotted as horizontal lines. Notice that, due to these bounds, $E^{\rm NP}$ cannot be lower than about 1 GeV. *Right:* Standard oscillation phase ϕ_{21} and phase including the energy-independent contribution, $\tilde{\phi}_{21}$, as functions of neutrino energy. The redshift $z = 1$. Note that the phases start to differ at $E^{\rm NP} = 10^6$ GeV, which corresponds to $b_{21} = 6.1 \times 10^{-29}$ GeV and $b_{32} = 1.9 \times 10^{-27}$ GeV. Below this energy, they are indistinguishable.

expected to become increasingly more dominant in the oscillation. Doing this, we obtain

$$E^{\rm NP}\,[\text{GeV}] = 6 \times 10^{-19} \frac{\Delta m^2_{ij}\,[\text{eV}^2]}{b_{ij}\,[\text{GeV}]} \frac{1-(1+z)^{-5/2}}{1-(1+z)^{-3/2}} \,. \tag{6.21}$$

The left panel of Fig. 6.1 shows a plot of b_{21} and b_{32} as functions of $E^{\rm NP}$. The current upper bounds are shown as horizontal lines. The lower the value of $E^{\rm NP}$, the earlier the NP effects would manifest. Notice that, due to the current bounds, $E^{\rm NP}$ cannot be lower than about 1 GeV. The plots have been generated for a fixed $z = 1$; for lower values of z we will have a higher value of b_{ij} (30% if we take $z = 0.03$), while we will obtain a decrease in the values of b_{ij} for large z (a 20% decrease for $z = 6$). The right panel of Fig. 6.1 shows the standard and the energy-independent NP phases, ϕ_{21} and $\tilde{\phi}_{21}$, respectively, as functions of neutrino energy, assuming that $E^{\rm NP} = 10^6$ GeV. Notice that the phases start to differ precisely at this energy.

For concreteness, we will study the detected ratio of ν_μ defined in Eq. (6.20), since our conclusions are independent of the chosen flavour. Fig. 6.2 shows the predicted ratio calculated for different values of b_{21} and b_{32} (we have assumed that $b_{31} = b_{32} + b_{21}$) as a function of E_o.

Fig. 6.2 shows that $\Upsilon^D_{\nu_\mu}$ indeed becomes constant and different from 1/3 after a certain energy threshold. This occurs when the standard phase $\phi_{ij} \to 0$, so that, effectively, the oscillation phase is reduced to the energy-independent NP contri-

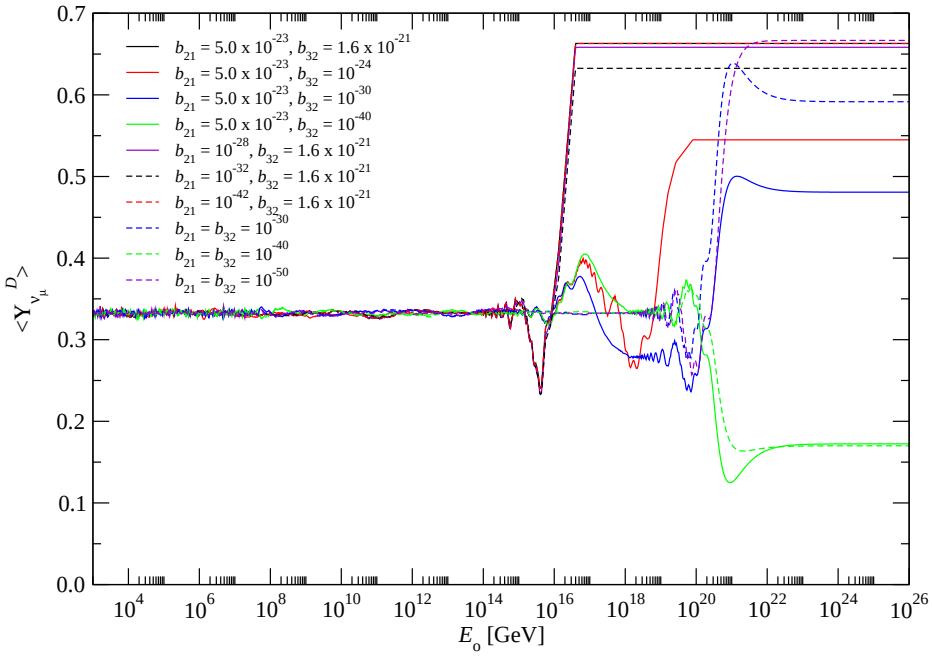

Figure 6.2: Energy-averaged detected ν_μ ratio $\Upsilon^D_{\nu_\mu}$, Eq. (6.20), as a function of neutrino energy E_o, for different values of the b_{ij}. Note that the ratio becomes constant only for unrealistically high energies: $\sim 10^{16.5}$ GeV in the best case, when the b_{ij} are set to their upper bounds. For lower values of the b_{ij}, the energy at which the ratio becomes constant is higher. The neutrino flux from cosmic accelerators is predicted to span up to about 10^{11} GeV; hence, the regime of constant $\Upsilon^D_{\nu_\mu}$ due to an energy-independent contribution to the oscillation phase would not be observable.

bution, i.e., $\tilde{\phi}_{ij} \to \xi^{(0)}_{ij}$, and the transition probabilities become constant. Note, however, that $\Upsilon^D_{\nu_\mu}$ is constant only for $E_o \gtrsim 10^{16.5}$ GeV in the most promising case, that is, when the b_{ij} equal their current upper bounds. This is about five orders of magnitude higher than the energy of the most energetic neutrinos expected from cosmic accelerators. For smaller values of these parameters, the energy at which the ratio becomes constant is even higher. Using closer or more distant sources, effectively decreasing or increasing z, does not affect the energy threshold, but only modifies the constant value reached by $\Upsilon^D_{\nu_\mu}$. Therefore, we conclude that, given the current upper bounds on the b_{ij}, an energy-independent NP contribution to neutrino oscillations would be visible in the high-energy astrophysical neutrino flux only if it modifies the oscillation amplitude (i.e., the mixing angles), as well as the phase.

In light of this conclusion, within the formalism used in the present work, a comparative calculation, with and without NP effects, of high-energy astrophysical neutrinos detected at a second-generation neutrino telescope such as IceCube becomes unnecessary.

6.3 Summary and conclusions

We have considered the effect of a modified dispersion relation on the detected flavour ratios of high-energy neutrinos from cosmic accelerators. In the scenario of new physics that we have explored, the flavour oscillation phases are modified by the addition of energy-independent terms which depend on the parameters b_{ij}. This contribution could correspond to a violation of CPT symmetry or to a nonuniversal neutrino coupling to a torsion field. The current upper bounds on the b_{ij} are strict: $b_{21} \leq 5.0 \times 10^{-23}$ GeV and $b_{32} \leq 1.6 \times 10^{-21}$ GeV.

At sufficiently high energies, the oscillation phases are dominated by the energy-independent terms and the flavour ratios become constant and, possibly (depending on the values of the b_{ij}) different from the average value of the ratios in the standard oscillation case, when new physics effects are absent. We have found, however, that even in the best case, when the b_{ij} are set to their upper bounds, the ratios are constant only for energies above $10^{16.5}$ GeV, about five orders of magnitude higher than the most energetic neutrinos that are expected from cosmic accelerators. Lower values of the b_{ij} will only result in higher energy thresholds for the ratios to become constant.

Therefore, we conclude that, even though there could be, in principle, a clear signature of the presence of energy-independent contributions to the neutrino flavour oscillations, these are not detectable in the flavour ratios of high-energy neutrinos from cosmic accelerators if they affect solely the oscillation phases. This will be the subject of the next chapter.

Chapter 7

CPT violation in astrophysical neutrinos in the Standard Model Extension

Note: the results in Section 7.2 have been adapted from [120, 121].

In Chapter 3, we saw that the lepton sector of the Standard Model Extension contains the Lorentz-violating contributions [13]

$$\mathcal{L}_{\text{LIV}} \supset -\left(a_L\right)_{\mu\alpha\beta}\overline{L}_\alpha\gamma^\mu L_\beta + \frac{1}{2}i\left(c_L\right)_{\mu\nu\alpha\beta}\overline{L}_\alpha\gamma^\mu \overleftrightarrow{D}^\nu L_\beta \ , \tag{7.1}$$

with α, β flavour indices. The first term is CPT-odd, with the coefficients a_L having dimensions of mass, while the second term is CPT-even, with the c_L dimensionless. Because we are interested in an energy-independent CPTV contribution, we have kept only the first term in the Lagrangian. In the neutrino sector, then, CPT violation can be introduced through an effective, model-independent, vector coupling of the form [122]

$$\mathcal{L}^\nu_{\text{CPTV}} = b_{\mu\alpha\beta}\overline{\nu}_\alpha\gamma^\mu\nu_\beta \ . \tag{7.2}$$

The vector $\overline{\nu}_\alpha\gamma^\mu\nu_\beta$ is CPT-odd and the $b_{\mu\alpha\beta}$ are real coefficients, so $\mathcal{L}^\nu_{\text{CPTV}}$ is CPT-odd, i.e., $\text{CPT}\left(\mathcal{L}^\nu_{\text{CPTV}}\right) = -\mathcal{L}^\nu_{\text{CPTV}}$. When the effective energy-independent Hamiltonian associated to $\mathcal{L}^\nu_{\text{CPTV}}$ is added to the standard mass-driven neutrino oscillation Hamiltonian, it modifies the energy eigenvalues and, as a result, the mixing matrix is modified as well.

7.1 Two–neutrino case

The simpler, two-neutrino formalism of CPTV in neutrino oscillations was the subject of ref. [123]. Here we present their results, with more detailed derivations, before examining the more realistic case of three-neutrino CPTV.

Consider the following Hamiltonian in the flavour basis:

$$H_{f,2\nu} = \frac{\Delta m^2}{2E} U_{0,2\nu} \begin{pmatrix} -1 & 0 \\ 0 & 1 \end{pmatrix} U_{0,2\nu}^\dagger + \Delta b \, U_{b,2\nu} \begin{pmatrix} -1 & 0 \\ 0 & 1 \end{pmatrix} U_{b,2\nu}^\dagger \, , \tag{7.3}$$

where the first term accounts for oscillations in the vacuum and the second one, for CPTV-induced flavour transitions. The mixing

The coefficient $\Delta b \equiv b_2 - b_1$ is energy-independent, and its origin is made evident by writing the Hamiltonian in the mass basis, i.e.,

$$H_{f,2}^m = \frac{1}{2} M M^\dagger + b \, , \tag{7.4}$$

where $M = \mathrm{diag}\,(m_1, m_2)$, and b a Hermitian matrix. For anti-neutrinos, the sign of b is flipped. Thus, there are three different bases at play:

$$\text{flavour basis:} \qquad (\nu_e, \nu_\mu) \tag{7.5}$$

$$\text{mass basis:} \qquad (\nu_1, \nu_2) \tag{7.6}$$

$$\text{basis in which } b \text{ is diagonal:} \qquad \left(\nu_1^b, \nu_2^b\right) \tag{7.7}$$

and they are connected through the vacuum mixing matrix, $U_{0,2\nu}$, and the CPTV mixing matrix, $U_{b,2\nu}$. Explicitly,

$$|\nu_\alpha\rangle = \sum_i [U_{0,2\nu}]_{\alpha i}^* \, |\nu_i\rangle \tag{7.8}$$

$$|\nu_\alpha\rangle = \sum_i [U_{b,2\nu}]_{\alpha i}^* \, |\nu_i^b\rangle \, . \tag{7.9}$$

The vacuum and CPTV mixing matrices are given, respectively, by

$$U_{0,2\nu} = \begin{pmatrix} \cos(\theta) & \sin(\theta) \\ -\sin(\theta) & \cos(\theta) \end{pmatrix} \tag{7.10}$$

and

$$U_{b,2\nu} = \begin{pmatrix} \cos(\theta_b) & \sin(\theta_b)\, e^{i\eta} \\ -\sin(\theta_b)\, e^{-i\eta} & \cos(\theta_b) \end{pmatrix} \, . \tag{7.11}$$

Here, θ and θ_b are the rotation angles that diagonalise the vacuum and CPTV

contributions, respectively. The phase η in Eq. (7.11) is the difference between the phases that diagonalise the first and second terms in Eq. (7.3); only one of these two phases can be rotated away by the redefinition of the neutrino states.

Operating, we obtain

$$H_{f,2\nu} = \begin{pmatrix} -\frac{\Delta m^2}{2E}\cos(2\theta) - \Delta b \cos(2\theta_b) & \frac{\Delta m^2}{2E}\sin(2\theta) + \Delta b \sin(2\theta_b)\, e^{i\eta} \\ \frac{\Delta m^2}{2E}\sin(2\theta) + \Delta b \sin(2\theta_b)\, e^{-i\eta} & \frac{\Delta m^2}{2E}\cos(2\theta) + \Delta b \cos(2\theta_b) \end{pmatrix} . \tag{7.12}$$

We will calculate the eigenvalues of $H_{f,2\nu}$ in some details, since in the three-neutrino case, due to the existence of several more splittings and phases, it would be too involved. The characteristic equation reads

$$\det\left(H_{f,2\nu} - \lambda\right) = 0 \, , \tag{7.13}$$

with λ the eigenvalue. Solving this leads to

$$\lambda^2 = \left[\Delta\cos(2\Theta)/2\right]^2 + \left[\Delta\sin(2\Theta)/2\right]^2 = \Delta^2/4 \, , \tag{7.14}$$

with Δ and Θ defined implicitly by

$$\Delta\cos(2\Theta) = \frac{\Delta m^2}{E}\cos(2\theta) + 2\Delta b\cos(2\theta_b) \tag{7.15}$$

$$\Delta\sin(2\Theta) = \left|\frac{\Delta m^2}{E}\sin(2\theta) + 2\Delta b \sin(2\theta_b)\, e^{i\eta}\right| . \tag{7.16}$$

The rotation angle Θ diagonalises $H_{f,2\nu}$ through

$$U_{f,2\nu} = \begin{pmatrix} \cos(\Theta) & \sin(\Theta) \\ -\sin(\Theta) & \cos(\Theta) \end{pmatrix} . \tag{7.17}$$

We will denote by $\left\{|\nu_i^T\rangle\right\}$ the orthonormal basis in which $H_{f,2\nu}$ is diagonal, i.e.,

$$H^T_{f,2\nu} = U^\dagger_{f,2\nu} H_{f,2\nu} U_{f,2\nu} = \begin{pmatrix} \Delta/2 & 0 \\ 0 & -\Delta/2 \end{pmatrix} , \tag{7.18}$$

with $\pm\Delta/2$ the eigenvalues. From Eqs. (7.15) and (7.16), we can find explicit ex-

pressions for Δ and Θ, namely

$$\begin{aligned}\Delta &= \left\{\left(\frac{\Delta m^2}{2E}\right)^2 + 4\left(\Delta b\right)^2 \right. \\ &\qquad \left. + 4\frac{\Delta m^2}{E}\Delta b\left[\cos\left(2\theta\right)\cos\left(2\theta_b\right) + \sin\left(2\theta\right)\sin\left(2\theta_b\right)\cos\left(\eta\right)\right]\right\}^{1/2} \quad (7.19)\\ \tan\left(2\Theta\right) &= \frac{\left|\left(\Delta m^2/E\right)\sin\left(2\theta\right) + 2\Delta b\sin\left(2\theta_b\right)e^{i\eta}\right|}{\left(\Delta m^2/E\right)\cos\left(2\theta\right) + 2\Delta b\cos\left(2\theta_b\right)} \ . \quad (7.20)\end{aligned}$$

The evolved state of a neutrino created with flavour α is

$$\begin{aligned}\left|\nu_\alpha\left(L\right)\right\rangle &= \sum_i \left[U_{f,2\nu}\right]^*_{\alpha i}\left|\nu_i^T\left(L\right)\right\rangle \\ &= \sum_i \left[U_{f,2\nu}\right]^*_{\alpha i} e^{-i\frac{\Delta_i}{2}L}\left|\nu_i^T\right\rangle \\ &= \cos\left(\Theta\right)e^{i\frac{\Delta}{2}L}\left|\nu_1^T\right\rangle + \sin\left(\Theta\right)e^{-i\frac{\Delta}{2}L}\left|\nu_2^T\right\rangle \ , \quad (7.21)\end{aligned}$$

and, on account of the definition of the other neutrino in the system as

$$\left|\nu_\beta\right\rangle = -\sin\left(\Theta\right)\left|\nu_1^T\right\rangle + \cos\left(\Theta\right)\left|\nu_2^T\right\rangle \ , \quad (7.22)$$

the probability $P_{\alpha\beta} = \left|\left\langle\nu_\beta|\nu_\alpha\left(L\right)\right\rangle\right|^2$ for the transition $\nu_\alpha \to \nu_\beta$ to occur is therefore

$$\begin{aligned}P_{\alpha\beta} &= P_{\beta\alpha} = \sin^2\left(2\Theta\right)\sin^2\left(\frac{\Delta}{2}L\right) \quad (7.23)\\ P_{\alpha\alpha} &= P_{\beta\beta} = 1 - P_{\alpha\beta} \ . \quad (7.24)\end{aligned}$$

Thus, observable CPT violation is a consequence of the interference between the standard Δm^2 term (which is CPT-even) and the Δb term (which is CPT-odd). From Eq. (7.12), it is evident that if $\Delta m^2 = 0$ or $\Delta b = 0$, there will be no observable CPTV in neutrino oscillations. Were $\Delta m^2/E \gg \Delta b$, then $\Theta \simeq \theta$ and $\Delta \simeq \Delta m^2/e$, whereas, if $\Delta m^2/E \ll \Delta b$, then $\Theta \simeq \theta_b$ and $\Delta \simeq \Delta b$. Therefore, the strength of the CPTV can vary dramatically with E.

Note from Eq. (7.20) that there is a CPT-odd resonance for neutrinos, reminiscent of the resonance due to matter effects (see Section 4.1.3), when $\cos\left(2\Theta\right) = 0$ or, equivalently,

$$\left(\Delta m^2/E\right)\cos\left(2\theta\right) + 2\Delta b\cos\left(2\theta_b\right) = 0 \ . \quad (7.25)$$

For anti-neutrinos, the same condition holds, but with $\Delta b \to -\Delta b$. Hence, for neutrinos, in order for the resonance to occur, it is necessary that Δm^2 and Δb have opposite signs, while, for anti-neutrinos, they must have the same sign. The

resonance condition is independent of η, and so a resonance can occur regardless of the value of this phase. However, if $\theta = \theta_b$, a resonance can only occur if $\eta \neq 0$.

Following [123], we will explore three different examples of CPTV and CPT-odd resonances. To simplify the analysis, we assume herafter that the Δm^2 and Δb contributions are diagonalised by the same angle, i.e., $\theta_b = \theta$. With this, Eqs. (7.19) and (7.20) become

$$\Delta = \left\{ \left(\frac{\Delta m^2}{2E} \right)^2 + 4 (\Delta b)^2 + 4 \frac{\Delta m^2}{E} \Delta b \left[\cos^2 (2\theta) + \sin^2 (2\theta) \cos (\eta) \right] \right\}^{1/2} \tag{7.26}$$

$$\tan (2\Theta) = \frac{|(\Delta m^2/E) + 2\Delta b e^{i\eta}|}{(\Delta m^2/E) + 2\Delta b} \tan (2\Theta) \ . \tag{7.27}$$

7.1.1 $\eta = 0$

In this case,

$$\Delta = \frac{\Delta m^2}{E} + 2\Delta b \tag{7.28}$$

$$\Theta = \theta \ , \tag{7.29}$$

and no CPT-odd resonance is possible. The transition and survival probabilities, Eq. (7.23), are

$$P_{\overline{\alpha\beta}} = \sin^2 (2\theta) \sin^2 \left[\left(\frac{\Delta m^2}{4E} \pm \frac{\Delta b}{2} \right) L \right] \tag{7.30}$$

$$P_{\overline{\alpha}\,\overline{\alpha}} = 1 - \sin^2 (2\theta) \sin^2 \left[\left(\frac{\Delta m^2}{4E} \pm \frac{\Delta b}{2} \right) L \right] \ . \tag{7.31}$$

The effect of the CPTV term is to introduce an energy-independent phase shift $\Delta b L/2$. In this respect, the case of $\eta = 0$ is equivalent to introducing CPTV through a modified dispersion relation, as we did in Chapter 6. As within that formalism, only the oscillation phase, and not the amplitude (i.e., the mixing angle), is modified.

One possible CPT observable can be the difference between the probabilities for neutrinos and anti-neutrinos, i.e.,

$$P_{\alpha\alpha} (L) - P_{\overline{\alpha}\,\overline{\alpha}} (L) = -2 \sin^2 2\theta \sin \left(\frac{\Delta m^2}{2E} L \right) \sin (\Delta b L) \ . \tag{7.32}$$

If $\Delta b = 0$, evidently, this quantity is identically zero. In [123], estimates are made using the ratio of $\overline{\nu}_\mu \to \overline{\nu}_\mu$ to $\nu_\mu \to \nu_\mu$ eventos in a neutrino factory.

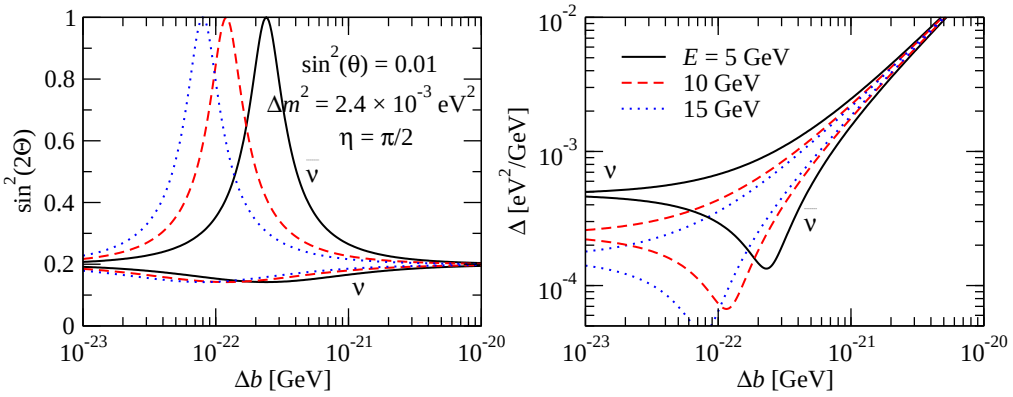

Figure 7.1: Variation of the oscillation amplitude $\sin^2(2\Theta)$ (*left*) and argument Δ (*right*) with the CPT-odd parameter Δb, for neutrinos and anti-neutrinos. We have set $\sin^2(\theta) = 0.01$ and $\Delta m^2 = 2.4 \times 10^{-3}$ eV^2, corresponding to the central values of θ_{13} and Δm^2_{31}, respectively. The phase $\eta = \pi/2$.

7.1.2 $\eta = \pi/2$

In this case,

$$\Delta^2 = \left[\frac{\Delta m^2}{E} + 2\Delta b\right]^2 - 4\frac{\Delta m^2}{E}\Delta b \sin^2(2\theta) \tag{7.33}$$

$$\tan(2\Theta) = \frac{\sqrt{(\Delta m^2/E)^2 + (2\Delta b)^2}}{(\Delta m^2/E) + 2\Delta b}\tan(2\theta)\ . \tag{7.34}$$

If either $\Delta m^2/E \gg 1$ or $\Delta b \gg 1$, then $\tan(2\Theta) \simeq \tan(2\theta)$. Hence, in order for the effect of the Δb contribution to be observable we require $|\Delta m^2/E| \sim |2\Delta b|$. Whenever $\Delta m^2/E \simeq -2\Delta b$, a resonance occurs for neutrinos and $\Theta = \pi/4$, whatever the value of $\tan(2\theta)$ is. For anti-neutrinos, the resonance occurs whenever $\Delta m^2/E \simeq -2\Delta b$. Figure 7.1 shows plots of $\sin^{2\Theta}$ and Δ versus the CPT-odd parameter Δb, for fixed $\sin^2(\theta)\,0.01$, $\Delta m^2 = 2.4 \times 10^{-3}$ eV^2, and $\eta = \pi/2$, for neutrinos and anti-neutrinos.

7.1.3 CPTV with matter effects

If either ν_α or ν_β is a ν_e, then matter effects may be present (see Section 4.1.3). In such a case, the full Hamiltonian is built from Eq. (7.3) by adding to it the matter interaction term in Eq. (4.33), i.e.,

$$\frac{V_W}{2}\begin{pmatrix} 1 & 0 \\ 0 & -1 \end{pmatrix}\ . \tag{7.35}$$

Diagonalising the full Hamiltonian, we find

$$\Delta \sin(2\Theta) = \left|\left(\Delta m^2/E\right)\sin(2\theta) + 2\Delta b e^{i\eta}\sin(2\theta_b)\right| \quad (7.36)$$

$$\Delta \cos(2\Theta) = \left(\Delta m^2/E\right)\cos(2\theta) + 2\Delta b\cos(2\theta_b) - 2\sqrt{2}G_F N_e\ , \quad (7.37)$$

for neutrinos, and the same expressions with $\Delta b \to -\Delta b$ and $N_e \to -N_e$ for anti-neutrinos.

Assuming again $\theta = \theta_b$ and $\eta = 0$, we find, for neutrinos,

$$\tan(2\Theta) = \frac{\left[(\Delta m^2/E) + 2\Delta b\right]\sin(2\theta)}{\left[(\Delta m^2/E) + 2\Delta b\right]\cos(2\theta) - 2\sqrt{2}G_F N_e}\ , \quad (7.38)$$

$$\Delta^2 = \left\{\left[\left(\Delta m^2/E\right) + 2\Delta b\right]\cos(2\theta) - 2\sqrt{2}G_F Ne\right\}^2 + \left[\left(\Delta m^2/E\right) + 2\Delta b\right]^2\sin^2(2\theta)\ , \quad (7.39)$$

with $\Delta b \to -\Delta b$ and $N_e \to -N_e$ for anti-neutrinos. The resonance occurs for (anti-)neutrinos whenever

$$\left[\left(\Delta m^2/E\right) + 2\Delta b\right]\cos(2\theta) = \pm 2\sqrt{2}G_F N_e\ . \quad (7.40)$$

For a resonance to occur both for neutrinos and anti-neutrinos, we require that the CPTV term dominates over the vacuum term, i.e., $\Delta m^2/E \ll \Delta b$.

7.2 Three–neutrino case

7.2.1 CPT violation in the neutrino sector

Motivated by the vector coupling in Eq. (7.2), and in analogy to the standard oscillation scenario, we can introduce an energy-independent contribution in the form of the Hamiltonian (also in the flavour basis)

$$H_b = U_b\ \mathrm{diag}\,(0, b_{21}, b_{31})\, U_b^\dagger\ , \quad (7.41)$$

where $b_{ij} \equiv b_i - b_j$. Following [122], we write the mixing matrix in this case as

$$U_b = \mathrm{diag}\left(1, e^{i\phi_2}, e^{i\phi_3}\right) U_0\left(\{\theta_{bij}\}, \delta_b\right). \quad (7.42)$$

The mixing angles associated with this Hamiltonian are θ_{b12}, θ_{b13}, θ_{b23}, and δ_b fills the role of δ_{CP} in the standard Hamiltonian. The two extra phases, ϕ_2 and ϕ_3, appear because, once the flavour states and the mass eigenstates have been related through

Eq. (4.1), the former are completely defined, and the two extra phases cannot be rotated away.

H_b is dependent on eight parameters –two eigenvalues (b_{21}, b_{31}), three mixing angles (θ_{b12}, θ_{b13}, θ_{b23}) and three phases (δ_b, ϕ_2, ϕ_3)– whose values are currently unknown. There are, however, experimental upper limits [122] on b_{21}, obtained using solar and Super-Kamiokande data, and on b_{32}, obtained using atmospheric and K2K data:

$$b_{21} \leq 1.6 \times 10^{-21} \text{ GeV} , \qquad b_{32} \leq 5.0 \times 10^{-23} \text{ GeV} . \tag{7.43}$$

The full Hamiltonian, including standard oscillations and the energy-independent contribution, is then

$$H_f = H_m + H_b . \tag{7.44}$$

In Chapter 6, we saw that H_m has been experimentally demonstrated to be the dominant contribution to the oscillations in the low to medium energy (MeV–TeV) regime: there are no indications of new energy-independent physics at these energies and accordingly the limits on b_{ij} shown in Eq. (7.43) were placed. Because of the $1/E$ dependence of H_m, however, it remains possible that, at higher energies, where the contribution of H_m is suppressed, the effect of a hypothetical energy-independent term H_b becomes comparable to it or even dominant. Such energy requirement is expected to be fulfilled by the UHE astrophysical neutrino flux (see Chapter 5).

The effect of CPTV on the flavour ratios of high-energy astrophysical neutrinos has been explored elsewhere literature: in [123], for instance, a two-neutrino approximation was employed and it was assumed that H_m and H_b are diagonalised by the same mixing matrix, i.e., that $\theta_{bij} = \theta_{ij}$, while, in [73], neutrinos and antineutrinos were treated differently due to CPTV. Ref. [122] used a formalism similar to the one we have used, but applied it to long-baseline terrestrial experiments and, due to the lower energies involved, introduced the CPTV effects as perturbations. The main difference between the existing literature on the effects of CPTV on the flavour fluxes of high-energy astrophysical neutrinos and the present work is that we have not treated the CPTV contribution as a perturbation, but, rather, we have allowed for the possibility that it becomes dominant at a high enough energy scale.

We would like to write the flavour transition probability corresponding to this Hamiltonian in a form analogous to Eq. (4.55). In order to do this, we need to know what is the mixing matrix U_f that connects the flavour basis and the basis in which H_f is diagonal. Using basic linear algebra, this is achieved simply by diagonalising H_f, finding its normalised eigenvectors, and building U_f by arranging

them in column form. The components of the resulting matrix are in general complicated functions of the standard mixing parameters ($\{\theta_{ij}\}$, $\{\Delta m^2_{ij}\}$, $\delta_{\rm CP}$) and of the parameters of H_b ($\{\theta_{bij}\}$, $\{b_{ij}\}$, δ_b, ϕ_2, ϕ_3). By comparing the mixing matrix obtained by diagonalisation of H_f with a general PMNS matrix, given explicitly by Eq. (4.47) with mixing angles Θ_{ij} and phase δ_f, we are then able to calculate how the effective mixing angles Θ_{ij} vary with the parameters of H_b and $\delta_{\rm CP}$. Succintly put, we have

$$U_f = U_f\left(\{\theta_{ij}\},\{\theta_{bij}\},\{\Delta m^2_{ij}\},\{b_{ij}\},\delta_{\rm CP},\delta_b,\phi_{b2},\phi_{b3}\right) = U_0\left(\{\Theta_{ij}\},\delta_f\right). \quad (7.45)$$

Note that we have not used a perturbative expansion in the b_{ij}, as in [122], to calculate U_f. This was done in order to allow for the possibility that the new physics effects become dominant at high energies, a possibility that would be negated if we had assumed that the effects are small from the start. As a result, the functional forms of the Θ_{ij} and δ_f, while calculated in a straightforward manner, result in lengthy expressions and, due to their unilluminating character, we have chosen not to present them here.

Thus defined, U_f is 14-parameter function. However, the standard mixing parameters Δm^2_{21}, Δm^2_{31}, θ_{12}, θ_{13} and θ_{23} have been fixed by neutrino oscillation experiments (see Eq. (4.52)). Additionally, in order to simplify the analysis, we have set the phases $\delta_b = \phi_2 = \phi_3 = 0$. The standard CP-violating phase $\delta_{\rm CP}$ has been allowed to vary in the range $[0, 2\pi]$ in some of our plots, but otherwise we have set it to zero as well. As a further simplification, we have made the eigenvalues of H_m proportional to those of H_b, at a fixed energy of $E^\star = 1$ PeV, that is,

$$b_{ij} = \lambda \frac{\Delta m^2_{ij}}{2E^\star}\ , \quad (7.46)$$

with λ the proportionality constant. The upper bounds on the b_{ij}, Eq. (7.43), are satisfied for $\lambda \lesssim 10^4$. Standard, purely mass-driven oscillations are recovered when $\lambda = 0$. Thus we are left with only four free parameters to vary: λ, θ_{b12}, θ_{b13} and θ_{b23} (and $\delta_{\rm CP}$, where noted).

In analogy to Eq. (4.55), the average flavour transition probability associated to the full Hamiltonian H_f is then

$$\langle P_{\alpha\beta}\rangle = \sum_i |[U_f]_{\alpha i}|^2 |[U_f]_{\beta i}|^2\ . \quad (7.47)$$

We will use this expression for the flavour-transition probability hereafter. It is worth noting that, if the CPTV contribution were introduced instead through a

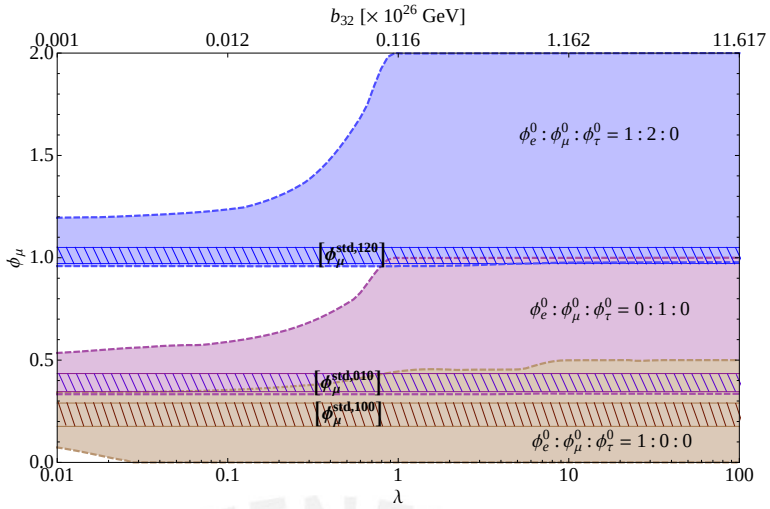

Figure 7.2: Allowed regions of values of the detected muon-neutrino flavour ratio, ϕ_μ, as a function of λ for different neutrino production models. The three standard mixing angles (θ_{12}, θ_{13}, θ_{23}) were varied within 3σ bounds and the three CPTV angles (θ_{b12}, θ_{b13}, θ_{b23}) were varied within $[0, \pi]$, while $\delta_{\text{CP}} = 0$. The hatched regions are the allowed regions of ϕ_μ when only standard oscillations are allowed, and allowing the θ_{ij} to vary within their 3σ bounds.

modified energy-momentum relation, only the oscillation phase would be affected, and this information would be lost when the average probability was used in place of the oscillatory one [103].

7.2.2 Detection of only muon-neutrinos

In Figure 7.2 we present a plot of the muon-neutrino flavour ratio, ϕ_μ, as a function of λ. The coloured bands correspond to different neutrino production scenarios, namely: $\phi_e^0 : \phi_\mu^0 : \phi_\tau^0 = 1 : 2 : 0$ (blue), $0 : 1 : 0$ (purple) and $1 : 0 : 0$ (brown), which have been generated by varying the three CPTV angles (θ_{b12}, θ_{b13}, θ_{b23}) within $[0, \pi]$, and the three standard mixing angles (θ_{12}, θ_{13}, θ_{23}) within their 3σ bounds, with $\delta_{\text{CP}} = 0$. For comparison, we have included the hatched bands which represent the pure standard oscillation case, that is, without CPTV. These have been generated by setting $\lambda = 0$ and varying the three standard mixing angles within their 3σ bounds, again with $\delta_{\text{CP}} = 0$. As expected, the standard-oscillation bands are contained within the corresponding CPTV region.

When CPTV is allowed, we observe large deviations of ϕ_μ with respect to the pure standard-oscillation bands, especially for the scenarios $\phi_e^0 : \phi_\mu^0 : \phi_\tau^0 = 1 : 2 : 0$ and $0 : 1 : 0$, and less so for the scenario $1 : 0 : 0$. Starting from $\lambda \sim 0.1$ ($b_{32} \simeq 1.2 \times 10^{-28}$ GeV), the CPTV bands start growing with λ, as was expected, since λ measures the

strength of the CPT violation. Thus, the influence of the CPTV contribution to the oscillations grows and, as a consequence, the accessible region also grows. This is due to the wide range of values that the CPTV mixing angles can take, in comparison with the standard ones. Past $\lambda = 1$, the CPTV regions reach a plateau, owing to the fact that the CPTV term becomes dominant over the standard-oscillation term in the Hamiltonian.

An interesting feature is the overlap between the standard-oscillation band for the scenario $1 : 2 : 0$ and the CPTV region for scenario $0 : 1 : 0$. A similar overlap occurs between the scenarios $0 : 1 : 0$ (without CPTV) and $1 : 0 : 0$ (with CPTV). As a consequence of these overlaps, if CPTV exists for certain values of the parameters, a measurement of ϕ_μ will be insufficient to distinguish what the neutrino production model is. For instance, if a value of $\phi_\mu \simeq 0.4$ were measured, and $\lambda \gtrsim 0.2$, we would not be able to assert whether the initial fluxes were $0 : 1 : 0$ or $1 : 0 : 0$. Analogously, since the standard-oscillation bands are contained within the CPTV regions, for these cases we will be unable to conclude, from the measurement of ϕ_μ, whether or not CPTV effects are present.

Although we have not presented it here, we have tested that when varying $\delta_{\rm CP}$ within $[0, 2\pi]$, the regions change only in a few percent. Therefore, the features observed in Fig. 7.2 are largely independent of the value of $\delta_{\rm CP}$.

7.2.3 Detection of muon- and electron-neutrinos

In this section, we consider an scenario where only muon- and electron-neutrinos are detected in an available neutrino telescope. Assuming that flavour identification is possible, we can define the ratio of observed flavour ratios

$$R \equiv \phi_\mu / \phi_e \ , \tag{7.48}$$

which, in the presence of CPTV, depends on λ and on the three CPTV mixing angles through the definition of the ϕ_α in terms of the flavour-transition probabilities. Figure 7.3 shows the regions of values of R as a function of λ by varying the three CPTV angles within $[0, \pi]$.

The coloured regions in Fig. 7.3 grow with λ, for the same reason as they did in Fig. 7.2. Under the assumption of a $0 : 1 : 0$ production model, R can attain very large values, between 10^6 and 10^7, as a result of very low electron-neutrino fluxes. On the other hand, the CPTV region associated to the $1 : 2 : 0$ production model reaches a maximum of $R = 2$ after $\lambda \simeq 5$, while the one associated to $1 : 0 : 0$ reaches a maximum of $R = 1$ after $\lambda \simeq 1$. Therefore, a measurement of $R \gg 4$ could imply

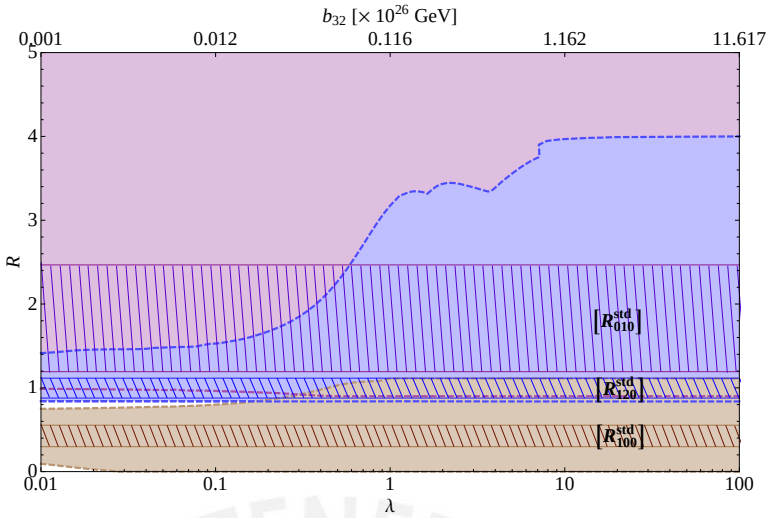

Figure 7.3: Allowed regions of values of $R \equiv \phi_\mu/\phi_e$ as a function of λ, for three scenarios of initial flavour ratios: $\phi_e^0 : \phi_\mu^0 : \phi_\tau^0 = 1 : 2 : 0$ (blue), $0 : 1 : 0$ (purple) and $1 : 0 : 0$ (brown). For each one of them, at each value of λ, the three CPTV mixing angles, θ_{b12}, θ_{b13} and θ_{b23}, were independently varied within $[0, \pi]$, and the three standard mixing angles, θ_{12}, θ_{13} and θ_{23}, were varied within their 3σ bounds (Eq. (4.52)): the lowest and highest value of R obtained in this way define, respectively, the lower and upper bounds of the corresponding region, for this particular value of λ. The CP-violating phase $\delta_{\rm CP} = 0$. The upper horizontal axis is $b_{32} = \lambda\, \Delta m^2_{32}/\,(2E^*)$, with $E^* = 1$ PeV; to find the corresponding values of b_{21}, notice that $b_{21}/b_{32} = \Delta m^2_{21}/\Delta m^2_{32} \simeq 1/30$. The hatched horizontal bands are the allowed regions of R assuming only standard oscillations and allowing the standard mixing angles θ_{ij} to vary within their 3σ bounds.

that the production model is $0 : 1 : 0$, and that CPTV effects are present, but will not be enough to set strong bounds on λ. The minimum value in both the $0 : 1 : 0$ and $1 : 2 : 0$ regions is located around $R = 0.8 \sim 1$, while for the $1 : 0 : 0$ flux, it is zero for most of the range of λ.

If a value of $R \lesssim 4$ is found, the ability to single out a production model depends on the exact value of R that is measured. A single production model can be distinguished univocally for some measured values of R (e.g., for $R < 0.84$, the model is $1 : 0 : 0$), while for others, two (when $1 \lesssim R \lesssim 4$, depending on λ) or three models (when $R \simeq 1$) can account for the same measured value. In the same way, for some values of R, CPTV and standard oscillations cannot be distinguished. The conclusions, from Fig. 7.3, that can be obtained from the measurement of different values of R are shown in Table 7.1.

Measured R	Conclusion
$R > 4$	Initial ratios $0:1:0$ and CPTV
$\left[R^{\rm std}_{010}\right] < R < 4$	Initial ratios $0:1:0$ or $1:2:0$, and CPTV
$R \in \left[R^{\rm std}_{010}\right]$	(Initial ratios $0:1:0$ and std. osc.) or ($1:2:0$ and CPTV)
$\left[R^{\rm std}_{120}\right] < R < \left[R^{\rm std}_{010}\right]$	Initial ratios $0:1:0$ or $1:2:0$, and CPTV
$R \in \left[R^{\rm std}_{120}\right]$	(Initial ratios $1:2:0$ and std. osc.) or (initial ratios $0:1:0$ or $1:0:0$, and CPTV)
$0.84 < R < \left[R^{\rm std}_{120}\right]$	Initial ratios $1:2:0$ or $1:0:0$, and CPTV
$\left[R^{\rm std}_{100}\right] < R < 0.84$	Initial ratios $1:0:0$ and CPTV
$R \in \left[R^{\rm std}_{100}\right]$	Initial ratios $1:0:0$ and std. osc.
$R < \left[R^{\rm std}_{100}\right]$	Initial ratios $1:0:0$ and CPTV

Table 7.1: Conclusions that can be obtained depending on the measured value of R, according to Fig. 7.3. $\left[R^{\rm std}_{120}\right]$, $\left[R^{\rm std}_{010}\right]$ and $\left[R^{\rm std}_{100}\right]$ represent, respectively, the standard-oscillation bands corresponding to the $\phi^0_e : \phi^0_\mu : \phi^0_\tau = 1:2:0$, $0:1:0$ and $1:0:0$ production models. When we refer to standard oscillations, we mean either the inexistence of CPTV ($\lambda = 0$) or the existence of too small a CPTV ($\lambda \ll 1$).

7.2.4 Detection of three flavours

Given the approach of this work, we have considered as a natural step to extend our analysis by taking into account the possibility of tau-neutrino detection. For this purpose, we have defined the ratio

$$S = \phi_\tau / \phi_\mu \ , \tag{7.49}$$

and studied the effects of the new physics in the R vs. S plane.

Before we describe the results of this section, it will be useful to turn our attention to the values of R and S associated to the different production models when only standard oscillations are allowed, along with the correspondong standard values of the detected fluxes ϕ_α. These values are shown in Table 5.1. The CPTV regions in Figures 7.4–7.6 have been generated by setting $\lambda = 100$ (Figs. 7.4 and 7.5) and $\lambda = 1, 10, 100$ (Fig. 7.6), fixing the standard mixing parameters at their best-fit values (see Eq. (4.52)), and varying the CPTV mixing angles θ_{bij} within the range $[0, \pi]$, while the standard-oscillation regions have been generated by setting $\lambda = 0$ and varying the standard mixing angles within their 3σ bounds. With the exception of Figure 7.7, where $\delta_{\rm CP}$ has been allowed to vary, we have set all phases equal to zero.

In Fig. 7.4 we display in three R vs. S panels the allowed regions of values that correspond to pure standard oscillations at 3σ, in dark tones, and the correspond-

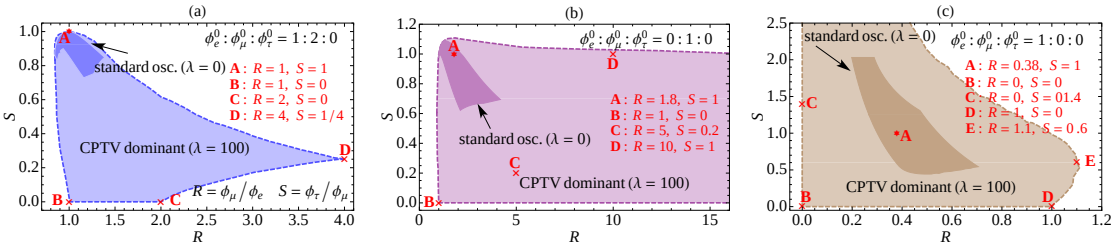

Figure 7.4: Regions of R and S accessible with CPTV by assuming different neutrino production scenarios. Different colours correspond to different initial ratios: $\phi_e^0 : \phi_\mu^0 : \phi_\tau^0 = 1 : 2 : 0$ (blue), $0 : 1 : 0$ (purple), $1 : 0 : 0$ (brown). Darker regions are generated with standard (CPT-conserving) neutrino flavour oscillations, by allowing the standard mixing angles to vary within their 3σ experimental bounds. Lighter regions correspond to the case when we include a dominant CPTV contribution with $\lambda = 100$, and allow the CPTV angles θ_{bij} to vary within $[0, \pi]$. All phases are set to zero.

ing regions allowed by the mixed solution composed of the standard oscillation plus CPTV effects, with $\lambda = 100$, in lighter tones. At this value of λ, the CPTV contributions are the dominant ones in the Hamiltonian, i.e., $H_f \simeq H_b$. Each plot corresponds to a different neutrino production scenario: (a) to $1 : 2 : 0$, (b) to $0 : 1 : 0$, and (c) to $1 : 0 : 0$.

From these plots we can extract two observations: one is the potentially dramatic deviation of the allowed values of the pair (R, S) when CPTV is turned on, and the other is the presence of points that are common to all scenarios. The latter implies that, if there is CPTV, there could exist pairs (R, S), such as $(1, 0)$, that can be generated by any of the three production models, each with a different set of values for the CPTV mixing angles. There are also (R, S) pairs which could be generated by one production model with standard oscillations or with a different model with CPTV, e.g., those lying around $(1, 0.95)$. It is convenient to remark that this figure and Fig. 7.3 are consistent with each other, which can be shown by projecting the CPTV regions of Fig. 7.4 onto the horizontal axis and checking that the limits on R agree with those on Fig. 7.3. We have marked a few notable points in each plot: for the three production models, the points labelled with A correspond to the best-fit values of the standard-oscillation mixing parameters in Eq. (4.52).

In Fig. 7.5, the allowed $R-S$ regions corresponding to the three neutrino production models are shown together: $1 : 2 : 0$ in blue, $0 : 1 : 0$ in purple, and $1 : 0 : 0$ in brown, where, as before, the darker tones correspond to pure standard oscillations, and the lighter tones, to a dominant CPTV with $\lambda = 100$. Following the argument in Section 5.2, we have also included the regions of (R, S) pairs allowed by neutrino

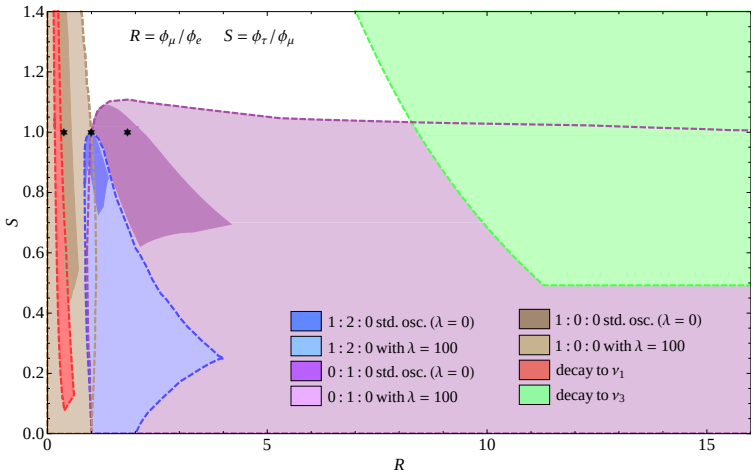

Figure 7.5: Regions of R and S accessible by assuming different neutrino production scenarios: $\phi_e^0 : \phi_\mu^0 : \phi_\tau^0 = 1 : 2 : 0$ (blue), $0 : 1 : 0$ (purple) and $1 : 0 : 0$ (brown). Darker shades of blue, purple and brown correspond to standard, CPT-conserving (i.e., $\lambda = 0$), flavour transitions, while lighter shades correspond to flavour transitions dominated by CPT violation ($\lambda = 100$). The former were generated by varying the standard mixing angles θ_{ij} within their current 3σ experimental bounds; the latter, by fixing the θ_{ij} to their best-fit values and varying the new mixing angles θ_{bij} within 0 and π. All of the phases were set to zero: $\delta_{\rm CP} = \delta_b = \phi_{b2} = \phi_{b3} = 0$. Also shown are the regions accessible through decay of the neutrinos into invisible products, when ν_1 is the lightest mass eigenstate (red) and when ν_3 is the lightest one.

decay into invisible products, considering both the cases of a normal mass hierarchy (decay into the ν_1 eigenstate), in red, and of an inverted hierarchy (decay into ν_3), in green. The decay regions were also generated by varying the standard-oscillation mixing angles within their 3σ bounds.

While the regions corresponding to $1 : 2 : 0$ do not overlap those corresponding to neutrino decay, this is not the case for the $0 : 1 : 0$ scenario, for which there is a clear overlap between the CPTV region and the one from neutrino decay into ν_3. The region corresponding to decay into ν_1 is completely contained within the $1 : 0 : 0$ CPTV region. Projecting onto the horizontal axis, we see that, apart from the same overlaps between the allowed R intervals that existed in the two-neutrino case, as observed in Fig. 7.3, new overlaps appear due to the inclusion of the neutrino-decay regions. Particularly, whereas prior to the inclusion of decays, a value of $R \gg 4$ was a clear indication of the existence of CPTV and of a $0 : 1 : 0$ production model, now Fig. 7.5 shows that, after $R = 7$, the decay into ν_3, assuming an inverted mass hierarchy, can also be accountable for a high value of R. On the other hand, values of $0.25 \lesssim R \lesssim 0.75$ can be reached by the $1 : 0 : 0$ production model, with or without CPTV, as well as with neutrino decay into ν_1, assuming

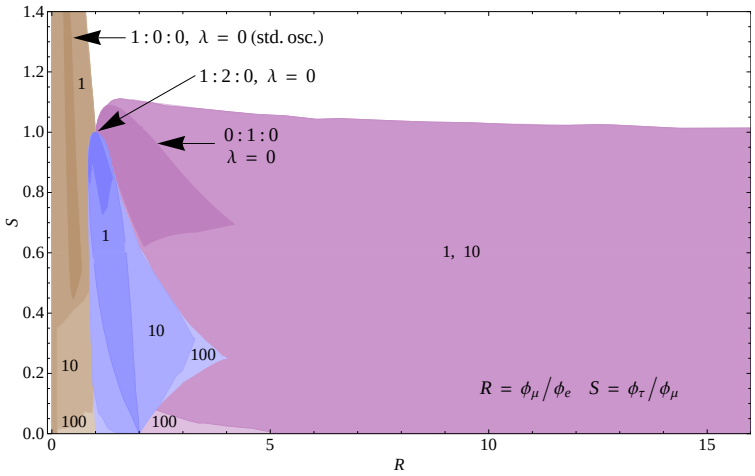

Figure 7.6: Regions of values of R and S accessible when varying the parameter λ between 0 (no CPT breaking) and 100 (dominant CPTV term), for different neutrino production models. In blue: $\phi_e^0 : \phi_\mu^0 : \phi_\tau^0 = 1 : 2 : 0$; in purple, $0 : 1 : 0$; in brown, $1 : 0 : 0$. The region corresponding to pure standard oscillations ($\lambda = 0$) was generated by varying the standard mixing angles within their 3σ experimental bounds, Eq. (4.52). To generate the regions corresponding to $\lambda = 1, 10, 100$, the standard mixing angles were fixed to their best-fit values, and the three CPTV mixing angles θ_{bij} were varied independently within $[0, \pi]$. The CP-violating phase $\delta_{\rm CP} = 0$ for all of the regions.

a normal hierarchy. A normal mass hierarchy is able to yield values of S as low as ~ 0.075, leaving only the small window between zero and this value as unique feature of CPTV. Taking into account experimental uncertainty, it is likely that this window is actually non-existent. Only if the measured $S \gtrsim 1.1$, and in the absence of decays, would it be possible to identify a single production model, $1 : 0 : 0$, as the one responsible. If decays are allowed, however, they can also account, irrespectively of the mass hierarchy, for $S > 1.1$, and the ability to single out a production model is lost. Thus, the signatures of CPTV become less unique in the presence of decays. A more complete analysis of neutrino decays [73], exploring also the possibility of incomplete decays and decay into visible products, further reduces our ability to uniquely identify the presence of CPTV.

In the absence of neutrino decays, a measurement of $R \gtrsim 4.1$ and $S \lesssim 1.1$ could indicate the presence of dominant CPTV and a $0 : 1 : 0$ production model. Also, for $R \lesssim 0.9$, the production model is $1 : 0 : 0$; if $S \lesssim 0.45$, there is dominant CPTV and, for other values of S, the existence of CPTV will depend on the value of R measured. Close to $R = 1$, and for $S \lesssim 0.9$, any of the three production models with dominant CPTV can explain the measured (R, S) pair, while for $0.9 \lesssim S < 1$,

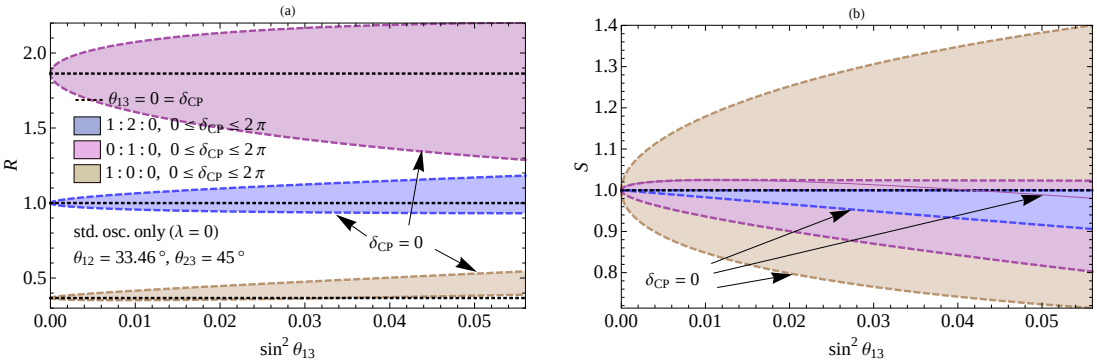

Figure 7.7: Variation of R and S with θ_{13}, when the CP-violation phase $\delta_{\rm CP}$ is allowed to vary between 0 and 2π. The upper limit for θ_{13} is given by the current bound $\sin^2(\theta_{13}) \leq 0.056$ (3σ) and the mixing parameters θ_{12}, θ_{23}, Δm^2_{21} and Δm^2_{32} have been set to their current best-fit values; standard flavour oscillations have been assumed throughout (i.e., $\lambda = 0$). Three different scenarios of initial flavour ratios have been considered: $\phi^0_e : \phi^0_\mu : \phi^0_\tau = 1 : 2 : 0$ (in blue), $0 : 1 : 0$ (in purple) and $1 : 0 : 0$ (in brown). To allow for comparison, the arrows point to the curves on which $\delta_{\rm CP} = 0$.

the pair could be generated either by the $0 : 1 : 0$ or $1 : 0 : 0$ models with CPTV, or by the $1 : 2 : 0$ model with standard oscillations. For $1.1 \lesssim R < 4$ and $S \lesssim 0.6$, there is a large region of overlap between the $1 : 2 : 0$ and $0 : 1 : 0$ models with dominant CPTV.

Fig. 7.6 shows the effect of the variation of the parameter λ between 0 (no CPTV, i.e., $H_f = H_m$) and 100 (dominant CPTV term, i.e., $H_f \simeq H_b$) on the allowed $R-S$ regions, for the different neutrino production scenarios. For the three of them, we can observe significant deviations from the predictions of the standard-oscillation case, even for low values of λ. In this sense, it is interesting to point out that in the case of an experimental non-detection of CPTV in the neutrino flavour ratios, R and S can be used to set limits on the related parameters. In fact, when $\lambda = 1$, and for a neutrino energy of 1 PeV, we can attain limits for the CPTV eigenvalues b_{ij} in the order of 10^{-29} and 10^{-27} GeV, for b_{21} and b_{23}, respectively. It is also important to mention that these results can be easily rescaled to any energy, just by doing $b_{ij} \times (\text{PeV}/E)$. This would mean a very significant improvement over the current bounds of $10^{-23} - 10^{-21}$ GeV for b_{21} and b_{32}, respectively [122].

Finally, it is worth exploring the effect of the choice of value of $\delta_{\rm CP}$ on R and S. From Fig. 7.7, we see that the effect on R of a non-zero value of $\delta_{\rm CP}$ in the standard-oscillation regions is more prominent for a choice of initial ratios of $0 : 1 : 0$, and less so for $1 : 2 : 0$ and $1 : 0 : 0$. For S, the effect of a non-zero phase is greater for $1 : 0 : 0$, and less for $0 : 1 : 0$ and $1 : 2 : 0$. Note that using a non-zero value of $\delta_{\rm CP}$

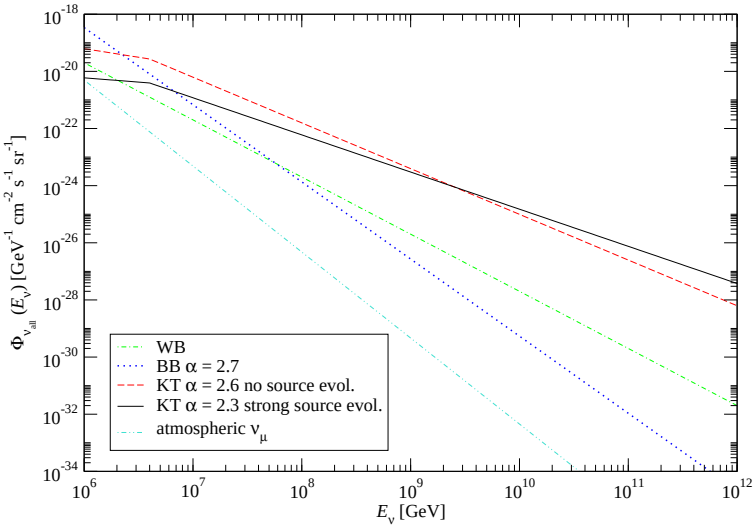

Figure 7.8: High-energy astrophysical neutrino flux models as function of neutrino energy. The spectral index $\alpha = 2.7$ for the Becker-Biermann (BB) and 2.3, 2.6 for the Koers-Tinyakov (KT) fluxes with and without source evolution, respectively. For the BB flux, we have set $\Gamma_\nu/\Gamma_{\rm CR} = 3$ and $z_{\rm CR}^{\rm max} = 0.03$ (see [87]). The atmospheric muon-neutrino flux, modelled according to [86], which is considered as a background to the astrophysical neutrino signal, lies below the predictions of these models in the plotted energy range.

can lead to a variation in R of up to 42% (in the $0:1:0$ case) and in S of up to 40% (in the $1:0:0$ case) with respect to the standard case of $\theta_{13} = \delta_{\rm CP} = 0$, when the largest 3σ allowed value of $\sin^2(\theta_{13}) = 0.056$ is assumed.

7.3 Experimental prospects

7.3.1 Neutrino flux models

We will present our estimations of $N_{\nu_{\rm all}}^{\rm NC}$, $N_{\nu_{\rm all}}^{\rm CC}$, and $N_{\nu_{\rm all}}^{\rm NC}/N_{\nu_{\rm all}}^{\rm CC}$, in the context of four models of astrophysical neutrino fluxes. The Waxman-Bahcall [124] model makes use of the observation of ultra-high-energy ($> 10^{19}$ eV) cosmic rays to set an upper limit on the neutrino flux. The limit depends on the redshift evolution of the neutrino sources, which could be active galactic nuclei (AGN) or gamma-ray bursts. We have adopted, conservatively,

$$\Phi_{\nu_{\rm all}}^{\rm WB}(E_\nu) = 10^{-8}\,(E_\nu/{\rm GeV})^{-2}\ {\rm GeV}^{-1}\ {\rm cm}^{-2}\ {\rm s}^{-1}\ {\rm sr}^{-1}\ . \tag{7.50}$$

The second model, by Becker-Biermann [87], describes the production of neutrinos in the relativistic jets of FR-I galaxies (low-luminosity radio galaxies with extended ra-

dio jets) through the decay of pions produced in the interaction of shock-accelerated protons with the surrounding photon field. The sources are assumed to evolve with redshift according to certain luminosity functions. The flux is given by

$$\Phi_{\nu_{\rm all}}^{\rm BB}\,(E_\nu) \simeq 5.4\times 10^{-3}\,(E_\nu/{\rm GeV})^{-2.7}\ {\rm GeV}^{-1}\ {\rm cm}^{-2}\ {\rm s}^{-1}\ {\rm sr}^{-1}\ . \tag{7.51}$$

The third and fourth models, by Koers-Tinyakov [86], predict an astrophysical neutrino flux based on the assumption that the neutrinos originate predominantly at AGN and that these behave like Centaurus A, the nearest active galaxy. The difference between these last two models lies in the assumption about the redshift evolution of the source: in one of them, sources are assumed not to evolve with redshift, while in the other one, they are assumed to have a strong redshift evolution, following the star-formation rate of $\sim (1+z)^3$. These two fluxes are given, respectively, by

$$\begin{aligned}\Phi_{\nu_{\rm all}}^{\rm KT,\ no\ evol.}\,(E_\nu) &\simeq 3.5\times 10^{-10}\,(E_\nu/{\rm GeV})^{-1.6}\times \\ &\quad \times \min\left(1, E_\nu/E_{\nu,{\rm br}}\right)\ {\rm GeV}^{-1}\ {\rm cm}^{-2}\ {\rm s}^{-1}\ {\rm sr}^{-1} \qquad (7.52)\\ \Phi_{\nu_{\rm all}}^{\rm KT,\ evol.}\,(E_\nu) &\simeq 4.6\times 10^{-12}\,(E_\nu/{\rm GeV})^{-1.3}\times \\ &\quad \times \min\left(1, E_\nu/E_{\nu,{\rm br}}\right)\ {\rm GeV}^{-1}\ {\rm cm}^{-2}\ {\rm s}^{-1}\ {\rm sr}^{-1}\ , \qquad (7.53)\end{aligned}$$

with $E_{\nu,{\rm br}} = 4\times 10^6$ GeV the break energy. Both the Becker-Biermann and Koers-Tinyakov models account for the change in cosmic-ray energy due to the adiabatic cosmological expansion, but only the latter take into account also energy losses due to pion photoproduction and electron-positron pair production in the interaction with the CMB photons. See Chapter 4 for details on the WB, BB, and KT fluxes.

Currently, the most stringent upper bound on the astrophysical muon-neutrino flux is the one obtained by the AMANDA-II experiment [93], which restricts the integrated muon-neutrino flux to be lower than 7.4×10^{-8} GeV cm^{-2} s^{-1} sr^{-1}, within the interval 16 TeV – 2.5 PeV. We have checked that the four fluxes used in our analysis satisfy this upper bound in the standard-oscillation case, i.e., when the detected flavour ratios are $\phi_e : \phi_\mu : \phi_\tau = 1:1:1$. The spectral indices of the power laws for the Koers-Tinyakov fluxes, -1.6 and -1.3, have been chosen so that the integrated fluxes between 16 TeV and 2.5 PeV yield exactly the upper bound value set by AMANDA. A plot of the four different fluxes is presented in Fig. 7.8.

7.3.2 Experimental setup

The IceCube neutrino telescope [125, 126], located at the South Pole, can detect both muons and showers initiated by incoming high-energy astrophysical neutrinos. Muon-neutrinos are detected through the high-energy muon produced in charged-current (CC) deep inelastic neutrino-nucleon scattering: the Čerenkov light emitted by the fast-moving muon in ice is detected by the photomultipliers buried in ice and used to reconstruct the muon track. Electron-neutrinos can generate electromagnetic and hadronic showers in CC interactions. Tau-neutrino CC events have a distinct topology: they either show two hadronic showers joined by a tau track (a double bang) or a tau track ending with the decay of the tau in a hadronic shower (lollipop). Additionally, every flavour of neutrino is able to generate hadronic showers in neutral-current (NC) interactions. Flavour identification is expected to be difficult at IceCube [74] and the number of lollipops expected is about one every two years (for a neutrino flux of 10^{-7} GeV^{-1} s^{-1} cm^{-2} sr^{-1} [74]), so the useful observables turn out to be the total number of NC plus CC showers, $N_{\rm sh} = N_{\rm sh}^{\rm NC} + N_{\rm sh}^{\rm CC}$ and the number of muon tracks, N_{ν_μ}. From this, we can construct the closest experimental analogue of the variable $R \equiv \phi_\mu/\phi_e$ as $R_{\rm exp} \equiv N_{\nu_\mu}/N_{\rm sh}$. Due to the very low number of tau-neutrinos expected at IceCube, there is no practical experimental analogue of $S \equiv \phi_\tau/\phi_\mu$.

Following our analysis of CPTV in the previous sections, where we set the scale of CPTV at $E^* = 1$ PeV, we have adopted the energy range $E_\nu^{\rm min} = 10^6 \leq E_\nu/{\rm GeV} \leq E_\nu^{\rm max} = 10^{12}$ for our predictions. Within this energy range, the Earth is opaque to neutrinos due to the increased number of NC interactions which degrade their energy [127], so we have calculated only the number of downgoing events. Bear in mind, however, that due to the tighter background filtering that is required for the observation of downgoing neutrinos, which we have not taken into account in the following calculations, our estimates may be optimistic. Conveniently, for most of this range the atmospheric ν_μ background flux will be well below the fluxes from the neutrino production models that we have probed (see Figure 7.8). Using the expressions of [128], we can estimate the number of CC and NC events at IceCube, for a given astrophysical all-flavour diffuse neutrino flux, denoted here by $\Phi^{\nu_{\rm all}}$:

$$N_{\nu_{\rm all}}^{\rm CC} = T n_T V_{\rm eff} \Omega \int_{E_{\rm sh}^{\rm min}}^{E_\nu^{\rm max}} \Phi^{\nu_{\rm all}}(E_\nu) \frac{1}{2} \left[\sigma_{\rm CC}^{\nu N}(E_\nu) + \sigma_{\rm CC}^{\overline{\nu} N}(E_\nu)\right] dE_\nu \quad (7.54)$$

$$N_{\nu_{\rm all}}^{\rm NC} = T n_T V_{\rm eff} \Omega \int_{E_{\rm sh}^{\rm min}}^{E_\nu^{\rm max}} dE_\nu \int_{E_\nu - E_{\rm sh}^{\rm min}}^{E_\nu^{\rm max}} dE'_\nu \Phi^{\nu_{\rm all}}(E_\nu) \times \times \frac{1}{2} \left[\frac{d\sigma_{\rm NC}^{\nu N}}{dE'_\nu}(E_\nu, E'_\nu) + \frac{d\sigma_{\rm NC}^{\overline{\nu} N}}{dE'_\nu}(E_\nu, E'_\nu)\right] , \quad (7.55)$$

where E'_ν is the energy of the secondary neutrino in the NC interaction, T is the exposure time, $n_T = 5.1557 \times 10^{23}$ cm^{-3} is the number density of targets (nucleons) in ice, V_{eff} is the effective detector volume (1 km^3 for IceCube) and $\Omega = 5.736$ sr is the detector's opening angle (up to 85°). The total cross sections for neutrino and anti-neutrino deep inelastic scattering, $\sigma^{\nu N}_{\text{CC}}$, $\sigma^{\overline{\nu} N}_{\text{CC}}$, $\sigma^{\nu N}_{\text{NC}}$ and $\sigma^{\overline{\nu} N}_{\text{NC}}$, have been extracted from [129]. The differential cross sections used are written as a function of both the primary and the secondary neutrino energies, which in NC interactions are related through $E'_\nu = (1 - \langle y_{\text{NC}} \rangle) E_\nu$, with $\langle y_{\text{NC}} \rangle$ the NC inelasticity parameter, extracted from [127]. If the interval of interest ($10^6 - 10^{12}$ GeV) is partitioned into small enough subintervals, then within each, the NC cross section can be approximated by $\sigma_{\text{NC}} = A E_\nu^B$ with A, B constants for each subinterval. We can then write

$$\sigma^{\nu N}_{\text{NC}} = A E_\nu^B = A \left[\left(1 - \langle y_{\text{NC}}(E_\nu) \rangle\right)^{-1} E'_\nu \right]^B \ , \tag{7.56}$$

so that

$$\frac{d\sigma_{\text{NC}}}{dE'_\nu}(E_\nu, E'_\nu) = AB \left[1 - \langle y_{\text{NC}}(E_\nu) \rangle\right]^{-B} (E'_\nu)^{B-1} \ . \tag{7.57}$$

Using this expression in Eq. (7.55) and performing the E'_ν integral, we obtain the simplified form

$$\begin{aligned} N^{\text{NC}}_{\nu_{\text{all}}} \simeq \ & \tfrac{1}{2} \ T n_T V_{\text{eff}} \Omega \int_{E^{\text{min}}_{\text{sh}}}^{E^{\text{max}}_\nu} dE_\nu \Phi^{\nu_{\text{all}}}(E_\nu) \times \\ & \times \left[\frac{\sigma^{\nu N}_{\text{NC}}(E^{\text{max}}_\nu) - \sigma^{\nu N}_{\text{NC}}\left(E_\nu - E^{\text{min}}_{\text{sh}}\right)}{\left[1 - \langle y^{\nu N}_{\text{NC}}(E_\nu) \rangle\right]^B} + \frac{\sigma^{\overline{\nu} N}_{\text{NC}}(E^{\text{max}}_\nu) - \sigma^{\overline{\nu} N}_{\text{NC}}\left(E_\nu - E^{\text{min}}_{\text{sh}}\right)}{\left[1 - \langle y^{\overline{\nu} N}_{\text{NC}}(E_\nu) \rangle\right]^{\overline{B}}} \right] \end{aligned} \tag{7.58}$$

with B and $\overline{B}$ taking the appropriate values in each subinterval.

The number of CC showers generated by electron- and tau-neutrinos are, respectively, $N^{\text{CC}}_{\text{sh},e} = \tilde{\phi}_e N^{\text{CC}}_{\nu_{\text{all}}}$ and $N^{\text{CC}}_{\text{sh},\tau} = \tilde{\phi}_\tau N^{\text{CC}}_{\nu_{\text{all}}}$, where

$$\tilde{\phi}_\alpha \equiv \frac{\phi_\alpha}{\phi_e + \phi_\mu + \phi_\tau} \in [0, 1] \tag{7.59}$$

are the normalised flavour ratios. The number of CC showers is given by

$$N^{\text{CC}}_{\text{sh}} = N^{\text{CC}}_{\text{sh},e} + N^{\text{CC}}_{\text{sh},\tau} = \left(\tilde{\phi}_e + \tilde{\phi}_\tau\right) N^{\text{CC}}_{\nu_{\text{all}}} \tag{7.60}$$

and the total number of CC plus NC showers is therefore

$$N_{\text{sh}} = N^{\text{CC}}_{\text{sh}} + N^{\text{NC}}_{\text{sh}} = \left(1 - \tilde{\phi}_\mu\right) N^{\text{CC}}_{\nu_{\text{all}}} + N^{\text{NC}}_{\nu_{\text{all}}} \ , \tag{7.61}$$

Flux	$N_{\nu_{\rm all}}^{\rm NC}$	$N_{\nu_{\rm all}}^{\rm CC}$	$N_{\nu_{\rm all}}^{\rm NC}/N_{\nu_{\rm all}}^{\rm CC}$
Waxman-Bahcall [124]	1781.64	33.12	53.79
Becker-Biermann $\alpha = 2.7$ [87]	9248.58	130.68	70.77
Koers-Tinyakov no source evolution $\alpha = 2.6$ [86]	9013.86	354.96	25.39
Koers-Tinyakov strong source evolution $\alpha = 2.3$ [86]	16495.92	1866.42	8.84

Table 7.2: Expected number of neutral-current and charged-current events (summed over all flavours) at IceCube, $N_{\nu_{\rm all}}^{\rm NC}$ and $N_{\nu_{\rm all}}^{\rm CC}$, respectively, in the energy range $10^6 \leq E_\nu/\text{GeV} \leq 10^{12}$, for different choices of the incoming astrophysical neutrino flux. The exposure time used was $T = 15$ yr, and the effective detector volume, $V_{\rm eff} = 1$ km^3. Only downgoing events are considered. The Waxman-Bahcall flux assumes an E^{-2} spectrum, while for the Becker-Biermann and the Koers-Tinyakov fluxes we have used a power law of the form $E^{-\alpha}$, with α specified for each model. The different values of α have been selected so that the upper bound on the diffuse astrophysical muon-neutrino flux set by AMANDA-II [93] is satisfied. Details of the neutrino production models can be found in the indicated references.

where we have used the fact that $\sum_{\beta=e,\mu,\tau} \tilde{\phi}_\beta = 1$. In a similar way, the number of downgoing muon-neutrinos is given by

$$N_{\nu_\mu} = \tilde{\phi}_\mu N_{\nu_{\rm all}}^{\rm CC} \,. \tag{7.62}$$

Using Eqs. (7.54), (7.58), (7.61) and (7.62), we find

$$R_{\rm exp} = \frac{N_{\nu_\mu}}{N_{\rm sh}} = \frac{\tilde{\phi}_\mu}{\left(1 - \tilde{\phi}_\mu\right) + N_{\nu_{\rm all}}^{\rm NC}/N_{\nu_{\rm all}}^{\rm CC}} \,, \tag{7.63}$$

and we see that $R_{\rm exp}$ depends on only one of the normalised flavour ratios, $\tilde{\phi}_\mu$, and that it is independent of the exposure time and the effective detector size. Increasing T and $V_{\rm eff}$, however, results in a larger event yield and consequently in lower statistical uncertainty. Considering $N_{\nu_{\rm all}}^{\rm NC}$ and $N_{\nu_{\rm all}}^{\rm CC}$ as independent variables with Poissonian errors, i.e., $\sqrt{N_{\nu_{\rm all}}^{\rm NC}}$ and $\sqrt{N_{\nu_{\rm all}}^{\rm CC}}$ respectively, we find the error on $R_{\rm exp}$ to be

$$\sigma_{R_{\rm exp}} = \frac{R_{\rm exp}}{\left(1 - \tilde{\phi}_\mu\right) + N_{\nu_{\rm all}}^{\rm NC}/N_{\nu_{\rm all}}^{\rm CC}} \frac{N_{\nu_{\rm all}}^{\rm NC}}{N_{\nu_{\rm all}}^{\rm CC}} \sqrt{\frac{1}{N_{\nu_{\rm all}}^{\rm NC}} + \frac{1}{N_{\nu_{\rm all}}^{\rm CC}}} \,. \tag{7.64}$$

As expected, $\sigma_{R_{\rm exp}} \propto (TV_{\rm eff})^{-1/2}$, so that, for a given neutrino flux, the statistical error on $R_{\rm exp}$ decreases with the time of exposure and the size of the detector.

We have evaluated Eqs. (7.54) and (7.58) numerically in the range $10^6 \leq E_\nu/\text{GeV} \leq 10^{12}$ for the four different fluxes, assuming $T = 15$ yr and $V_{\rm eff} = 1$ km^3 (the IceCube

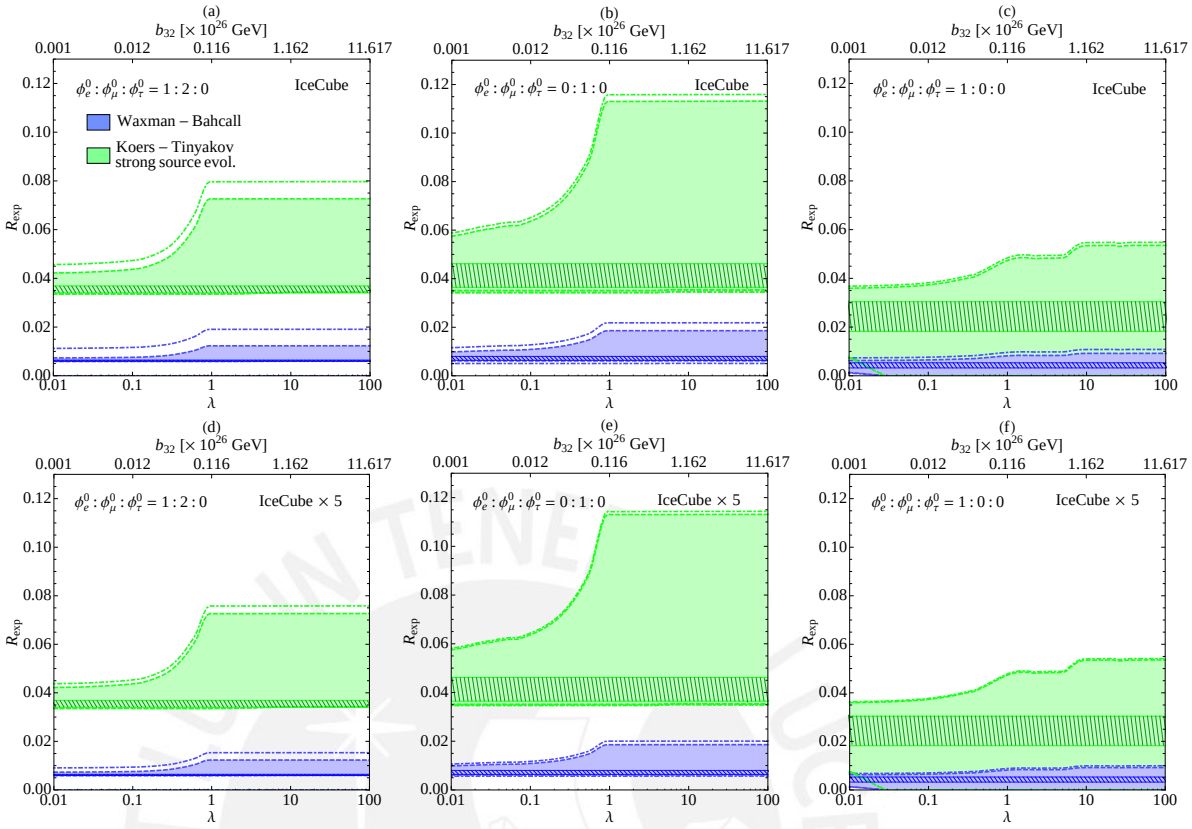

Figure 7.9: $R_{\rm exp} \equiv N_{\nu_\mu}/N_{\rm sh}$ vs. λ for two neutrino flux models: the Waxman-Bahcall flux (in blue) and the Koers-Tinyakov flux with spectral index $\alpha = 2.3$ and strong source evolution (in green). Three initial flavour ratios have been considered: $\phi_e^0 : \phi_\mu^0 : \phi_\tau^0 = 1:2:0$ (plots (a) and (d)), $0:1:0$ (plots (b) and (e)) and $1:0:0$ (plots (c) and (f)). The coloured areas, bounded by dashed coloured lines, have been calculated plugging the values of $\tilde{\phi}_\mu$ from Fig. 7.2 into Eq. (7.63) and using the event count data in Table 7.2. The dot-dashed coloured lines mark the 1σ uncertainty on $R_{\rm exp}$ for each assumption of initial ratios, calculated with Eq. (7.64). For comparison, the standard value of $R_{\rm exp}$ for the different initial ratios are shown in hatched bands of the corresponding colours; these values are calculated assuming no CPTV effects and using the current 3σ bounds on the standard mixing angles. In the upper row, an effective detector area $V_{\rm eff} = 1$ km^3 (IceCube size) was assumed; for the bottom one, $V_{\rm eff} = 5$ km^3 (IceCube $\times$ 5).

effective volume). The results are presented in Table 7.2. The Waxman-Bahcall model yields the lowest number of CC and NC events, while the Koers-Tinyakov model with strong source evolution yields the highest number, more than two orders of magnitude over Waxman-Bahcall.

7.3.3 Results

In this section, we will display the regions of $R_{\rm exp}$ vs. λ, allowing for CPTV, for the Waxman-Bahcall model and the Koers-Tinyakov model with strong source evolution, which correspond, respectively, to the cases with the lowest and highest event yields. In order to generate these regions we have used the values in Table 7.2 to calculate $R_{\rm exp}$ in the presence of CPTV, Eq. (7.63), using for $\tilde{\phi}_\mu$ the range of values allowed by the variation of the standard mixing angles θ_{ij} within their current 3σ experimental bounds and of the new mixing angles θ_{bij} in the range $[0, \pi]$. This range of values of $\tilde{\phi}_\mu$ vs. λ can be obtained from the plot of ϕ_μ vs. λ shown in Fig. 7.2, after applying the transformation in Eq. (7.59). The resulting regions as functions of λ are shown colour-filled in Figure 7.9, for the Waxman-Bahcall (blue) and Koers-Tinyakov (green) models. We have explored two different detector effective volumes, 1 km^3 (IceCube-sized) and 5 km^3, and the three different choices for the initial fluxes $\phi_e^0 : \phi_\mu^0 : \phi_\tau^0 = 1 : 2 : 0$, $0 : 1 : 0$ and $1 : 0 : 0$, that we introduced in the previous sections. Furthermore, this figure includes boundaries of 1σ statistical uncertainty on $R_{\rm exp}$ that were obtained by adding (subtracting) 1σ to (from) the upper (lower) boundaries of the coloured regions. The values of σ were calculated by plugging into Eq. (7.64) the corresponding values of $\tilde{\phi}_\mu$ that occur on the borderlines of the coloured regions.

We note that the shapes of the coloured regions in Fig. 7.9 are similar to those in Fig. 7.2. This can be understood if we note that $R_{\rm exp}$, Eq. (7.63), is proportional to $\tilde{\phi}_\mu$. In Fig. 7.2 we saw that there exists overlap among the regions related to the different hypotheses of the initial flux. In fact, in Fig. 7.9, there is overlap between the three production models, with the region corresponding to $\phi_e^0 : \phi_\mu^0 : \phi_\tau^0 = 1 : 2 : 0$ almost entirely enclosed within the region for $0 : 1 : 0$. This last fact can be explained on account of the reduction in size of the region for $1 : 2 : 0$, caused by the normalisation of $\tilde{\phi}_\mu$ applied for this case, i.e., $\tilde{\phi}_\mu = \phi_\mu/3$. As we can anticipate, due to the higher event yield, the statistical uncertainty on $R_{\rm exp}$ associated to the Koers-Tinyakov flux is lower than the one associated to the Waxman-Bahcall flux, and is reduced when the larger detector volume is used. The size of this uncertainty is also proportional to the value of $\tilde{\phi}_\mu$ (see Eq. (7.64)). As a consequence, the size of the 1σ regions is larger for an initial flux of $1 : 2 : 0$, intermediate for $0 : 1 : 0$, and smallest for $1 : 0 : 0$.

When a detector volume of 1 km^3 is considered, there is a clear overlap among regions corresponding to different assumptions of the neutrino flux model when the production scenario is $1 : 0 : 0$. This observation is reinforced when we consider also the regions spanned by the statistical uncertainty. In comparison, for the $1 : 2 : 0$

and $0:1:0$ scenarios, the regions corresponding to the two flux models do not overlap. When the 5 km^3 detector is assumed, the regions associated to $1:2:0$ and $0:1:0$ are further separated at the 1σ level. However, there is still an overlap between the two flux models in the $1:0:0$ scenario. Here we do not show the results for the Becker-Biermann model and the Koers-Tinyakov model with no source evolution, since their results are embodied in what we have already presented. For instance, the mean value of R_{exp} and $\sigma_{R_{\text{exp}}}$ for Becker-Biermann is similar to the one for Waxman-Bahcall. Similar estimates can be easily obtained by plugging the values of Table 7.2 into Eqs. (7.63) and (7.64).

7.4 Summary and conclusions

Motivated by the CPT-violating (CPTV) neutrino coupling considered in the Standard Model Extension, we have added a CPTV, energy-independent, contribution to the neutrino oscillation Hamiltonian and explored its effects on the flavour ratios of the high-energy (1 PeV and higher) astrophysical neutrino flux predicted to come from active galactic nuclei. We have parametrised the strength of the CPTV contribution by the parameter λ, defined as the quotient between the eigenvalues of the CPTV Hamiltonian, b_{21} and b_{32}, and those of the standard-oscillation one, $\Delta m^2_{21}/\left(2E^\star\right)$ and $\Delta m^2_{32}/\left(2E^\star\right)$, with $E^\star = 1$ PeV, and allowed λ to vary between 10^{-2} and 100, corresponding to standard-oscillation dominance and CPTV dominance, respectively. We have used three different neutrino production scenarios for the flavour ratios at the astrophysical sources: production by pion decay, which results in $\phi^0_e : \phi^0_\mu : \phi^0_\tau = 1:2:0$; muon cooling, which results in $0:1:0$; and neutron decay, resulting in $1:0:0$, and explored the effect of a potential CPTV on the neutrino flavour ratios at Earth, ϕ_α ($\alpha = e, \mu, \tau$), and on the ratios between them. With this objetive, we have studied the behaviour of ϕ_μ, $R = \phi_\mu/\phi_e$, and $S = \phi_\tau/\phi_\mu$, by letting the standard-oscillation mixing parameters vary within their current 3σ experimental bounds, and varying the unknown CPTV parameters as broadly as possible, while keeping b_{21} and b_{32} below their current upper limits (obtained from atmospheric and solar experiment data).

From the observation of ϕ_μ, if CPTV is dominant, we found that there could be large deviations with respect to the pure standard-oscillation case, depending on the values of the CPTV parameters. These deviations start at $\lambda = 0.1$ ($b_{32} \sim 10^{-28}$ GeV, $b_{21} \sim 10^{-26}$ GeV) and reach a plateau at $\lambda = 1$. There are overlaps between the different neutrino production models, in such a way that a measurement of certain values of ϕ_μ could be satisfied by two different production models, either including

CPTV or not.

When we consider the possibility of detecting ϕ_μ and ϕ_e, from which $R \equiv \phi_\mu/\phi_e$ can be built, we find that the regions corresponding to $1:2:0$ and $0:1:0$ exhibit a similar behaviour than when ϕ_μ alone is measured, though the former is now nearly contained by the latter. This is not the case for $1:0:0$, where the value of R could blow up owing to a potentially very low value of ϕ_e, in comparison to ϕ_μ.

If tau-neutrinos can also be detected, then we can use the ratio $S \equiv \phi_\tau/\phi_\mu$. When we combine R and S, i.e., when we assume the ability to measure ϕ_τ with enough statistics, we improve the chances of discovering CPTV effects. In fact, large CPTV regions of (R, S) values that are well distinguished from the standard-oscillation case are obtained for the three neutrino production models that we have considered here. As a consequence of the wideness of these regions, there are many overlapping areas where a given pair (R, S) can be generated by any of the production models that we have explored, assuming a dominant CPTV.

On the other hand, in the case of the non-observation of deviations in the flavour ratios, it will be possible to impose very stringent limits on the parameters related to CPTV in the neutrino sector, such as $b_{21} \lesssim 10^{-29}$ GeV and $b_{32} \lesssim 10^{-27}$ GeV, to be compared with the current limits of 10^{-23} GeV and 10^{-21} GeV, respectively.

In order to compare CPTV with other competitive new physics scenarios, we have included the possibility of neutrino decay to invisible products, both in the normal and inverted mass hierarchies. As a result, there are additional overlaps between the CPTV regions and the regions accessible by neutrino decays, for certain values of the CPTV parameters.

With the purpose of presenting a more realistic perspective, we have performed an analysis of the potential CPTV signals at a large ice Čerenkov detector such as IceCube. On top of the three neutrino production models, $1:2:0$, $0:1:0$ and $1:0:0$, we have used two different models for the neutrino astrophysical flux, one by Waxman and Bahcall and the other by Koers and Tinyakov, and compared their respective signals at the detector. For this analysis, we have found that there are still overlaps among the three production models, even more pronounced than the ones that were obtained in the theoretical plots. In 15 years of exposure time, a 1 km^3 detector (or, equivalently, $tV_{\text{eff}} = 15$ yr km^3) would be able to distinguish between the two fluxes, in the $1:2:0$ and $0:1:0$ scenarios, while a 5 km^3 detector with the same exposure (or $tV_{\text{eff}} = 75$ yr km^3), would provide clearer separation between the flux models at the 1σ level.

When $\lambda \geq 1$, a separation of a few standard deviations between the CPT-conserving and the CPTV scenarios is possible, depending on the values of the

CPTV mixing parameters, both for the Waxman-Bahcall and the Koers-Tinyakov fluxes. This separation is more clearly visible in the $1:2:0$ and $0:1:0$ cases. Our main result is that, while it is in principle possible to detect the presence of CPTV with IceCube, it will not be possible, for many values of (R, S), to find which one of the production models is the actual one. The detection of CPTV can be aided by a more precise knowledge of the standard-oscillation mixing parameters and by a considerably higher event yield, brought by a larger effective volume or probably from a non-Čerenkov detector, but these two improvements do not eliminate the overlaps that exist between (R, S) regions associated to different production models. In the event of measuring values of R, S, or both, that fall inside an overlap region, then, in the absence of knowledge of the values of the CPTV mixing parameters, one is able to trade one production model, with a certain set of values of the CPTV parameters, by one of the other overlapping models, with another set of values of the parameters. These degeneracies could be lifted by an independent measurement of the CPTV parameters in the neutrino sector, in a different kind of experiment.

Nevertheless, as a tool for detecting the presence of CPT breaking in the neutrino sector, if not for measuring it in detail, IceCube might be a useful one. If CPT is broken, and if the parameters introduced by the breaking have certain values, then IceCube could be able to detect the deviation from the standard-oscillation scenario after 15 years of data taking.

Chapter 8

Summary and conclusions

Lorentz and CPT invariance are a fundamental property of any local quantum field theory, such as the Standard Model (SM), which is briefly summarised in Chapter 2. Every term in the SM Lagrangian is Lorentz-invariant and CPT-even, i.e., they are invariant under a combined C, P, and T transformation (Section 2.2). However, in Chapter 3 we saw that it is possible to add extra terms to the SM Lagrangian that break Lorentz invariance and which can be classified into CPT-even and CPT-odd terms, the latter of which change sign under a CPT transformation. A general theoretical framework, called the Standard Model Extension (SME), was introduced by Kostelecky *et al.* [13, 14, 46], as a generalisation of the SM which adds Lorentz-violating couplings in all of the particle sectors, parametrised by coefficients, some of which are bounded by experimental data [47]. The SME is an effective field theory: it assumes that a fundamental Lorentz-invariant theory exists at a high energy scale (in string theory, this may be the Planck scale, $m_{Pl} \approx 10^{19}$ GeV) and that Lorentz symmetry is spontaneously broken at a lower energy scale, the Lorentz-violating terms arising as a consequence of this breaking. However, the SME does not assume a particular form of the fundamental theory; in this sense, the Lorentz violation in the SME is model-independent.

Neutrino flavour transitions, or "oscillations", were introduced in Chapter 4. There we saw that a neutrino of a certain flavour does not have a definite mass, but rather that it is a linear combination of several neutrino mass eigenstates of a propagation Hamiltonian, each of which does have a definite mass value. For the case of three active neutrino flavours, ν_e, ν_μ, and ν_τ, three accompanying mass eigenstates, ν_1, ν_2, and ν_3, are necessary. The two neutrino bases are connected by means of a unitary transformation, represented by the Pontecorvo-Maki-Nakagawa-Sakata (PMNS) mixing matrix U: a neutrino of flavour α is defined as $|\nu_\alpha\rangle = \sum_{i=1}^{3} U^*_{\alpha i}|\nu_i\rangle$. The PMNS matrix can be parametrised in terms of three mixing

angles, which are bounded by experiment [50], and one CP-violation phase, whose value remains unknown.

As a result of the interference between the different mass eigenstates, each of mass m_i, that make up a flavour state, there is a probability that a neutrino of energy E created with flavour α is detected, after having propagated for a distance L, as having flavour $\beta \neq \alpha$. This probability contains sinusoidal terms (hence the name neutrino *oscillations*) with a typical dependence of the form $\sim \sin^2\left(\Delta m^2_{ij} L/\left(4E\right)\right)$, with the mass-squared differences $\Delta m^2_{ij} = m^2_i - m^2_j$ $((i,j) = (2,1),(3,1),(3,2))$ bounded by experiment. The L/E oscillation phase is typical of standard, mass-driven, neutrino oscillations. Furthermore, the amplitude of the oscillations depends on the values of the mixing angles in the PMNS matrix.

When neutrinos travel through matter, e.g., when neutrinos created in the Sun or the atmosphere travel through the Earth, neutral- and charged-current forward scattering off the nucleons results in modifications to the energy eigenvalues and, therefore, to the oscillation probability. We saw in Section 4.1.3 that the effect of matter interactions can be introduced in a straightforward manner by writing the vacuum-oscillation Hamiltonian, H, in the flavour basis (that is, by calculating $H_f = UHU^\dagger$) and adding to it extra terms that account for the interaction with matter. Re-deriving the oscillation probability with this modified Hamiltonian (see Section 4.1.2) we find the same functional form of the oscillation formula, but with the vacuum mixing angles and mass-squared differences replaced by their respecitve effective values in matter.

Effects different from matter interactions could be added to the vacuum oscillation Hamiltonan following the same procedure. In general, the result would be similar: the mixing angles and mass differences would be modified with respect to their vacuum values. In the present work, we have explored CPT violation by adding a CPT-odd term to the neutrino sector of the SM. As a result, energy-independent, CPT-violating, contributions will apear, together with the vacuum terms, in both the mixing angles and the mass differences. Since the vacuum oscillation terms have a $1/E$ dependence, they will be more suppressed the higher the energy, while the CPT-violating contribution remains constant. Therefore, the effect of the constant terms should be more easily detected in the flux of very high-energy neutrinos.

The most energetic neutrinos are the ones that are expected to originate at distant astrophysical or cosmological sources, such as supernovae, gamma ray bursts (GRBs), and active galactic nuclei (AGN). In the latter two, it is presumed that shock-accelerated protons interact with background photons and create pions: the neutral ones decay into X-ray and gamma-ray photons, whereas the charged ones

decay into neutrinos. Additionally, observations performed during the last decade have identified AGN and GRBs as the production sites of the highest-energy X-rays detected. If the origin of these lies in the decay of neutral pions, then an accompanying high-energy neutrino flux is to be expected also from these sources. In Chapter 5 we saw that recent results from the Pierre Auger Observatory (PAO) indicate that the reconstructed directions of the highest-energy cosmic rays, with energies greater than 57 EeV, are correlated with the known positions of some AGN [82]. The neutrinos from AGN are expected to reach energies of up to 10^{12} GeV, and would provide, if detected, an ideal probe of CPT violation in neutrinos.

In the same chapter we introduced three different high-energy neutrino production models at AGN: by Waxman & Bahcall (WB) [89], by Koers & Tinyakov (KT) [86], and by Becker & Biermann (BB) [87]. The models differ in their assumptions: for instance, while in the KT model the protons, and the $p\gamma$ interactions, are confined in a region close to the center (where a supermassive black hole possibly exists), in the BB model the $p\gamma$ interactions are assumed to occur in the jets of the AGN. Furthermore, the KT model considers two possibilities regarding the distribution of the sources: either they are distributed homogeneously in redshift and luminosity, or they follow the star formation rate (see Section 5.1.3).

At the sources, different neutrino flavours are produced in different proportions (see Secion 5.1). Assuming the unobstructed decay of the pions generated in $p\gamma$ interactions, twice the number of muon-neutrinos are created with respect to electron-neutrinos, and no tau-neutrinos are produced. Succintly put, $\phi_e^0 : \phi_\mu^0 : \phi_\tau^0 = 1 : 2 : 0$. However, if the muons produced in the decay of pions lose most of their energy through interactions before decaying into neutrinos, then the high-energy flavour fluxes will be $0 : 1 : 0$. In a third scenario, the nuclei emitted from, say, AGN, are broken up by photodisintegration due to their interaction with the cosmic-microwave-background photons, and the freed nucleons produce $\overline{\nu}_e$ through beta decay, thus yielding fluxes of $1 : 0 : 0$. Note that, since neutrino detectors are not able to distinguish between neutrinos and anti-neutrinos, we make no such distinction also in the flavour fluxes.

The neutrinos thus generated undergo flavour oscillations on their way to Earth. As a result, the flavour fluxes at Earth, ϕ_α, are different from those at production, namely, $\phi_\alpha = \sum_{\beta=e,\mu,\tau} P_{\beta\alpha}\phi_\beta^0$, for $\alpha = e, \mu, \tau$. Hence, new physics effects that affect the oscillation probability $P_{\beta\alpha}$, such as CPT violation, might yield flavour fluxes at Earth which greatly deviate from the values of the fluxes under standard oscillations. In our exploration of CPT violation in astrophysical neutrinos, we have used these detected flavour ratios as our key observables.

Before attempting to study CPT violation with high-energy astrophysical neutrinos in the context of the SME, we have done so in the context of modified dispersion relations, in Chapter 6. Motivated by candidate theories of quantum gravity, the special-relativistic dispersion relation, $E^2 = p^2 + m^2$, is augmented by an extra term that introduces Lorentz- and CPT-violation and that is suppressed by some power of the Planck energy. The suppression is parametrised by three real coefficients b_{ij}, which have experimental upper bounds of 10^{-21} GeV or lower. This extra term induces an energy-independent oscillation phase, but does not affect the mixing angles. In other words, the oscillation wavelength is modified, but not the amplitude.

Naively, one could expect that, for neutrinos of very high energy, the standard L/E oscillation phase would vanish, leaving only the constant CPT-violating term. Were this to occur, the oscillation probability would become constant after such an energy value. However, we found that, in order to satisfy the current upper bounds on b_{ij}, the minimum energy at which the probability could become constant is $\sim 10^{16.5}$ GeV, about five orders of magnitude higher than the most energetic astrophysical neutrinos expected [103]. Therefore, while modified dispersion relations are useful in constraining the values of the suppression parameters b_{ij} in terrestrial neutrino experiments, where, due to the high statistics, the deviations of the expected shape of the energy spectrum can be used to set bounds on the b_{ij} using neutrinos of lower enregy, the dispersion relation formalism fails at higher energies, where the low statistics precludes the reconstruction of the energy spectrum and only the event count above a certain energy (say, 1 PeV) is available as a potential means to bound the b_{ij}.

In Chapter 7 we explored the modification of neutrino flavour fluxes at Earth due to CPT violation, in the context of the Standard Model Extension. By adding a CPT-odd Lorentz-violating contribution to the neutrino sector, $b_{\mu\alpha\beta}\overline{\nu}_\alpha\gamma^\mu\nu_\beta$, the oscillation Hamiltonian, written in the flavour basis, is modified by the CPT-violating, energy-independent, terms $b_{0\alpha\beta}$. When diagonalising this augmented Hamiltonian, as part of the procedure to calculate the oscillation probability (see Section 7.2.1), it is found that both the mass-squared differences and the mixing angles are affected, or, equivalently, both the oscillation phase and amplitude are affected, whereas when using the modified dispersion relation formalism only the phase is. Furthermore, we have assumed that the eigenvalues associated to the CPT-violating contribution, b_{ij}, are λ times the standard oscillation eigenvalues, i.e., the squared-mass differences $\Delta m^2_{ij}/2E^\star$, at a neutrino energy of $E^\star = 1$ PeV. For $\lambda \ll 1$, the standard oscillation contribution to the Hamiltonian is the dominant one, while for $\lambda \gg 1$, the CPT-violating contribution is dominant; for $\lambda \sim 1$, both parts contribute equally.

In this context, we have explored the magnitude of the deviation of the flavour fluxes, and of the ratios between them, with respect to their values expected from standard oscillations. By varying the standard mixing parameters within their current 3σ experimental bounds [50] and the parameters (three mixing angles and two eigenvalues) associated with the CPT violation in the broadest possible way, we have generated regions of values corresponding to the two scenarios: the standard-oscillations one, and the CPT-violating one. In each one, we separately the three different production flavour fluxes, $1:2:0$, $0:1:0$, and $1:0:0$.

First, in Section 7.2.2, we assumed that only muon-neutrinos are detected. We found that even for relatively low values of λ, around 10^{-2}, there is already a deviation from the standard region of values of ϕ_μ. As expected, the deviation grows with λ, as the CPT-violating term grows in importance. At $\lambda \approx 1$, ϕ_μ reaches a plateau and remains essentially unchanged as λ grows further. An interesting observation is that the regions of ϕ_μ corresponding to the three different production flavour fluxes have certain zones where they superimpose. As a result, if the measured value of ϕ_μ were to lie inside one of these regions, we might be able to assert that CPT-violation is indeed present (depending on whether or not the point lies far enough from the standard-oscillations region), but we would not be able to attribute the observation to a single scenario of production flavour fluxes.

In Section 7.2.3 we considered that muon- and electron-neutrinos are detected, and defined the ratio $R \equiv \phi_\mu/\phi_e$. The regions of values of R also grow with λ. Under the assumption of a $0:1:0$ production model, R can attain very large values, between 10^6 and 10^7, as a result of very low electron-neutrino fluxes. On the other hand, the CPT-violating region associated to the $1:2:0$ production model reaches a maximum of $R = 2$ after $\lambda \simeq 5$, while the one associated to $1:0:0$ reaches a maximum of $R = 1$ after $\lambda \approx 1$. Therefore, a measurement of $R \gg 4$ could imply that the production model is $0:1:0$, and that CPT-violation effects are present, but will not be enough to set strong bounds on λ. The minimum value in both the $0:1:0$ and $1:2:0$ regions is located around $R = 0.8 \sim 1$, while for the $1:0:0$ flux, it is zero for most of the range of λ. If a value of $R \lesssim 4$ is found, the ability to distinguish between production models depends on the magnitude of the experimental errors with which ϕ_e and ϕ_μ are measured. A single production model can be distinguished univocally for some measured values of R, while for others, two (when $1 \lesssim R \lesssim 4$, depending on λ) or three models (when $R \simeq 1$) can account for the same measured value.

Detection of the three neutrino flavours is the subject of Section 7.2.4. Given the tau-neutrino flux we have defined also the ratio $S \equiv \phi_\tau/\phi_\mu$ and studied the

deviations from the standard-oscillations regions in the $R-S$ plane. Since we have considered the propagation of neutrinos over distances of hundreds or thousands of Mpc, neutrino decays are a possibility. For comparison, we have included the predictions of neutrino decay into invisible productions in two scenarios: one in which the lightest mass eigenstated is ν_1 (normal mass hierarchy) and one in which it is ν_3 (inverted mass hierarchy). The $R-S$ plane exhibits is rich in its features: there are zones where the CPT-violating predictions of all the three production models superimpose, zones that can be attributed either to one production model under standard oscillations or to a different one under CPT violation, and zones where the predictions from CPT violation intersect with those of neutrino decay. As expected, the CPT-violating regions in the $R-S$ plane grow with λ; beyond $\lambda = 100$, corresponding to dominant CPT violation, they do not change shape or size. We have also explored the variation of R and S with $\delta_{\rm CP}$, and found that a variation of the ratios of up to $\sim 40\%$ is possible as a result of varying the mixing angle θ_{13} within its 3σ allowed region.

It is also interesting to point out that in the case of an experimental non-detection of CPT violation in the neutrino flavour ratios, R and S can be used to set limits on the related parameters. In fact, when $\lambda = 1$, and for a neutrino energy of 1 PeV, we can attain limits for the CPTV eigenvalues b_{ij} in the order of 10^{-29} and 10^{-27} GeV, for b_{21} and b_{23}, respectively. It is also important to mention that these results can be easily rescaled to any energy, just by doing $b_{ij}\times(\text{PeV}/E)$. This would mean a very significant improvement over the current bounds of $10^{-23}-10^{-21}$ GeV for b_{21} and b_{32}, respectively [122].

Finally, in Section 7.3, we have estimated the high-energy neutrino signals at the IceCube Čerenkov neutrino detector, located in the ice near the South Pole, and at a detector with five times IceCube's effective volume, in the presence of CPT violation. In order to do this, we have used the AGN neutrino fluxes introduced in Chapter 5 and calculated the number of charged- and neutral-current events initiated by the neutrinos of different flavours at IceCube. We have defined the experimental analogue of R, denoted by $R_{\rm exp}$, as the ratio of the number of muon tracks to the total number of showers detected, within the energy range 10^6-10^{12} GeV. Since the astrophysical tau-neutrino flux is expected to be very low, we have not considered an experimental analogue of S.

We selected the two fluxes which yield the lowest and highest event counts: the Waxman-Bahcall flux and the Koers-Tinyakov flux with strong source evolution, respectively. Due to the higher event yield, the statistical uncertainty on $R_{\rm exp}$ associated to the Koers-Tinyakov flux is appreciably lower than the one associated

to the Waxman-Bahcall flux, and is reduced when the larger (5×) detector volume is used. The size of this uncertainty is also proportional to the value of ϕ_μ. As a consequence, the size of the 1σ regions is larger for an initial flux of $1:2:0$, intermediate for $0:1:0$, and smallest for $1:0:0$.

When a detector volume of 1 km^3 is considered, there is a clear overlap among regions corresponding to different assumptions of the neutrino flux model when the production scenario is $1:0:0$. This observation is reinforced when we consider also the regions spanned by the statistical uncertainty. In comparison, for the $1:2:0$ and $0:1:0$ scenarios, the regions corresponding to the two flux models do not overlap. When the 5 km^3 detector is assumed, the regions associated to $1:2:0$ and $0:1:0$ are further separated at the 1σ level. However, there is still an overlap between the two flux models in the $1:0:0$ scenario.

In conclusion, we have found that IceCube might be able to detect the presence of a CPT-odd term in the high-energy astrophysical neutrino flavour fluxes. However, IceCube's capacity to confidently claim discovery of CPT violation is limited due to our current lack of knowledge of the standard and of the CPT-violating mixing parameters. The coming years will undoubtedly bring an improved determination of the standard mixing parameters, so that the potential distinction between standard-oscillation and CPT-violating regions will be clearer.

Appendix A

Derivation of the two–neutrino oscillation probability with an arbitrary time-independent Hamiltonian

A.1 With a general Hamiltonian

Consider a general, time-independent, two-neutrino Hamiltonian H_2 –effectively a 2×2 matrix– and write it as

$$H_2 = h_0 I + h_k \sigma^k \ , \quad k = 1, 2, 3 \ , \tag{A.1.1}$$

where σ^k, $k = 1, 2, 3$, are the traceless Pauli matrices which, together with the identity I constitute a basis for the space of 2×2 matrices (sum over k is assumed). h_0 and the h_k are functions of the components of the Hamiltonian, $(H_2)_{ij}$, $i, j = 1, 2$. In the two-neutrino case,

$$|\nu_\alpha\rangle = f_e |\nu_e\rangle + f_\mu |\nu_\mu\rangle \tag{A.1.2}$$

is a two-component column vector, with f_e and f_μ the amplitudes associated to detecting an electron- and muon-neutrino, respectively. The former is represented by $|\nu_e\rangle = (1\ 0)^T$, while the latter is represented by $|\nu_\mu\rangle = (0\ 1)^T$.

The time-evolution operator associated to H_2 is thus $U_2(L) = e^{-i(h_0 I + h_k \sigma^k)L}$. Given that the conmutator $C_2 \equiv \left[h_0 I, h_k \sigma^k\right] = 0$ and so $[h_0 I, C_2] = \left[h_k \sigma^k, C_2\right] = 0$, we are able to separate the exponential into $e^{-i h_0 I L} e^{-i h_k \sigma^k L}$. Furthermore, making

use of the well-known Euler identity

$$e^{\pm i|r|\hat{r}_k\sigma^k} = \cos(|r|) \pm i\hat{r}_k\sigma^k \sin(|r|) \ , \tag{A.1.3}$$

with $\hat{r}$ a unitary vector in the direction of r, and noting that $e^{-ih_0 IL}|\nu_\alpha\rangle = e^{-ih_0 L}|\nu_\alpha\rangle$, we can finally write

$$\begin{aligned} U_2(L) &= e^{-ih_0 L}\left[\cos(|h|\,L) - i\hat{h}_k\sigma^k \sin(|h|\,L)\right] &\text{(A.1.4)}\\ &\to \cos(|h|\,L) - i\hat{h}_k\sigma^k \sin(|h|\,L) \ , &\text{(A.1.5)}\end{aligned}$$

with $|h| \equiv \sqrt{h_k h^k}$ the module of the vector h_k and where to obtain the last expression we have discarded the global phase $e^{-ih_0 L}$. Note that

$$h\cdot\sigma = \begin{pmatrix} h_3 & h_1 - ih_2 \\ h_1 + ih_2 & -h_3 \end{pmatrix} . \tag{A.1.6}$$

The evolved state of a neutrino that was produced with flavour α (i.e., $f_\alpha = 1$, $f_\beta = 0$) is

$$|\nu_\alpha\rangle = U_2(L)\left(f_\alpha|\nu_\alpha\rangle + f_\beta|\nu_\beta\rangle\right) = U_2(L)\,|\nu_\alpha\rangle. \tag{A.1.7}$$

The probability of the transition $\nu_\alpha \to \nu_\beta$ is then calculated as

$$\begin{aligned} P_{\alpha\beta} &\equiv P_{\nu_\alpha\to\nu_\beta}(L) = |\langle\nu_\beta\,|\nu_\alpha(L)\rangle|^2 = |\langle\nu_\alpha|\,U(L)\,|\nu_\alpha\rangle|^2 \\ &= \left|\cos(|h|\,L)\,\langle\nu_\beta|\nu_\alpha\rangle - i\frac{\sin(|h|\,L)}{|h|}\,\langle\nu_\beta|\,h\cdot\sigma\,|\nu_\alpha\rangle\right|^2 \\ &= \left|-i\frac{\sin(|h|L)}{|h|}\langle\nu_\beta|h\cdot\sigma|\nu_\alpha\rangle\right|^2 = \frac{\sin^2(|h|L)}{|h|^2}|\langle\nu_\beta|h\cdot\sigma|\nu_\alpha\rangle|^2 \\ &= \frac{h_1^2+h_2^2}{|h|^2}\sin^2(|h|\,L)\,. \end{aligned} \tag{A.1.8}$$

Because of the conservation of probability, $P_{\alpha\alpha}(L) = 1 - P_{\alpha\beta}(L)$. In a single expression, we can write

$$P_{\alpha\beta}(L) = \delta_{\alpha\beta} + (-1)^{\delta_{\alpha\beta}}\frac{h_1^2+h_2^2}{|h|^2}\sin^2(|h|\,L) \ . \tag{A.1.9}$$

Thus, by making use of Eq. (A.1.9), we are able to calculate the transition probabilities corresponding to any time-independent Hamiltonian, in the two-neutrino scenario.

A.2 Oscillations in the vacuum

Consider, for instance, flavour oscillations in the vacuum. These are driven by the mass-squared difference between two mass eigenstates $|\nu_1\rangle$ and $|\nu_2\rangle$, with respective masses m_1 and m_2, out of which the flavour states $|\nu_e\rangle$ and $|\nu_\mu\rangle$ are constructed (or $|\nu_\mu\rangle$ and $|\nu_\tau\rangle$ if we are studying atmospheric neutrinos). In this case, the Hamiltonian is

$$H_2^{\text{vac}} = \frac{1}{2E} \begin{pmatrix} \cos(\theta) & \sin(\theta) \\ -\sin(\theta) & \cos(\theta) \end{pmatrix} \begin{pmatrix} \Delta m^2 & 0 \\ 0 & -\Delta m^2 \end{pmatrix} \begin{pmatrix} \cos(\theta) & -\sin(\theta) \\ \sin(\theta) & \cos(\theta) \end{pmatrix} , \tag{A.2.10}$$

with E the neutrino energy, $\Delta m^2 \equiv m_2^2 - m_1^2$, and θ the mixing angle between $|\nu_1\rangle$ and $|\nu_2\rangle$. Using this Hamiltonian,

$$|h_1|^2 = \frac{\Delta m^2}{2E} \sin^2(2\theta) \quad , \quad |h_2|^2 = 0 \quad , \quad |h_3|^2 = \frac{\Delta m^2}{2E} \cos^2(2\theta) \quad , \quad |h|^2 = \frac{\Delta m^2}{2E} , \tag{A.2.11}$$

so that

$$\frac{|h_1|^2 + |h_1|^2}{|h|^2} = \sin^2(2\theta) \tag{A.2.12}$$

and, from Eq. (A.1.9), the probability in this scenario is

$$P_{\alpha\beta}(E, L) = \sin^2(2\theta) \sin^2\left(\frac{\Delta m^2}{4E} L\right) \quad , \quad \alpha \neq \beta , \tag{A.2.13}$$

$$P_{\alpha\alpha}(E, L) = 1 - P_{\alpha\beta}(E, L) , \tag{A.2.14}$$

which is the standard expression for standard two-neutrino mixing. Inserting the necessary factors of $\hbar$ and c, we can write

$$P_{\alpha\beta}(E, L) = \sin^2(2\theta) \sin^2\left(1.27 \frac{\Delta m^2\,[\text{eV}^2]}{E\,[\text{GeV}]} L\,[\text{km}]\right) \quad , \quad \alpha \neq \beta . \tag{A.2.15}$$

Instead of the vacuum-oscillation Hamiltonian, we could have used one that incorporates interaction with matter (see the next section), non-standard interactions (NSI) such as flavour-changing neutral currents or one that allows for violation of Lorentz or CPT invariance. Thus, by writing the Hamiltonian as the sum of a part proportional to the identity and a part which is a linear combination of the Pauli matrices, and making use of the identity in Eq. (A.1.3), we have a general method for calculating flavour-transition probabilities in a closed form.

Appendix B

Derivation of the three–neutrino vacuum oscillation probability

Neutrinos of a definite flavour are linear combinations of neutrino mass eigenstates, i.e., of neutrinos with definite mass:

$$|\nu_\alpha\rangle = \sum_i [U_0]^*_{\alpha i} |\nu_i\rangle \ , \tag{B.0.1}$$

with U_0 the complex unitary matrix that represents the transformation between the flavour and mass bases.

Since the mass eigenstates $|\nu_i\rangle$ are eigenstates of the Hamiltonian (in the mass basis) $H = \mathrm{diag}\,(E_1, E_2, E_3)$, the eigenvalue equation reads

$$H|\nu_i\rangle = E_i|\nu_i\rangle = \sqrt{m_i^2 + p_i^2}|\nu_i\rangle \ , \tag{B.0.2}$$

with E_i, m_i and p_i the energy, mass and momentum, respectively, of the i-th eigenstate. Using the fact that neutrinos are highly relativistic, i.e., that $m_i \ll E_i$, and assuming that all of the mass eigenstates share the same energy, i.e., that $E_i = E$ for all i, we can write the momentum of the i-th eigenstate as

$$p = \sqrt{E^2 - m_i^2} \simeq m_i^2/\left(2E\right) \ . \tag{B.0.3}$$

Hence, the mass eigenstate propagates as

$$|\nu_i\left(L\right)\rangle = e^{-iHL}|\nu_i\rangle = e^{-i\frac{m_i^2}{2E}L}|\nu_i\rangle \ , \tag{B.0.4}$$

After having propagated a distance L since its production, the neutrino created with

flavour α is

$$|\nu_\alpha(L)\rangle = \sum_i [U_0]^*_{\alpha i} |\nu_i(L)\rangle = \sum_i [U_0]^*_{\alpha i} e^{-i\frac{m_i^2}{2E}L} |\nu_i\rangle \ . \tag{B.0.5}$$

Inverting Eq. (B.0.1) yields

$$|\nu_i\rangle = \sum_\beta [U_0]_{\beta i} |\nu_\beta\rangle \ , \tag{B.0.6}$$

where the sum is over all neutrino flavours. Inserting this in Eq. (B.0.5) makes it evident that the neutrino created with flavour α is now a linear combination of neutrinos of all flavours, i.e.,

$$|\nu_\alpha(L)\rangle = \sum_\beta [U_0]^*_{\alpha i} e^{-i\frac{m_i^2}{2E}L} [U_0]_{\beta i} |\nu_\beta\rangle \ . \tag{B.0.7}$$

Hence, the probability amplitude of detecting the neutrino with flavour β is

$$\langle\nu_\beta|\ \nu_\alpha(L)\rangle = \sum_i [U_0]^*_{\alpha i} [U_0]_{\beta i} e^{-i\frac{m_i^2}{2E}L} \ , \tag{B.0.8}$$

where we have made use of the orthonormality of the flavour basis, i.e., $\langle\nu_\beta|\nu_\alpha\rangle = \delta_{\beta\alpha}$. The transition probability for $\nu_\alpha \to \nu_\beta$ can then be written as

$$P_{\alpha\beta} = |\langle\nu_\beta|\ \nu_\alpha(L)\rangle|^2 = \sum_{i,j} [U_0]^*_{\alpha i} [U_0]_{\beta i} [U_0]_{\alpha j} [U_0]^*_{\beta j} e^{-i\frac{\Delta m_{ij}^2}{2E}L} \ , \tag{B.0.9}$$

with $\Delta m_{ij}^2 \equiv m_i^2 - m_j^2$.

Now, let

$$J^{ij}_{\alpha\beta} \equiv [U_0]^*_{\alpha i} [U_0]_{\beta i} [U_0]_{\alpha j} [U_0]^*_{\beta j} \tag{B.0.10}$$

and

$$\Delta_{ij} \equiv \frac{\Delta m_{ij}^2}{2E} L \ , \tag{B.0.11}$$

so that Eq. (B.0.9) can be written succintly as $P_{\alpha\beta} = \sum_{i,j=1}^3 J^{ij}_{\alpha\beta} e^{-i\Delta_{ij}}$. After expanding the sum, we obtain

$$\begin{aligned} P_{\alpha\beta} \ = \ & \sum_i J^{ii}_{\alpha\beta} \\ & + \left(J^{12}_{\alpha\beta} e^{-i\Delta_{12}} + J^{21}_{\alpha\beta} e^{-i\Delta_{21}}\right) \\ & + \left(J^{13}_{\alpha\beta} e^{-i\Delta_{13}} + J^{31}_{\alpha\beta} e^{-i\Delta_{31}}\right) \\ & + \left(J^{23}_{\alpha\beta} e^{-i\Delta_{23}} + J^{32}_{\alpha\beta} e^{-i\Delta_{32}}\right) \ . \end{aligned} \tag{B.0.12}$$

Note that $J^{ji}_{\alpha\beta} = \left(J^{ij}_{\alpha\beta}\right)^*$. With this, and with the trivial identity $\Delta_{ij} = -\Delta_{ji}$, we can write

$$J^{ij}_{\alpha\beta}e^{-i\Delta_{ij}} + J^{ji}_{\alpha\beta}e^{-i\Delta_{ji}} = J^{ij}_{\alpha\beta}e^{-i\Delta_{ij}} + \left(J^{ij}_{\alpha\beta}e^{-i\Delta_{ij}}\right)^* = 2\ \mathrm{Re}\left(J^{ij}_{\alpha\beta}e^{-i\Delta_{ij}}\right) \tag{B.0.13}$$

and so the oscillation probability becomes

$$P_{\alpha\beta} = \sum_i J^{ii}_{\alpha\beta} + 2\sum_{i>j} \mathrm{Re}\left(J^{ij}_{\alpha\beta}e^{-i\Delta_{ij}}\right)\ . \tag{B.0.14}$$

Next, we develop

$$\begin{aligned} \mathrm{Re}\left(J^{ij}_{\alpha\beta}e^{-i\Delta_{ij}}\right) &= \mathrm{Re}\left(J^{ij}_{\alpha\beta}\cos\left(\Delta_{ij}\right) - iJ^{ij}_{\alpha\beta}\sin\left(\Delta_{ij}\right)\right) \\ &= \mathrm{Re}\left(J^{ij}_{\alpha\beta}\right)\cos\left(\Delta_{ij}\right) - \mathrm{Re}\left(iJ^{ij}_{\alpha\beta}\right)\sin\left(\Delta_{ij}\right)\ . \end{aligned} \tag{B.0.15}$$

But

$$\mathrm{Re}\left(iJ^{ij}_{\alpha\beta}\right) = \mathrm{Re}\left(i\left[\mathrm{Re}\left(J^{ij}_{\alpha\beta}\right) + i\mathrm{Im}\left(J^{ij}_{\alpha\beta}\right)\right]\right) = -\mathrm{Im}\left(J^{ij}_{\alpha\beta}\right) \tag{B.0.16}$$

and with this, we can write the previous expression as

$$\mathrm{Re}\left(J^{ij}_{\alpha\beta}e^{-i\Delta_{ij}}\right) = \mathrm{Re}\left(J^{ij}_{\alpha\beta}\right)\cos\left(\Delta_{ij}\right) + \mathrm{Im}\left(J^{ij}_{\alpha\beta}\right)\sin\left(\Delta_{ij}\right)\ . \tag{B.0.17}$$

Plugging this into Eq. (B.0.14) results in

$$P_{\alpha\beta} = \sum_i J^{ii}_{\alpha\beta} + 2\sum_{i>j}\mathrm{Re}\left(J^{ij}_{\alpha\beta}\right)\cos\left(\Delta_{ij}\right) + 2\sum_{i>j}\mathrm{Im}\left(J^{ij}_{\alpha\beta}\right)\sin\left(\Delta_{ij}\right)\ . \tag{B.0.18}$$

Finally, putting $\cos\left(\Delta_{ij}\right) = 1 - 2\sin^2\left(\Delta_{ij}/2\right)$, the oscillation probability becomes

$$\begin{aligned} P_{\alpha\beta} &= \sum_i J^{ii}_{\alpha\beta} + 2\sum_{i>j}\mathrm{Re}\left(J^{ij}_{\alpha\beta}\right) - 4\sum_{i>j}\mathrm{Re}\left(J^{ij}_{\alpha\beta}\right)\sin^2\left(\frac{\Delta_{ij}}{2}\right) \\ &\quad + 2\sum_{i>j}\mathrm{Im}\left(J^{ij}_{\alpha\beta}\right)\sin\left(\Delta_{ij}\right) \end{aligned} \tag{B.0.19}$$

$$\begin{aligned} &= \sum_{i,j} J^{ij}_{\alpha\beta} - 4\sum_{i>j}\mathrm{Re}\left(J^{ij}_{\alpha\beta}\right)\sin^2\left(\frac{\Delta_{ij}}{2}\right) \\ &\quad + 2\sum_{i>j}\mathrm{Im}\left(J^{ij}_{\alpha\beta}\right)\sin\left(\Delta_{ij}\right)\ . \end{aligned} \tag{B.0.20}$$

From the unitarity of U_0, it follows that

$$\sum_i \left[U_0\right]_{\alpha i}\left[U_0\right]_{i\beta} = \sum_i \left[U_0\right]_{\alpha i}\left[U_0\right]^*_{\beta i} = \delta_{\alpha\beta}\ , \tag{B.0.21}$$

and hence

$$\sum_{i,j} J^{ij}_{\alpha\beta} = [U_0]^*_{\alpha i}\,[U_0]_{\beta i}\,[U_0]_{\alpha j}\,[U_0]^*_{\beta j} = \delta_{\alpha\beta}\ . \tag{B.0.22}$$

With this, the oscillation probability, Eq. (B.0.20), reduces to the well-known expression

$$P_{\alpha\beta} = \delta_{\alpha\beta} - 4\sum_{i>j} \mathrm{Re}\left(J^{ij}_{\alpha\beta}\right) \sin^2\left(\frac{\Delta_{ij}}{2}\right) + 2\sum_{i>j} \mathrm{Im}\left(J^{ij}_{\alpha\beta}\right) \sin\left(\Delta_{ij}\right)\ , \tag{B.0.23}$$

as expected.

Bibliography

[1] R. Davis, Jr., D. S. Harmer, and K. C. Hoffman, "Search for neutrinos from the sun," *Phys. Rev. Lett.* **20** (1968) 1205–1209.

[2] SNO Collaboration, B. Aharmim *et al.*, "Electron energy spectra, fluxes, and day-night asymmetries of B-8 solar neutrinos from the 391-day salt phase SNO data set," *Phys. Rev.* **C72** (2005) 055502, arXiv:nucl-ex/0502021.

[3] Borexino Collaboration, C. Arpesella *et al.*, "Direct Measurement of the Be-7 Solar Neutrino Flux with 192 Days of Borexino Data," *Phys. Rev. Lett.* **101** (2008) 091302, arXiv:0805.3843 [astro-ph].

[4] Super-Kamiokande Collaboration, Y. Ashie *et al.*, "Evidence for an oscillatory signature in atmospheric neutrino oscillation," *Phys. Rev. Lett.* **93** (2004) 101801, arXiv:hep-ex/0404034.

[5] MACRO Collaboration, M. Ambrosio *et al.*, "Measurements of atmospheric muon neutrino oscillations, global analysis of the data collected with MACRO detector," *Eur. Phys. J.* **C36** (2004) 323–339.

[6] KamLAND Collaboration, K. Eguchi *et al.*, "First results from KamLAND: Evidence for reactor anti-neutrino disappearance," *Phys. Rev. Lett.* **90** (2003) 021802, arXiv:hep-ex/0212021.

[7] K2K Collaboration, M. H. Ahn *et al.*, "Measurement of Neutrino Oscillation by the K2K Experiment," *Phys. Rev.* **D74** (2006) 072003, arXiv:hep-ex/0606032.

[8] MINOS Collaboration, P. Adamson *et al.*, "Measurement of Neutrino Oscillations with the MINOS Detectors in the NuMI Beam," *Phys. Rev. Lett.* **101** (2008) 131802, arXiv:0806.2237 [hep-ex].

[9] C. W. Walter, "Experimental Neutrino Physics," arXiv:0810.3937 [hep-ex].

[10] G. L. Fogli, E. Lisi, A. Marrone, and G. Scioscia, "Testing violations of special and general relativity through the energy dependence of $\nu_\mu \leftrightarrow \nu_\tau$ oscillations in the Super-Kamiokande atmospheric neutrino experiment," *Phys. Rev.* **D60** (1999) 053006, arXiv:hep-ph/9904248.

[11] N. E. Mavromatos, "Neutrinos and the phenomenology of CPT violation," arXiv:hep-ph/0402005.

[12] N. E. Mavromatos, "CPT Violation and Decoherence in Quantum Gravity," *J. Phys. Conf. Ser.* **171** (2009) 012007, arXiv:0904.0606 [hep-ph].

[13] D. Colladay and V. A. Kostelecky, "Lorentz-violating extension of the standard model," *Phys. Rev.* **D58** (1998) 116002, arXiv:hep-ph/9809521.

[14] V. A. Kostelecky and M. Mewes, "Lorentz and CPT violation in the neutrino sector," *Phys. Rev.* **D70** (2004) 031902, arXiv:hep-ph/0308300.

[15] V. De Sabbata and M. Gasperini, "Neutrino oscillations in the presence of torsion," *Nuovo Cim.* **A65** (1981) 479–500.

[16] P. Q. Hung and C. Quigg, "Intermediate Bosons: Weak Interaction Couriers," *Science* **210** (1980) 1205–1211.

[17] S. Weinberg, "From BCS to the LHC," *Int. J. Mod. Phys.* **A23** (2008) 1627–1635.

[18] C. Quigg, "Unanswered Questions in the Electroweak Theory," arXiv:0905.3187 [hep-ph].

[19] M. Bustamante, L. Cieri, and J. Ellis, "Beyond the Standard Model for Montaneros," arXiv:0911.4409 [hep-ph].

[20] Gargamelle Neutrino Collaboration, F. J. Hasert *et al.*, "Observation of neutrino-like interactions without muon or electron in the Gargamelle neutrino experiment," *Phys. Lett.* **B46** (1973) 138–140.

[21] UA1 Collaboration, G. Arnison *et al.*, "Experimental observation of isolated large transverse energy electrons with associated missing energy at $s^{1/2} = 540$ GeV," *Phys. Lett.* **B122** (1983) 103–116.

[22] UA2 Collaboration, M. Banner *et al.*, "Observation of single isolated electrons of high transverse momentum in events with missing transverse energy at the CERN anti-p p collider," *Phys. Lett.* **B122** (1983) 476–485.

[23] UA2 Collaboration, P. Bagnaia *et al.*, "Evidence for $Z^0 \to e^+e^-$ at the CERN anti-p p collider," *Phys. Lett.* **B129** (1983) 130–140.

[24] C. Rubbia, "Experimental Observation of the Intermediate Vector Bosons W^+, W^-, and Z^0," *Rev. Mod. Phys.* **57** (1985) 699–722.

[25] M. Delmastro, "Searches for the Higgs boson at the LHC," `arXiv:0909.0493 [hep-ex]`.

[26] K. Jakobs, "Higgs bosons at the LHC," *Eur. Phys. J.* **C59** (2009) 463–495.

[27] ATLAS Collaboration, E. Solfaroli Camillocci, "Standard model Higgs boson search at the Large Hadron Collider," *Nuovo Cim.* **123B** (2008) 790–792.

[28] C. Quigg, *Gauge Theories of the Strong, Weak, and Electromagnetic Interactions*. Addison-Wesley, 1997.

[29] Particle Data Group Collaboration, C. Amsler *et al.*, "Review of particle physics," *Phys. Lett.* **B667** (2008) 1.

[30] D. D. Ryutov, "Using Plasma Physics to Weigh the Photon," *Plasma Phys. Control. Fusion* **49** (2007) B429.

[31] ALEPH, CDF, D0, DELPHI, L3, OPAL, SLD, LEP Electroweak Working Group, Tevatron Electroweak Working Group, and SLD Electroweak Heavy Flavour Group, "Precision Electroweak Measurements and Constraints on the Standard Model," `arXiv:0911.2604 [hep-ex]`.

[32] H. Flacher *et al.*, "Gfitter - Revisiting the Global Electroweak Fit of the Standard Model and Beyond," *Eur. Phys. J.* **C60** (2009) 543–583, `arXiv:0811.0009 [hep-ph]`.

[33] J. R. Ellis and G. L. Fogli, "Neutral currents, $M\,(Z)$ and $m\,(t)$," *Phys. Lett.* **B231** (1989) 189.

[34] J. R. Ellis, G. L. Fogli, and E. Lisi, "Bounds on $M\,(H)$ from electroweak radiative corrections," *Phys. Lett.* **B274** (1992) 456–462.

[35] ALEPH Collaboration, S. Schael *et al.*, "Search for neutral MSSM Higgs bosons at LEP," *Eur. Phys. J.* **C47** (2006) 547–587, `arXiv:hep-ex/0602042`.

[36] B. Kayser, "Neutrino physics," `arXiv:hep-ph/0506165`.

[37] R. N. Mohapatra *et al.*, "Theory of neutrinos: A white paper," *Rept. Prog. Phys.* **70** (2007) 1757–1867, arXiv:hep-ph/0510213.

[38] M. C. Peskin and D. V. Schroeder, *An introduction to quantum field theory.* Westview Press, 1995.

[39] F. Mandl and G. G. Shaw, *Quantum field theory.* Wiley, 1993.

[40] C.-W. Chiang, "Theoretical Review on CP Violation in Rare B decays," arXiv:0808.1336 [hep-ph].

[41] R. Fleischer, "Theoretical review of CP violation," arXiv:hep-ph/0310313.

[42] J. L. Rosner, "CP violation: A Brief review," arXiv:hep-ph/0005258.

[43] C. Giunti and C. W. K., *Fundamentals of neutrino physics and astrophysics.* Oxford University Press, 2007.

[44] S. M. Bilenky, "Neutrinoless Double β-Decay: Status and Future," *Phys. Atom. Nucl.* **69** (2006) 2134–2140, arXiv:hep-ph/0509098.

[45] O. Cremonesi, "Neutrino masses and Neutrinoless Double Beta Decay: Status and expectations," arXiv:1002.1437 [hep-ex].

[46] D. Colladay and V. A. Kostelecky, "CPT violation and the standard model," *Phys. Rev.* **D55** (1997) 6760–6774, arXiv:hep-ph/9703464.

[47] V. A. Kostelecky and N. Russell, "Data Tables for Lorentz and CPT Violation," arXiv:0801.0287 [hep-ph].

[48] ALEPH Collaboration, D. Decamp *et al.*, "Determination of the Number of Light Neutrino Species," *Phys. Lett.* **B231** (1989) 519.

[49] B. Kayser, "Neutrino Mass, Mixing, and Flavor Change," arXiv:0804.1497 [hep-ph].

[50] T. Schwetz, M. A. Tortola, and J. W. F. Valle, "Three-flavour neutrino oscillation update," *New J. Phys.* **10** (2008) 113011, arXiv:0808.2016 [hep-ph].

[51] S. J. Parke, "CP Violation in the Neutrino Sector," arXiv:0807.3311 [hep-ph].

[52] H. Minakata, "Do neutrinos violate CP?," arXiv:hep-ph/0604088.

[53] M. Ishitsuka, T. Kajita, H. Minakata, and H. Nunokawa, "Resolving Neutrino Mass Hierarchy and CP Degeneracy by Two Identical Detectors with Different Baselines," *Phys. Rev.* **D72** (2005) 033003, arXiv:hep-ph/0504026.

[54] O. Mena, "Unveiling Neutrino Mixing and Leptonic CP Violation," *Mod. Phys. Lett.* **A20** (2005) 1–17, arXiv:hep-ph/0503097.

[55] P. D. Serpico and M. Kachelriess, "Measuring the 13-mixing angle and the CP phase with neutrino telescopes," *Phys. Rev. Lett.* **94** (2005) 211102, arXiv:hep-ph/0502088.

[56] HESS Collaboration, F. Aharonian, "Upper Limits from HESS AGN Observations in 2005-2007," arXiv:0711.3196 [astro-ph].

[57] HESS Collaboration, F. Aharonian, "Discovery of very high energy gamma-ray emission from Centaurus A with H.E.S.S," *Astrophys. J. Lett.* **695** (2009) L40–L44, arXiv:0903.1582 [astro-ph.CO].

[58] VERITAS, HESS and MAGIC Collaboration, V. A. Acciari *et al.*, "Radio Imaging of the Very-High-Energy Gamma-Ray Emission Region in the Central Engine of a Radio Galaxy," *Science* **325** (2009) 444–448, arXiv:0908.0511 [astro-ph.HE].

[59] MAGIC Collaboration, J. Albert *et al.*, "Detection of VHE radiation from the BL Lac PG 1553+113 with the MAGIC telescope," *Astrophys. J.* **654** (2007) L119–L122, arXiv:astro-ph/0606161.

[60] MAGIC Collaboration, J. Albert *et al.*, "Observations of Mkn 421 with the MAGIC Telescope," *Astrophys. J.* **663** (2007) 125–138, arXiv:astro-ph/0603478.

[61] MAGIC Collaboration, J. Albert *et al.*, "Discovery of Very High Energy gamma-rays from 1ES1011+496 at $z = 0.212$," *Astrophys. J.* **667** (2007) L21–L23, arXiv:0706.4435 [astro-ph].

[62] H. Anderhub, "Discovery of Very High Energy gamma-rays from the blazar S5 0716+714," arXiv:0907.2386 [astro-ph.CO].

[63] VERITAS Collaboration, V. Acciari *et al.*, "Discovery of Very High-Energy Gamma-Ray Radiation from the BL Lac 1ES 0806+524," arXiv:0812.0978 [astro-ph].

[64] VERITAS Collaboration, V. A. Acciari *et al.*, "VERITAS observations of the BL Lac 1ES 1218+304," *AIP Conf. Proc.* **1085** (2009) 565–568, arXiv:0901.4561 [astro-ph.HE].

[65] VERITAS Collaboration, V. A. Acciari *et al.*, "VERITAS Observations of a Very High Energy Gamma-ray Flare from the Blazar 3C 66A," *Astrophys. J. Lett.* **693** (2009) L104–L108, arXiv:0901.4527 [astro-ph.HE].

[66] Milagro Collaboration, D. A. Williams, "Studies of nearby blazars with Milagro," *AIP Conf. Proc.* **745** (2005) 499–504.

[67] Milagro Collaboration, J. A. Goodman, "Recent results from Milagro," *AIP Conf. Proc.* **917** (2007) 202–205.

[68] F. Halzen, "IceCube: Neutrinos Associated with Cosmic Rays," *AIP Conf. Proc.* **1182** (2009) 14–21, arXiv:0906.3470 [astro-ph.HE].

[69] IceCube Collaboration, X. W. Xu, "Results achieved with AMANDA," *Nucl. Phys. Proc. Suppl.* **175-176** (2008) 401–406.

[70] F. Halzen, "IceCube Science," *J. Phys. Conf. Ser.* **171** (2009) 012014, arXiv:0901.4722 [astro-ph.HE].

[71] A. M. Brown and f. t. A. Collaboration, "The ANTARES Neutrino Telescope: status and first results," *AIP Conf. Proc.* **1178** (2009) 76–82, arXiv:0908.1035 [astro-ph.HE].

[72] A. Esmaili and Y. Farzan, "An Analysis of Cosmic Neutrinos: Flavor Composition at Source and Neutrino Mixing Parameters," *Nucl. Phys.* **B821** (2009) 197–214, arXiv:0905.0259 [hep-ph].

[73] G. Barenboim and C. Quigg, "Neutrino observatories can characterize cosmic sources and neutrino properties," *Phys. Rev.* **D67** (2003) 073024, arXiv:hep-ph/0301220.

[74] J. F. Beacom, N. F. Bell, D. Hooper, S. Pakvasa, and T. J. Weiler, "Measuring flavor ratios of high-energy astrophysical neutrinos," *Phys. Rev.* **D68** (2003) 093005, arXiv:hep-ph/0307025.

[75] H. Athar, C. S. Kim, and J. Lee, "The intrinsic and oscillated astrophysical neutrino flavor ratios," *Mod. Phys. Lett.* **A21** (2006) 1049–1066, arXiv:hep-ph/0505017.

[76] P. Lipari, M. Lusignoli, and D. Meloni, "Flavor Composition and Energy Spectrum of Astrophysical Neutrinos," *Phys. Rev.* **D75** (2007) 123005, arXiv:0704.0718 [astro-ph].

[77] K.-C. Lai, G.-L. Lin, and T. C. Liu, "Determination of the Neutrino Flavor Ratio at the Astrophysical Source," *Phys. Rev.* **D80** (2009) 103005, arXiv:0905.4003 [hep-ph].

[78] Z.-Z. Xing and S. Zhou, "Towards determination of the initial flavor composition of ultrahigh-energy neutrino fluxes with neutrino telescopes," *Phys. Rev.* **D74** (2006) 013010, arXiv:astro-ph/0603781.

[79] J. P. Rachen and P. Meszaros, "Photohadronic neutrinos from transients in astrophysical sources," *Phys. Rev.* **D58** (1998) 123005, arXiv:astro-ph/9802280.

[80] T. Kashti and E. Waxman, "Flavoring Astrophysical Neutrinos: Flavor Ratios Depend on Energy," *Phys. Rev. Lett.* **95** (2005) 181101, arXiv:astro-ph/0507599.

[81] Z.-z. Xing, "Neutrino telescopes as a probe of broken mu tau symmetry," *Phys. Rev.* **D74** (2006) 013009, arXiv:hep-ph/0605219.

[82] Pierre Auger Collaboration, J. Abraham *et al.*, "Correlation of the highest-energy cosmic rays with the positions of nearby active galactic nuclei," *Astropart. Phys.* **29** (2008) 188–204, arXiv:0712.2843 [astro-ph].

[83] M.-P. Véron-Cetty and P. Véron, "A catalogue of quasars and active nuclei: 12th edition," *A&A* **455** (2006) 773–777.

[84] H. B. J. Koers and P. Tinyakov, "Testing large-scale (an)isotropy of ultra-high energy cosmic rays," *JCAP* **0904** (2009) 003, arXiv:0812.0860 [astro-ph].

[85] G. R. Farrar, I. Zaw, and A. A. Berlind, "Correlations between Ultrahigh Energy Cosmic Rays and AGNs," arXiv:0904.4277 [astro-ph.HE].

[86] H. B. J. Koers and P. Tinyakov, "Relation between the neutrino flux from Centaurus A and the associated diffuse neutrino flux," *Phys. Rev.* **D78** (2008) 083009, arXiv:0802.2403 [astro-ph].

[87] J. K. Becker and P. L. Biermann, "Neutrinos from active black holes, sources of ultra high energy cosmic rays," *Astropart. Phys.* **31** (2009) 138–148, arXiv:0805.1498 [astro-ph].

[88] M. Kachelriess, "Lecture notes on high energy cosmic rays," arXiv:0801.4376 [astro-ph].

[89] E. Waxman and J. N. Bahcall, "High energy neutrinos from astrophysical sources: An upper bound," *Phys. Rev.* **D59** (1999) 023002, arXiv:hep-ph/9807282.

[90] E. Waxman, "Cosmological origin for cosmic rays above 10^{19} eV," *Astrophys. J.* **452** (1995) L1–L4, arXiv:astro-ph/9508037.

[91] The Pierre Auger Collaboration, J. Abraham *et al.*, "Upper limit on the diffuse flux of UHE tau neutrinos from the Pierre Auger Observatory," *Phys. Rev. Lett.* **100** (2008) 211101, arXiv:0712.1909 [astro-ph].

[92] IceCube Collaboration, J. Ahrens *et al.*, "Sensitivity of the IceCube detector to astrophysical sources of high energy muon neutrinos," *Astropart. Phys.* **20** (2004) 507–532, arXiv:astro-ph/0305196.

[93] IceCube Collaboration, A. Achterberg *et al.*, "Multi-year search for a diffuse flux of muon neutrinos with AMANDA-II," *Phys. Rev.* **D76** (2007) 042008, arXiv:0705.1315 [astro-ph]. Erratum-ibid. D **77**, 089904 (2008).

[94] B. J. Boyle and R. Terlevich, "The cosmological evolution of the QSO luminosity density and of the star formation rate," arXiv:astro-ph/9710134.

[95] A. Cuoco and S. Hannestad, "Ultra-high energy Neutrinos from Centaurus A and the Auger hot spot," *Phys. Rev.* **D78** (2008) 023007, arXiv:0712.1830 [astro-ph].

[96] K. Mannheim, R. J. Protheroe, and J. P. Rachen, "On the cosmic ray bound for models of extragalactic neutrino production," *Phys. Rev.* **D63** (2001) 023003, arXiv:astro-ph/9812398.

[97] C. J. Willott, S. Rawlings, K. M. Blundell, M. Lacy, and S. A. Eales, "The radio luminosity function from the low-frequency 3CRR, 6CE & 7CRS complete samples," *Mon. Not. Roy. Astron. Soc.* **322** (2001) 536–552, arXiv:astro-ph/0010419.

[98] J. S. Dunlop and J. A. Peacock, "The Redshift Cut-Off in the Luminosity Function of Radio Galaxies and Quasars," *Mon. Not. Roy. Astron. Soc.* **247** (1990) 19.

[99] M. Maltoni and W. Winter, "Testing neutrino oscillations plus decay with neutrino telescopes," *JHEP* **07** (2008) 064, arXiv:0803.2050 [hep-ph].

[100] J. F. Beacom, N. F. Bell, D. Hooper, S. Pakvasa, and T. J. Weiler, "Decay of high-energy astrophysical neutrinos," *Phys. Rev. Lett.* **90** (2003) 181301, arXiv:hep-ph/0211305.

[101] J. F. Beacom and N. F. Bell, "Do solar neutrinos decay?," *Phys. Rev.* **D65** (2002) 113009, arXiv:hep-ph/0204111.

[102] A. Mirizzi, D. Montanino, and P. D. Serpico, "Revisiting cosmological bounds on radiative neutrino lifetime," *Phys. Rev.* **D76** (2007) 053007, arXiv:0705.4667 [hep-ph].

[103] J. L. Bazo, M. Bustamante, A. M. Gago, and O. G. Miranda, "High energy astrophysical neutrino flux and modified dispersion relations," *Int. J. Mod. Phys.* **A24** (2009) 5819–5829, arXiv:0907.1979 [hep-ph].

[104] M. Bustamante, A. M. Gago, J. L. Bazo, and O. G. Miranda, "On the sensitivity of neutrino telescopes to a modified dispersion relation," *AIP Conf. Proc.* **1026** (2008) 251–253.

[105] M. Maltoni, T. Schwetz, M. A. Tortola, and J. W. F. Valle, "Status of global fits to neutrino oscillations," *New J. Phys.* **6** (2004) 122, arXiv:hep-ph/0405172.

[106] KamLAND Collaboration, S. Abe *et al.*, "Precision Measurement of Neutrino Oscillation Parameters with KamLAND," *Phys. Rev. Lett.* **100** (2008) 221803, arXiv:0801.4589 [hep-ex].

[107] M. C. Gonzalez-Garcia and M. Maltoni, "Atmospheric neutrino oscillations and new physics," *Phys. Rev.* **D70** (2004) 033010, arXiv:hep-ph/0404085.

[108] G. Battistoni *et al.*, "Search for a Lorentz invariance violation contribution in atmospheric neutrino oscillations using MACRO data," *Phys. Lett.* **B615** (2005) 14–18, arXiv:hep-ex/0503015.

[109] G. L. Fogli, E. Lisi, A. Marrone, D. Montanino, and A. Palazzo, "Probing non-standard decoherence effects with solar and KamLAND neutrinos," *Phys. Rev.* **D76** (2007) 033006, arXiv:0704.2568 [hep-ph].

[110] D. Hooper, D. Morgan, and E. Winstanley, "Lorentz and CPT invariance violation in high-energy neutrinos," *Phys. Rev.* **D72** (2005) 065009, arXiv:hep-ph/0506091.

[111] S. R. Coleman and S. L. Glashow, "High-Energy Tests of Lorentz Invariance," *Phys. Rev.* **D59** (1999) 116008, arXiv:hep-ph/9812418.

[112] D. Mattingly, "Modern tests of Lorentz invariance," *Living Rev. Rel.* **8** (2005) 5, arXiv:gr-qc/0502097.

[113] M. C. Gonzalez-Garcia, F. Halzen, and M. Maltoni, "Physics reach of high-energy and high-statistics Icecube atmospheric neutrino data," *Phys. Rev.* **D71** (2005) 093010, arXiv:hep-ph/0502223.

[114] D. Morgan, E. Winstanley, J. Brunner, and L. F. Thompson, "Neutrino telescope modelling of Lorentz invariance violation in oscillations of atmospheric neutrinos," arXiv:0705.1897 [astro-ph].

[115] G. Amelino-Camelia, J. Kowalski-Glikman, G. Mandanici, and A. Procaccini, "Phenomenology of doubly special relativity," *Int. J. Mod. Phys.* **A20** (2005) 6007–6038, arXiv:gr-qc/0312124.

[116] C. Lunardini and A. Y. Smirnov, "High-energy neutrino conversion and the lepton asymmetry in the universe," *Phys. Rev.* **D64** (2001) 073006, arXiv:hep-ph/0012056.

[117] J. Christian, "Testing quantum gravity via cosmogenic neutrino oscillations," *Phys. Rev.* **D71** (2005) 024012, arXiv:gr-qc/0409077.

[118] H. Athar, "Neutrino conversions in active galactic nuclei," arXiv:hep-ph/0001128.

[119] The AMANDA Collaboration, J. Ahrens *et al.*, "New results from the Antarctic Muon And Neutrino Detector Array," *Nucl. Phys. Proc. Suppl.* **143** (2005) 343–350, arXiv:astro-ph/0409423.

[120] M. Bustamante, A. M. Gago, and C. Pena-Garay, "Extreme scenarios of new physics in the UHE astrophysical neutrino flavour ratios," *J. Phys. Conf. Ser.* **171** (2009) 012048, arXiv:0906.5329 [hep-ph].

[121] M. Bustamante, A. M. Gago, and C. Pena-Garay, "Energy-independent new physics in the flavour ratios of high-energy astrophysical neutrinos," *JHEP* **04** (2010) 066, arXiv:1001.4878 [hep-ph].

[122] A. Dighe and S. Ray, "CPT violation in long baseline neutrino experiments: a three flavor analysis," *Phys. Rev.* **D78** (2008) 036002, arXiv:0802.0121 [hep-ph].

[123] V. D. Barger, S. Pakvasa, T. J. Weiler, and K. Whisnant, "CPT odd resonances in neutrino oscillations," *Phys. Rev. Lett.* **85** (2000) 5055–5058, arXiv:hep-ph/0005197.

[124] E. Waxman, "Astrophysical sources of high energy neutrinos," *Nucl. Phys. Proc. Suppl.* **118** (2003) 353, arXiv:astro-ph/0211358.

[125] T. DeYoung, "Neutrino Astronomy with IceCube," *Mod. Phys. Lett.* **A24** (2009) 1543–1557, arXiv:0906.4530 [astro-ph.HE].

[126] F. Halzen, "IceCube: The Rationale for Kilometer-Scale Neutrino Detectors," arXiv:0910.0436 [astro-ph.HE].

[127] R. Gandhi, C. Quigg, M. H. Reno, and I. Sarcevic, "Ultrahigh-energy neutrino interactions," *Astropart. Phys.* **5** (1996) 81–110, arXiv:hep-ph/9512364.

[128] L. A. Anchordoqui *et al.*, "Probing Planck scale physics with IceCube," *Phys. Rev.* **D72** (2005) 065019, arXiv:hep-ph/0506168.

[129] R. Gandhi, C. Quigg, M. H. Reno, and I. Sarcevic, "Neutrino interactions at ultrahigh-energies," *Phys. Rev.* **D58** (1998) 093009, arXiv:hep-ph/9807264.